Water quality-based real time control of combined sewer systems

Duy Khiem Ly

N°d'ordre NNT : 2019LYSEI032

THESE de DOCTORAT DE L'UNIVERSITE DE LYON
opérée au sein de
INSTITUT NATIONAL DES SCIENCES APPLIQUEES DE LYON

Ecole Doctorale ED162
MECANIQUE, ENERGETIQUE, GENIE CIVIL, ACOUSTIQUE
Spécialité : **Génie Civil**

Soutenue publiquement le 28/05/2019, par :
Duy Khiem LY

WATER QUALITY-BASED REAL TIME CONTROL OF COMBINED SEWER SYSTEMS

GESTION EN TEMPS RÉEL DES RÉSEAUX D'ASSAINISSEMENT UNITAIRES BASÉE SUR LA QUALITÉ DE L'EAU

Devant le jury composé de :

BARRAUD, Sylvie	INSA LYON	Présidente
MUSCHALLA, Dirk	TU GRAZ	Rapporteur
CAMPISANO, Alberto	UNIVERSITY OF CATANIA	Rapporteur
CHEBBO, Ghassan	ENPC	Examinateur
MARUÉJOULS, Thibaud	SUEZ EAU France	Co-encadrant de thèse
BERTRAND-KRAJEWSKI, Jean-Luc	INSA LYON	Directeur de thèse

Département FEDORA – INSA Lyon - Ecoles Doctorales – Quinquennal 2016-2020

SIGLE	ECOLE DOCTORALE	NOM ET COORDONNEES DU RESPONSABLE
CHIMIE	**CHIMIE DE LYON** **http://www.edchimie-lyon.fr** Sec. : Renée EL MELHEM Bât. Blaise PASCAL, 3e étage **secretariat@edchimie-lyon.fr** INSA : R. GOURDON	M. Stéphane DANIELE Institut de recherches sur la catalyse et l'environnement de Lyon IRCELYON-UMR 5256 Équipe CDFA 2 Avenue Albert EINSTEIN 69 626 Villeurbanne CEDEX **directeur@edchimie-lyon.fr**
E.E.A.	**ÉLECTRONIQUE, ÉLECTROTECHNIQUE, AUTOMATIQUE** **http://edeea.ec-lyon.fr** Sec. : M.C. HAVGOUDOUKIAN **ecole-doctorale.eea@ec-lyon.fr**	M. Gérard SCORLETTI École Centrale de Lyon 36 Avenue Guy DE COLLONGUE 69 134 Écully Tél : 04.72.18.60.97 Fax 04.78.43.37.17 **gerard.scorletti@ec-lyon.fr**
E2M2	**ÉVOLUTION, ÉCOSYSTÈME, MICROBIOLOGIE, MODÉLISATION** **http://e2m2.universite-lyon.fr** Sec. : Sylvie ROBERJOT Bât. Atrium, UCB Lyon 1 Tél : 04.72.44.83.62 INSA : H. CHARLES **secretariat.e2m2@univ-lyon1.fr**	M. Philippe NORMAND UMR 5557 Lab. d'Ecologie Microbienne Université Claude Bernard Lyon 1 Bâtiment Mendel 43, boulevard du 11 Novembre 1918 69 622 Villeurbanne CEDEX **philippe.normand@univ-lyon1.fr**
EDISS	**INTERDISCIPLINAIRE SCIENCES-SANTÉ** **http://www.ediss-lyon.fr** Sec. : Sylvie ROBERJOT Bât. Atrium, UCB Lyon 1 Tél : 04.72.44.83.62 INSA : M. LAGARDE **secretariat.ediss@univ-lyon1.fr**	Mme Emmanuelle CANET-SOULAS INSERM U1060, CarMeN lab, Univ. Lyon 1 Bâtiment IMBL 11 Avenue Jean CAPELLE INSA de Lyon 69 621 Villeurbanne Tél : 04.72.68.49.09 Fax : 04.72.68.49.16 **emmanuelle.canet@univ-lyon1.fr**
INFOMATHS	**INFORMATIQUE ET MATHÉMATIQUES** **http://edinfomaths.universite-lyon.fr** Sec. : Renée EL MELHEM Bât. Blaise PASCAL, 3e étage Tél : 04.72.43.80.46 **infomaths@univ-lyon1.fr**	M. Luca ZAMBONI Bât. Braconnier 43 Boulevard du 11 novembre 1918 69 622 Villeurbanne CEDEX Tél : 04.26.23.45.52 **zamboni@maths.univ-lyon1.fr**
Matériaux	**MATÉRIAUX DE LYON** **http://ed34.universite-lyon.fr** Sec. : Stéphanie CAUVIN Tél : 04.72.43.71.70 Bât. Direction **ed.materiaux@insa-lyon.fr**	M. Jean-Yves BUFFIÈRE INSA de Lyon MATEIS - Bât. Saint-Exupéry 7 Avenue Jean CAPELLE 69 621 Villeurbanne CEDEX Tél : 04.72.43.71.70 Fax : 04.72.43.85.28 **jean-yves.buffiere@insa-lyon.fr**
MEGA	**MÉCANIQUE, ÉNERGÉTIQUE, GÉNIE CIVIL, ACOUSTIQUE** **http://edmega.universite-lyon.fr** Sec. : Stéphanie CAUVIN Tél : 04.72.43.71.70 Bât. Direction **mega@insa-lyon.fr**	M. Jocelyn BONJOUR INSA de Lyon Laboratoire CETHIL Bâtiment Sadi-Carnot 9, rue de la Physique 69 621 Villeurbanne CEDEX **jocelyn.bonjour@insa-lyon.fr**
ScSo	**ScSo*** **http://ed483.univ-lyon2.fr** Sec. : Véronique GUICHARD INSA : J.Y. TOUSSAINT Tél : 04.78.69.72.76 **veronique.cervantes@univ-lyon2.fr**	M. Christian MONTES Université Lyon 2 86 Rue Pasteur 69 365 Lyon CEDEX 07 **christian.montes@univ-lyon2.fr**

*ScSo : Histoire, Géographie, Aménagement, Urbanisme, Archéologie, Science politique, Sociologie, Anthropologie

Tưởng nhớ đến ông nội và
ông ngoại kính yêu của con

Acknowledgements

I wish to express my gratitude and appreciation to all who have contributed to this thesis.

I would like to thank most specially my supervisors, Jean-Luc Bertrand-Krajewski from Laboratoire DEEP, INSA Lyon, and Thibaud Maruéjouls from Le LyRE, Suez. Without their continuous guidance, fruitful discussions and invaluable support, this work would not have been possible. They both gave me very constructive comments and were always there when I needed help. Working with them over the past three years helped me greatly to improve my research skills and to learn meaningful things beyond the academic world.

I am grateful to the thesis committee members for accepting to read this manuscript and to take part in the defense of this thesis. Their kind support is truly appreciated.

I am also indebted to the LIFE EFFIDRAIN European project for funding this thesis, together with the other financial and technical support by Bordeaux Métropole and Société de Gestion de l'Assainissement de Bordeaux (SGAC) for data collection and monitoring tasks.

I wish to extend my sincere gratitude to Guillaume Binet for his inspiring remarks and precious discussions. I wish to thank Albert Montserrat, Fares Aouichat, Jing Feng, Christophe Chauvin, Xavier Litrico, Bernat Joseph-Duran, and other team members for their contributions to the LIFE EFFIDRAIN project, which are important for the progress of this thesis. Besides, I particularly thank my other friends and colleagues at Le LyRE, Suez and Laboratoire DEEP, INSA Lyon. To Jean-Claude Dorignac, Alexandre Ventura and Aude Garda, I will remember all their assistance and company.

Finally, I must say thanks to the most important people of my life: my big family in Vietnam and my dear wife. They gave me endless care and permanent encouragement during the past years. They are simply my main source of motivation to overcome all challenges in life.

Abstract

Real time control (RTC) is considered as a cost-efficient solution for combined sewer overflow (CSO) reduction as it optimises the available capacity of sewer networks. RTC helps to prevent the need for construction of additional retention volumes, increases the network adaptability to changes in water management policies, and above all alleviates the environmental impact of CSOs. Following increasing interest in water quality-based RTC (QBR), this thesis demonstrates a simple and nothing-to-lose QBR strategy to reduce the amount of CSO loads during storm events. The performance of the QBR strategy, based on Mass-Volume (MV) curves prediction, is evaluated by comparison to a typical hydraulics-based RTC (HBR) strategy. A proof-of-concept study is first performed on a small catchment of 205 ha to test the new QBR concept using 31 storm events during a two-year period. Compared to HBR, QBR delivers CSO load reduction for more than one third of the events, with reduction values from 3 to 43 %. The QBR strategy is then implemented on the Louis Fargue catchment (7700 ha) in Bordeaux, France and similarly compared with the HBR strategy. By implementing QBR on 19 storm events over 15 months, its performance is consistent, bringing valuable benefits over HBR, with 17 out of 19 events having load reduction varying between 6 and 28.8 %. The thesis further evaluates the impact of MV curve prediction uncertainty (due to model prediction uncertainty) on the performance of the QBR strategy, using a representative storm event. The resulting range of uncertainty is limited. Besides, results of the sensitivity study show that the choice of the QBR or HBR strategy should take into account the current tank volumes and their locations within the catchment.

Résumé

La gestion en temps réel (GTR) est considérée comme une solution économiquement efficace pour réduire les déversements par temps de pluie car elle optimise la capacité disponible des réseaux d'assainissement. La GTR permet d'éviter la construction de volumes de rétention supplémentaires, d'augmenter l'adaptabilité du réseau aux changements de politiques de gestion de l'eau et surtout d'atténuer l'impact environnemental des déversoirs d'orage. À la suite de l'intérêt croissant pour la GTR fondée sur la qualité de l'eau (QBR), cette thèse démontre une stratégie simple et efficace pour les charges polluantes déversées par temps de pluie. La performance de la stratégie QBR, basée sur la prédiction des courbes masse-volume (MV), est évaluée par comparaison avec une stratégie typique de GTR à base hydraulique (HBR). Une étude de validation de principe est d'abord réalisée sur un petit bassin versant de 205 ha pour tester le nouveau concept de QBR en utilisant 31 événements pluvieux sur une période de deux ans. Par rapport à HBR, QBR offre une réduction des charges déversées pour plus d'un tiers des événements, avec des réductions de 3 à 43 %. La stratégie QBR est ensuite mise en œuvre sur le bassin versant de Louis Fargue (7700 ha) à Bordeaux, France et comparée à nouveau à la stratégie HBR. En implémentant QBR sur 19 événements pluvieux sur 15 mois, ses performances sont constantes et apportent des avantages précieux par rapport à HBR, 17 des 19 événements ayant une réduction de charge variant entre 6 et 28.8 %. La thèse évalue en outre l'impact de l'incertitude de prédiction de la courbe MV (due à l'incertitude de prédiction du modèle) sur la performance de la stratégie QBR, en utilisant un événement pluvieux représentatif. La marge d'incertitude qui en résulte est faible. En outre, l'étude de sensibilité montre que le choix de la stratégie QBR ou HBR doit tenir compte des dimensions réelles des bassins et de leur emplacement sur le bassin versant.

Table of Contents

List of Abbreviations and Acronyms

Antecedent Dry Weather Period	ADWP
Biological Oxygen Demand	BOD
Caudéran-Naujac	CDN
Chemical Oxygen Demand	COD
Combined Sewer Overflow	CSO
Control Time Interval	CTI
cumulative distribution function	cdf
Dissolved Oxygen	DO
Explanatory Variables	EV
Forward Stepwise Algorithm	FSA
Gestion Dynamique	GD
Hydraulics-based Real Time Control	HBR
Leave-One-Out Cross Validation	LOOCV
Mass-volume curve	MV curve
Monte Carlo	MC
Multiple Linear Regression	MLR
Nash-Sutcliffe efficiency index	NS
out-of-bag	oob
Population Equivalent	PE
probability density function	pdf
Random Forest Regression	RFR
Real Time Control	RTC
Root-Mean-Square Error	RMSE
Sewer Network	SN
State Variable	SV
Suspended Solids	SS
Total Kjeldahl Nitrogen	TKN
Total Organic Carbon	TOC
Total Suspended Solids	TSS
Ultraviolet	UV
Ultraviolet-Visible	UV-Vis
Urban Drainage System	UDS

Urban Wastewater System	UWS
Wastewater Treatment Plant	WWTP
Water Quality-based Real Time Control	QBR

CHAPTER 1: INTRODUCTION

This chapter aims to provide basic knowledge to better understand the research area and to present the work, the objectives, and the structure of the thesis. In the first section, an overview of urban drainage systems (UDSs), i.e. their components and functions, is presented. To bring added values for the thesis and to satisfy the author's own curiosity, the first section also looks into UDS development along the humankind history. The second section starts with an introduction of the LIFE EFFIDRAIN European project, which can be considered as the foundation of this thesis. Subsequently the next parts in the section present the thesis objective and outline.

1.1 General overview and historic evolution of urban drainage systems

1.1.1 General overview

UDSs or sewer networks (SNs) have been developed to support the interactions between human activities and natural water resources within an urban area. There are two types of water handled by UDSs: wastewater and stormwater. Wastewater arises from human use of distributed water, and stormwater refers to the water that drains off a land area due to rainfall, i.e. surface runoff. Wastewater carries numerous pollutants e.g. domestic and industrial consumptions, and is usually far more contaminated than stormwater. The latter type includes mainly pollutants coming from the air and catchment surfaces (Butler *et al.*, 2018).

SNs contain networks of pipes and associated structures, e.g. pumps, valves, gates, etc. to serve the purpose of water collection and transport. In dry weather, SNs collect and convey wastewater to wastewater treatment plants (WWTPs) through underground pipes. Following the manner of dealing with stormwater, SNs can be principally classified into two categories: combined and separate SNs. In combined SNs, stormwater is mixed with wastewater and both

are transported together in the same pipes to WWTPs during rainfall events (as illustrated by Figure 1). Under wet weather conditions, flow in the pipes may increase rapidly due to stormwater contribution. As reported by Butler *et al.* (2018), the stormwater flow can be 50 or even 100 times the average wastewater flow in heavy rainfall events. It is not economically efficient to furnish capacity for such flows on the whole system, given that most of the time the sewers are operated under dry weather conditions. Combined SNs are therefore designed to overflow excessive stormwater into nearby water bodies via combined sewer overflow (CSO) structures located at outlet points of the catchments in order to avoid flooding and hydraulic overloading of WWTPs. CSO discharges containing polluted stormwater are frequently considered real risks to the environments (discussed in section 2.1.3). In separate SNs, the risks are lowered because different types of water flow in different pipes. Nevertheless, as presented by Butler *et al.* (2018), the installations of separate SNs often require higher cost, and the strong impact of even few incorrect connections can easily diminish their advantage.

WWTPs are meant to remove pollutants in wastewater and/or stormwater, producing water that meets certain treatment criteria and is considered safe to be released to the receiving water bodies. At the present time, WWTPs are often designed for three key processes: preliminary treatment to screen out coarse materials and sand, primary treatment to separate suspended solids (SS) by gravity sedimentation, and secondary treatment to further remove remaining suspended and dissolved organic matters by biological methods (Henze *et al.*, 2008). Depending on the regulations and budget availability, additional treatment processes of physical, chemical or tertiary types can be brought into to further remove pollutant loads. Most of the WWTPs are designed with bypasses, allowing rapid discharges of water when the WWTPs are hydraulically overloaded.

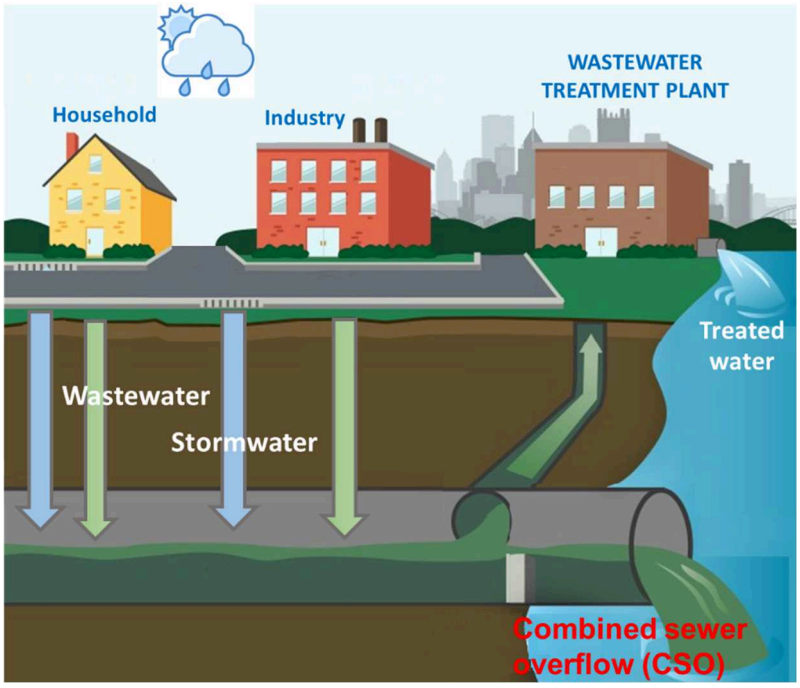

Figure 1. An example of UDS with a combined SN and a WWTP (adapted from Flood, K. (2017)).

1.1.2 Historic evolution

One of the earliest evidences of UDSs was possibly from the excavations of Harappa and Mohenjo-Daro, which are ancient archaeological sites in Pakistan (Webster, 1962). The ancient structures are reported to be dated as early as 2500 BCE, belonging to the Indus Valley civilization of the Bronze Age. As described by the same author, both wastewater from the bath, kitchen and latrine of each home and stormwater from the roof drainage ran into a little brick-lined settling pit. There also existed terra-cotta pipes that drained wastewater from the high floors into the pit. When three-quarters of the pit volume was fulfilled, water overflowed through an outlet to the street drains. The width and depth of the street drains ranged between 23 and 46 cm and between 30 and 60 cm respectively. They were often covered by flat bricks or stone slabs that could be taken away for cleaning or maintenance (Gray, 1940). It was not documented where the final destination of all the street drains was, but the findings show the first signs of the SNs functional for collection and transport of wastewater and stormwater.

The next interesting evidence of SNs was from the remnants of the Minoan civilization, more particularly during the period ca. 2100-1400 BCE (Angelakis *et al.*, 2005). Archaeologists discovered elaborate facilities for drainage built in several palaces and towns of ancient Greece, e.g. Knosso, Zakros and Hagia Triadha. The SNs of these places shared many similarities in design and construction principles. They were of combined type, usually well covered and mostly made of stone structures or smaller terra-cotta ones. Water was conveyed by gravity, and the conduits sometimes included zigzag shapes and were connected with basins to control the flow velocity. In addition, the main disposal points of the system were identified as rivers or sea (Angelakis and Rose, 2014). The study also highlighted that in Minoan times, stormwater enriched by sewage was utilized for agricultural irrigation.

A higher level of the UDS evolution was associated with the Roman civilization, ca. 753 BCE - 476 CE. During this period, fresh water was widely supplied by the famous Roman aqueducts through public latrines, baths and fountains to reduce the issues of epidemics and fires (Vuorinen *et al.*, 2007). This also led to remarkable wastewater management strategies of the Romans, with complex and diverse networks of pipes and cesspools in multiple cities. One representative success of the Roman engineers is the Cloaca Maxima (i.e. the Greatest Sewer), the largest known ancient SN in the world. It is still existent and partly functional today, after over 2500 years (De Feo *et al.*, 2014). It served initially to drain marshes, but then was extended throughout the center of the ancient Rome for wastewater and stormwater transport to the Tiber river. The main channel was 12 m underneath the ground, up to 4.5 m wide and 3.30 m high, and accessible via manholes (Lofrano and Brown, 2010). The large conduits of the Cloaca Maxima could be regarded as an unwitting application of treatment because wastewater was diluted by much bigger quantities of stormwater before being discharged to the receiving waters (Angelakis and Rose, 2014). Unfortunately, following the end of the Roman Empire, wastewater management was almost abandoned in Europe throughout the Middle Ages except

in monasteries where sometimes elaborated systems were built. Until the seventeenth century, no evidence of significant improvement was discovered (Lens *et al.*, 2001). Since the 19th century, there have been massive improvements in wastewater management such as installation of separate SNs to protect the receiving waters, new construction materials and equipment to improve the SNs' performance.

Another evolutional aspect of UDSs concerns handling sediments in the pipes. Deposition has long been the main cause of blockages, floods, odour and gas emissions. From the old times, the conduits were not well designed to overcome deposition. Flat inverts, small slopes and rough walls were addressed as typical causes of deposition, which demanded enormous manpower, fresh or drinking water to remove trapped sediments (Graham, 1972; Malissard, 1994; Sickert, 1999). As presented by Bertrand-Krajewski (2003), starting from the eighteenth century, innovative approaches were applied on designing the shapes of the sewer conduits. Egged shape was commonly preferred for medium size conduits (depth between 0.6 m and 0.9 m) and circular shape was the choice for the small ones to facilitate self-cleansing. Furthermore, multiple flushing tanks were built since the late eighteenth century to enable flushing periodically the downstream mains. Because of their economic constraints, the flushing tanks were latter replaced by other more efficient tools, e.g. high pressure jetting, vacuum lorries, etc.

Compared to the SNs, the first WWTP was likely born thousands years after despite early signs of drinking water treatment in the Bronze Age, e.g. hydraulic filters and siphons to remove impurities from source waters (Spanakis, 1981; Mays *et al.*, 2012). Settling in trenches and pits was possibly the earliest attempt of wastewater treatment and the pristine form of primary treatment. For secondary treatment, it consists of two types: biofilm and activated sludge. The first biofilm treatment facility was the trickling filter constructed in Salford, England in 1893, mainly based on the principles of filtration proposed by Sir Edward Frankland (Stanbridge, 1976). On the other hand, the activated sludge process was developed by two British engineers:

Edward Arden and William Lockett. This ground-breaking study was published and patented in 1914 (Ardern and Lockett, 1914). The application of activated sludge process instead of trickling filters has become the trend afterwards. Activated sludge WWTPs are generally known to provide smaller footprint and higher effluent quality (Jenkins and Wanner, 2014), e.g. higher removal rates of organic matter, smaller land requirements and lower need to handle fly or odour nuisance. Following the strong expansion of cities, increasing pollutant loads and severe effects on the environments led to more rigorous standards for wastewater treatment. As a result, many more treatment techniques and WWTPs have been implemented over the recent decades, as shown in Figure 2.

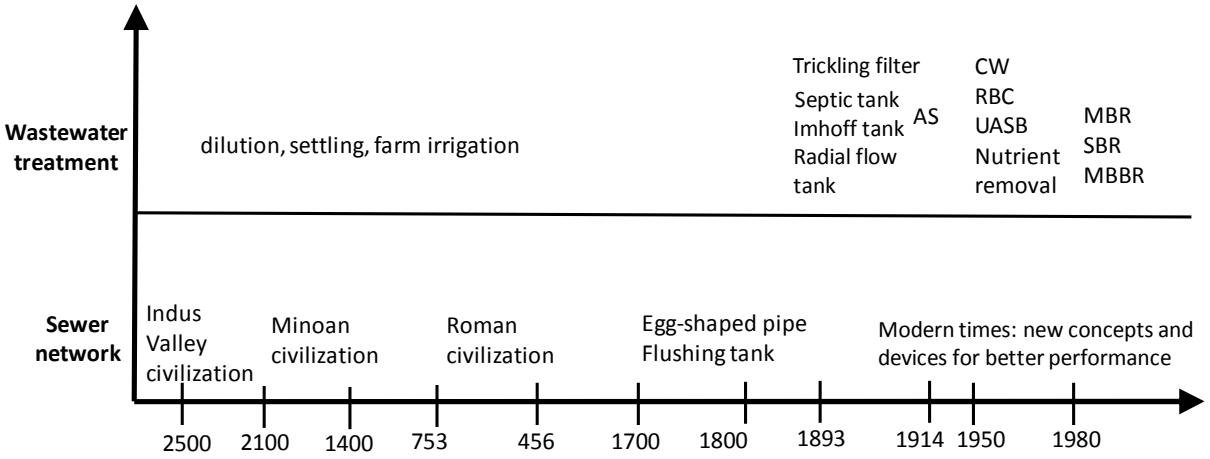

Figure 2. Summary of key milestones in the historical evolution of SNs and WWTPs (adapted from Lofrano and Brown (2010)). AS: activated sludge; CW: constructed wetlands; RBC: rotating biological reactors; UASB: upward-flow anaerobic sludge blanket; MBR: membrane biological reactors; SBR: sequencing batch reactors; MBBR: moving bed biofilm reactors.

1.2 The LIFE EFFIDRAIN project, thesis objective, and outline

1.2.1 The LIFE EFFIDRAIN project

Following the evolution of UDSs, modern sewers are significantly enhanced by innovative ideas and concepts. There have been abundant theoretical and practical projects aiming to raise the operational efficiency of UDSs, and thereby alleviate detrimental environmental impacts

from wastewater. Amongst these projects, many involve the participation of multiple entities, public and private, sharing the primary goal of better protection of human health and the environment. The LIFE EFFIDRAIN (Efficient Integrated Real-time Control in Urban Drainage and Wastewater Treatment Plants for Environmental Protection, http://www.life-effidrain.eu/) European project is one typical example, which was co-financed by the LIFE programme of the European Commission and Suez Group from 2015 to 2019, and involves five institutional partners[1]. The main goal of LIFE EFFIDRAIN was to demonstrate an integrated real time control (RTC) strategy of SNs and WWTPs to minimize the pollution of receiving waters, through the use of real-time quantity and quality data. This PhD work results from the collaboration between Laboratoire DEEP (Déchets Eaux Environnement Pollutions), INSA Lyon and LyRE (Lyonnaise REcherche), Suez Water France to contribute to the project work.

In the LIFE EFFIDRAIN project, there are two pilot sites for demonstration: Louis Fargue in Bordeaux, France and Badalona in Barcelona, Spain. Their general characteristics are displayed in Table 1.

[1] LIFE EFFIDRAIN partners: Aquambiente, Aquatec, Cetaqua (project coordinator), CSIC, and LyRE.

Table 1. General characteristics of the two pilot sites in the LIFE EFFIDRAIN project (adapted from Rouge *et al.* (2016)).

	Louis Fargue (Atlantic pilot site)	Badalona (Mediterranean pilot site)
Climate	Oceanic climate (near the Atlantic coast), with frequent rainfall events and mean annual rainfall depth of 1000 mm	Mediterranean climate (near the Mediterranean coast), with irregular rainfall events and mean annual rainfall depth of 650 mm
Area and population	7700 ha and 300000 inhabitants	2200 ha and 220000 inhabitants
Sewers	1340 km pipe length, 80 % combined, tank storage capacity of around one million m^3	318 km pipe length, mainly combined, tank storage capacity of around 30000 m^3
Receiving water body	Garonne River	Mediterranean Sea

Key actions of the LIFE EFFIDRAIN project are shown in Figure 3 and actions A3, B1, B2, and B6 play main roles in defining and developing the integrated RTC strategy for the Atlantic pilot site, which is the experimental site of this thesis. This research work was the main contribution to actions A3, B1, B2 and B6.

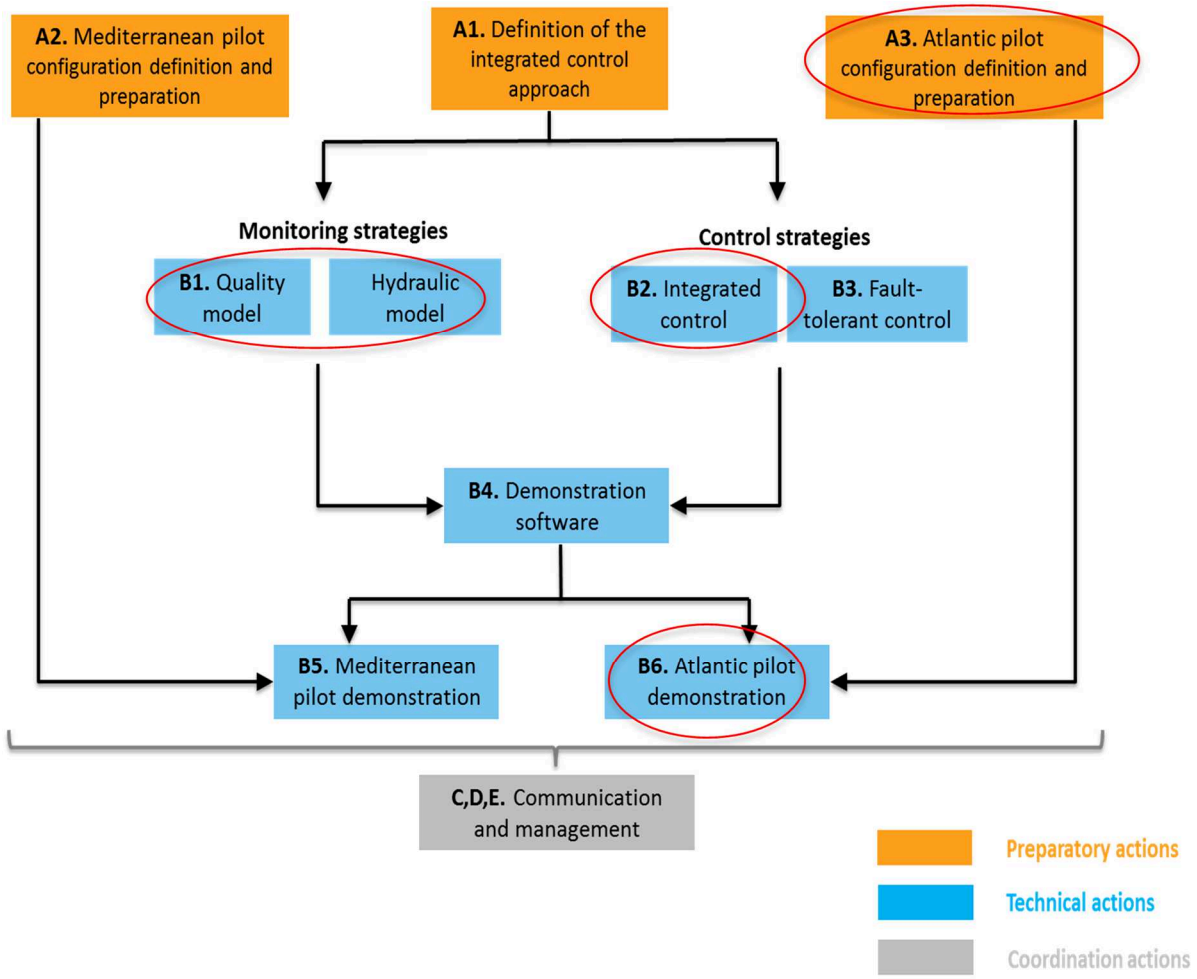

Figure 3. Main actions of the LIFE EFFIDRAIN project. Actions circled by red colour are led by LyRE and closely connected with this PhD work (adapted from Cetaqua (2015)).

1.2.2 Objective and outline of the thesis

This thesis aims at developing of a new water quality-based RTC (QBR) strategy, tested for the Louis Fargue combined SN to reduce the amount of CSO loads during storm events. The reduction of CSO loads is calculated by comparing with the existing operation of the SN, which is based on a traditional hydraulics-based RTC (HBR). Given the above objective, the main steps of the work were:

i. Review of major quality processes in SNs, associated with detrimental environmental effects caused by urban discharges onto the receiving waters.

ii. Review of underlying concepts, classifications, motivations and implementations of RTC methods.
iii. Review of monitoring strategies for the QBR strategy.
iv. Definition of a new QBR concept, including simulation setup, algorithm, and deriving a Python-based controller that provides appropriate control actions during storm events.
v. Proof-of-concept study on a small test site over a sufficiently large number of storm events (i.e. 31 events).
vi. Full-scale study on the Louis Fargue catchment with assessment of the performance over representative storm events and long term.
vii. Sensitivity study on the influence of the retention tank volume and a study on the impact of model prediction uncertainty on the controller performance.

The first three steps are based on literature studies. They are strongly connected and provide relevant knowledge to the development of the new QBR strategy. Step iv involves the conceptual development of the new QBR strategy. To perform this step, the author attempted to propose several concepts before reaching the most potential choice. For instance, there was the idea of using quick and simple regression models for process predictions of the QBR controller. Although this statistics-based concept was not pursued further, the results from the development of the regression models is worth presented in this thesis (see chapter 5). The last three steps are devoted to the development and demonstration of the new QBR strategy.

According to the objective and steps described above, the structure of this PhD thesis is formed by eight chapters. Table 2 provides the outline of the thesis, including the main contents of each chapter.

Table 2. Outline of the thesis.

Chapter 1	▪ Basic knowledge to better understand the field of urban drainage. ▪ The project, objectives, and structure of the thesis.
Chapter 2	▪ Review of major quality processes in SNs, associated with detrimental environmental effects caused by urban discharges onto the receiving water bodies. ▪ Review of underlying concepts, classifications, motivations and implementations of RTC methods for SNs.
Chapter 3	▪ Review of monitoring strategies for QBR.
Chapter 4	▪ Description of the case study area, data-base and selected detailed hydrodynamic model.
Chapter 5	▪ Development of two statistical approaches for estimating total CSO loads of storm events: multiple linear regression versus random forest regression.
Chapter 6	▪ Demonstration of the proof-of-concept study for the new QBR strategy
Chapter 7	▪ Explanation of the reference strategy and application of the new strategy to the Louis Fargue case study. ▪ Evaluation of the new strategy versus the reference strategy. ▪ Sensitivity analysis on the influence of the retention tank volume and assessment of the impact of prediction uncertainty by the controller.
Chapter 8	▪ Conclusions and perspectives of the thesis.

CHAPTER 2: MAJOR WATER QUALITY PROCESSES AND REAL TIME CONTROL OF SEWER SYSTEMS

This chapter first describes important wastewater quality processes in sewer systems, associated with adverse wastewater quality impacts on the environment due to urban discharges. Understanding these wastewater quality processes is imperative for the development and usage of water quality modelling tools used for the QBR of sewer systems. The first section of this chapter is based on the report of Deliverable D5 (Ly *et al.*, 2017) to complete action B1 of the LIFE EFFIDRAIN project. The next section is devoted to an overview of underlying concepts and classifications of RTC methods. The principles related to model predictive control, a core part applied in this work to develop the new QBR strategy, are also introduced. Furthermore, there is a review of RTC applications in literature as well as the motivations for QBR.

2.1 Major wastewater quality processes

2.1.1 Catchment surface and sewer network

As provided by Schütze *et al.* (2002), basic processes associated with wastewater quality and pollutant transport in SNs consist of:

- Surface build-up and wash-off
- Conduit transport, i.e. solute and sediment transport
- Biochemical conversion of pollutants
- Processes in storage tanks

Since the early 1970s, these processes have been accounted for in most of the state-of-the-art modelling approaches for wastewater quality and pollutant transport in SNs (Rauch *et al.*, 2002).

2.1.1.1 Surface build-up and wash-off

Surface build-up refers to the accumulation of sediments and attached pollutants on impervious surfaces of the catchment under dry weather conditions and receding storm run-off. Butler *et al.* (2018) presented the list of factors influencing the surface build-up: land use, population, traffic flow, effectiveness of street cleaning, season period, meteorological conditions, antecedent dry period, and street surface type and condition. The mass of accumulated sediments is frequently regarded as being linear or exponentially asymptotic with time (Bertrand-Krajewski *et al.*, 1993). Because observed data is sparse and affected by high uncertainties, the choice of a model for surface build-up mostly relies on numerical fittings, rather than physical reasons (Rauch *et al.*, 2002).

On the other hand, surface wash-off indicates the removal of accumulated of particles on impervious surfaces of the catchment under wet weather conditions. Main factors influencing this process are rainfall characteristics, topography, particles characteristics, and street surface type and condition (Butler *et al.*, 2018). Bertrand-Krajewski *et al.* (1993) highlighted that rainfall intensity, especially the square of maximum rainfall intensity, was found in some previous studies as the most important factor. Due to its complexity, the surface wash-off is usually represented by conceptual or global models, instead of physically based models. In particular, the process is assumed to be directly proportional to the accumulated mass on the impervious areas, rainfall intensity and/or the overland flow rate.

Recently, Sandoval and Bertrand-Krajewski (2018) present that existing model structure for build-up/wash-off models still lacks of a global deterministic process (if it exsits). Results from the same authors also evince that there might be no link between the missing process and the real build-up phenomenon.

2.1.1.2 Conduit transport

According to Rauch *et al.* (2002), pollutants transported in the combined sewer system originate from three major sources:

(i) Surface wash-off: pollutants enter SNs through street inlets, with or without gully pots.

(ii) Accumulated mass occurring inside the pipes during dry weather (e.g. deposits, near bed solids and biofilms): pollutants are re-suspended when there is a sufficient increase of shear stress and turbulence.

(iii) Dry weather flow: pollutants stem from domestic and industrial activities.

Typically, solute transport in SNs can be represented by advection and dispersion processes. Advection is the process whereby dissolved and finely suspended substances are carried along with the unidirectional flow of wastewater. The substances velocity is equated with the mean flow velocity in this case. Dispersion describes the spread out of pollutants due to the spatial differences of the velocity profile (Langeveld, 2004). In other words, dispersion implies how the actual pollutant transport deviates from the mean flow velocity. Generally, pollutants follow the advection and dispersion transport will maintain their existing form unless they are affected by biochemical conversion processes. In terms of modelling, advection and dispersion transport is commonly reproduced in detailed models by solving advection-dispersion partial differential equations. A simplified approach can be considering each conduit as a reservoir or a continuously stirred tank reactor (Schütze *et al.*, 2002).

Sediment transport or the movement of particles of different sizes in SNs is far more comprehensive. This multi-stage process involves settling, resuspension and subsequent transport of sediments and attached pollutants. Settling and resuspension are similar to the

surface build-up and wash-off respectively, but happening within sewer structures. According to Langeveld (2004), sewer sediment in SNs can be fractioned as follows:

- SS
- gross solids
- near-bed solids
- granular bed load and bed deposits
- biofilm.

The movement of each fraction however corresponds to one or more types of transport depending on its size, specific gravity, cohesion properties and external factors like the characteristics of the flow and the conduit. For instance, at sufficient values of the flow, certain SS are led by advection and dispersion as suspended load, but at a decreasing flow, they may be transported as bed load and/or form bed deposits through settling. For water quality prediction, existing detailed sewer quality models usually account for the transport of SS. Some models apply various equations to include both suspended load and bed load transport and rely upon adapting settling and resuspension criteria from sediment transport theories in fluvial environments to take into account settling, resuspension, and cohesion of sediment (Langeveld *et al.*, 2005). There is especially the approach of particle settling velocity distribution (PSVD) that has been proven to be able reproduce the distribution of the settling velocities of different particle classes (see Vallet *et al.* (2014) and Bachis *et al.* (2015)).

2.1.1.3 Biochemical conversion of pollutants

A gravity sewer pipe can be divided into four interacting compartments: sewer atmosphere, bulk water, sediment and biofilm (see Figure 4). It is slightly different in the case of a pressure sewer pipe because the atmospheric part does not exist and the biofilm is distributed around the

pipe circumference (Butler *et al.*, 2018). During the transport of wastewater inside SNs, there are different biochemical processes occurring within and between the four compartments and transforming the wastewater composition considerably (Nielsen *et al.*, 1992). This PhD work deals only with important processes that may have significant effects on the performance of SNs and other interacted sub-systems.

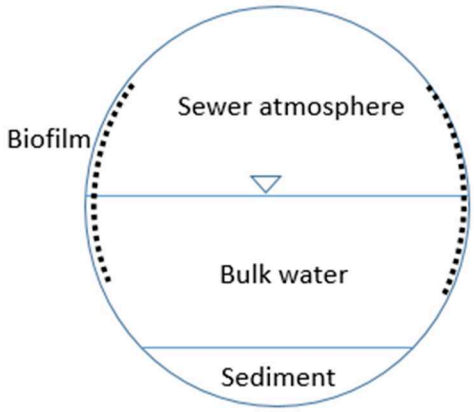

Figure 4. Interacting compartments inside a sewer pipe (after Butler *et al.*, 2018).

Hydrolysis

This process refers to the breakdown of complex organic compounds into more simple ones after natural reactions with water in the presence of enzymes. Hydrolysis precedes and greatly influences aerobic and anaerobic conversion processes. In addition, it is temperature dependent and its products can be utilized by bacteria later on. One typical illustration of hydrolysis is when suspended organic matters are hydrolysed and turn into solution. This also implies the transformation of chemical oxygen demand (COD) from a more slowly biodegradable form into a readily biodegradable one, before it can be consumed by the heterotrophic biomass (Vollertsen and Hvitved-Jacobsen, 2002).

Besides, phosphorus in wastewater mostly exists in the inorganic form, comprising of polyphosphates and orthophosphates. However, because of hydrolysis, polyphosphates are

gradually transformed into orthophosphates, which are more simple compounds and either in soluble phase or attached to particles.

Ammonification

Ammonification refers to the process that most of organic nitrogen in wastewater is hydrolysed and becomes ammonia-nitrogen. It was observed that urea, which amounts up to 80% of the nitrogen content of fresh wastewater, is hydrolysed with the assistance of the enzyme urease at a rate of of 3 mg.N/L per hour at 12°C in stored samples (Painter, 1958).

Processes under anaerobic conditions

Main microbial processes under anaerobic conditions involve the partial breakdown of large organic molecules and the generation of simple organic gases as end products. The reactions are performed by the anaerobic heterotrophic bacteria, which have to utilize oxygen from dissolved inorganic salts to compensate for the absence of oxygen in wastewater (Butler *et al.*, 2018).

One important microbial process is sulphate reduction. This process takes places in the absence of nitrate and oxygen, when sulphurous compounds in the form of either organic compounds or sulphates are reduced to sulphides, mercaptans and other products. The most concerned product is hydrogen sulphide (H_2S) which is formed mostly within the biofilm or sediment compartments (Ashley *et al.*, 2004). H_2S is regarded as a flammable and poisonous gas even at low concentration, and may cause severe odour problems. Furthermore, it can be biochemically oxidized under aerobic conditions to create sulphuric acid, which leads to the corrosions of concrete pipes and other facilities such as pumping stations, manholes, etc. (Delgado *et al.*, 1999).

In general, the transformations of wastewater composition under anaerobic conditions happen more slowly than under aerobic conditions (Fronteau *et al.*, 1997). For instance, the rate of

hydrolosis of biodegradation substrate at aerobic conditions was proven to be 15% slower (Tanaka and Hvitved-Jacobsen, 1998).

Processes in storage tanks

Storage tanks are used to store excess rainfall runoff which may threaten the hydraulic capacity of the WWTPs. With regards to quality aspects, the storage tanks also contribute to the partial treatment of SS and consequently particulate COD (Maruéjouls *et al.*, 2010). According to Johansen (1985) and Durchschlag (1991), the maximum removal rate of SS was between 60% and 80%; whereas for particulate COD, Michelbach and Wöhrle (1994) provided that it was possible to reach the removal rate of around 70%.

2.1.2 Adverse effects on receiving waters

As previously mentioned, CSO discharges from sewer systems are considered a major risk of pollution for the environment. Besides, under transient conditions caused by rainfall events, discharges from the effluents of WWTPs may also contain higher concentrations of SS or ammonia due to the loss of biomass.

2.1.2.1 Water quality processes due to urban discharges

House *et al.* (1993) divided water quality processes occurring in the receiving waters due to urban discharges into three types:

- Physical processes: transport, mixing, dilution, flocculation, erosion, sedimentation, thermal effects and re-aeration.
- Biochemical processes: aerobic and anaerobic oxidation, nitrification, adsorption and desorption of metals and organic micropollutants.
- Microbial processes: growth and die-off of bacteria

The temporal and spatial scales of these processes decide the extent of their impact on receiving waters, as exemplified in Figure 5.

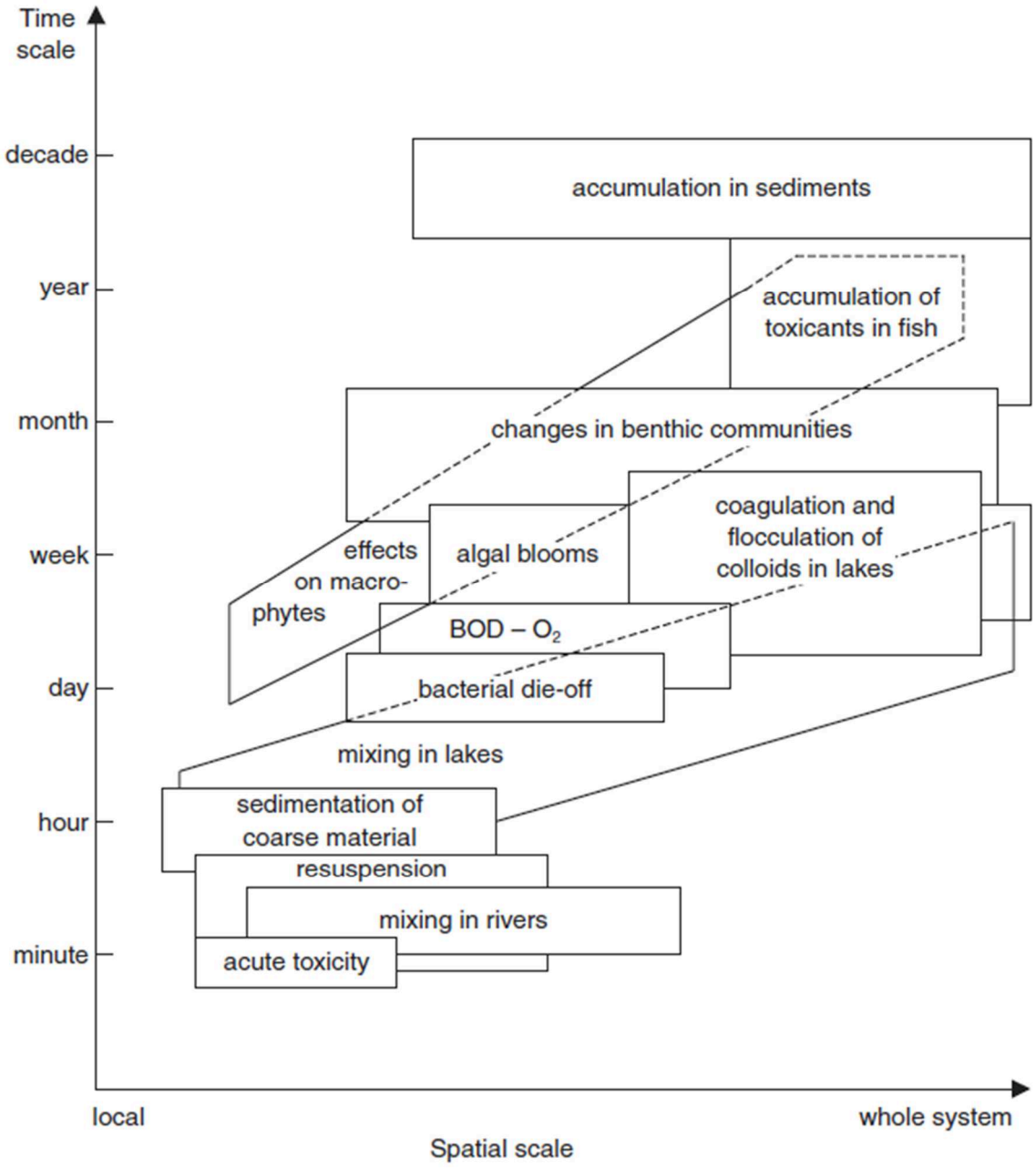

Figure 5. Temporal and spatial scales of processes within receiving water bodies due to urban discharges (after Aalderink and Lijklema, 1985).

2.1.2.2 Categorization of quality effects

With regards to the impact of the discharges from SNs and WWTPs on the receiving water bodies, it has been an inspiring topic for numerous studies over a few decades (Hvitved-

Jacobsen, 1982; House *et al.*, 1993; Rauch and Harremoës, 1997; Vanrolleghem *et al.*, 1999; Mannina and Viviani, 2010). The impact can be categorized as chemical, bio-chemical, physical, hygienic, aesthetic, hydraulic and hydrologic. In addition, the impact can be further distinguished according to its timescale, i.e. acute (hours), delayed (days) or accumulative (weeks to seasons or years) (Schilling *et al.*, 1997), as seen in Table 3.

Table 3. Effects of SNs WWTPs discharges on receiving water bodies (after Schilling *et al.*, 1997)).

Timescales	Characteristics	Indicators
Acute (hours)	hydraulic	flow, shear stress, bed erosion
	chemical	toxic substances (NH3)
	physical	suspended solids
	bio-chemical	oxygen depletion in the water body
	hygienic	bacteria, virus
	aesthetic	floating material, odor
Delayed (days)	hydraulic	sediment carrying capacity
	chemical	toxic substances (NH3, NO2)
	bio-chemical	oxygen depletion in the sediments
	hygienic	bacteria, virus
	aesthetic	floatables, debris, oil
Accumulative (weeks to years)	hydrological	flow regime, morphology
	chemical	heavy metals, persistent organics, inorganic and organic sediments
	bio-chemical	oxygen depletion (i.e. eutrophication caused by accumulated nitrogen and phosphorous)

2.1.2.3 Typical acute effects

In reality, it is not necessary and not possible to monitor every water quality process or adverse effect on the receiving waters. To reduce the complexity and cost, the focus should be on

identifying the main problems of the studied receiving waters, e.g. dominant processes that cause direct and crucial influences. Starting from there the objective and methodology to tackle the problems can be developed (Rauch *et al.*, 2002).

The type of the receiving water is important for characterizing the main problems caused by urban discharges. For instance, in terms of water quality, a stagnant water body is often far more vulnerable to the urban discharges than a running water body similar in size. There are many large- and medium-sized cities in the world where urban discharges pose great environmental risks to the running water bodies, including the project site of this study. These cities usually experience strong acute effects from urban discharges, which comprise of: oxygen depletion, toxics due to unionized ammonia and hygienic problems by faecal coliforms (Rauch *et al.*, 1998; Benedetti *et al.*, 2013).

Oxygen depletion

Degradation of organic matter from urban discharges may substantially increase the DO demand of the receiving waters and is considered a dominating acute effect. The effect can be propagated downstream in the case of moving water bodies such as rivers and seas. Besides, sediments from the discharge pose a threat of delayed oxygen depletion because these sediments contain slowly degradable organic matter (Langeveld, 2004). Finally, the detrimental consequence of oxygen depletion is the loss of aquatic lives.

Toxic impact

Urban discharges containing high amounts of toxic pollutants, e.g. heavy metals, hydrocarbons, pesticides, micropollutants, etc. can engender immediate effects on the receiving waters. Of main concern is ammonia discharges since its unionized form is a strong and acute fish toxicant. As a result, ammonia concentration can be an alternative quality indicator unless the oxygen depletion is a matter (Rauch *et al.*, 1998).

For other toxic pollutants, considerable acute effects are rarely spotted, except in abnormal cases like spillages from industrial areas. They are more concerned where there are long term exposures to aquatic life, resulting in accumulation effects. Micropollutants have not received much attention in literature although there were reported cases that CSO discharge is a significant pathway for a broad range of organic micropollutants entering the receiving waters, e.g. Launay *et al.* (2016).

Hygienic issues

Another important issue refers to the hygienic inadequacy of the receiving waters under the consideration of public health. Butler *et al.* (2018) showed that relatively high concentrations of pathogenic bacteria and viruses can still be observed from urban discharges, especially via CSOs. Rauch *et al.* (1998) presented that faecal coliforms have been often selected as a representative indicator of pathogens in receiving waters, and their high concentration in the receiving waters hints a risk for human activities. One interesting fact is that pathogens mostly adhere to SS and they can survive longer in receiving waters if they follow the settling process (Butler *et al.*, 2018).

2.2 Real time control of sewer systems

2.2.1 Fundamental concepts

2.2.1.1 Real time control

Control is the effort to achieve pre-set operational goals of the system by taking advantage of its degrees of freedom. A SN is under RTC when variables related to the sewer processes (water level, flow, and water quality) are monitored continuously at certain positions in the network, and almost at the same time the obtained information is used to derive the positions of actuators (Schütze *et al.*, 2004). Actuators are devices that can be used to modify processes. A key task

in RTC of SNs is determining the control strategy, which is defined as appropriate time sequences for all actuators' set-points to meet the control objectives.

As discussed by Schütze *et al.* (2008), RTC of SNs will most likely be considered as an efficient choice when the operator aims to improve the performance of SNs through the following objectives:

- Reduction of sewer flooding
- Reduction of pollutant loads discharged into receiving
- Maximisation of WWTPs use, but not overloading WWTPs
- Minimisation of operational cost (e.g. energy and chemicals)
- Minimisation of capital expenditure (e.g. storage and conveyance)

Historic planning and design of SNs usually follow static conditions (i.e. SNs only perform optimally for the design event, as explained by Jørgensen *et al.* (1995)), but in reality, the systems are under dynamic loading conditions (Borsányi *et al.*, 2008). As a result, the application of RTC can be beneficial to improve the performances of SNs. Compared to static control, RTC incorporates the dimension of time into its solution process. With this additional degree of freedom, RTC can respond more flexibly to disturbances and external effects (Campisano *et al.,* 2013). Numerous studies demonstrate that considerable cost benefits compared to static capacity expansions can be obtained by RTC (Weyand, 2002; Erbe and Schütze, 2005). For instance, Beeneken *et al.* (2013) estimated that the global RTC of the sewer system implemented in the city of Dresden, Germany (around 530000 inhabitants) for over 10 years reduced the COD load spilled to the receiving water body by 39%, and saved 60 million euros when compared with conventional solutions such as building additional retention ponds.

2.2.1.2 Basic components

As explained by Campisano *et al.* (2013), core hardware components of RTC contain controllers, actuators, sensors and data transmission systems. The conceptual organisation of any RTC system can be schematised by means of a control loop (see Figure 6). Sensor is used to measure the controlled process variables which reflect the present state of SNs. Data transmission system transfers measured data between various devices. Actuator refers to controllable device of SNs, e.g. valves, movable weirs, pumps. Controller provides actuator positions by means of control action to minimise deviations of the process variable from its desired value (set-point).

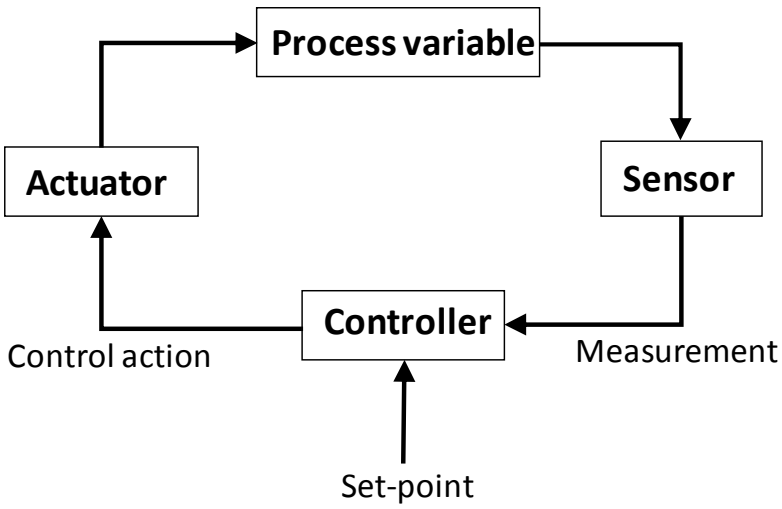

Figure 6. Scheme of data flows in a control loop of RTC, adapted from Schütze *et al.* (2002) (direction of data transfer follows the arrows).

There are two types of control loops: feedback and feedforward. In feedback loop, the control action is proposed only if measurement shows deviations of the process variables. In feedforward loop, the controller is based on a model to forecast the immediate future values of the deviations and to propose the control action (Butler *et al.*, 2018). Measurement in this case is intended to correct the model to improve the forecast ability.

Sensors used for RTC include rain gauges (or meteorological radars), water level gauges, flow gauges and water quality gauges. These sensors should be applicable for continuous data logging and remote data transfer. Their reliability and robustness need to be appropriate to endure the harsh sewer environment. In addition, RTC systems depend on the configurations of the existing actuators. Typical actuators used for RTC of are described by Campisano *et al.* (2000) and Schütze *et al.* (2004) as follows:

- Gates: used for flow restriction. They are usually actuated by motors and paramount for managing in-line storage or rerouting flow into different branches of the system.
- Pumps: function to transport water to a point of higher elevation in SNs. In emergency cases (e.g. strong storm events), they are needed to release accumulated water out of depressed areas. Pumps are also frequently used to empty storage facilities. Pumping flow rate can be constant or variable, depending on the pump type.
- Valves: also used for flow restriction. They are usually located in small circular pipes to control the flow entering larger interceptors.
- Weirs: can be moveable or static. They are typically used to provide storage volume, e.g. they can be placed in main interceptors to activate in-line storage upstream. Besides, they can also act as overflow devices which lessen overflow volumes over a CSO.
- Other actuators: flow splitters for flow separation under specific conditions; chemical dosing devices for control of the conditions of water in storage facilities; and aeration devices for enhancement of pollutant removals.

2.2.2 Types of control methods

Control methods for SNs can be classified by different criteria. Table 4 shows the classification in detail, based on the definitions by Meirlaen (2002) and Lund *et al.* (2018). Amongst many criteria of categorizing control methods, the criterion based on the control objective is important

for this research because our main goal is to propose a QBR strategy and evaluating its performance in comparison with a HBR strategy.

Table 4. Different criteria to classify control methods of SNs (inspired by Meirlaen (2002) and Lund *et al.* (2018)).

Criteria	Types	Explanations
Degree of automation	Manual	Actuators are adjusted manually by an operator.
	Supervisory	Actuators are regulated automatically but their set-points are defined or approved by an operator or a supervisory system.
	Automatic	The whole system is operated automatically.
Degree of control	Passive	Actuators are fixed at static positions.
	Real time	Online measurements are used to adjust the actuators dynamically.
Physical extension	Local	Actuators are not actuated remotely from a control centre and measurements are obtained directly at the actuator site.
	Global	A controller collects observed data throughout the network and actuators are adjusted in a coordinated manner.
	Integrated	The level of control includes other components such as WWTPs and receiving waters. Under integrated control, the control methods can be further categorized by emission-based (WWTP effluent and/or CSO water quality) versus immission-based (receiving water quality) consideration of the control objectives.
Timing of input	Reactive	The control is performed only based on measurements. It is normally characterised by predefined ruled-based control actions (e.g. in the form of if-then rules).
	Predictive	The control is performed based on both measurements, rainfall forecast and prediction of the

		future process variables (e.g. using mathematical models).
Control objective	Hydraulics-based	Priority objective of the control strategy is reduction of the volume of polluted water entering receiving waters. It is also called volume-based control strategy.
	Water quality-based	Priority objective is reduction of the pollutant loads entering receiving waters. It is also called pollution-based control strategy.
Development method of the control strategy	Heuristic	Control strategy is derived solely from the experience of the operating staff.
	Offline optimisation	Historic database is used to derive an "optimal" control strategy using mathematical techniques.
	Online optimisation	Optimisation is done for each control time interval of the controlled event to propose the most appropriate control action for each interval. Real time measurements are used in this case.

2.2.3 Model predictive control

MPC is one of the most widely used advanced techniques in industrial control engineering. Since it was first presented as a theory in the 1960s, MPC has been applied by multiple industries, for instance: aerospace, automotive, energy, food processing, papers, etc. (Qin and Badgwell, 2003). It can tackle multivariable control problems while allowing consideration of constraints and accounting for actuator limitations (Rawlings and Mayne, 2009). As defined by Lund *et al.* (2018), MPC involves two fundamental principles: receding horizon control (i.e. recursive repetition of the control actions within a finite control time interval (CTI) and optimisation (i.e. determination of the optimal sequence of control actions within this CTI). According to Ocampo-Martinez (2010), three pivotal tasks to formulate an MPC solution therefore include:

(i) Usage of a process model (detailed or statistical model) to anticipate the future states of the system.

(ii) Implementation of an optimisation algorithm to solve the objective (cost) function that is based on key performance indices to be achieved.

(iii) Application of the receding horizon principle.

Table 5 displays the general advantages and disadvantages of the MPC method, adapted from Bordóns (2000) and Ocampo-Martinez (2010).

Table 5. Advantages and disadvantages of the MPC method.

Advantages	**Disadvantages**
1. Widespread applicability for a large variety of processes, from simple to complex systems.	1. High demand of computational resources to derive sequences of control actions.
2. A relatively intuitive concept with less efforts for parameter tunings compared to other methods	2. Strong dependence on the accuracy of the process models.
3. Competency for solving multivariable system.	3. Reliance on past knowledge about the system's behaviour to develop the controller, thus the quality of the knowledge is highly important.
4. Possibility to account for system constraints, actuator limitations, and delay compensation.	
5. User-friendliness, even for people lacking deep knowledge of control engineering.	

MPC for combined SNs is considered as an adaptive control method in which the optimisation is recomputed recursively as new information about the state of SNs and new rainfall forecasts become available. The global HBR system implemented on the large and complex Quebec Urban Community's Westerly SN since 1999 is considered one of the earliest practical RTC

applications. This system was based on the MPC method, solving multi-objective optimisation problem to reduce the frequency and volumes of CSOs discharged into the receiving rivers (Pleau *et al.*, 2001; Schütze *et al.*, 2004). Detailed descriptions about the different phases of this work in Quebec are further presented by Pleau *et al.* (2005) and Fradet *et al.* (2011). Besides, several past studies on RTC of SNs using MPC also demonstrated the additional use of online measurements to update the process model, i.e. online calibration (Joseph-Duran *et al.*, 2014).

2.2.4 Implementations of RTC and motivations for QBR

As reported by Borsányi *et al.* (2008), the first RTC prototype for SNs was built in the late 1960s in Minneapolis-St. Paul, United States. Potential of control of SNs was first discussed in publications in the 1970s (Beck, 1976). Accordingly, the earliest state-of-the-art evaluation was performed by Schilling (1989) showing the benefits of RTC to lower the frequency and magnitude of CSOs with minimal capital investments. From the 1990s, the start of revolution of microprocessors motivated the growth of RTC application (Borsányi *et al.*, 2008). Since then, publications related to RTC have been increasingly seen in literature. There have been a number of review papers presenting the advances of the method (Schütze *et al.*, 2004; Campisano *et al.*, 2013; García *et al.*, 2015; Mollerup *et al.*, 2017, van Daal *et al.*, 2017), along with several studies concentrating on the theoretical aspects of RTC (Capodaglio, 1994; Rauch and Harremoës, 1999; Vanrolleghem *et al.,* 2005; Muschalla *et al.*, 2014) or some showing the results of real experiments (Schilling *et al.*, 1996; Petruck *et al.*, 1998). Up to now, the majority of RTC research or real implementations across the world are HBR, which aims at minimizing CSO volume or frequency through the use of real time hydraulic measurements. Several cities in the world have been reported as successful operational sites for HBR systems such as Quebec (Pleau *et al.*, 2005), Wilhelmshaven (Seggelke *et al.*, 2013), and Bordeaux (Andréa *et al.*, 2013).

QBR was initiated more lately mainly due to the shortage of available and reliable quality data in the UDS. There also used to be the common misconception that the dynamics of pollutant loads and stormwater volumes are always correspondent. Reduction of pollutant loads emitted by CSOs is usually expressed as the main objective of the QBR method. Various research studies, e.g. Lacour and Schütze (2011), and Vezzaro *et al.* (2014), have proven the benefit of the method via lowering pollutant loads released into receiving waters. Lacour (2009) presents a new QBR concept that is based on the observed mass-volume (MV) curve to construct an optimised MV curve, and intercepting more polluted flows by assessing the deviations between the two curves. Still, there are very few existing practical implementations of QBR found in literature. One example is the QBR system developed and installed for the separate SN of Wuppertal, Germany. This system has been put into operation since 2009, aiming to separate the more polluted surface runoffs from the less polluted river flows. It utilises threshold values of total suspended solids (TSS) to generate control actions diverting polluted runoff into the main sewer interceptor (Hoppe *et al.*, 2011; Fricke *et al.*, 2016).

Campisano *et al.* (2013) reports that the QBR has received increasing attention because of gradual advancements in wastewater quality sensors. Recent studies have demonstrated the possibility of monitoring water quality of SNs continuously, e.g. using photometric (turbidity meter) and optical (spectrophotometer) sensors (Winkler *et al.*, 2008). These sensors can function well in the foul wastewater environment (e.g. high humidity level, corrosive atmosphere, exposure to oils, greases, waste, debris and sediments) over a long period, given that regular maintenance works must be done (see Hoppe *et al*., 2009; Lacour *et al*., 2009). Nowadays, online monitoring data can be obtained directly or indirectly (through local calibration, explained in Chapter 3) with adequate quality for the following process variables: temperature, pH, turbidity, SS, organic carbon, COD, conductivity, ammonia, nitrate and total

nitrogen (Gamerith, 2011). Chapter 3 provides in-depth review of the functions and characteristics of the representative sensors.

As discussed by Maruéjouls and Binet (2018), the European Union Urban Waste Water Directive (Council Directive, 1991) was one of the first official documents concerning CSOs particularly. It pronounces the obligation of the European Union Member States to avoid stormwater overflows except under exceptional circumstances, or if the cost of CSO prevention is inordinate. More stringent regulations have been enforced over past decades, such as the European Framework Directive (Council Directive, 2000), stating the objective of achieving a 'good ecological status' for all of Europe's surface waters and groundwater. Subsequently the 28 European Union Member States have put the Directive into effect via their environmental guidelines and laws. A majority of the Member States choose hydraulic criteria for the assessment of CSO impact, e.g. number of spillages per CSO structure per year onto the receiving water bodies (e.g. Belgium, France, Netherlands, Poland, UK) and total CSO volume per year. Over time, some Member States have additionally included water quality criteria into the assessment. The French Decree dated 21 July 2015 rules that the compliance of UDSs is based on meeting one of the three criteria: (i) total CSO volumes are less than 5% of the total volumes of urban water discharges, (ii) total CSO loads are less than 5 % of the total pollutant loads of urban water discharges, and (iii) there are less than 20 days of CSOs per year and per CSO structure. In Austria, maximum 40-60 % of the incoming flow and 25-45 % the SS can be discharged annually as CSOs (Moreira *et al.*, 2016).

To sum up, the motivation for QBR application has continued to grow over time. The increasing interest in the water-quality based RTC mainly comes from the development of sensing technologies and the inclusion of reducing pollutant loads from urban discharges in environmental regulations.

2.3 Summary

Key knowledge on main processes related to water quality and pollutant transport in SNs together with dominant effects from these processes on the receiving waters are presented in this chapter. Surface build-up and wash-off, conduit transport, biochemical conversion of pollutants and processes in storage tanks are key consideration for SNs. Besides, dominant effects from these processes on the receiving waters, i.e. the acute, delayed, and accumulative impact, are discussed with focus on the acute ones during wet weather like oxygen depletion, which are of primary concern in the assessment of CSO impact on the running receiving water bodies (including the case study of this research).

Furthermore, this chapter highlights important concepts related to RTC, such as its definition, control loop and its elements. The classifications of RTC methods according to different criteria are also described. There are many criteria to distinguish the type of control, such as degree of automation, degree of control, physical extension, timing of input, control objective, and development method of the control strategy. In terms of control objective, RTC can be categorized in two types: HBR (i.e. aiming to reduce of the volume of polluted water entering receiving waters) and QBR (i.e. aiming to reduce the pollutant loads entering receiving waters). In addition, this chapter further explains the method of model predictive control, which can be characterised by receding horizon and optimisation principles. Lastly, the development of RTC over time is mentioned with the introduction of multiple past studies in the literature. Since the first installed prototype in the United States in the late 1960s, there have been considerable development of the RTC methods. Although literature on QBR is more limited than HBR, the motivation for QBR application has continued to grow over past decades. The increasing interest in the QBR mainly comes from the development of sensing technologies and the inclusion of reducing pollutant loads from urban discharges in environmental regulations.

CHAPTER 3: MONITORING STRATEGIES FOR WATER QUALITY-BASED REAL TIME CONTROL OF SEWER SYSTEMS

A good monitoring strategy is key towards the success of any QBR strategy of sewer systems. For most QBR applications, both real time measurements and historic database are needed for implementation of control strategies and development of modelling tools. Measurement data should be relevant, reliable, and with appropriate frequency. Accordingly, Chapter 3 is meant to provide knowledge on important factors to be considered in monitoring strategies: state variables, monitoring methods, and sensor placement methods. This chapter is based on the report Deliverable D5 (Ly *et al.*, 2017) of the LIFE EFFIDRAIN project.

3.1 State variable

Pollutants in combined SNs come from both wastewater and stormwater. If the flow is high enough, runoff can mobilise accumulated pollutants on the catchment surface and deposits in the sewers. According to Gamerith (2011), main water quality indicators of pollutants that are most often monitored and analysed for storm events consist of: sum parameters of organic materials (BOD, COD, total organic carbon (TOC)), TSS, TKN, phosphorus and heavy metals as Cd, Cr, Ni, Pb, Cu, Zn. Comprehensive overview of the pollutants and their concentrations are described in Brombach *et al.* (2005) and Butler *et al.* (2018).

State variable (SV) reflects the status of the system's processes during various time steps. In the context of the QBR, SV is considered as the representative indicator of water quality. Its dynamics can be measured by online sensors and reproduced by detailed models. Each component of the urban wastewater system has its own function and key water quality processes. In terms of modelling, the SVs of SNs are not identical to the ones of WWTPs or

receiving water bodies (as shown in Table 6). However, SNs are connected to the other components in several ways. For instance, SNs transfer wastewater to WWTPs for pollutant removals or generate CSO discharges to receiving waters during storm events. Due to such cause-effect interactions, for RTC of SNs, the selected SVs should be equivalent or at least convertible into the typical SVs of WWTPs and receiving water bodies. This facilitates the assessment of the RTC impact on the environment.

Table 6. Comparison of state variables used in models of the sewer network, WWTP (ASM1), and receiving water (adapted from Rauch *et al.* (1998)).

Sewer network	**WWTP**	**Receiving water**
Flow rate, depth	Flow rate, depth	Flow rate, depth
TSS	TSS	TSS
BOD or COD: - particulate - soluble	COD-fractions: - inert soluble - soluble readily biodegradable - inert particulate - slowly biodegradable - heterotrophic biomass - autotrophic biomass	BOD-fractions: - slowly biodegradable - readily biodegradable - sediment oxygen demand
TKN (i.e. organic nitrogen and ammonium)	Nitrogen: - ammonium - nitrate - soluble biodegradable - inert soluble - slowly biodegradable	Nitrogen: - nitrite - nitrate - TKN
	Dissolved Oxygen	Dissolved Oxygen
Total phosphorus	N.A.*	Phosphate: - organic - inorganic
Faecal coliform	N.A.	Faecal coliform
N.A.	N.A.	Chlorophyll a
N.A.	N.A.	pH

*N.A.: not available

It is clear from Table 6 that each model may have its own way to describe the same water quality feature, and the corresponding level of details to model is also different. As an example, sewer models utilize TKN as a measure of nitrogen in water whereas WWTP models account

for different fractions of nitrogen. Another example is that usually sewer models involve particulate and soluble COD while WWTP models are based on more complex COD-fractions. In addition, there are few SVs important for one model but negligible for the other, e.g. heterotrophic biomass or faecal coliform (Rauch *et al.*, 1998). Following Table 6, TSS, COD and TKN (or nitrogen) are important SVs of the detailed models of water quality for all component of the UDS.

3.2 Quality monitoring methods

In the context of this research, field monitoring is fundamental for generating model-based tools for RTC of SNs since monitoring data are required in calibration and verification of the tools and development of the control rules. There are different field monitoring techniques for water quality and this chapter provides an introduction about sampling and online monitoring, two most widely used techniques in the field.

3.2.1 Sampling

Sampling is defined by Hvitved-Jacobsen *et al.* (2010) as the collection of a representative part of a system, which is called sample and after taken from the site, it undergoes a handling procedure prior to detailed analysis in the laboratory. Handling here implies the storage and preservation of the sample before transporting it to the laboratory, given that adverse changes in quantity or quality of the sample must be minimized. Laboratory analysis pertains to another procedure carried out on the collected sample in the laboratory and typically following standardized methods. Its end goal is to give measured values of required quality parameters.

Although there is an increasing trend in applying modern online monitoring sensors, sampling still remains the backbone in field measurements. As mentioned before, sufficient sampling data is mandatory for local calibrations of online monitoring sensors (Caradot *et al.*, 2015; Lepot *et al.*, 2016). Local calibration increases modelers' confidence in using long-term

monitoring data for tool developments. More details about local calibration will be revealed later on in the discussion about online monitoring sensors. In addition, it was demonstrated by Fletcher and Deletic (2007) that sampling is a reliable way to characterize rainfall event loads, especially in extreme cases due to fast hydrologic response of the catchment, strong peak or fluctuation of quality parameters. The possible inclusion of a wide range of quality parameters further make this technique useful in obtaining complete knowledge about the system.

3.2.1.1 Typical sample collection methods

Manual sampling

Sampling involves submerging a container into the water to get the sample. The submersion can be done by hands or the container can be connected with ropes or rods and then lowered down into the water. The sample will then be transferred to the laboratory for analysis.

Automatic sampling

Sampling involves utilizing electronic or mechanical devices to get the sample. This method only requires the presence of operators to install and configure the device before the actual measurement, and then to collect the samples and uninstall the device (Strecker *et al.*, 2002). The advantages and disadvantages of automatic and manual sampling methods are summarized in Table 7.

Table 7. Advantages and disadvantages of the two sample collection methods.

Method	Advantages	Disadvantages
Manual	- Great flexibility during actual measurement process, especially if adjustments are needed due to unusual situations at the site. - Very low equipment cost.	- Man-hour labour cost, not appropriate for large or regular measuring programs. - Risk of inconsistencies in sample collection due to human errors. - Safety concerns. - High uncertainties of forecast (e.g. starting time of rainfall event so that the operator can be present at the site).
Automatic	- Low man-hour labour cost when sampling is planned on a frequent basis. - Less safety concerns. - Ability to automatically trigger the start of sampling based on a pre-specified signal threshold.	- Equipment cost and logistic constraints (mobilization and demobilization of the sampler, battery or power supply, etc.). - Risk of sampler damage at the site. - Maintenance cost (battery, cleaning, etc.). - No human presence during actual measurement process.

3.2.1.2 Types of sample

Grab samples

Discrete samples of fixed volume are collected in series during a defined period of time at a specific place and then analysed in the laboratory separately. The number and timing of samples is dependent on the goal of sampling. The sample volume is decided according to the number and type quality parameters to be analysed. Also it is desirable that the sample is representative

for the water conditions at the time of collection to enable true reflection of the measurement. Therefore, ideally sampling intake should be at well-mixed and laminar flow positions (Foladori (2015). Typical application of collecting grab samples is to characterize the dynamics of concentration and loads of pollutants during rainfall events or dry weather days, especially to detect the peaks (McCarthy *et al.*, 2018).

Composite samples

Discrete samples of fixed volume are collected in series during a defined period of time at a specific place and then mixed together to represent the average characteristics of water quality during the period. Commonly for composite samples, sampling is carried out according to time-proportional or flow-proportional basis, before all samples are merged into one final sample for laboratory analysis (Foladori (2015). Time-proportional samples are taken at constant time intervals and with constant sample volumes, which clearly do not take into consideration the change in flow volume between times of collection. Consequently, unless the flow variation is insignificant, these samples cannot give good estimation of mean concentration or pollutant load of the measured period. In contrast, flow-proportional samples are often taken using one of the followings ways:

- Constant volume and varying time: the volume of each sample is equal and they are collected at equal increments of flow volume, regardless of time. When sampling is automatic, this way is preferred as it reduces the risk of sample contamination due to splitting the sample volume.

- Constant time and varying volume: samples are collected at equal time intervals and the volume of each sample is proportional to: (i) flow rate at the time of collection or (ii) flow volume since the previous time of collection. The choice of flow rate proportion is practical in the case of manual sampling; however, it is the least accurate because it uses only an instantaneous flow value to account for the change in flow volume.

3.2.2 Online monitoring

Online monitoring denotes the measurement of certain indicators of the system performance through the use of sensors and other devices to transmit recorded data to a computer (Hvitved-Jacobsen *et al.*, 2010).

Upgraded wastewater management frameworks increase progressively the interest in measuring water quality in sewer network and WWTP for several purposes, e.g. examination of the water quality at different locations in the system, protection of WWTPs, control of the CSO pollutant loads, etc. Conventionally, measurements are done by sampling, either manually or with automatic sampler. With significant development of sensing technologies, it becomes possible nowadays to utilize online monitoring sensors as an alternative or a supplement for better measurements. Such sensors were already used successfully in WWTPs few decades ago but when employed in SNs, there appeared to have functioning and maintenance failure risks due to the hostile sewer environment (Gruber *et al.*, 2006). When the effects of urban discharge on receiving waters gain more attention, various types of sensors have been tested and some are found usable for both sewers and WWTP continuous measurement applications. The measurement frequency of these sensors can be selected flexibly according to the measuring purpose. In terms of QBR, this is highly meaningful for the efforts to unveil and simulate distinctly dynamic processes of rainfall events and CSOs or to quantify pollution loads at both event and long-term scales (Caradot *et al.*, 2015). The following sections deal with main online monitoring sensors that can be used for water quality monitoring in SNs nowadays.

3.2.2.1 Turbidity meter

Turbidity meter (or turbidimeter) is a sensor device to measure turbidity of water, which refers to the decrease in water transparency caused by suspended particles. According to Joannis *et*

al. (2008), turbidity is measured by comparison between the intensity I_0 of an incident light beam, and the intensity I_1 of the same beam after its travel through a medium of sampled water.

$$T = \frac{1}{L} log \frac{I_0}{I_1} \quad \text{(Eq. 1)}$$

where T is turbidity, L is the length of the optical path through the medium.

Figure 7 represents the typical elements of a turbidity meter: a light source, a filter, a lens, a sample cell and a detector. The four positions of the detector stand for basic classification of turbidity meter according to the measuring principle: attenuation or scattering light. Attenuation is the case when the intensity of transmitted light through the medium is measured (at 180^0 from the incident light beam) whereas scattering light, or nephelometry, contains the remaining three cases (back-scatter detector, 90^0 side scatter detector, and forward-scatter detector) when the intensity of the scattered light is measured at different detection angles.

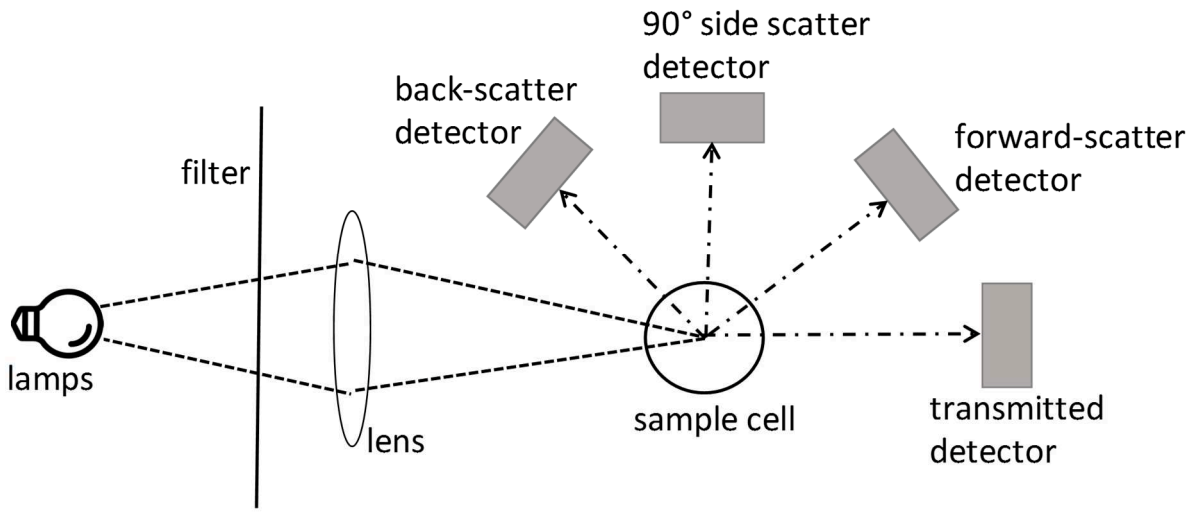

Figure 7. Basic components of a turbidity meter with four possible positions of the detector (adapted from Lawler (2005)).

Nowadays turbidity meters with 90^0 side scatter detector or transmitted detector are most widely used in the field. The unit of turbidity values recorded by a turbidity meter depend on the angle of detectors. Turbidity values retrieved by nephelometry-type turbidity meters are expressed

commonly in Formazin Nephelometric Units (FNU) or Nephelometric Turbidity Units (NTU). Both measure scattered light at 90^0 from the incident light beam; however, NTU is used for white light source turbidity meters while FNU is used for infrared light source turbidity meters. Turbidity values retrieved by attenuation-type turbidity meters are expressed in Formazin Attenuation Units (FAU). Joannis *et al.* (2008) indicate that two turbidity meters with two different turbidity units give substantially different numeric turbidity values of a water sample in spite of being calibrated with the same reference standard (e.g. 1 FAU or 1 FNU is observed with formazin standards of 0.72 mg/L). The same authors further provide an example that turbidity values recorded on wastewater during dry weather periods are usually between 100 and 200 in FNU, but between 250 and 500 in FAU.

Turbidity meters are increasingly utilized in water quality monitoring in sewers systems because of its ability to estimate equivalent concentrations of TSS and COD. Bertrand-Krajewski *et al.* (2007) propose the two calibration steps that can be applied for continuous measurement using turbidity meters:

Sensor calibration

The turbidity meter after delivered by the manufacturer should be calibrated with high precision certified standard formazin solutions. A calibration function is established to derive the relationship between observed values and true values. The function can be a linear, second or third order polynomial equation, depending on the targeted accuracy and significance of nonlinearity of the sensor itself. Sensor calibration should also be done periodically to avoid inaccuracies, e.g. data drifting.

Local calibration

The dynamics of quality parameters such as turbidity, COD and TSS is known to be site-specific, therefore it is essential for the turbidity meter to be calibrated and tuned to local

conditions. Sampling campaigns are thus performed to obtain laboratory measurements of TSS (or COD) data, and the data are then used to derive the correlation with corresponding turbidity data produced by the turbidity meter. Local calibration is however costly because of grab sampling efforts and laboratory analysis costs. As a result, the extent of calibrated data should be well planned in advance. Based on a study on four sites in different countries, Caradot *et al.* (2015) suggest that at least 15 to 20 samples are needed for the local calibration.

3.2.2.2 Ultraviolet-Visible (UV-Vis) spectrophotometers

A UV-Vis spectrophotometer is a submersible optical sensor that measures light absorption at various wavelengths within the UV and visible range and then derive equivalent concentrations of various quality parameters. Figure 8 depicts the basic components inside a typical UV-Vis spectrophotometer: the emitting unit, the measuring section, and the receiving unit (s::scan Messtechnik GmbH, 2011).

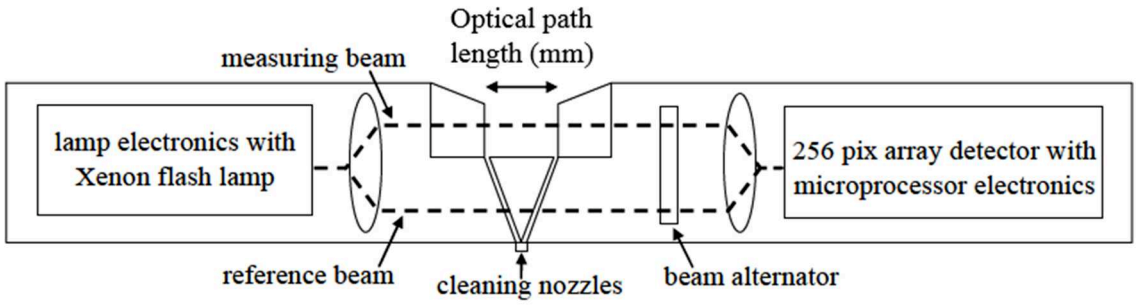

Figure 8. Basic design of a UV-Vis spectrophotometer (Langergraber *et al.*, 2003).

Emitting unit

The main element is a dual-beam xenon flash lamp as a light source emitting within UV and visible range at wavelengths between 200 nm and 750 nm. There is additionally an electronic control system to operate the lamp and an enlarging optical system to guide the beams.

Measuring section

There is an opening optical path where the measured water passes by. Spectrophotometers with various path lengths are available and the choice is based on the expected range of concentrations of the water matrix at the site (Lepot *et al.*, 2016). It is reported by Langergraber *et al.* (2003) that for wastewater measurement, the optical path length is around 5 mm. The measuring beam travels through the optical path filled by water medium whereas the reference beam is only transmitted within the instrument, acting as an internal reference to permit automatic compensation of disturbances in the measurement, e.g. fluctuations in energy of the light source, ageing of the detector. Light signals entering the medium experience gradual attenuation because of scattering and adsorption by constituents in the measured water. Furthermore, there is an automatic cleaning system added into the spectrophotometer whereby pressurized air is blown through the built-in nozzles to maintain the required cleanliness for the measuring section (Lepot *et al.*, 2016).

Receiving unit

There is a collecting optical system to focus the two incident beams on the entrance port of the detector. The light is afterwards separated according to its wavelength with typical resolution of 2.5 nm, and directed to 256 fixed photodiodes before estimating the equivalent concentration according to the observed attenuation at various wavelength ranges (s::scan Messtechnik GmbH, 2011). It commonly takes approximately 15 seconds to evaluate the whole spectrum (Rieger *et al.*, 2004). Figure 9 indicates the absorption of different substances within the spectrum of the spectrophotometer. For the field of urban drainage, the spectrophotometer is most widely used for continuous measurement of TSS, total COD, soluble COD, nitrite (NO_2) and nitrate (NO_3).

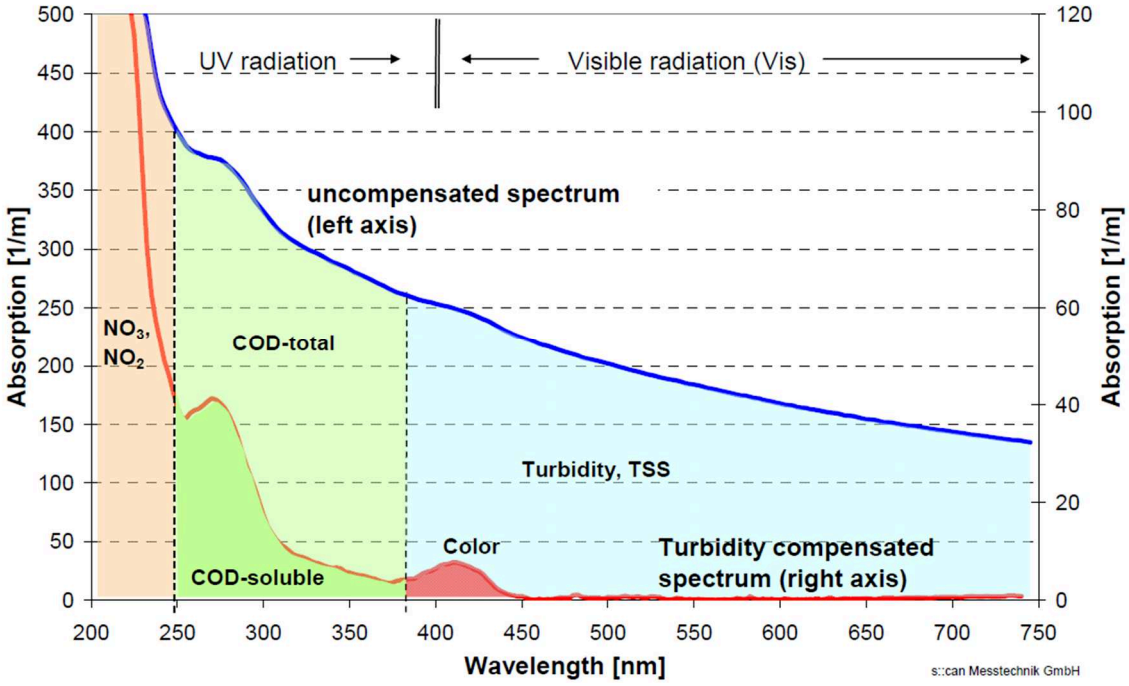

Figure 9. Absorbance profiles of various substances within the spectrum between 200 and 750 nm (van den Broeke *et al.*, 2006).

The basis for measurement of the UV-Vis spectrophotometer concentrates on the correlation between pollutant concentrations and the absorbance of light at different wavelengths. Spectra of observed absorbencies are converted into equivalent concentrations of substances by applying some statistical regression techniques, as per the next equation (Gruber *et al.*, 2006):

$$C_{eq} = \sum_{i=1}^{n} w_i A_i + K \qquad \text{(Eq. 2)}$$

where C_{eq}: equivalent concentration of pollutant (mg/L)

n : number of wavelengths used

w_i: weighing factor per wavelength i (m·mg/L), to be calibrated with laboratory measurements

A_i: measured absorption for wavelength i (m-L)

K: off-set factor

The manufacturer performs global calibration using the above correlation equation, applying the result as a default configuration for the sensor. Global calibration is however carried out for

typical municipal wastewaters, as reported by s::scan Messtechnik GmbH (2011). When the spectrophotometer is employed in water quality monitoring for a specific site, the water composition may differ due to several causes, such as different contributions of industrial wastewater or the mix with stormwater during wet weather periods. As a consequence, it is important to perform local calibration to adapt the sensor to the local conditions and increase its long term stability (Rieger *et al.*, 2004). This issue has been discussed in many studies, including the introduction of several correlation models for the local calibration (Gruber *et al.*, 2006; Gamerith, 2011; Schilperoort, 2011; Caradot *et al.*, 2015; Lepot *et al.*, 2016).

3.3 Sensor placement methods

3.3.1 Measurement locations

QBR requires data from online monitoring water quality sensors. Ideally, high density of quality sensors can enhance the accuracy of modelling and RTC and quality sensors should be deployed as close as possible towards the flow sensors. However, several constrains such as budget, ease of access and permitting usually bring down the number of sensors. Identification of critical locations for measurements should therefore be addressed insightfully to enable proper compensation for the limited number of sensors.

Within SNs, basic components comprise CSOs, retention tanks, and main sewers branches. Figure 10 displays potential locations for sensor placements. Urban water mainly enters receiving waters through CSOs and WWTP outlets, and moreover CSO discharges carry along untreated wastewater. Priority should thus be given to monitoring water quality at CSOs and WWTP outlets in order to determine the mass and dynamics of pollutants. Sensors can be placed either upstream or downstream CSO weirs to record the dynamics of pollutant concentration. Given simultaneous operation of a flow sensor, upstream placement allows understandings of total pollutant mass whereas downstream one can help correctly quantify the actual amount of

pollutants spilled to receiving waters. Inlet of the WWTP is the point linked with the SN, so information on the water quality is beneficial to better understand the influence of the SN on the WWTP. Bypass of WWTP is another place of interest for RTC application to obtain complete information about discharges to the receiving water.

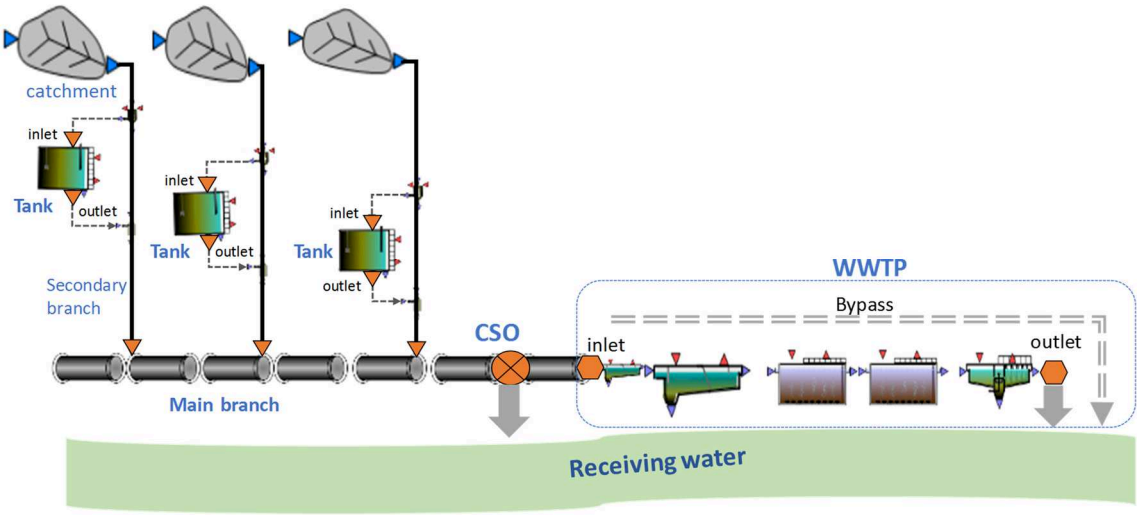

Figure 10. Main locations for sensor placements (orange color).

For QBR, retention tanks also play a crucial part in intercepting excess polluted water, so quality of water entering and leaving the tanks is useful for timing the interception and knowing its impact. Besides, quality data from the retention tanks is practical for model development. Finally, to improve calibration and verification of the sewer model, sensor placements can be further employed at positions on the secondary branches, before junctions where water flows into the main branch.

3.3.2 Installation methods

After identification of monitoring points on the system, the next stage is selection of methods for online measurement sensor installation. There are two common methods and the choice is made in accordance with the particular conditions of the site.

3.3.2.1 Direct installation

The approach of direct installation indicates that the sensor is positioned within the sewer structure. For instance, as in Figure 11, the sensor can be mounted to a frame and both are then placed through the manhole, at right angle to the sewer pipe. The frame is fixed to the manhole during measurement to keep the probe stable, but it can be easily retrieved for maintenance work. This solution is applied in the LIFE EFFIDRAIN project to monitor water quality at CSOs in Bordeaux. Other solutions include the one described by Gruber *et al.* (2004), which attaches the sensor under a mini pontoon floating in the sewer. The pontoon is connected with the chamber walls and the ceiling by ropes to prevent drifting.

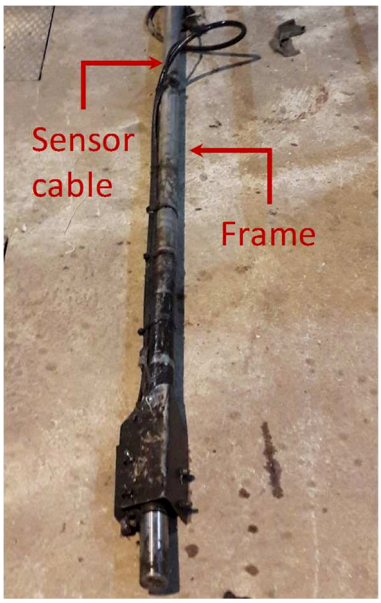

Figure 11. Example of how a sensor is mounted to a metal frame (photo: Duy Khiem Ly).

3.3.2.2 Bypass installation

This approach indicates that measurements are not directly done in the sewer, but in a bypass measuring container positioned right next to the sewer. Water is pumped from the sewer into the container where the quality sensor is installed. One example is the case presented by Bertrand-Krajewski *et al.* (2000) and Bertrand-Krajewski *et al.* (2007) in which a measuring

transit flume placed in a shelter next to the sewer system and a peristaltic pump are used. With the peristaltic pump, water matrix is mostly unaltered during the transfer and the pump also allows operation in the opposite direction to remove blockages in the sampling tube when necessary. The pump is nevertheless restricted to a maximum suction head of approximately 8-9 m (Gruber *et al.*, 2006).

Table 8 below is adapted from Gruber *et al.* (2006) to compare between the two abovementioned methods with regards to a number of possible issues. In general, direct installation is more preferred for short-term monitoring. On the other hand, bypass installation should not be neglected for long-term monitoring, particularly because this method can lessen maintenance efforts and provide more reliable data if the problem of lag-time measurement is tackled appropriately by constant pump velocities.

Table 8. Comparison between two installation methods for online monitoring sensors.

Possible problem	**Direct installation**	**Bypass installation**
Temporal delay in measurement	None	A few seconds of lag time but can be overcome with the data logger. A challenge for RTC
Unmixed samples due to pumping	None	Likely
Measurement conditions	Unstable	Very stable if the pump operation is reliable
Local calibration of sensor	Potential risk that grab sampling and sensor measurement results are different due to different intake points in the sewer.	More easy as the sampler can get grab samples in the same container.
Risks of sensor damage	Vulnerable to the high flow velocity, especially during strong rainfall events.	Much less likely
Energy consumption	Lower	Higher
Access for sensor maintenance	Access to the sewer is strictly needed.	More convenient, specifically if measurements are performed in a shelter.
Maintenance of additional parts	Frame or mini pontoon	Intake tube spot, pump, and the container (flume or tank)
Ease of installation and associated cost	Easier to install and less cost.	Additional spaces are required, e.g. for the shelter, pump; more permitting issues. Mandatory cost of extra parts: container, pump, shelter construction, etc.
Low water level in the sewer	Critical for non-floating system	Less affected (mobile sampling tube).

3.3.2.3 Sensor position in the water

When sensors are installed in the sewer for online monitoring either by bypass or direct installation, there is concern regarding the sampling position of the probe. Obviously the sensor provides merely point-measured values of pollutant concentration and typically, implicit assumption is that a point measured value at one time step is the same as the cross-section mean concentration at that time step.

Variations of TSS concentration profile are often insignificant under fully mixed conditions in the sewer. However, under other conditions, the variations of TSS concentration profile need to be assessed with care because compared to the water surface, TSS concentration values near the invert can be larger (Raudkivi, 1998). Sandoval and Bertrand-Krajewski (2016) applied two statistical methods with Monte Carlo simulations accounting for different sources of uncertainty to evaluate the probability of underestimating cross-section mean concentration values of TSS from measurements during wet weather events, and the results were 88% and 64% accordingly. These results were specific to the observed data in one catchment in Lyon (France).

Versini *et al.* (2015) proposed a guideline for turbidity measurements in the sewer networks and several relevant instructions include:

- Choose a spot which is spatially representative of the identified location/site, and the average flow velocity is at least 0.3 m/s under all conditions.
- The spot should not be close to any strong turbulence upstream which can cause air bubbles on optical parts, resulting in false high turbidity readings.
- Ensure sufficient water level: for direct installation, minimum level recorded at night and during dry weather should be at least of 20 to 30 cm and the probe should be 5-10 cm above the invert to avoid interference by sediments. For bypass installation, the minimum level is 10 cm.

In addition, two-dimensional samplers (2D samplers) were used by Jaumouillié *et al.* (2002) and Larrarte (2015) in several experiments in Nantes, France to characterize TSS concentration map throughout cross sections of an oval-shaped sewer channel with a side bank. It was reported by the authors that under wet weather conditions, certain fluctuations in TSS concentration could appear but there was no obvious vertical gradient for sites without any sediment layer on the pipe invert. Similar experiments completed during dry weather conditions using multipoint samplers were presented by Randrianarimanana *et al.* (2015). There were significant vertical gradients in TSS concentration profile when significant layer of sediments exists, e.g. from 200 mg/L near the surface to around 400 mg/L near the sediment layer at the bottom.

Generally, few published studies performed field experiments to investigate the effects of positioning the sensor probe inside the sewer on measurement of pollutant concentrations, to the best knowledge of the author. The difficulty is probably due to numerous factors to be accounted for when studying the effects, e.g. flow conditions, geometry of the cross section, size and slope of the pipe, type of measurement devices, and type of measured quality parameters. It is also not easy to have simultaneous sampling points across a cross section in the sewer channel.

3.4 Summary

TSS, COD or TKN can be considered as state variables for QBR of sewers systems. Past studies justified the possibility of using economic and easy-to-use sensors such as UV-Vis spectrophotometers and turbidity meters for online monitoring of these state variables. Their values can be obtained through UV-Vis spectra (for UV-Vis spectrophotometers) or local calibration (for turbidity meters), which is the correlation between turbidity data from these sensors and lab-analysed data from sampling campaigns.

Water quality sensors can be positioned at CSOs to quantify the dynamics of processes and pollutant loads by wet weather events. Information on the water quality at other locations, such as the inlets and outlets of WWTPs and retention tanks, and the secondary branches before junctions where water flows into the main branch is meaningful to model development and implementation of control decisions.

Next, two methods for sensor deployment are introduced and compared: direct installation and bypass installation. Direct installation is used in this research because it avoids the complication in requesting additional spaces, resources, and permitting from the authorities, and does not face the challenge of time lag in measurement due to pumping. Furthermore, literature review on the impact of different positioning of quality sensors on the water on pollutant concentrations is carried out and one of the highlights is the risk of high vertical gradients in TSS concentration profile due thick layers of sediments.

CHAPTER 4: LOUIS FARGUE CATCHMENT CASE STUDY

This chapter gives a comprehensive description of the Louis Fargue catchment case study. In particular, relevant background about climate, location, historical development of the catchment, etc. will be presented. Current sewer operation is also elaborated to enable better understanding of the type of existing control implemented on the site. Besides, the chapter provides information related to the current conditions of the receiving water body and the WWTP. Next, the detailed hydrodynamic model used to represent the main hydraulic and quality processes of SNs is introduced. This model is an important tool for control, whose application will be described in the next chapters. Lastly, the last two sections of this chapter are based on the report Deliverable D10 (Ly *et al.*, 2018) of the LIFE EFFIDRAIN project.

4.1 Study area

4.1.1 Background

The study area is the Louis Fargue catchment which is part of Bordeaux Métropole (known as "la communauté urbaine de Bordeaux" (la CUB) before 2015), and includes 28 municipalities and encompasses the central metropolitan area of Bordeaux city, the largest city of the Nouvelle-Aquitaine region in the southwest of France. The city lies on a bend of the Garonne River and is within 50 km from the river estuary (Figure 12). In 2012, Bordeaux Métropole had a total population of approximately 737000 inhabitants, and particularly about 241000 were from Bordeaux. Bordeaux Métropole extends over 58000 ha of urban catchments (Lerat-Hardy *et al.*, 2018) and those right next to the Garonne River have been long known to be prone to flooding (Figure 13). The flood risks are due to specific characteristics of the place (climate, topography and tidal bore) that are presented hereafter.

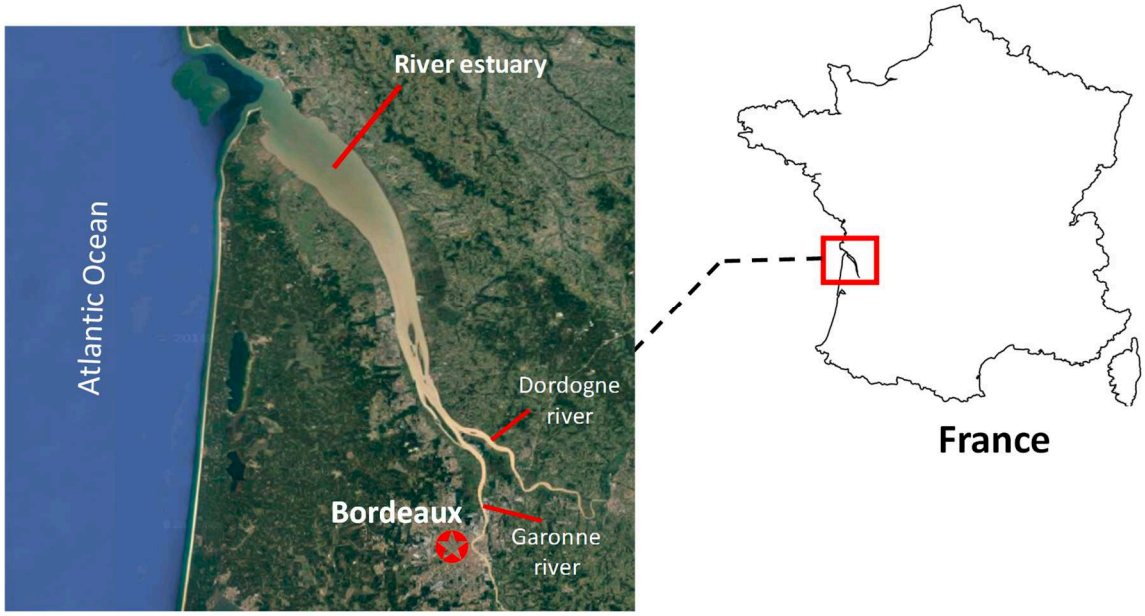

Figure 12. Map of Bordeaux with the Garonne river and its estuary (adapted from "France Outline Map" n.d.).

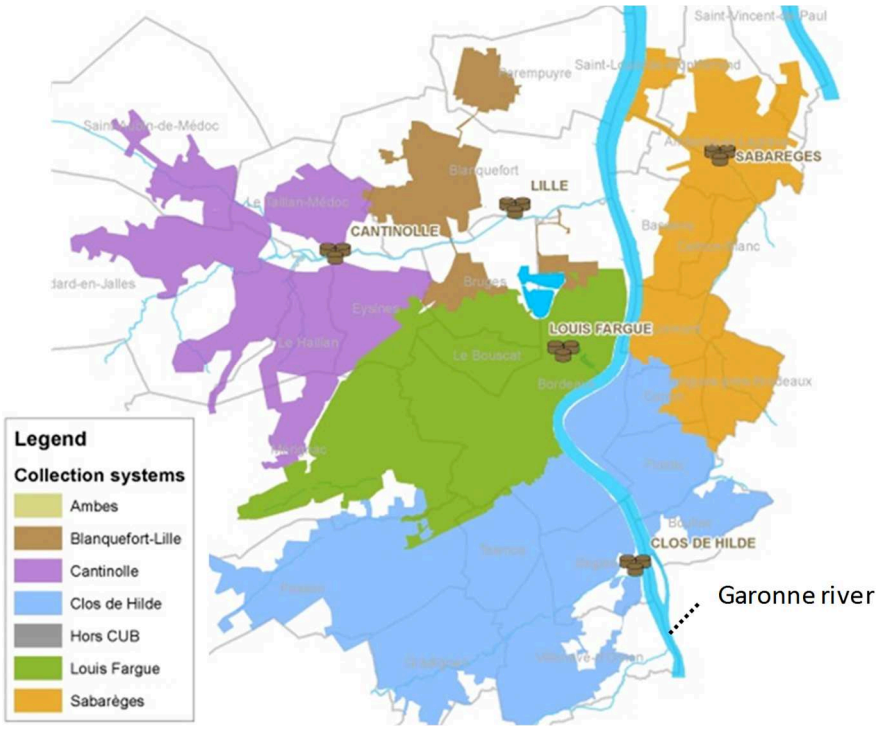

Figure 13. Main urban catchments and WWTPs of Bordeaux Métropole (after Komorowski, 2016).

4.1.1.1 Climate

Bordeaux is close to the Atlantic Ocean and its climate is oceanic, with frequent rainfall events observed throughout the year. Strong convective storms may appear in summer, resulting in high rainfall volumes and intensities. The yearly average rainfall depth is around 900 mm for the period between 1980 and 2008 (see Figure 14). Furthermore, on average there are around 66 rainy days per year (Maruéjouls and Montserrat, 2016). Figure 15 shows the time series of rainfall intensity at Abria rain gauge for the year of 2016.

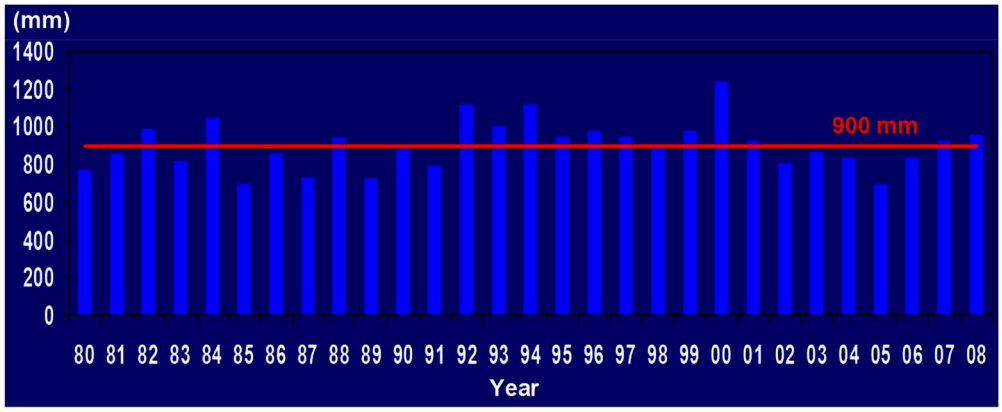

Figure 14. Average rainfall depth between 1980-2008 (after Komorowski, 2016).

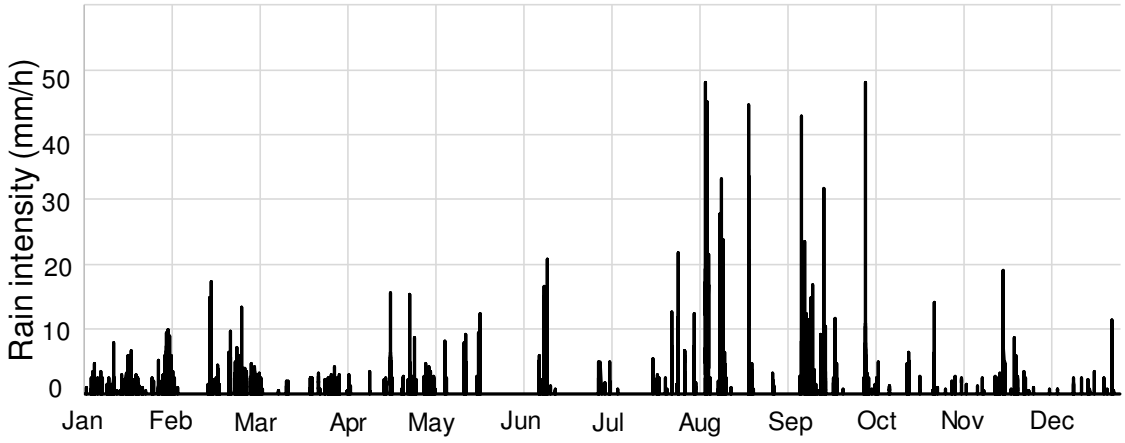

Figure 15. Observed rainfall data in Bordeaux (extracted from Abria rain gauge) in 2016.

4.1.1.2 Topography

The whole catchment area of 90000 ha has more than 150 streams. Several of them start from

far upstream and reach downstream combined sewers next to the Garonne River. The urban catchments along the left bank of the river (including the Louis Fargue catchment) are therefore similar to a concentration point of runoffs, as seen in Figure 16.

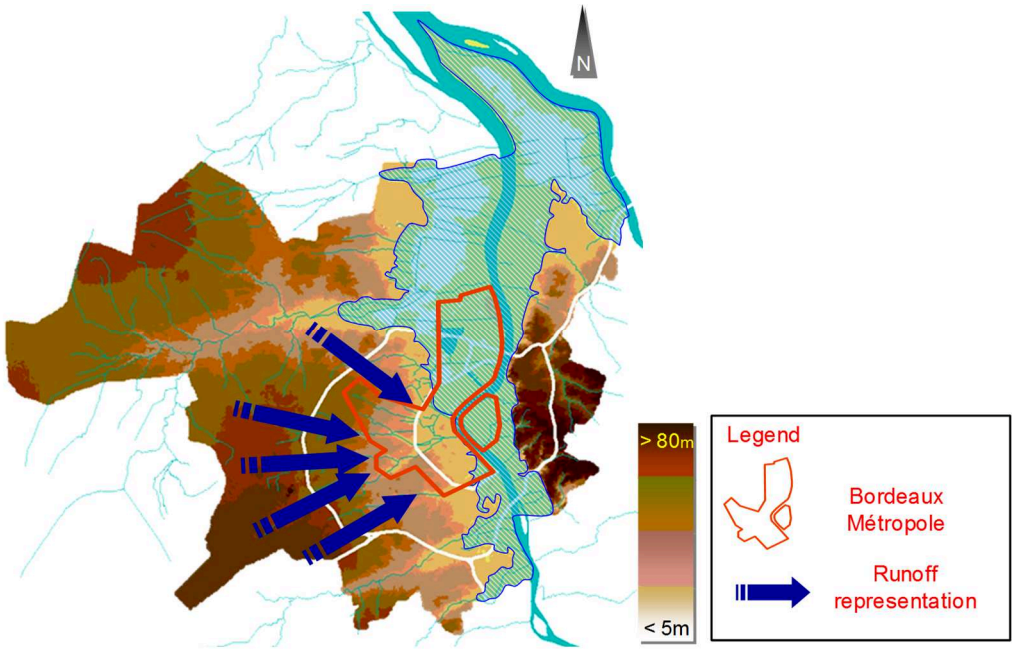

Figure 16. Topographic map with elevation showing the urban catchments of Bordeaux Métropole as a concentration point of runoffs (after Komorowski, 2016).

4.1.1.3 Tidal bore

The Garonne River is subject to tidal bore (alternatively known as “mascaret”) which happens when there is a rising tide with large amplitude entering a shallow, narrow and mild-sloping river. This phenomenon causes positive surges that can be propagated upstream along the river. Tidal wave propagation was once recorded to be up to 160 km from the estuary mouth of the Garonne River (Bonneton *et al.*, 2011). Given the influence of tidal bore, maximum tidal level of the river, dependent on wind, atmospheric pressure and strength of rainfall events, can reach 7 m. It is worth noted that 25% of the urban catchments of Bordeaux Métropole are lower than the highest tidal level of the river (Maruéjouls and Montserrat, 2016).

4.1.1.4 Historical development

Shortly after extensive damages caused by two violent storm events between 31 May 1982 (81 mm in 6 hours, more than 20-year return period) and 01 June 1982 (40 mm in 1 hour, 10-year return period), la CUB decided to implement a flood prevention strategy called “strategie des trois couronnes” (the three crowns strategy, as shown in Figure 17). It involves the below duties:

- Installation of pump stations at low-level zones
- Construction of many more retention tanks
- Further protection of the urban zones by runoff diversion, collection of excessive stormwater at each crown, underground transport of stormwater in downtown Bordeaux.

Accordingly, massive investments in flood protection infrastructures have been spent by the municipality, especially on left bank of the Garonne River. Since 1982, a wide network of retention tanks (with more than two million m^3 storage volume), tunnels and pumping stations with a total capacity of about 120 m^3/s have been constructed. In 1992, the RAMSES (Régulation de l’Assainissement par Mesures et Supervision des Equipements et Stations) project was commissioned by la CUB, aiming to build a powerful telecontrol system to monitor and control SNs during rainfall events to reduce flooding. As part of RAMSES, hydraulic sensors have been deployed across the system for monitoring purpose, and actuators can be controlled in real time to achieve the goal of flood prevention and proper functioning of the sewer systems.

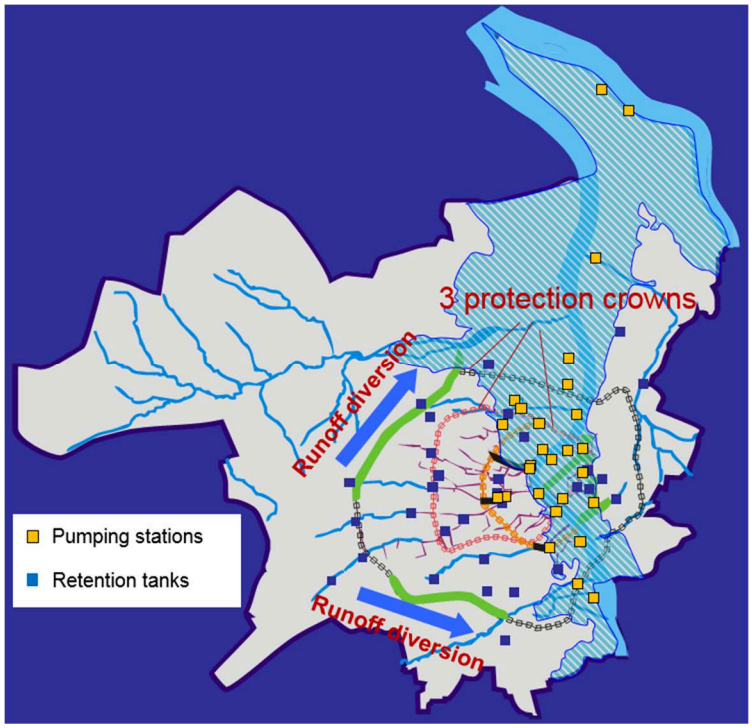

Figure 17. Illustration of flood prevention strategy implemented by la CUB since 1982 (after Komorowski, 2016).

4.1.2 The Louis Fargue catchment

4.1.2.1 General description

Louis Fargue is the most populated catchment of the Bordeaux Métropole. It covers an area of 7700 ha and accommodates approximately 300000 inhabitants. Its entire network length is around 1,340 km, of which 80 % are combined and 20 % are separate sewers. A majority of the pipes (i.e. 70%) have circular shapes with diameters ranging from 0.3 to 4.5 m. During dry weather days, wastewater is collected and transferred to the sub-catchment outlets. There is a large interceptor which receives wastewater from these outlets and then transfer it to the WWTP (shown in Figure 18). The pipe diameter of the interceptor varies between 3.6 and 4.2 m. At each connection point (at an outlet), there is a CSO structure to discharge excessive water into the Garonne River during storm events. The CSO structure at Le Lac is connected to the

Bordeaux Lake; however, as its discharge is negligible compared to other CSO structures, it is not included in the control and calculation of this research.

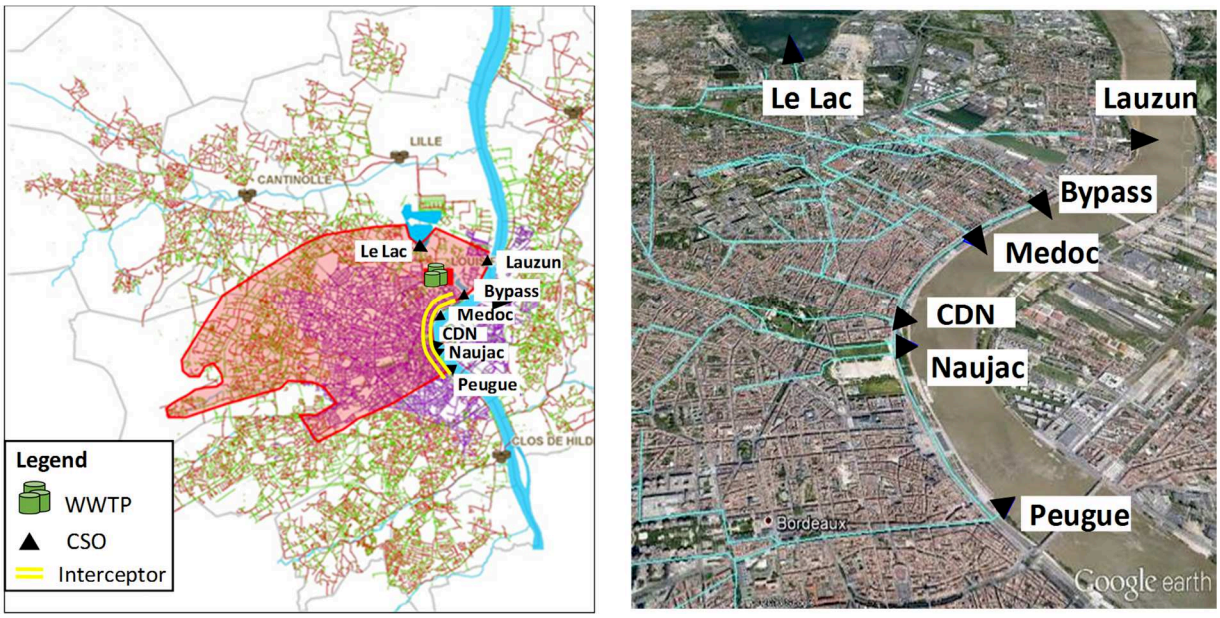

Figure 18. Map (left) and satellite (right) images of Louis Fargue catchment (red-coloured area in the map) with CSO structures, WWTP bypass and the main interceptor along the river (adapted from Komorowski (2016)).

4.1.2.2 Current sewers operation

As described above, the catchment was already equipped before this research with rain gauges, hydraulic measurements, and multiple retention tanks to deal with the persistent threat of flooding. The tank locations are shown in Figure 19. Most of the tanks are controlled thanks to local control rules. The principle of these local control rules is similar for all locations. Based on the water level at a node downstream of the tank and the rainfall intensity, the orifice position is adjusted (i.e. zero or limited opening) to force stormwater accumulation and then overflow into the tank. When runoff returns to dry weather conditions or the tank is full, orifice position is reset (i.e. full or higher opening), usually with triggering pumps, to gradually empty the tank. There are few tanks that are controlled by static rules only (i.e. hydraulic design to allow

overflow into the tank when water level in the pipe reaches certain thresholds), without the need of adjusting orifice positions.

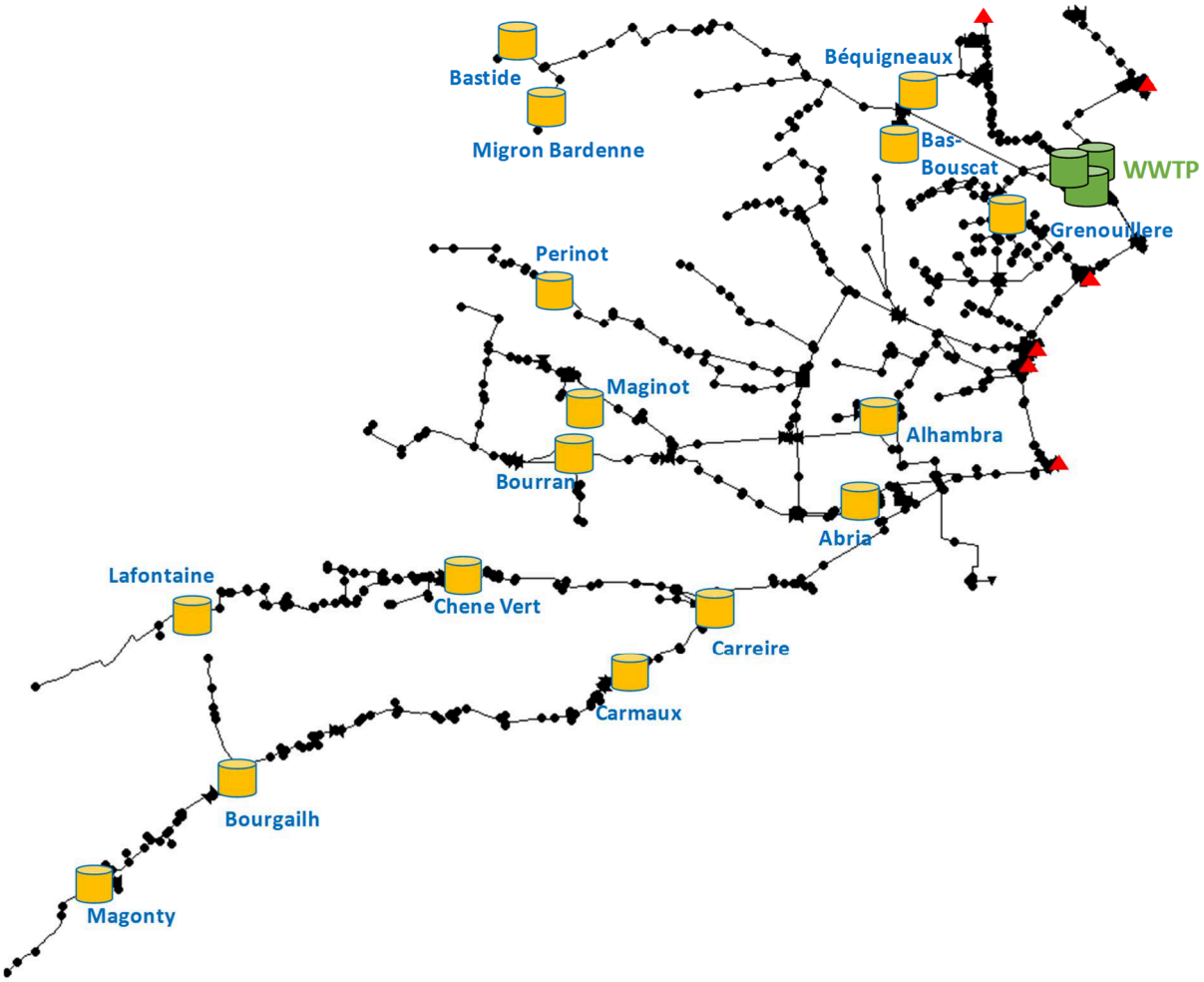

Figure 19. Sewer network layout with locations of the 16 retention tanks.

In addition, since 2013 a downstream part of the catchment has been implemented a global volume-based RTC system known as Gestion Dynamique (GD), as the last advance of RAMSES. Figure 20 displays the area where GD is presently operated. The management strategies of GD are summarized by Maruéjouls and Montserrat (2016):

- Watching mode: There is no provision of control actions and only forecast-related computations are carried out. It is activated under dry weather conditions.

- CSO reduction mode: Control actions are transmitted from the control centre to adjust the actuators. Its goal is maximisation of the WWTP use, followed by retention tanks and online storage facilities.
- Fast emptying mode: Control actions are transmitted from the control centre to adjust the actuators. Stored water should be released as quickly as possible to allow maximum storage capacity of the system before incoming storm events.
- Flood mode: Controllable actuators are set at static positions to keep water levels lower than critical thresholds. Maximisation of the WWTP use, flow through CSO structures, and filling of the retention tanks are the priorities.

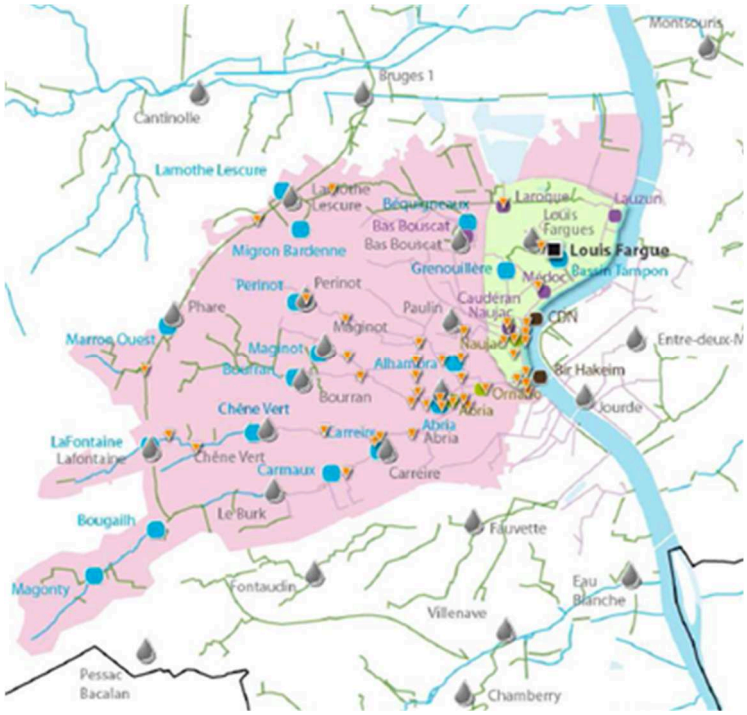

Figure 20. Louis Fargue catchment consists of the pink area (controlled by static or local dynamic rules) and the green area (under global control based on hydraulics) (after Maruéjouls and Montserrat, 2016).

4.1.2.3 Louis Fargue wastewater treatment plant

The Louis Fargue WWTP was constructed in 1974 and has been upgraded twice in 2003 and in 2011 to meet the population growth. It is located in the northern part of Bordeaux city, used

for treatment of wastewater mostly from Bordeaux and partially from surrounding municipalities (Mérignac, Pessac, Le Bouscat, Bruges, Eysines and Talence). Wastewater arriving at the plant under dry weather conditions mainly stems from domestic consumption, associated with other minor sources of industries and public establishments. The treatment is based on biological filters which takes advantage of packing (or filter media) along with attached biofilms. The WWTP also has a conventional activated sludge treatment line, including gas treatment facilities for electricity generation. Theoretical dry weather capacity of the WWTP is 367000 population equivalent (PE), plus additional capacity of 110000 PE during rainfall events. Main nominal capacity features of the WWTP is displayed in Table 9.

Table 9. Nominal capacity features of the Louis Fargue WWTP (after Maruéjouls and Montserrat, 2016).

	Unit	**Dry weather**	**Wet weather (additional capacity)**
Daily volume	m^3/d	210000	66500
Maximum flowrate	m^3/h	8750	2270
Biological Oxygen Demand (BOD_5)	kg/d	22000	6600
Chemical Oxygen Demand (COD)	kg/d	63500	20000
Total Suspended Solids (TSS)	kg/d	44500	14200

4.1.2.4 Garonne River receiving water body

The Garonne River originates from the streams of the Pyrenees, where it is fed by snowmelt. Resultantly, water levels may increase quickly in late spring, and sometimes generate flooding (Prosser, 2005). After passing by Bordeaux, the Garonne River is joined by the Dordogne River at the Gironde estuary, before reaching the Atlantic Ocean (see Figure 12). Average river discharge rate measured in Bordeaux is around 650 m^3/s, at the estuary around 1100 m^3/s (Etcheber *et al.*, 2011).

It is reported in literature that chronic metal pollution due to former mining and smelting activities in the late 19th century in the upper reaches of a tributary is one of the problems of the river (Schäfer *et al.*, 2006; Saari *et al.*, 2010). In addition, there is oxygen depletion. The Gironde estuary is one of the most spacious European estuaries, with an area of 625 km^2 (Etcheber *et al.*, 2007). Due to tidal activities (as described in section 4.1.1), residence times of water and suspended matter in the estuary can be around 20 days-3 months and 12-24 months respectively (Maruéjouls and Montserrat, 2016). This stimulates an increase in TSS concentration (higher than 1000 mg/L), directly affecting the oxygen consumption rate (Schmidt *et al.*, 2017). Few oxygen depletion events (DO around or less than 2 mg/L) were detected in the past along the river section close to the Bordeaux urban area (see Etcheber *et al.* (2011)). Furthermore, as provided by the same authors, further 30 km upstream Bordeaux, the riverbed, previously covered by gravels, is presently occupied by muds. The problem of oxygen depletion may thus become critical in the future, particularly during summer days, given stronger impact of global warming and pollutants from urban discharges.

The Garonne River has highly important ecological, social, and economic values (tourism, fishing industries, agriculture, etc.) to the city of Bordeaux. Therefore, better management of the sewer network, specifically the Louis Fargue one, should be prioritized to support the protection of the river.

4.2 Measurements and data

4.2.1 Choice of quality state variable and monitoring method

Within the LIFE EFFIDRAIN project, TSS is the main state variable to be monitored. As explained before in section 3.1, TSS, COD, and nitrogen are important state variables for QBR. TSS indicates the amount of SS in wastewater, which are proven as the primary source of pollution transfer within the sewer pipes (Ashley *et al.*, 2005). During wet weather, SS is

revealed to amount up to 80 % total mass of sediments, and reckoned as the main vector for numerous pollutants such as BOD, COD, heavy metals, and petroleum hydrocarbons (Delleur, 2001; Barraud *et al.*, 2005). Moreover, it has been proven from many past studies (e.g. Bertrand-Krajewski *et al.*, 2000; Barraud *et al.*, 2002; Bertrand-Krajewski, 2004; Sun *et al.*, 2015) that TSS data can be well obtained through the correlation with turbidity data, which can be measured by conventional and low-cost turbidity meters.

Given the choice of TSS as the state variable, turbidity is continuously monitored by using turbidity meters. The correlation between turbidity and TSS values is achieved through the local calibration procedure (explained in section 3.2.2). Sampling campaigns are a prerequisite for local calibration because lab-analysed values from grab samples of the campaigns are needed to derive the relationship with recorded values given by the online monitoring sensors. Additionally, the sampling campaigns data are also meaningful for understanding the catchment characteristics and model development.

4.2.2 Online monitoring

For the LIFE EFFIDRAIN project, four CSO structures along the Garonne River (i.e. Peugue, Naujac, Caudéran-Naujac (CDN) and Lauzun) have been selected. They are equipped with monitoring stations since October 2015 to measure continuously quality parameters. In addition, there are existing hydraulic sensors nearby (upstream and downstream some of these stations): their data are available for this research. Table 10 shows all available sensors and measured parameters at each CSO site. The sensors are autonomous in energy and retrieval of data is done by SMS to the control server with the assistance of Global System for Mobile Communications technology. Data downloaded from the server is then validated and treated by the tools built by LyRE (Suez) before being used for model developments (Figure 21).

Table 10. Summary of online sensors for each CSO site on the Louis Fargue catchment

Sensor type	Number	Measurement	Sampling interval
Ultra-sonic flowmeter	1	Flow	5 minutes
Piezometer	1	Water level	5 minutes
Nephelometric turbidity meter	1	turbidity	5 minutes
Conductivity meter	1	Conductivity, temperature	5 minutes

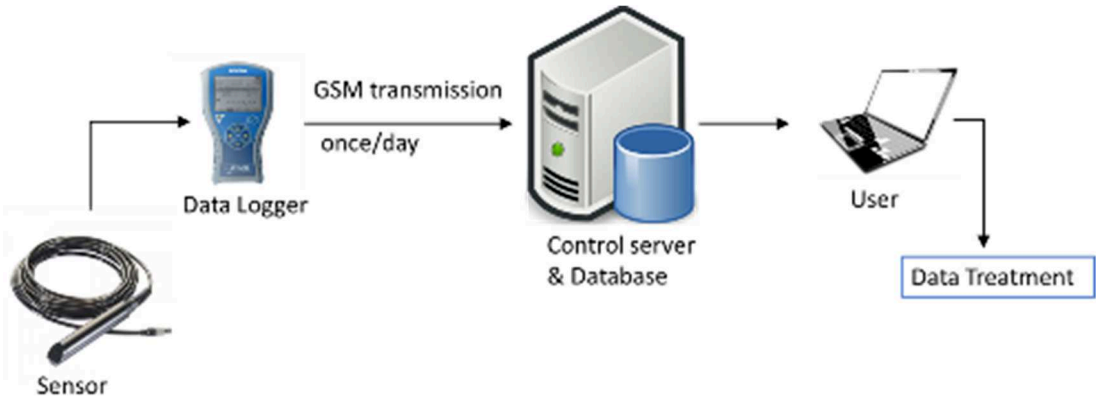

Figure 21. Scheme of observed data transmission.

The online sensors are deployed using the direct installation method. Although there are few differences due to the particular conditions of each site, the installation principle is generally the same for all the four sites. Turbidity and conductivity sensors are attached metal frames or chains which can slide inside a guide sleeve, allowing easy maintenance from the ground. The probes of the sensors are fixed and protected at the bottom by holding systems. Furthermore, there is a cleaning system of brush-type wiper which is independent and helps to clean the surface of the turbidity probe.

Figure 22 to Figure 29 display the locations and how the turbidity and conductivity sensors are installed in the four sites. For CDN, there is usually no wastewater during dry weather so a floating system to retain water is made to always keep the turbidity probe submerged in the water, avoiding sensor damage. The system consists of a water retainer in the sensor end and a

float in the other end (as shown in Figure 27). During increasing water level, the retainer is inclined. When water inflow is reduced till minor or zero level, the retainer is in horizontal position and water remained from the high level time can still be held inside.

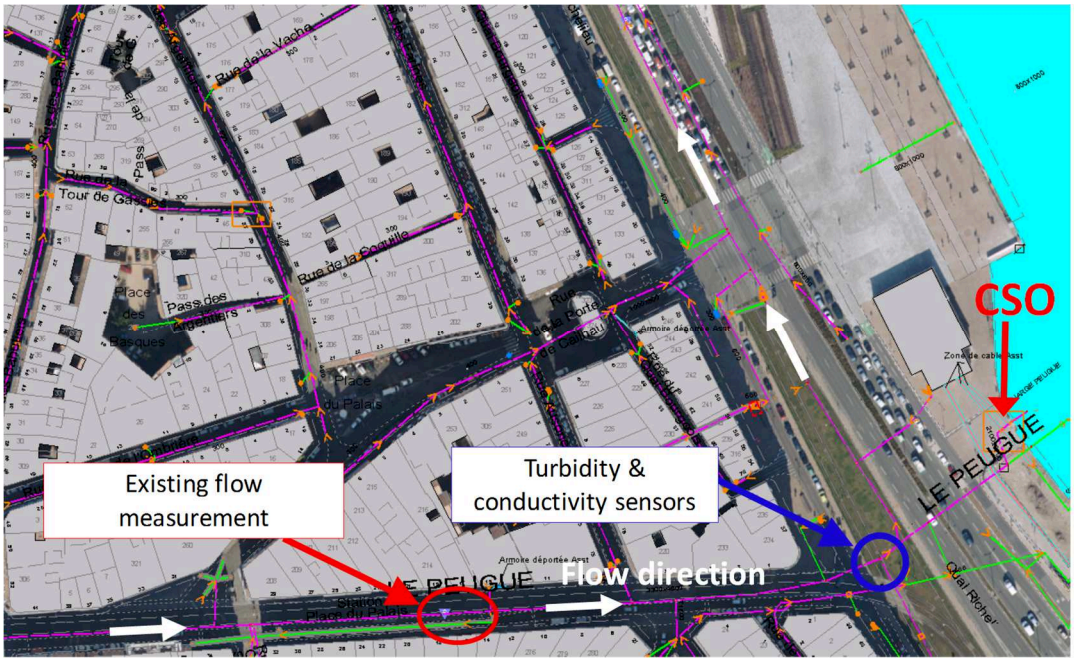

Figure 22. Location of sensors at Peugue (after Granger *et al.*, 2016).

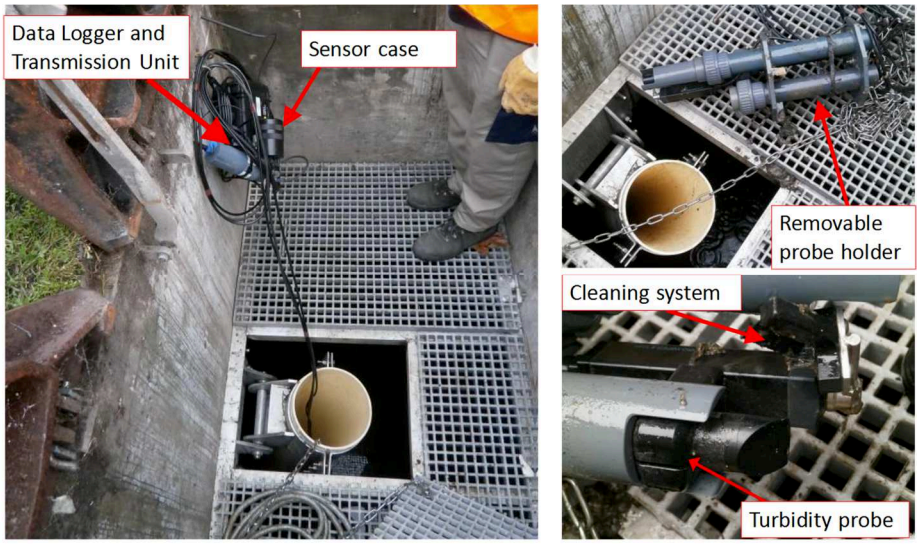

Figure 23. Installation of sensors and associated units at the CSO manhole at Peugue (after Granger *et al.*, 2016).

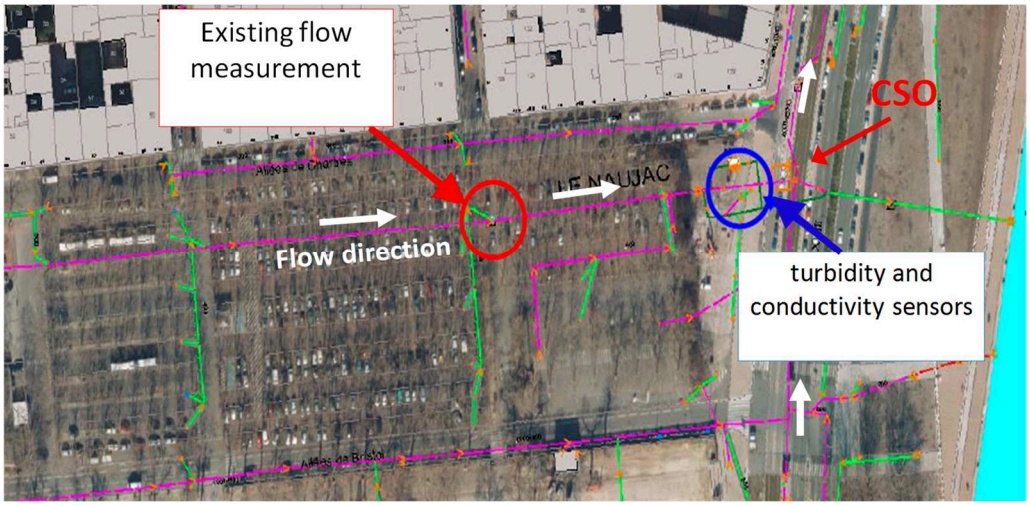

Figure 24. Location of sensors at Naujac (after Granger *et al.*, 2016).

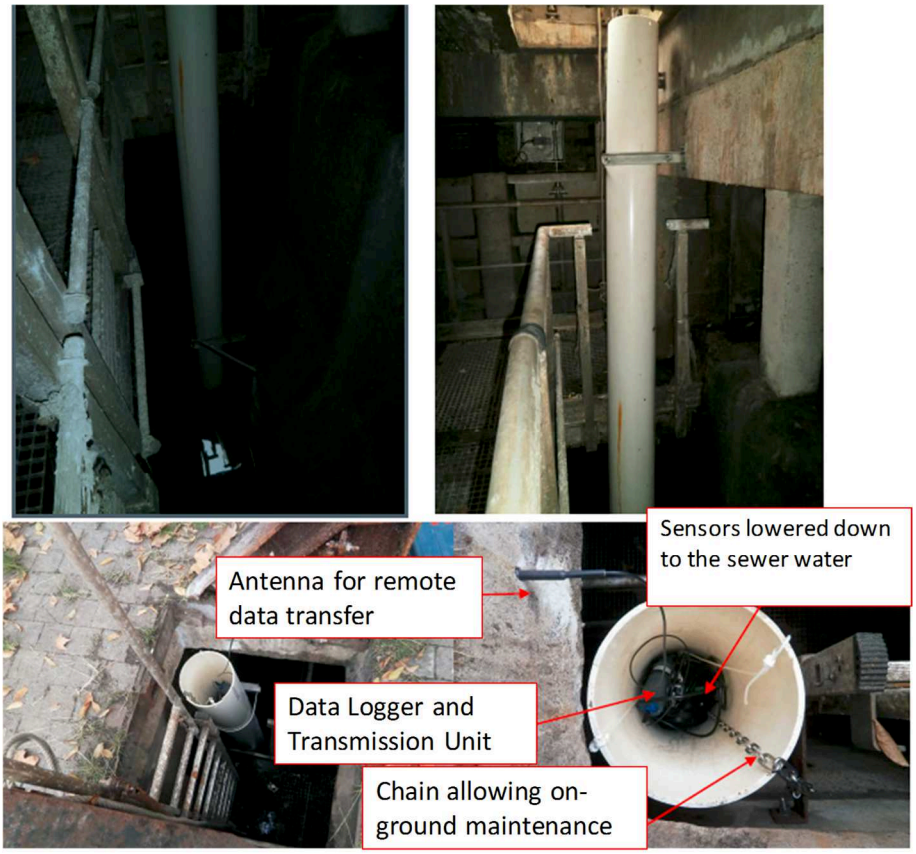

Figure 25. Installation of sensors and associated units at the CSO manhole at Naujac (after Granger *et al.*, 2016).

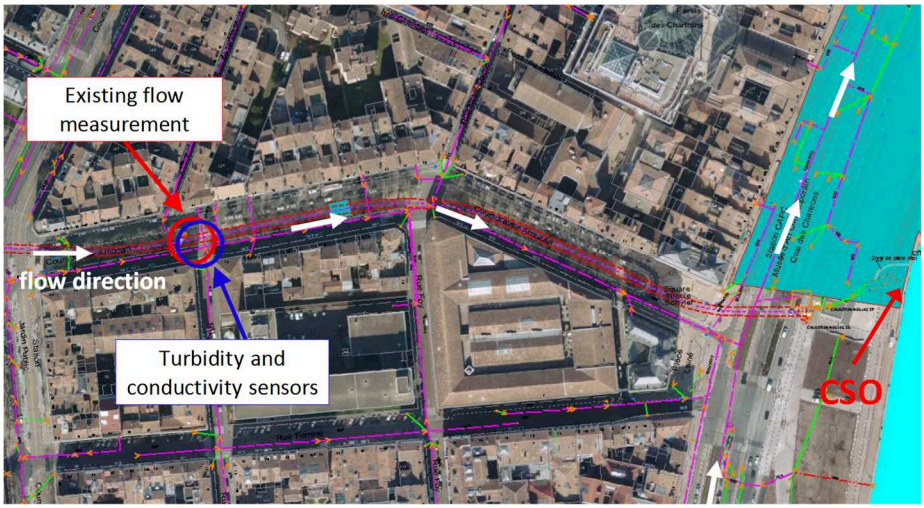

Figure 26. Location of sensors at CDN (after Granger *et al.*, 2016).

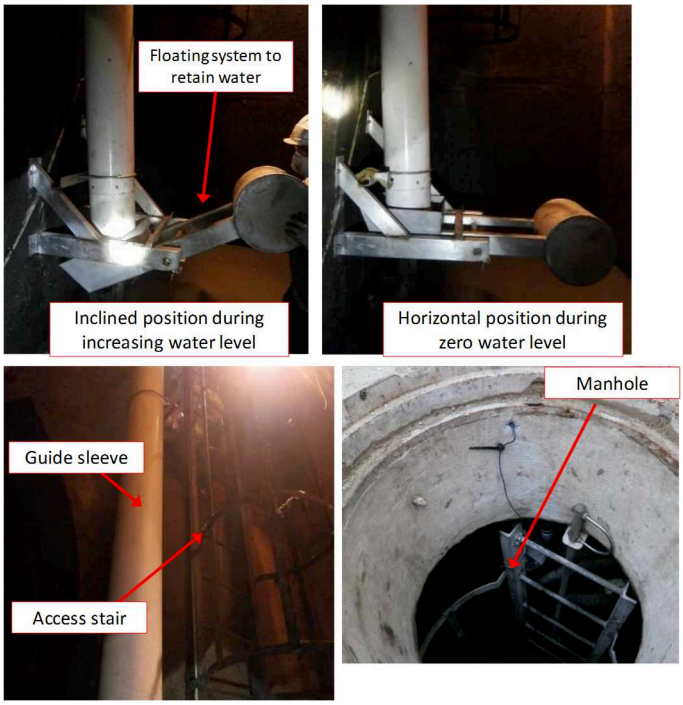

Figure 27. Installation of sensors and associated units at the CSO manhole at CDN (after Granger *et al.*, 2016).

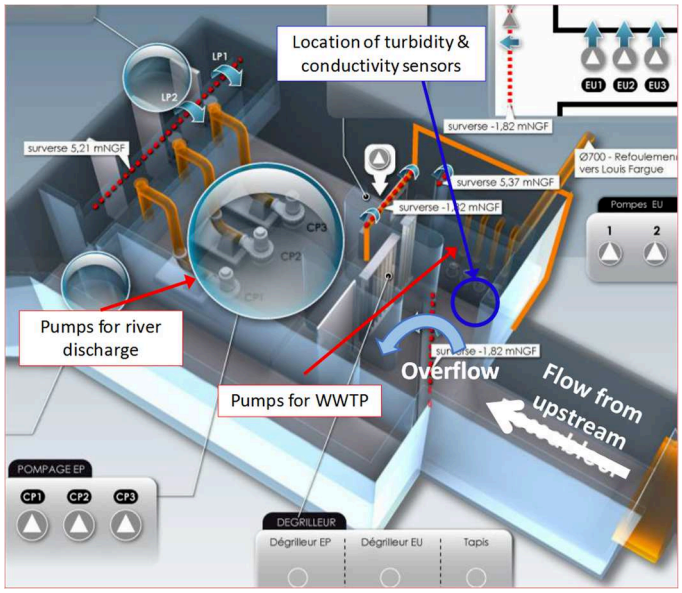

Figure 28. Location of quality sensors based on 3D plan of Lauzun CSO (after Granger *et al.*, 2016).

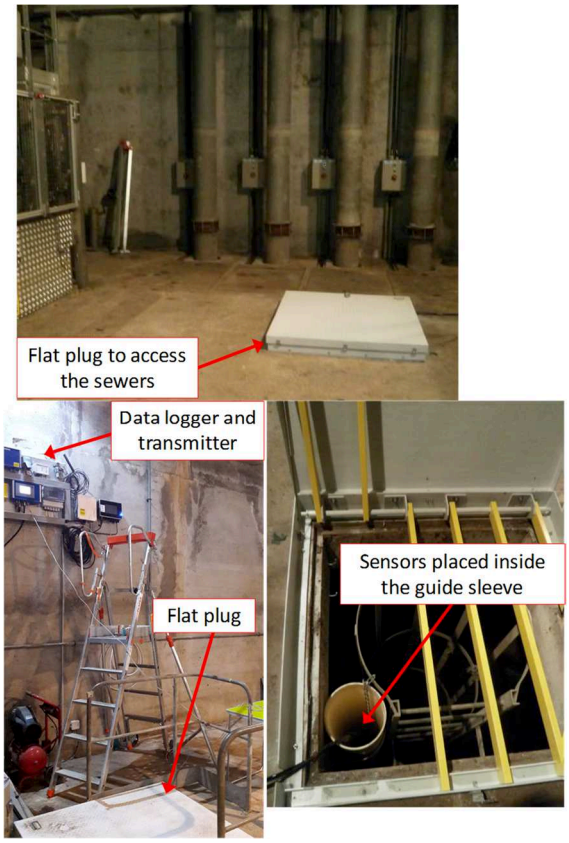

Figure 29. Installation of sensors and associated units at the CSO manhole at Lauzun (after Granger *et al.*, 2016).

Maintenance of the sensors is performed every month by SGAC (Société de Gestion de l'Assainissement de Bordeaux Métropole), the operator of the sewers in Bordeaux. Quality sensors operated in harsh sewer conditions are usually vulnerable to clogging and may provide highly inaccurate readings. Therefore, periodic maintenance is required so that the sensors can work properly. The maintenance frequency is decided according to the rate of fouling of the probes. Thanks to the incorporated automatic cleaning system, the turbidity meter does not usually require heavy maintenance (Maruéjouls *et al.*, 2017).

After commission, it is important to inspect the sensor frequently in the beginning to assess the fouling rate and any other possible effects on the sensor caused by surrounding environments of the site. Thereafter, based on online track of quality of the received data, one can decide an appropriate routine for visual inspection and cleaning of the sensor. Figure 30 illustrates two examples of sensor clogging that can be detected by data monitoring. Cleaning is imperative under these circumstances to ensure proper functioning of sensors. During maintenance, the sensor parts are rinsed meticulously with distilled water and acetone, using a soft cloth or an absorbent paper to remove deposits like biofilm, mud or dirt. At present, maintenance of the quality sensors at the four CSOs is performed once per month (see Figure 31). Nevertheless, regular monitoring of the recorded values is done at least twice a month to allow identification of any potential issue and to act when necessary.

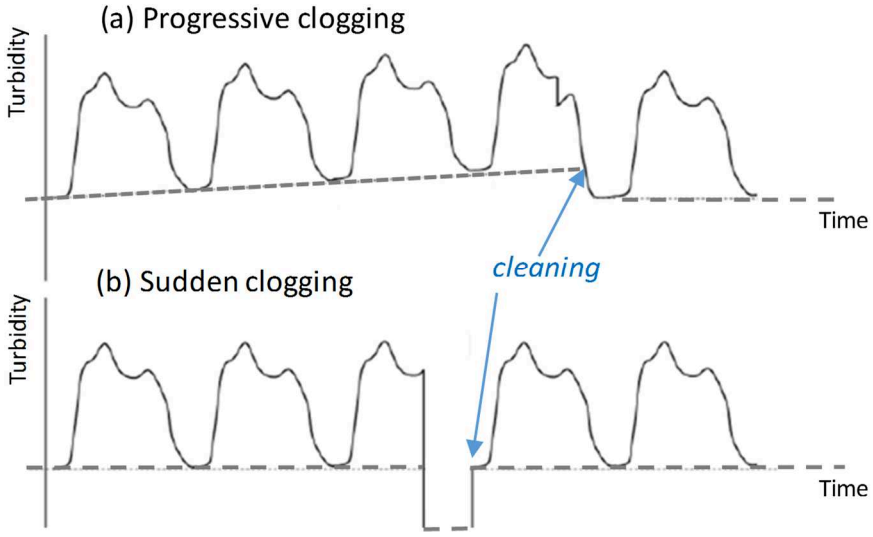

Figure 30. Examples of inaccurate readings due to clogging of the turbidity meter (after Granger *et al.*, 2016).

Figure 31. Visual inspection and cleaning of the quality sensors (photo: Duy Khiem Ly).

4.2.3 Automatic sampling campaigns

Over the three-year duration of the LIFE EFFIDRAIN project, there have been several wet weather sampling campaigns at the four CSOs. The selection of storm events for the campaigns aims to cover a wide range of TSS concentration but exclude extreme values in terms of rainfall characteristics such rainfall intensity, duration, etc. For the Louis Fargue catchment, the goal is to avoid either brief and intense summer events or long and low intensity winter events. Therefore, the most favourable periods are from mid-April to June and from September to mid-

November. The choice of the period is nevertheless highly subject to the operator's and equipment's availability.

Major steps included in the protocol of a wet weather sampling campaign are adapted from the technical report of Granger *et al.* (2016):

- Rainfall event selection: rainfall events can be anticipated in advance using weather forecast. The selected rainfall events should not fall under cases of extreme values of rainfall characteristics, i.e. rainfall duration, depth or intensity. Furthermore, the selection needs to account for seasonal variations. In reality, the choice of rainfall events is unfortunately limited by other reasons such as the availability of the equipment and the site operators.
- Threshold configuration of the sampler: the sampler should be brought to the site early enough to allow buffer time for starting up and configuring the sampler well before the rain. It is significant to set the hydraulic threshold for the sampler, which is typically water level or flow rate measured by a probe connected to the sampler. This threshold is understood by the sampler that when the water level or flow rate at the site reaches the specified value, the sampler will self-activate the first sampling. Right values for the threshold requires sufficient historical data analysis and/or experience from local operators. The values need to be specific to typical wet weather conditions of the sampling location to avoid false activation.
- Sampling time interval configuration: to capture the beginning of the event, the sampler is generally configured with higher frequency in the early rainfall runoff period. The time intervals between sampling times are configured such that they are short in the beginning, then gradually increase with time and then the longest interval are between the last sampling times at the dilution stage of the runoff. On top of that, the catchment characteristics (e.g. time of concentration) should be carefully considered before making any decision about the time intervals and the sampling duration. Figure 32 provides an illustration for the variation of defined time intervals versus the pollutant concentration profile.

- Sample selection, handling and transfer to the laboratory: if not all of the collected bottles from the sampler are used for laboratory analysis, it is necessary to pick the representative bottles. The dynamics of the pollutograph can be identified visually when the collected bottles are arranged in chronological order of sampling. Selected bottles should cover a wide range of concentration, from the lowest to the highest. Finally, selected samples are brought to the laboratory as early as possible to prevent any bio-chemical transformation of the pollutants.

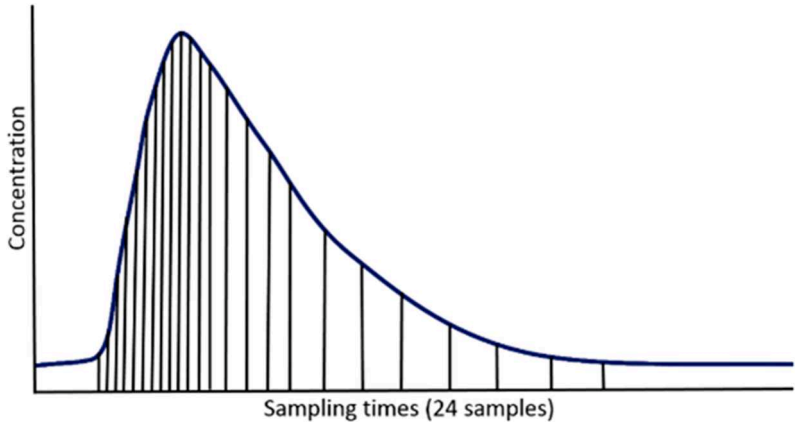

Figure 32. Sampling time intervals versus pollutant concentration profile during a rainfall event (inspired by Granger *et al.* (2016)).

The automatic samplers used by the operators for the campaigns are Teledyne ISCO portable samplers (3700 or 6712 series) (see Figure 33), which can be automatically triggered according to pre-set hydraulic thresholds (flow or water level at the site).

Figure 33. Automatic sampler used in the project (photo: Duy Khiem Ly).

Hydraulic threshold to trigger the automatic sampler is specific to each site, as displayed in Table 11 and identically, the sampling intervals for the automatic sampler is also programmed before a selected rainfall event. Automatic samplers used for the campaigns contain 24 bottles of 1 litre each. A few notes are derived from the author's own experience with the sampling campaigns:

- Pump intake of the sampler should be close to the turbidity probe and facing the water current.
- Check the clock of the sampler to make sure its timing is identical to the one of the quality sensors.
- Check the battery of the sampler to make sure it cannot be emptied before the sampling campaign is completed.
- Each lab bottle to collect water from a sampler bottle should be labelled (in filling order) and the label should be always visible till the end of the sampling campaign.
- If not all the sampler bottles are used, visual check on the water colour of each bottle is important to select the right bottles that can reflect the first flush effects on the pollutants.

- Once all the bottles are filled, laboratory analysis must be performed as soon as possible. The laboratory should be notified in advance to process the samples quickly after their arrival.

Table 11. Hydraulic thresholds to trigger the automatic samplers.

	Peugue	Naujac	CDN	Lauzun
Water level (m NGF*)	1.72	1.2	1.2	-2.10

Regarding the setting of sampling time intervals, the four CSOs are within the same catchment, so the same sampling intervals are set at all sites (as in Table 12). This setting is based on past observed data and the size of the Louis Fargue catchment.

Table 12. Programmed sampling intervals of the automatic sampler used for campaigns in the Louis Fargue catchment.

Bottle Number	Sampling Interval (minutes)	Total Duration (minutes)
1	0	0
2	3	3
3	3	6
4	3	9
5	3	12
6	3	15
7	5	20
8	5	25
9	5	30
10	5	35
11	5	40
12	5	45
13	10	55
14	10	65
15	10	75
16	10	85
17	20	105
18	20	125
19	20	145
20	40	185
21	40	225
22	40	265
23	60	325
24	60	385

4.2.4 Rainfall measurement and storm events

There are fully available observed data from various rain gauges in the catchment (Figure 34) during the time between January 2015 and May 2017. For this research, rainfall data are processed and stored as volume (unit mm) every 5 minutes. The criteria to define a storm event is adapted from (Métadier *et al.*, 2013) and the expertise of the site operators:

- Minimum average rainfall intensity of the event is 0.1 mm/h
- Minimum total rainfall depth of 2 mm
- Minimum rainfall duration of 10 minutes

- Minimum 8-hour dry period between two storm events. This criterion is to account for the necessary period for the flow to go back to its dry weather conditions.

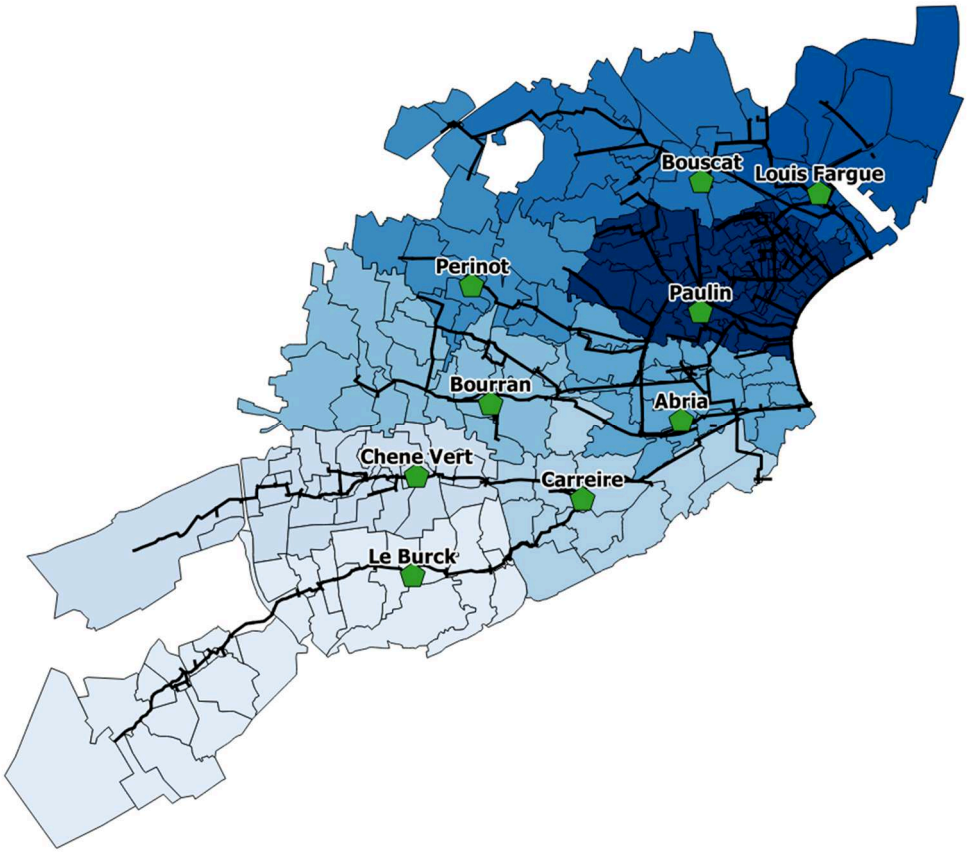

Figure 34. Distribution of rain gauges in the Louis Fargue catchment (after Maruéjouls and Montserrat (2016)).

Table 13 presents the characteristics of rainfall events for the sub-catchments with monitoring stations in the pilot site. For each sub-catchment, the statistics are derived from data obtained at the rain gauge nearest to the outlet, e.g. Abria for Peugue, Paulin for Naujac, Paulin for CDN, and Louis Fargue for Lauzun. It can be seen from the table that the features of storm events from the four sub-catchments are very similar.

Table 13. Characteristics of rainfall events in main sub-catchments from January 2015 to May 2017.

	Peugue			Naujac			CDN			Lauzun		
Number of rainfall events	155			145			146			137		
	min	mean	max	min	mean	max	min	mean	max	min	mean	max
Total depth (mm)	2	11	120	2	11.7	123	2	11.5	118	2	10.4	106
Duration (h)	0.5	17.5	130	0.75	18.4	185	1.3	17.8	121.7	0.8	16	119
Average intensity (mm/h)	0.1	1.0	10.8	0.1	0.9	10.9	0.1	0.9	6.7	0.2	0.9	4.9
Maximum intensity, 5 minutes (mm/h)	1.6	12.2	87.5	2.3	12.1	101.9	2.3	12.2	58.3	1.2	10.9	52.9
Antecedent dry weather period (h)	8	119	953	8	128	1010	8	128	1055	8	139	1010

4.3 SWMM-TSS detailed quality model for the sewer network

To perform RTC, it is crucial to develop a tool that can simulate main hydraulic and water quality processes within SNs. For the LIFE EFFIDRAIN project, the tool used for the Louis Fargue catchment is the SWMM-TSS model, which is based on the US Environmental Protection Agency's Storm Water Management Model (SWMM) version 5.1.11 (Rossman, 2015), associated with a user-defined improved library for water quality (Maruéjouls *et al.*, 2012; Montserrat *et al.*, 2017). The applications of this detailed model for RTC is presented in detail in the next sections. This section is meant to provide an overview on the model's background and development.

4.3.1 Background and theories

The SWMM software was first developed by the US Environmental Protection Agency in 1971, and since then many upgraded versions have been released. It is open source and commonly

utilized for planning, analysis and design related to urban stormwater runoff, and drainage systems. The software's graphical user interface furnishes an integrated environment for editing input data, defining parameters, running simulations, viewing and extracting the results easily. Furthermore, the software allows the inclusion of useful RTC elements such as storage units and actuators (pumps, weirs, and orifices). It gives possibilities to adjust the settings of the actuators throughout a simulation run by means of control rules written on a control editor.

SWMM is based on a node/reach concept to represent the hydraulics of the system. Flow routing within a network is governed by the conservation of mass and momentum equations for gradually varied, unsteady flow. The model provides the option of dynamic wave routing, which takes into account backwater, channel storage, entrance and exit losses, flow reversal, and pressurized flow. This can help to improve the model accuracy, but extends the computation time because a smaller routing time step is usually required to reduce numerical instabilities. Routing time step in SWMM is defined as the time step length used for calculation of routing flows and water quality constituents through the conveyance system. Figure 35 summarizes the most important processes included in the SWMM model and their interactions.

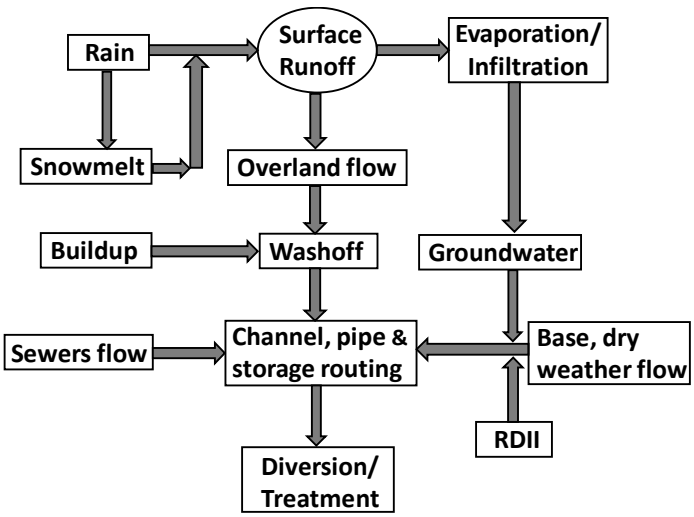

Figure 35. Main processes included in the SWMM model (inspired by Niazi *et al.* (2017)).

The user-defined improved library for water quality has been developed by LyRE since 2015 (see Montserrat *et al.* (2017)). The new library aims to reproduce better the solid transport processes in sewer systems:

- Buildup and washoff on catchments
- Distinction of particle size distribution depending on their origin (dry or wet weather)
- Sedimentation and erosion in the sewer
- Settling and solids removal in retention tanks

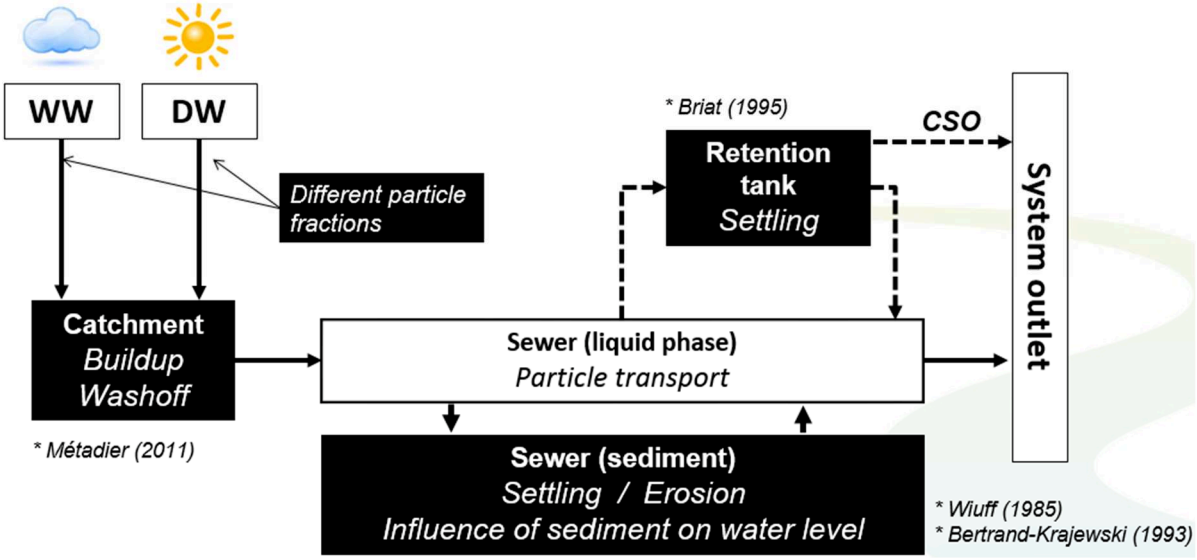

Figure 36. Water quality processes included in the SWMM-TSS model (after Montserrat *et al.*, (2017)). Black boxes indicate the processes improved by the new library, with given references for the used equations.

4.3.2 Model development for the Louis Fargue catchment

Model development for the Louis Fargue catchment is performed by Albert Monserrat (post-doctoral researcher) and Jing Feng (master student whose internship was co-supervised by the author of this thesis). This section is wholly devoted to present the main results of their works on calibrating and verifying the Louis Fargue model.

Model configuration of the Louis Fargue catchment is defined by transferring an existing hydraulic model built with the Infoworks ICM software. This existing hydraulic model was already fully calibrated. Calibration and verification of the Louis Fargue model are done using long-term measurement of turbidity, flow, and water level at the catchment outlets (Montserrat *et al.*, 2017), and focusing more on water quality. Detailed information about the treatment of raw water quality data, correlation between turbidity and TSS and measurement uncertainty are presented in Maruéjouls *et al.* (2018).

First of all, dry weather patterns are derived manually in order to reproduce the flow rates and TSS concentrations at the measurement points (i.e. four monitoring stations at the CSOs) during dry weather conditions. One week of dry weather per month is used to calibrate the model over one year. Different dry weather patterns (i.e. daily, weekly, monthly and seasonal) are thus obtained for each sub-catchment.

For wet weather conditions, buildup and washoff parameters are the most sensitive parameters to be calibrated. In addition, other parameters related to the hidden contributions due to rainfall dependent inflow and infiltration (RDII) are additionally calibrated to better simulate the discharges of sewers during the dilution period of storm events. RDII refers to the portion of stormwater that enters the pipes through direct connections of downspouts, foundation drains, etc., or the one of subsurface water via cracked pipes, leaky joints, faulty manhole connections (Rossman, 2015).

The model is calibrated using a one-month period in May 2016, which includes several storm events (see Figure 37).

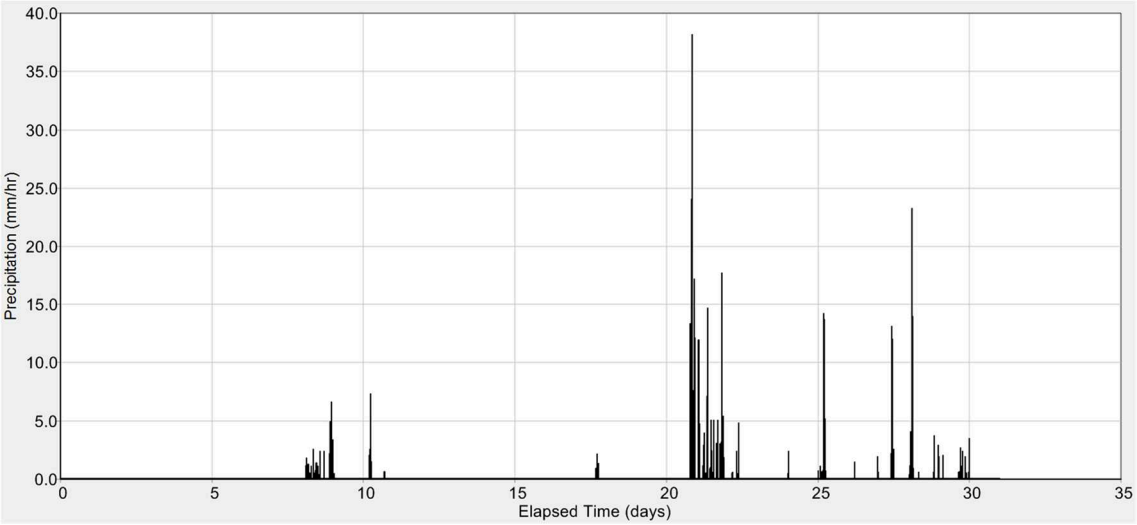

Figure 37. Observed rainfall data during May 2016 (after Feng, 2018).

Figure 38 to Figure 41 show the calibration results at Peugue and Naujac over the one-month period. Although the peaks of TSS at the two sites are generally overestimated, the model can basically reproduce the dynamics of observed data and the response of the catchments and networks during storm events.

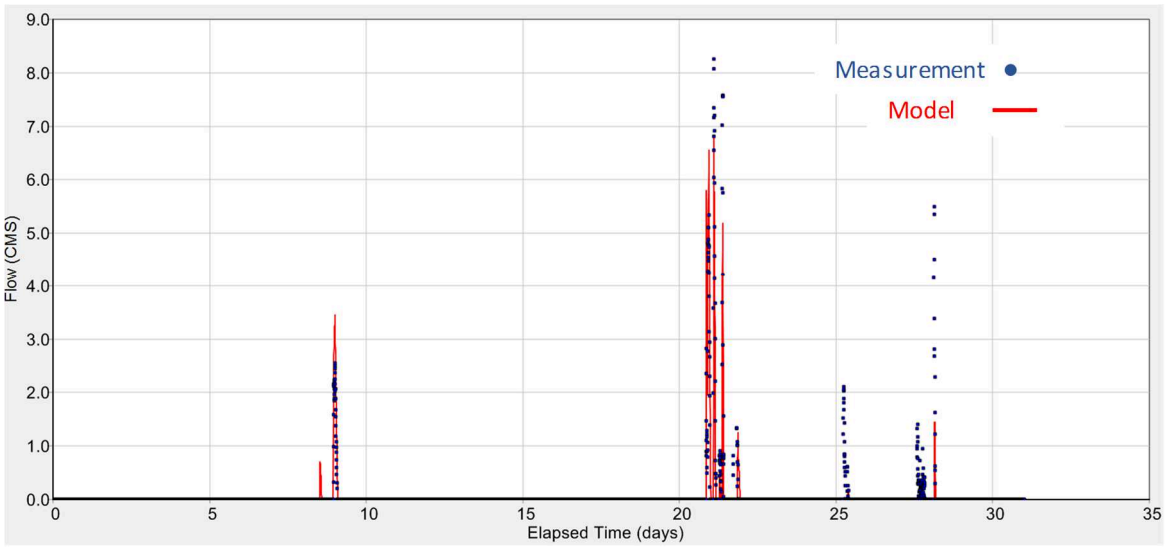

Figure 38. Observation versus modelling results of CSO flow at Peugue during May 2016 (after Feng, 2018).

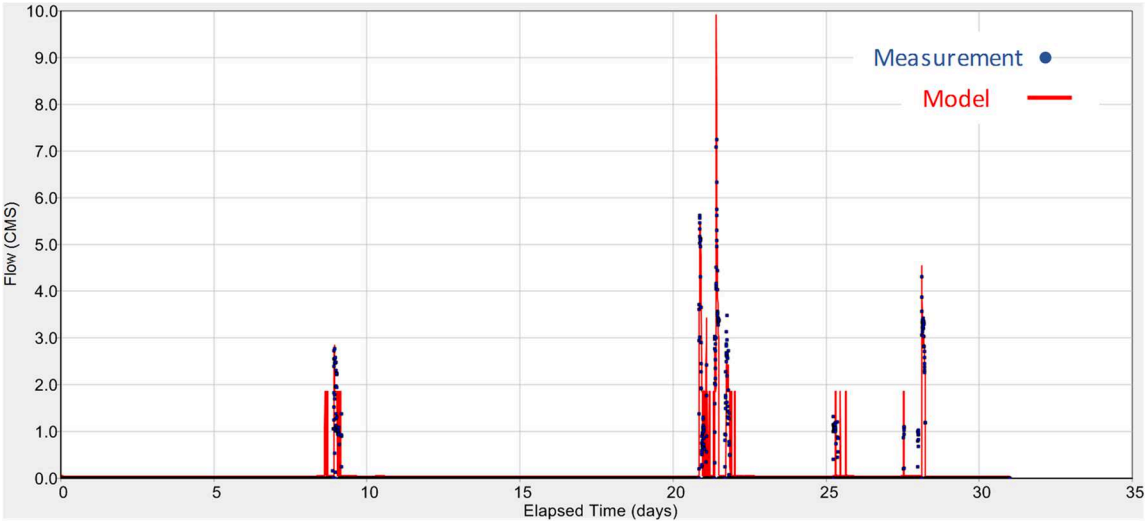

Figure 39. Observation versus modelling results of CSO flow at Naujac during May 2016 (after Feng, 2018).

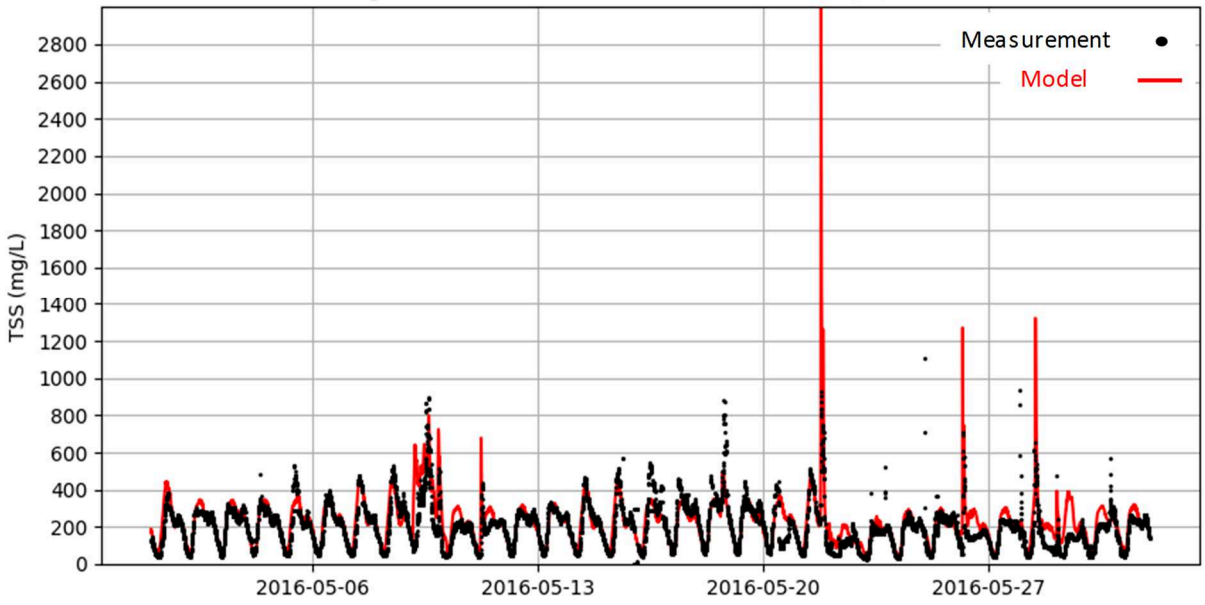

Figure 40. Observation versus modelling results of TSS concentration at Peugue during May 2016 (after Feng, 2018).

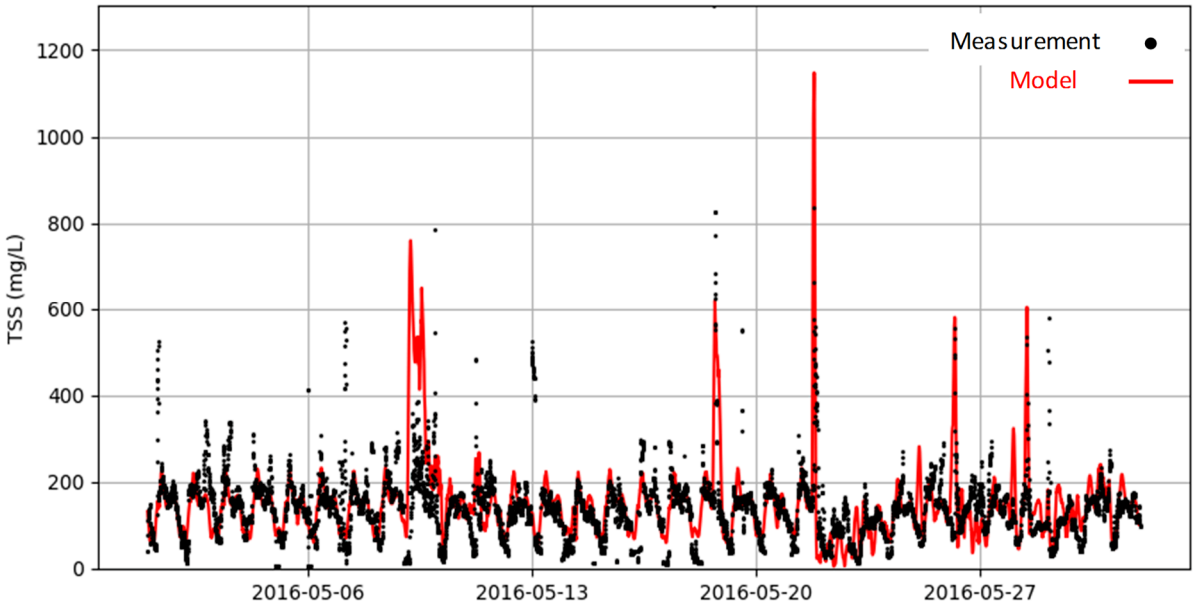

Figure 41. Observation versus modelling results of TSS concentration at Naujac during May 2016 (after Feng, 2018).

To verify the model performance, the model is run over a long period, between October 2015 and December 2016. Figure 42 and Figure 43 present the model performance at the four monitoring stations by plotting flow and TSS correlation graphs individually during the 15-month duration. The horizontal axis represents the observed data with five-minute intervals. The vertical axis represents the simulated data with the same time interval. The datasets of both observation and simulation are pre-filtered to remove the effect of extreme values. Consequently, 5% of each dataset are classified as outliers (shown as red points) and the remaining 95% (shown as blue points) are used to compute the performance indicators, i.e. Nash-Sutcliffe Efficiency index (NSE), Root Mean Squared Error (RMSE) and bias, according to the probability density function of distance. At CDN site, the online turbidity meter does not function well, so the availability of the TSS data is not sufficient to perform the correlation check.

In terms of flow correlations (Figure 42), it can be seen that NSE values of all the CSO sites are higher than 0.5 (e.g. 0.825 at Peugue, 0.713 at Naujac). Bias values smaller than 0.025 also show low impact of over- or under-estimation of the flows. Regarding TSS correlations (Figure

43), although the resulting performance indicators are lower, Figure 44 demonstrates that the model can give the contribution ratios of each sub-catchment outlets with always less than 5 % of differences between the simulated and the observed contributions.

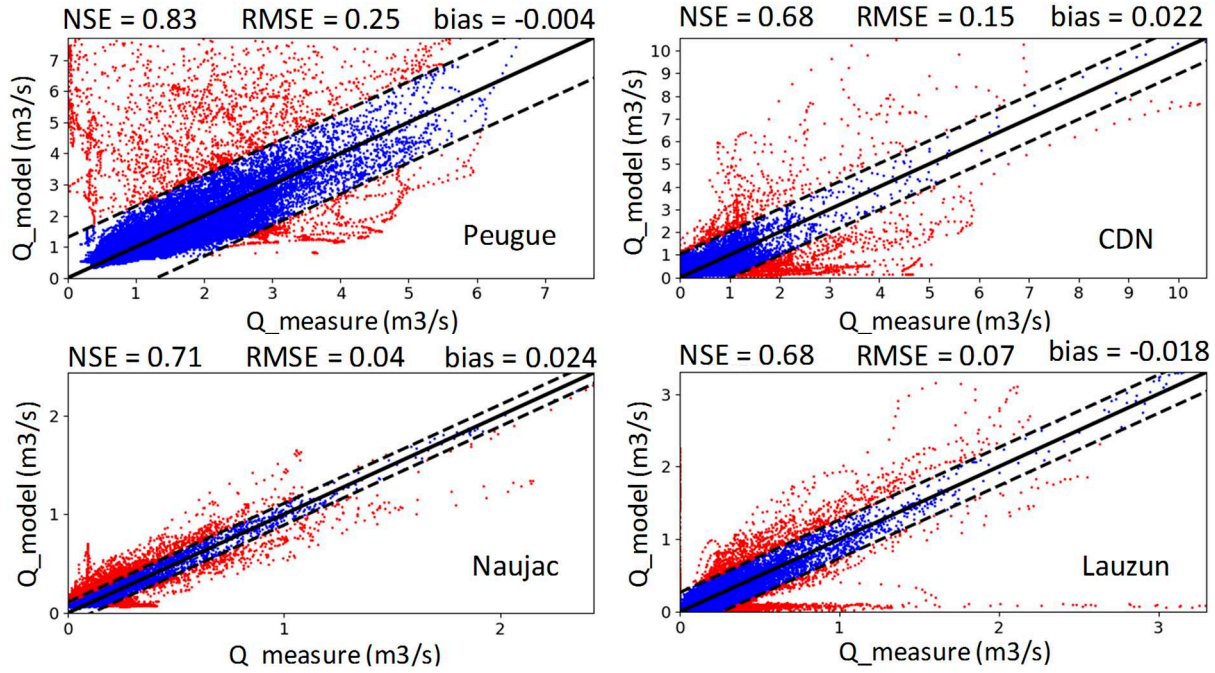

Figure 42. Flow correlation curves at 4 sub-catchments over 15 months (after Feng, 2018).

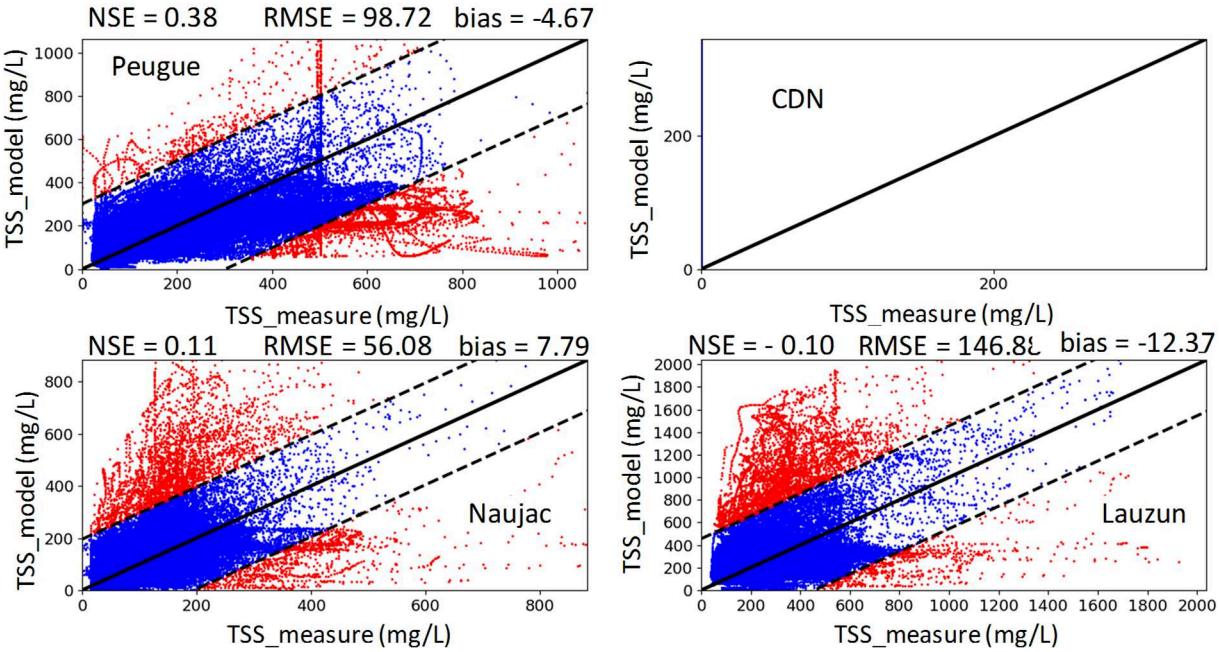

Figure 43. TSS correlation curves at 4 sub-catchments over 15 months (after Feng, 2018).

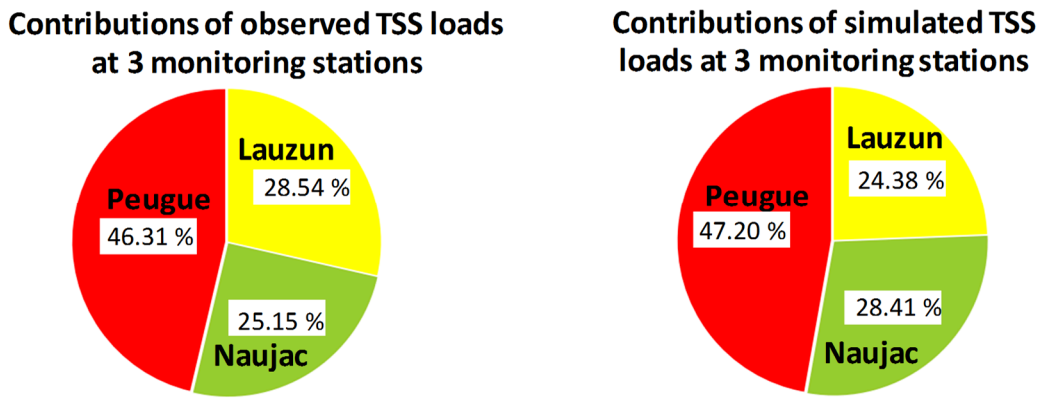

Figure 44. Contributions of the three outlets (Peugue, Naujac, Lauzun) in terms of TSS loads over 15 months (after Feng, 2018).

4.4 Summary

This chapter consists of three main sections. The beginning section first provides background of the Louis Fargue catchment in Bordeaux, which is prone to flooding due to several factors: climate, topography and tidal bore. As a result, a flood protection strategy has been implemented by the municipality since 1982. A large number of retention tanks, tunnels and pumping stations have been invested together with a telecontrol system (RAMSES) to manage UDSs and avoid flooding. Next, the first section also provides detailed description of the Louis Fargue. The catchment of 7700 ha has a wide network of retention tanks with storage capacity amounting up to around one million m^3. Currently, most of these tanks are operated by local or static control to protect the catchment from flooding. Additionally, since 2013 a global volume-based RTC system, named GD, has been implemented downstream the Louis Fargue catchment to further reduce flooding and CSO volumes. The receiving water of the SN may be exposed to the risk of oxygen depletion.

For this research, quality data (by turbidity meters), hydraulic data (by flow and level sensors) and rainfall data (by rain gauges) are collected from October 2015 to May 2017. Online hydraulic and quality sensors are located at the sub-catchment outlets, right upstream the CSOs

structures at Peugue, Naujac, CDN, and Lauzun. Sampling campaigns are also conducted to derive the correlations between turbidity and TSS, which is selected as the state variable for control in this research. To perform RTC, a core task is developing a detailed model that can simulate main water quality and hydraulic processes within the SN. The model used for the Louis Fargue catchment is the SWMM-TSS model, which is based on the US Environmental Protection Agency's SWMM version 5.1.11, associated with a user-defined improved library for water quality that allows better reproduction of solid transport processes sewer systems. On top of that, the procedure to develop the detailed quality model for the study area is elaborated, along with representative results when comparing between observed data and modelled data. In general, the model performance is considered as satisfactory (for hydraulics) and as acceptable (for TSS pollutographs) to allow RTC assessment.

CHAPTER 5: EVALUATION OF TWO STATISTICAL APPROACHES FOR ESTIMATING POLLUTANT LOADS AT ADJACENT COMBINED SEWER OVERFLOW STRUCTURES

As explained in section 1.2.2, there was an initial idea of using quick and simple regression models for process predictions of the QBR controller. Although this statistics-based approach was not pursued further to give priority to the mass-volume curve approach, the outputs from the development of the regression models are interesting and worth presented in this thesis. This chapter therefore describes the development of two statistical methods used for estimating total CSO loads of storm events: multiple linear regression versus random forest regression. The chapter is the pre-print version of the following paper with some minor changes indicated by italics and an additional figure (Figure 46):

Ly, D. K., Maruéjouls, T., Binet, G., Litrico, X., & Bertrand-Krajewski, J.-L. (2018). Evaluation of two statistical approaches for estimating pollutant loads at adjacent combined sewer overflow structures. *Water Science and Technology*, 78(3), 699–707.

5.1 Introduction

CSOs are long known as a major cause of receiving water quality degradation. Their processes and effects on receiving water have been comprehensively investigated and documented in previous papers, e.g. House *et al.* (1993) and Métadier and Bertrand-Krajewski (2011). There are several solutions to alleviate CSO effects; typical ones include disconnecting impervious surfaces, upgrading treatment capacity of the WWTP, adding retention tanks or sewer tunnels, and RTC of an integrated system. In Bordeaux, France, a system of HBR has already been implemented and operated at one of its catchments, Louis Fargue, since 2013 (Andréa *et al.*,

2013). Within the LIFE EFFIDRAIN project (www.life-effidrain.eu/en), the same catchment is further simulated with a QBR approach. As part of this project, one of the initial ideas was to develop local statistical models to predict TSS loads caused by CSO events, based on rainfall parameters derived from measurements by rain gauges.

Multiple options to develop statistical stormwater quality models can be found in the literature and regression is considered an effective and practical application of existing data to derive the relation between variables (Vaze and Chiew, 2003). Using rainfall and/or hydraulic observations, several regression models have been applied and presented in past publications to calculate storm event loads or event mean concentrations. However, few regression models use the same information to predict the pollutant load by a CSO event, e.g. the partial least square regression models by Sandoval *et al*. (2013). This study therefore proposes and compares two approaches for estimating CSO loads: the MLR (Multiple Linear Regression) approach implemented by Sun and Bertrand-Krajewski (2013) and the RFR (Random Forest Regression) approach proposed by Breiman (2001).

This paper aims to overcome major issues to the predictive ability of any regression model: proper selections of explanatory variables (EVs) and calibration data subsets. When there are many candidate EVs, a strategy to balance between under-fitting (with too few inputs) and over-fitting (with too many inputs) should be identified (McQuarrie and Tsai, 1998). Furthermore, different splitting methods of calibration and verification data subsets result in different model parameter evaluations. Data splitting can be performed in several manners. For instance, chronological splitting can be used to group all the observations before a specific point in time for calibration whereas the later observations are reserved for verification. However, this method as well as other random splitting methods would degrade the predictive capacity of the model if the calibration data subset contains observations with close ranges of recorded values (Montgomery and Peck, 1992).

5.2 Materials and methods

5.2.1 Study area and data-base

The Louis Fargue urban catchment has an area of 7700 ha and a population of approximately 300000 inhabitants. Its total sewer length is about 1340 km, of which 80 % are combined and 20 % are separate sewers. Its main outlet is the Garonne River. Along the river, there are five CSO structures within the catchment. However due to data availability, this study only focuses on three of them. Figure 45 displays the distribution of these CSO structures: Peugue, Naujac, and Lauzun, accompanied by the positions of nearby rain gauges used to analyse rainfall characteristics. In particular, the rain gauge named Abria is utilized for the Peugue CSO, Paulin for the Naujac CSO, and Louis Fargue for the Lauzun CSO. Distances between Peugue and Naujac, Naujac and Lauzun are around 1 km and 4.3 km respectively.

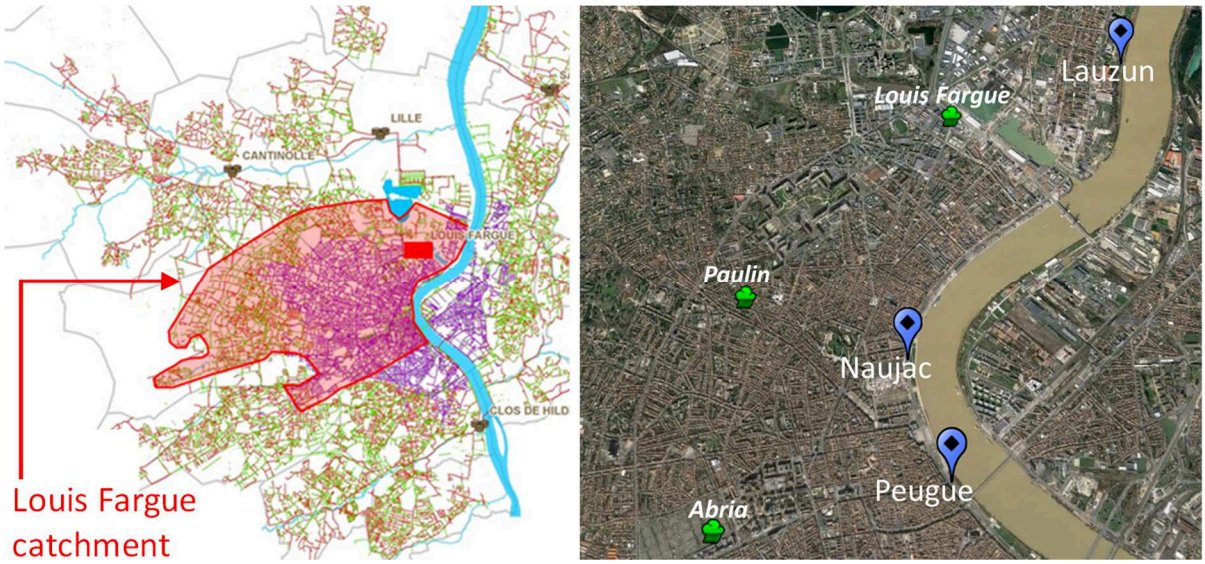

Figure 45. Louis Fargue catchment and locations of the CSO structures and nearby rain gauges.

Each CSO structure is equipped with a nephelometric turbidity meter and an ultrasonic flow meter, which allow continuous measurements of turbidity and flow rates downstream of each CSO weir. The recording time step for these sensors is set at 5 minutes, which is reasonable to

balance between measurement frequency for a 7700 ha catchment and required storage memory. TSS concentration is estimated through local calibration, which derives a correlation function between data provided by the online turbidity sensor and wet weather sampling campaigns for each CSO (Caradot *et al.*, 2015; Lepot *et al.*, 2016). Wet weather sampling campaigns are key for local calibration because lab-analysed values from grab samples of the campaigns are needed to determine the relationship with recorded values given by the turbidity meter. The resulting correlations for the four CSO sites are presented in Maruéjouls *et al.* (2017). Table 14 summarises the characteristics and measurement ranges of rainfall, volume and TSS load data from CSO events selected for developing the models. There are 32, 37, and 27 events used for model development for Peugue, Naujac and Lauzun respectively, and data collection period is between March 2015 and October 2016. There are other CSO events excluded from this study because of gaps in measurements.

Table 14. Rainfall characteristics, volume and TSS load of selected CSO events at three CSO structures.

	Peugue			Naujac			Lauzun		
Number of events	32			37			27		
Collection period	Mar 2015- Aug 2016			Mar 2015- Aug 2016			Oct 2015- Aug 2016		
	min	mean	max	min	mean	max	min	mean	max
Rainfall (RF)									
total depth (mm)	2.2	11.9	37.6	2.2	15.8	70.8	2.4	13.9	64.6
duration (hour)	1.0	14.2	61.2	1.6	17.8	84.4	1.7	15.3	75.6
average intensity (mm/hour)	0.3	1.7	10.8	0.2	1.4	5.6	0.3	1.2	3.1
max intensity, 5 min (mm/hour)	1.9	17.8	48.1	2.8	17.7	62.5	1.2	16.2	42.5
ADWP*** (hour)	8.1	105.1	792.3	8.9	117.6	1099.9	7.5	118.1	796.4
CSO volume									
total volume (m^3)	686	33200	147245	546	28727	425821	628	12341	113440
TSS									
total load (kg)	132	8297	41536	129	8100	99060	144	6454	32268

***ADWP: Antecedent Dry Weather Period

5.2.2 Multiple linear regression model

Two most common possibilities for the equation of a MLR model include:

$$Y = b_0 \prod_{i=1}^{n} X_i^{b_i} \quad \text{(Eq. 3)}$$

or

$$Y = b_0 + \sum_{i=1}^{n} b_i X_i^{b_i} \quad \text{(Eq. 4)}$$

where Y refers to the response variable (i.e. TSS load), X_i are explanatory or input variables obtained from rainfall characteristics, b_0 and b_i are model parameters to be calibrated.

Developing the MLR model is performed using the Python Numpy and Scipy packages (Oliphant, 2007) and contains three steps:

5.2.2.1 Pre-screening of candidate variables

Initially, the list of potential EVs contains all possible variables representing rainfall characteristics. To lessen the impact of multicollinearity, if two candidate variables are highly correlated (i.e. Pearson correlation coefficient is higher than 0.9), only one should be used to develop the model. After this pre-evaluation, the list of potential EVs is filtered and can be used in the next two steps of model development.

5.2.2.2 Selection of explanatory variables

The second step involves the use of leave-one-out cross validation (LOOCV) technique (Rudemo, 1982) and forward stepwise algorithm (FSA) *(Sun and Bertrand-Krajewski, 2013)* to select only useful EVs for the MLR model. For each run of a LOOCV procedure, one CSO event is reserved for verification while all the remaining CSO events are utilized in calibration. The procedure involves multiple runs and completes when all CSO events take part in verification. The verification performances of all runs are then averaged to represent the model's predictive capacity through the LOOCV procedure. The application of LOOCV generally helps to account for uncertainty due to separation of data subsets for calibration and verification.

In addition, FSA is incorporated to reduce the efforts of searching for the best combination of EVs. In order to find the first EV of the MLR model, it is first assumed that the MLR model has solely one EV. Each variable from the list of potential EVs is tested by applying the LOOCV procedure. The selected EV is the one which gives the highest model's predictive capacity. Similarly, the MLR model is then assumed to contain two EVs (the first one is already known) and each variable from the list of remaining variables is added to the model together with the known EV. The results of the LOOCV procedure are then evaluated to identify the second EV,

corresponding to the model with the highest predictive capacity. The selection of more EVs is repeated until the predictive capacity of the model cannot be further improved.

5.2.2.3 Splitting of dataset

The final step involves the application of hierarchical clustering to split the dataset for calibration and verification. The clustering method is adapted from Sun and Bertrand-Krajewski (2013) to group similar CSO events into distinct groups called clusters. In brief, the similarity between two CSO events is assessed by means of their standardized Euclidean distance. Using the computed distances, two similar CSO events are paired into a binary cluster. Similar binary clusters are gradually merged to form larger clusters until a hierarchical tree is built. Depending on the number of CSO events needed in calibration, the tree can be cut into different branches to form the expected number of clusters. If k CSO events are needed in calibration, the dataset is divided into k clusters and the most representative event from each cluster *(i.e. having the smallest sum of standardized Euclidean distances to other events in the cluster)* is picked for the calibration data subset. The remaining events are kept for the verification data subset.

In this study, calibration is performed with an increasing number k of CSO events until all events are chosen. In order to verify the proficiency of the cluster technique in selecting events for calibration, 2000 combinations of events are generated by random selection and used for calibration at each corresponding k number of calibration events. Higher number of the combinations of events were tested but given the size of the dataset, no significant variations in the results were observed. The resulting modified Nash-Sutcliffe efficiency indices (NS), as seen in Sun and Bertrand-Krajewski (2012), are summarized by five statistical values, i.e. minimum, lower quartile, median, upper quartile and maximum, and then compared with the modified NS given by using cluster technique. Besides, these statistical values are also

applicable for analysing the difference between MLR and RFR in terms of the range of error due to calibration data selection.

5.2.3 Random forest regression model

Random forest is an ensemble machine learning method based on bootstrap aggregation to enhance the decision tree method. By sampling with replacement of the original calibration data subset, a large number of trees are grown to maximum size without pruning, and aggregation is done by averaging the results from all trees (see Figure 46).

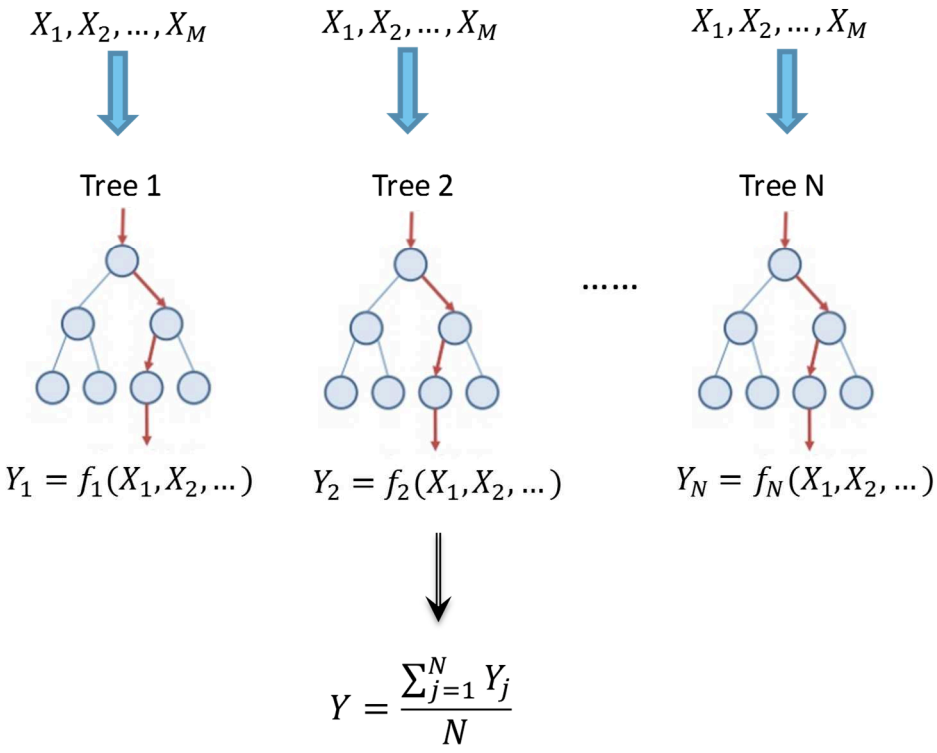

**Y: response variable; X: EV; M: total number of EVs; N: total number of regression trees

Figure 46. Illustration of the concepts of regression tree and forest.

For each tree, the set of EVs utilized to determine the best split at each node is randomly chosen from the total number of EVs (Prasad *et al.*, 2006). Due to bootstrapping, on average, approximately one-third of the events in calibration data subset are not used to build a tree. They are regarded as the out-of-bag (oob) events and used to compute the internal prediction

performance of the model (i.e. oob score, indicated by NS value) and then to evaluate the prediction strength of each variable (i.e. feature importance), avoiding the need of any cross-validation method (Archer and Kimes, 2008). Feature importance of a variable indicates how much the oob score would decrease if only that variable is permuted from the data subsets of oob events. More information on the conceptual aspects of RFR can be found in Grömping (2009).

The development of RFR is implemented by Python Scikit-learn package (Pedregosa *et al*., 2011) and involves an analogous three-step procedure as for MLR to allow straight assessments of the two approaches' performances. The main difference lies in the second step of selecting EVs, which utilizes RFR's measures of feature importance to eliminate trivial variables. Given the relatively small number of potential EVs, this study tailors the technique presented by Genuer *et al.* (2010) for the selection. Firstly, all the M potential EVs remaining after the first step of pre-screening are used as inputs of the RFR model. According to their feature importance outputs, they are subsequently ranked in a list of decreasing order of importance. Lastly, multiple runs of RFR models with increasing m number of inputs taken from the above list are performed (m = 1 to M). The variables involved in the model leading to the highest oob score are selected as the final EVs.

5.2.4 Model performance indication

Modified NS by which the variance of all observations is used for normalization (Sun and Bertrand-Krajewski, 2012) is applied as a goodness-of-fit indicator for all the models to enable direct comparisons and interpretation of different data subsets of the same or different sizes. Without normalization, a CSO event with a very large TSS load may substantially increase the overall variance of observed values in the selected data subset, resulting in a high NS value although the model performance is not satisfactory. As a result, the judgement when comparing

the performances of different models may be biased. The equation of the modified NS is proposed as follows:

$$modified\ NS = 1 - \frac{\sum_{i=1}^{n} \frac{e_i^2}{n}}{\sum_{j=1}^{N} \frac{(Y_j - \mu_Y)^2}{N}} \quad \text{(Eq. 5)}$$

where N is the total number of the available observations, n is the number of observations used for calibration or verification, μ is the mean of all observed values of Y, and e is the residual error.

In addition, modified root-mean-square error (RMSE), which is the RMSE normalized by the mean value of the response variable (Dembélé *et al.*, 2010), is also computed. Because of the good agreement between the results from these two indicators, this paper only presents the figures showing modified NS values.

5.2.5 Assessment of uncertainty

Based on the results obtained by hierarchical clustering, one RFR model and one MLR model are chosen for each CSO to assess their uncertainties. A chosen model should be amongst the models with leading verification performances while its calibration performance remains acceptable. Furthermore, the size of its verification data subset ought to be at least 10 % of the dataset.

The method of assessment requires each EV of the model to be associated with a probability density function (pdf). As an initial hypothesis, the pdf for each EV is assumed as normal (as applied e.g. by Dembélé *et al.*, 2011) with a standard deviation of 10 % of the mean value. Review of previous work shows that rainfall measurement uncertainty can vary in the order of 0 - 50 % (Willems, 2001), but the typical values are within the range of 0 - 15 % (Habib *et al.*, 2001; Weerts and Serafy, 2006). The selected value of 10 % is therefore considered as realistic and was used previously by Leonhardt *et al.* (2014). For the MLR approach, the 95 %

confidence interval of the response variable is derived by propagating the pdf associated to EVs using Monte Carlo (MC) simulations of 10^6 runs (Muste *et al.*, 2012). For the RFR approach, estimation of uncertainty is far more challenging due to its non-parametric nature. In this study, standard errors in a RFR prediction are obtained by applying the Jackknife and infinitesimal Jackknife procedures proposed by Wager *et al.* (2014). 1000 runs of MC simulations for the RFR model containing 1000 trees are carried out to propagate pdf of EVs and assess the 95 % confidence interval.

5.3 Results and discussions

5.3.1 Selection of explanatory variables

Pre-evaluation shows that model performance using the existing dataset is generally higher with equation (4), thus it is chosen for MLR model development. After pre-screening of candidate variables, potential EVs are obtained and listed in the first column of Table 15. *In addition to variables related to typical rainfall characteristics (depth, duration, ADWP, etc.), there are others variables formed by the products of ADWP and typical rainfall characteristics from the previous storm event. This could be explained by the importance of ADWP on the accumulation processes of SS.* From this list of potential EVs, selecting EVs is applied to sort out the useful EVs for each model. Table 15 shows the selected EVs for MLR and RFR models of the three CSO structures. It is obvious that the models for the three CSO structures do not share the same type and number of variables although the catchments of these structures are contiguous, with similar land use activities, and a majority of their rainfall, flow and quality characteristics are comparable (see Table 14). For Lauzun, the lower number of EVs compared to the other sites is due to the substantially high correlation between TSS load and rainfall depth (Pearson correlation coefficient amounts up to 0.92). MLR deems requiring more EVs than RFR, apart from the Lauzun case. It is equally interesting to observe that RFR tends to prefer input

variables having higher correlation with the measurand and excludes ADWP-related candidates, *which are usually part of published models*.

Table 15. Candidate EVs and EVs selected by the two approaches for each CSO structure model. Tick symbol indicates that a variable is selected as an EV for a model.

	Peugue		**Naujac**		**Lauzun**	
Variables	MLR	RFR	MLR	RFR	MLR	RFR
ADWP	✓					
RF depth	✓	✓	✓	✓	✓	✓
RF duration	✓		✓	✓		✓
Average RF intensity		✓	✓			
Max RF intensity, 5mins				✓		
Max RF intensity, 15 mins						
Max RF intensity, 30 mins		✓	✓	✓		
ADWP x last event's RF depth						
ADWP x last storm event's RF duration						
ADWP x last storm event's average RF intensity						
ADWP x last storm event's max RF intensity, 5 mins	✓		✓			
ADWP x last storm event's max RF intensity, 15 mins						
ADWP x last storm event's max RF intensity, 30 mins			✓			

5.3.2 Dataset division for calibration and verification

Model calibration and verification by the two approaches are performed with increasing sizes of calibration data subset using both random selection and cluster techniques. Resulting NS values are illustrated in Figure 47 and Figure 48. For plotting the outputs, the number of CSO events used for calibration starts from at least the number of EVs selected by either MLR or RFR, whichever is higher. The cluster technique clearly demonstrates improved prediction

ability (lower errors) compared to random selection as its verification NS values are mostly higher than the corresponding median values *(Figure 48)*. The box plots indicate that MLR typically shows lower performance in calibration compared to RFR *(Figure 47)*; nevertheless, in terms of verification *(Figure 48)*, MLR provides narrower range of NS values. Its median NS values are usually higher than the ones of RFR in the cases of Peugue and Lauzun, when there is higher correlation between explanatory and response variables *(Figure 48)*. On the other hand, RFR is better in capturing the non-linearity of the data for the Naujac case. Error in verification results *(Figure 48)* generally decreases when adding more calibration events and appears to be lower with MLR.

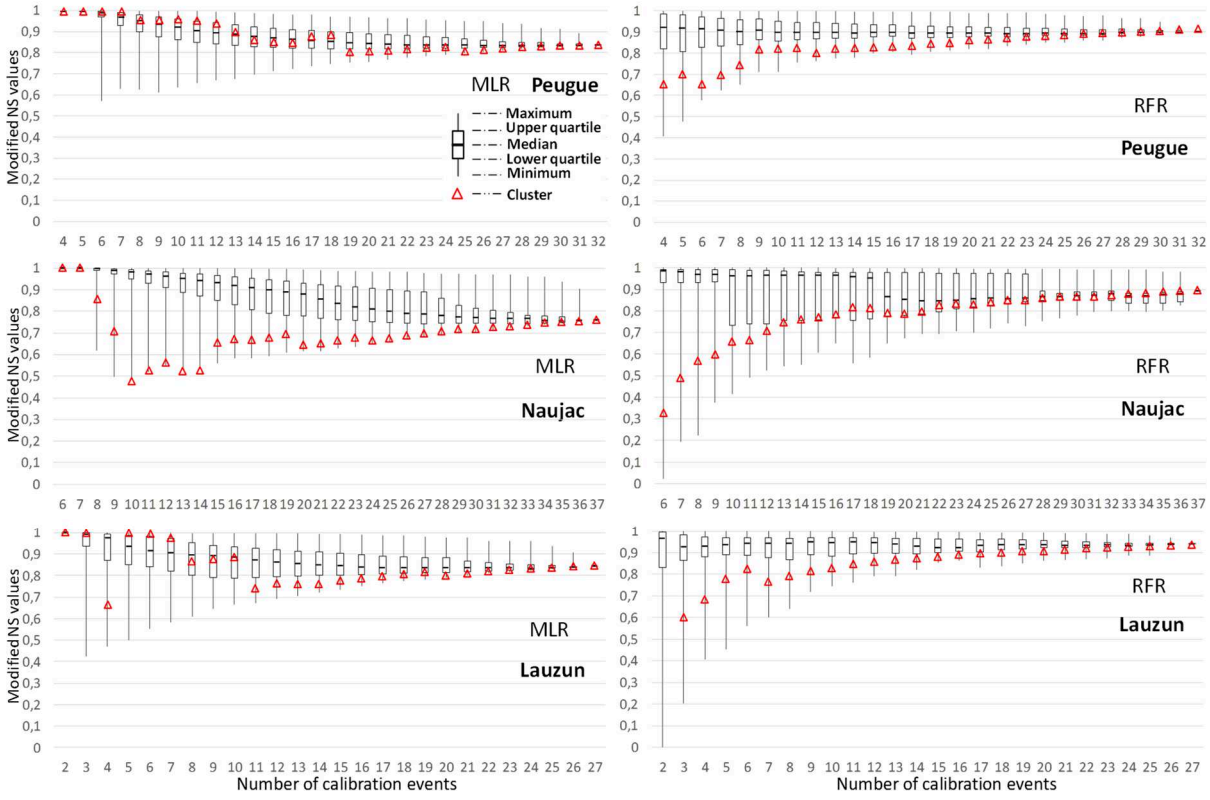

Figure 47. Calibration results at the three CSO structures obtained by the two approaches, left charts: modified NS by MLR and right charts: modified NS by RFR.

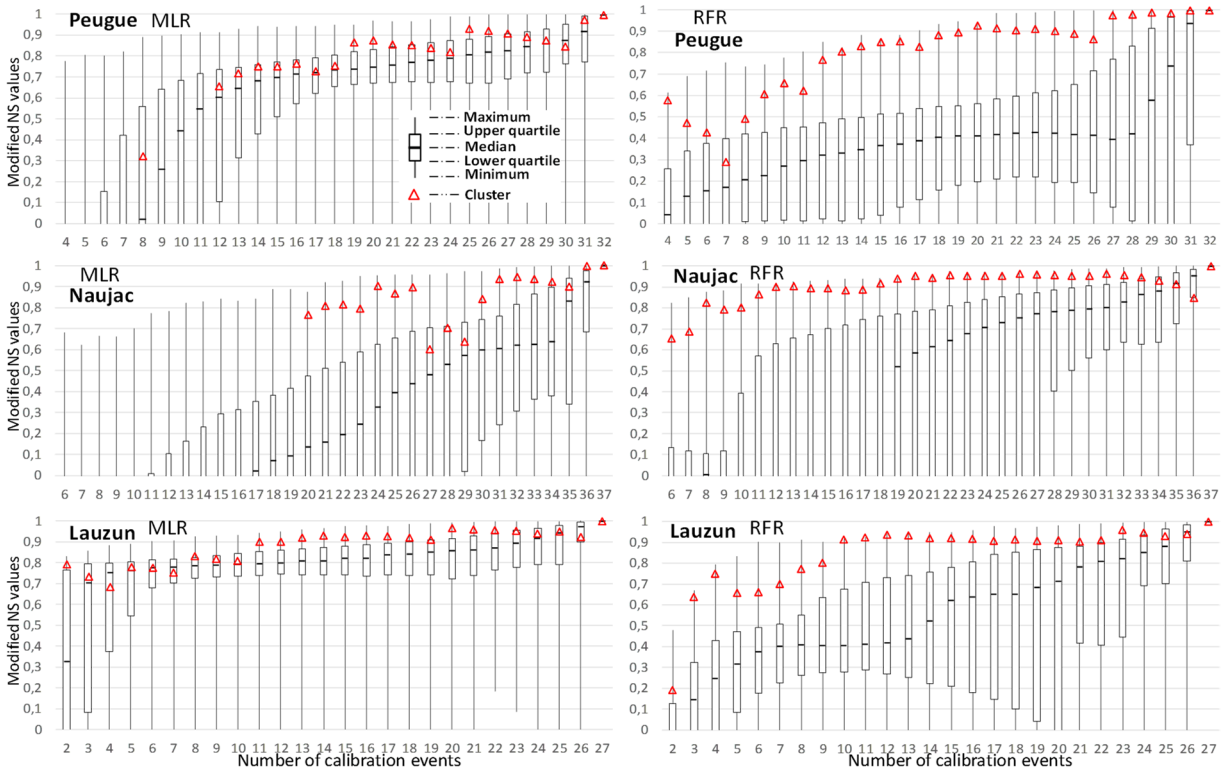

Figure 48. Verification results at the three CSO structures obtained by the two approaches, left charts: modified NS by MLR and right charts: modified NS by RFR.

5.3.3 Model uncertainty

MC simulation results are used to estimate the expanded uncertainty (with a coverage factor of 2, as applied in Muste *et al.* (2012)) for each CSO event. The units of expanded uncertainty are presented in both percentage and kg. For RFR models, the average expanded uncertainty of verification events of Peugue, Naujac, and Lauzun are about 50 % [±2781 kg], 28 % [±790 kg], and 18 % [±707 kg] respectively. For MLR models, most of them provide high expanded uncertainties and the lowest one belongs to the Lauzun model, which amounts to 78 % [±1958 kg]. The MLR model for Naujac *are* not satisfactory due to the very high expanded uncertainty [±35402 kg].

Given the widely varying magnitude of CSO events, from very small to large ones, it is convenient and operationally practical to sort the expanded uncertainties according to different ranges of simulated load values, as in Table 16. Particularly, all CSO events within the same

range of simulated loads (i.e. 0-5000 kg or 5000-10000 kg or > 10000 kg) are considered one group and the group's expanded uncertainty is obtained by averaging all values of individual expanded uncertainties. The expanded uncertainties of RFR models are globally lower than the ones of MLR model, both in calibration and verifications results. This could imply the RFR's benefit of the ensemble modelling to lessen the effect of measurement uncertainty. Figure 49 gives an example about the expanded uncertainties of MLR and RFR models at Lauzun. High expanded uncertainties are observed in the modelling results of MLR, particularly low-TSS-load events (less than 5000 kg) show significant larger expanded uncertainties than the other ones, e.g. approximately 85 % [±1940 kg] versus 30 % [±2068 kg] for the other events. Besides, it is interesting to note that RFR can be significantly more reliable for some predictions than for other ones. This is consistent with the observation by Wager *et al.* (2014) that RFR can give wider confidence intervals if the predicted values are considerably different from the measured ones.

Table 16. Expanded uncertainties of the two models according to the ranges of the simulated loads of CSO events.

	Expanded uncertainty in calibration results (± kg)						Expanded uncertainty in verification results (± kg)					
	PEUGUE		NAUJAC		LAUZUN		PEUGUE		NAUJAC		LAUZUN	
CSO events' loads (kg)	MLR	RFR	MLR	RFR	MLR	RFR	MLR	RFR	MLR	RFR	MLR	RFR
0-5000	4689	2627	15358	1241	1944	647	3590	1521	14937	790	1940	398
5000-10000	5599	3385	12140	4595	2310	3459	8613	4760	N.A**	N.A.	2068	3054
>10000	6746	6547	18023	12393	4557	3471	10335	10156	59960	N.A.	N.A.	32
Average	5593	4346	15806	4276	2658	2443	6235	2781	35402	790	1958	707

**N.A.: not available because the measured loads of selected events for verification do not fall in the considered range.

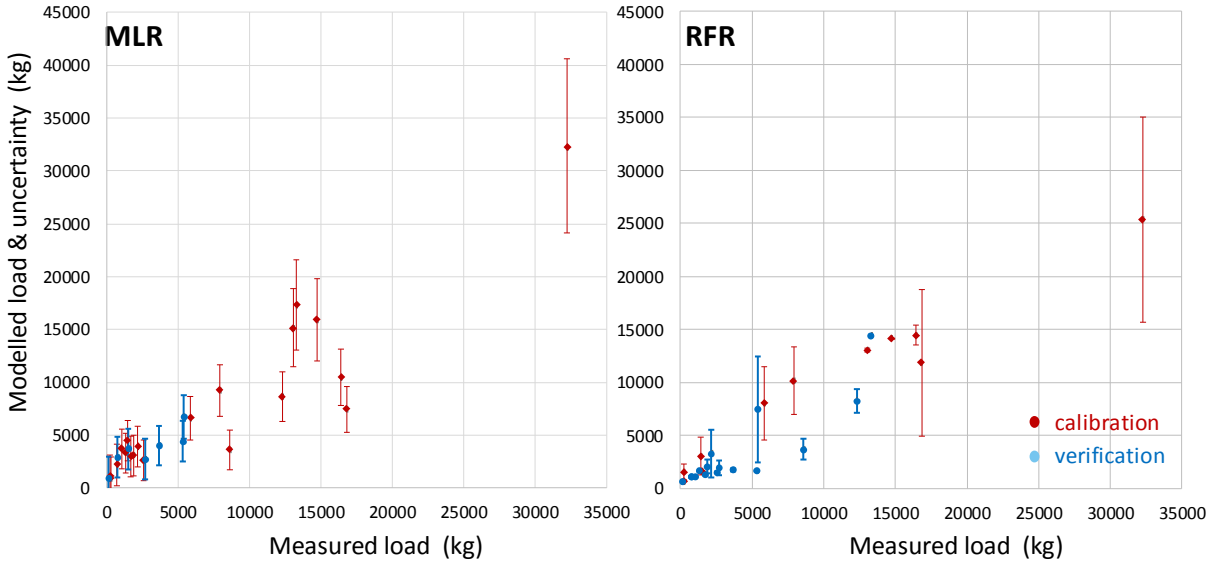

Figure 49. Observed versus simulated results with 95 % confidence intervals at Lauzun CSO structure.

5.4 Summary

This study on *empirical* modelling of TSS loads at three CSO structures in the Louis Fargue catchment, Bordeaux, France shows that the set of EVs depends on both the modelling approach (MLR or RFR) and varies with the CSO structure. For the available dataset, RFR requires fewer EVs than MLR. The cluster technique to select appropriate representative events for model calibration clearly enhances the model predictability for both approaches. MLR shows smaller variances of error due to calibration data selection, and higher performances of verification results. However, the uncertainties of simulated values in both calibration and verification of RFR models are seen to be lower than the ones of MLR models.

Given the current results, this paper provides a valuable means of evaluating CSO loads by regression models. In addition to the typical use of MLR, RFR may be an interesting alternative and worth consideration. Further improvement of the models for operational purposes can be achieved by applying a sensitivity analysis on the impact of the standard uncertainty of rainfall measurements and expanding the dataset by further data collection and analysis to include more CSO events. For this study, the developed regression models with better performance *can be*

applied to a simplified QBR strategy. Using rainfall forecast, the total CSO load of each sub-catchment can be quickly computed and recursively updated, facilitating the decisions of allocating excessive stormwater and prioritizing available storage capacities between different sub-catchments according to the magnitude of their CSO loads.

CHAPTER 6: APPLICATION OF STORMWATER MASS-VOLUME CURVE PREDICTION FOR WATER QUALITY-BASED REAL TIME CONTROL IN SEWER SYSTEMS: A PROOF-OF-CONCEPT STUDY

This chapter describes the concept and development of the new QBR strategy. To prove the concept, the QBR strategy is tested on a small test site over a large number of storm events. The chapter is the pre-print version of the following paper with some minor changes indicated by italics:

Ly, D. K., Maruéjouls, T., Binet, & Bertrand-Krajewski, J.-L. (2019). Application of Stormwater Mass-Volume Curve Prediction for Water Quality-based Real Time Control in Sewer Systems. *Urban Water Journal*, DOI: 10.1080/1573062X.2019.1611885.

6.1 Introduction

Pollutants discharged via combined sewer overflow (CSO) structures during storm events significantly deteriorate the quality of receiving water bodies. Real time control (RTC) is considered as a cost-efficient solution as it optimises the available capacity of a sewer network. RTC can help to prevent the need for construction of additional retention volumes, increases the network's adaptability to changes in water management policies, and above all alleviates the environmental impact of CSOs (Schütze *et al.*, 2008; Beeneken *et al.*, 2013). In RTC, real time measurements from the system are used to operate actuators (e.g. movable valves, weirs and pumps) by means of control rules in order to reach certain operational objectives. The majority of RTC implementations are hydraulics-based RTC (HBR), which aims at minimizing CSO volume or frequency through the use of real time hydraulic measurements. Several cities

in the world have been reported as successful sites for HBR system such as Quebec (Pleau *et al.*, 2005), Wilhelmshaven (Seggelke *et al.*, 2013), and Bordeaux (Andréa *et al*., 2013).

Water quality-based RTC (QBR) was initiated more lately due to the shortage of available and reliable quality data in urban drainage systems. Reduction of pollutant loads emitted by CSOs is normally expressed as the main objective of QBR. Campisano *et al.* (2013) reports that this control strategy has received increasing attention because of gradual advancements in wastewater quality sensors (turbidity, UV) and modelling tools. Various studies, e.g. Hoppe *et al.* (2011), Lacour and Schütze (2011), and Vezzaro *et al.* (2014), have proven the benefit of QBR by lowering pollutant loads released into receiving waters. Further motivation comes from adoption of more rigorous legislations to preserve receiving water bodies' ecological status, e.g. European Water Framework Directive and French Decree dated 21 July 2015 on the compliance of sewer networks.

This study is based on the application of mass-volume (MV) curves (Bertrand-Krajewski *et al.*, 1998) to propose a potential new and simple approach for QBR and presents the results of its application to a small sewer network, in comparison to HBR. Besides, sensitivity study is also performed to evaluate the impact of varying control parameters, such as the length of the control time interval (CTI) and the size of retention tank, on the performance of QBR.

6.2 Materials and methods

6.2.1 Study area and storm events

The hypothetical urban catchment in this study is adapted from the Périnot catchment to both facilitate quick and realistic features and represent a wide range of generic configuration for RTC demonstration (Figure 50). Périnot is part of the Louis Fargue catchment which covers most of the urban area in Bordeaux, France. The Périnot catchment has an area of 205 ha, an average imperviousness of 22.4 %, and accommodates approximately 2931 inhabitants. The

sewer network is combined and its total pipe length is 2054 m. The downstream part of the catchment includes a CSO structure and a retention tank of 1200 m^3 storage capacity. There is a rain gauge located inside the catchment and observed rainfall data are processed and stored as rainfall depth (mm) every 5 minutes.

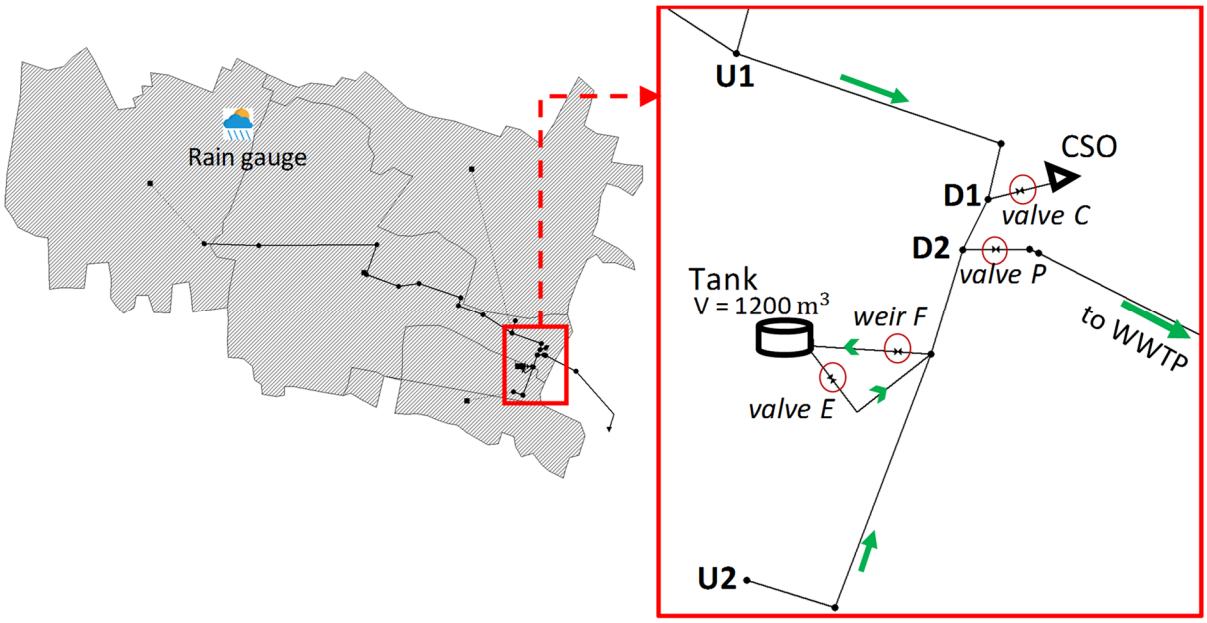

Figure 50. The sewer network and control elements.

The definition of an individual storm event in this study is based on criteria proposed for a nearby catchment in Bordeaux by Métadier *et al.* (2013). The concept of storm event in this study indicates a rainfall event that causes discharge through the CSO structure after filling the retention tank completely. The CSO event is considered as starting from the first rain droplet spilled to the environment and ending when the retention tank is entirely emptied, *including the whole CSOs period*. This study looks into storm events over a period of two years, between April 2015 and March 2017. Few storm events with extreme rainfall depth (around or more than 30 mm) are excluded because, in such cases, the priority operational goal of the operator is diminishing flood risks, *e.g. filling the tanks, transferring nominally maximum flow rate to the WWTP*, as quickly as possible *(see the description of GD's Flood mode in section 4.1.2.2)*. In total, 31 storm events with CSOs are available for testing the RTC strategies.

6.2.2 Quality state variable and modelling tool

The total suspended solids (TSS) concentration is used as the quality state variable for control since it is one of the primary sources of pollutant transfer within sewer pipes (Chebbo *et al.*, 1995). TSS indicates the amount of suspended solids (SS) in wastewater, which presents a surface for pollutant adsorption and consists mainly of organic matter. Specifically during wet weather, SS is reported to amount up to 80 % total mass of sediments, and regarded as the main vector for numerous pollutants such as BOD, COD, heavy metals, and petroleum hydrocarbons (Bertrand-Krajewski *et al.*, 1993).

Sewer hydraulics and main water quality processes related to TSS are simulated using the SWMM-TSS software, which contains an improved user-defined model library of the SWMM5.1.11. Compared to the original library developed by the US Environmental Protection Agency (Rossman 2015), important improvements include additional equations for better description of solids transport over the catchment surface, in the network and within the retention tank. The new library allows: classification of particles' settling potentials according to their origin, settling and solids removal in the retention tank, and the accumulation and erosion in the sewer network (Maruéjouls *et al.*, 2012). The model used for RTC strategies in this study is extracted from a full-scale model built for the whole 7700 ha Louis Fargue catchment, which is already calibrated and *verified* with long-term measurement data of turbidity, flow, and water level at four major catchment outlets (*see Chapter 4 and* Montserrat *et al.*, 2017). TSS time series are obtained from turbidity time series by means of their correlation derived from multiple sampling campaigns during storm events (as presented in *Chapter 4 and in* Maruéjouls and Binet, 2018).

6.2.3 Control elements

Referring to Figure 50, regulation of the weir F to fill the retention tank and the valve C to allow discharge through the CSO structure is based on the optimisation procedure which is described

below. Inlet offset of the side inlet valve C is at 0.54 m, three times the maximum dry weather (DW) water depth at junction node D1. Valve P settings depend on the water depth at junction node D2 to ensure that the flow to the WWTP remains always below 0.3 m^3/s, i.e. three times the maximum DW flow. Emptying of the tank is done after the rainfall event ends by adjusting valve E according to D2 depth too. All possible operational positions of the actuators are described in Table 17.

Table 17. Operation positions of the actuators used for RTC.

Actuators	Positions (opening of actuators: between 0 and 1)	Remarks
weir F	0: no fill 1: fill the retention tank	Settings are based on optimisation *(described in section 6.2.4.1 below).*
valve C	0: no CSO 1: allow discharge through CSO	Settings are based on optimisation *(described in section 6.2.4.1 below).*
valve P	0.033: if D2 depth is very high (> 0.57 m) 0.13: if D2 depth is high (between 0.31 m and 0.57 m) 0.25: if D2 depth is low (< 0.31 m)	Settings are dependent on the water depth of node D2.
valve E	0: no empty- the position of weir F or the position of valve C is set at 1 0.05: gradual empty- if D2 depth is low (between 0.19 m and 0.31 m) 0.25: fast empty- if D2 depth is very low (< 0.19 m)	Settings are dependent on the positions of weir F and valve C, and the water depth of node D2.

6.2.4 Control strategies

Two control strategies are performed in this study: QBR using MV curve *(section 6.2.4.1)* versus HBR *(section 6.2.4.2)*. Both share the primary objective of avoiding flooding in the network. The first strategy additionally targets reduction of CSO load while the second one

focuses on reduction of CSO volume.

6.2.4.1 QBR

The prediction of the event MV curve is key to the control concept of the QBR. An MV curve, by definition, refers to a dimensionless way of representing the variation of the cumulative pollutant load divided by the total pollutant load with respect to the cumulative volume divided by the total volume during a storm event. QBR aims to fill the tank during the highest peaks of the TSS flux. To capture such peaks, the QBR controller predicts the MV curve at an upstream pipe of the tank. From this curve, the controller can identify the CTIs with the highest increases of load versus volume, corresponding to the sharpest gradients of the MV curve.

Control simulation setup

The simulation setup is based on the principles of model predictive control (MPC) reported by Joseph-Duran *et al.* (2014) and Lund *et al.* (2018). The MPC involves two fundamental principles: receding horizon control (i.e. recursive repetition of the control actions within a finite CTI) and optimisation (i.e. determination of the optimal sequence of control actions within this CTI). Accordingly, the diagram in Figure 51a illustrates the closed-loop simulation scheme for QBR in this study.

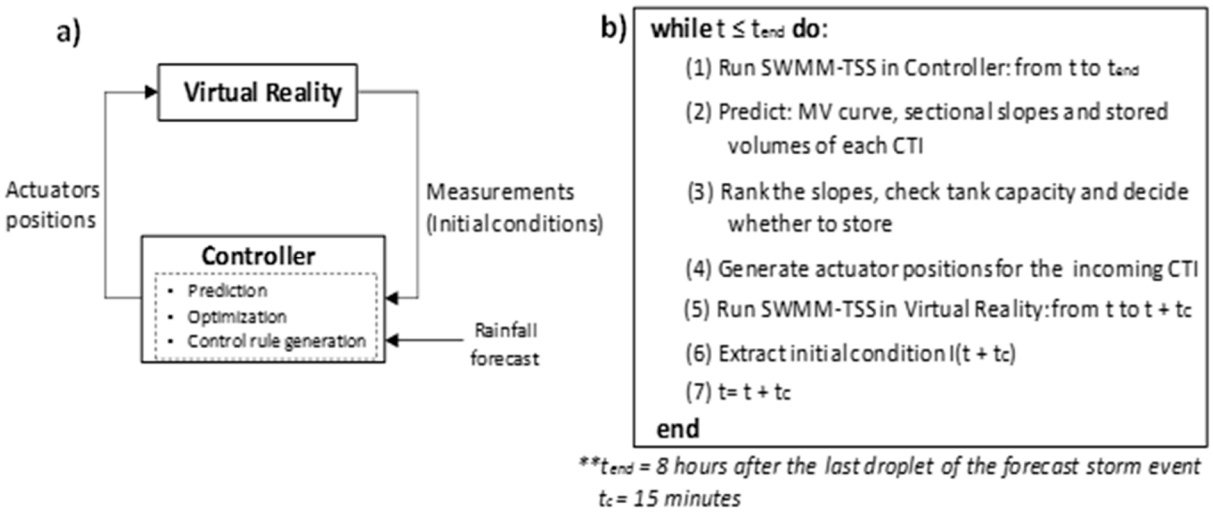

Figure 51. a) Block diagram of closed-loop simulation scheme; b) Summary of the QBR control algorithm.

The "Controller" block describes the function of the controller. It first runs a SWMM-TSS model simulation from rainfall forecast to flow and TSS processes, then performs optimisation *(described below, from page 164 to page 165)* and generates control rules for the incoming CTI. The "Virtual Reality" block is equivalent to the real system, but represented by another SWMM-TSS model to simulate what happens to the sewer network in reality. The control rules generated by the controller are implemented in the SWMM-TSS model by means of actuator positions, letting the model evolves from the beginning to the end of the CTI and measuring the system states to send initial conditions (i.e. corresponding to hydraulic and TSS measurements) to the next CTI. The initial length of each CTI is 15 minutes. The routing time step and the reporting time step of the SWMM-TSS models are set at very small values, one second and three seconds respectively, to ensure model convergence and accuracy. Given the time parameter settings, it takes, on average, around one hour to run QBR for a storm event of one-day duration with a computer server equipped with a 64-bit Intel® Xeon® CPU E5-2673 v4 2.3 GHz, 32 GB RAM.

In this study, uncertainty in rainfall forecast is not accounted for. As a starting point, this can be considered a reasonable approach to evaluate the potential of a new RTC method, reducing

the cost and challenge in searching for realistic and appropriate forecast rainfall data. If QBR does not perform better than HBR with assumed error free rainfall forecast, it is not worth to investigate further its potential.

Tasks of the controller

Figure 51b summarizes the main steps of the QBR control algorithm, including the tasks of the controller. The SWMM-TSS model in the controller is run for the period from the beginning of the incoming CTI until eight hours after the last droplet of the forecasted storm event. The eight-hour gap is sufficient to ensure that the tank can be completely emptied for all the 31 storm events. The simulated period consists of several CTIs: the incoming CTI and other later CTIs. Modelling outputs (flow and TSS) are used to draw the upstream MV curve for the simulated period. This MV curve can be divided into various curve sections; each curve section corresponds to one CTI. Estimation of each curve section's slope (i.e. sectional slope) is imperative to the optimisation task. In particular, the optimisation is carried out as follows:

- It first predicts the water depth at D1 during each CTI. Should D1 depth be predicted to be greater than 0.54 m during the incoming CTI, the sectional slopes of this CTI and all later CTIs with D1 depth also greater than 0.54 m are picked out. The selected sectional slopes are then sorted from the largest to the smallest values and assigned ranking numbers accordingly, e.g. rank #1 and rank #2 correspond to the largest and the second largest sectional slopes.
- Suppose that the sectional slope of the incoming CTI has ranking #*k*; if *k* is equal to one or two, it is necessary to fill the tank during this CTI. If not, exceeding volume in each CTI from rank #1 to rank #(*k*-1) can be obtained based on the difference between the simulated discharge upstream and its maximum DW discharge. When the sum of these stored volumes is less than the current tank capacity, it is possible to fill the tank during the incoming CTI,

ensuring that the storage capacity of the retention tank is fully utilized. Otherwise, filling of the tank is not allowed.

- Lastly, the control rules are based on the decision taken after optimisation, whether to fill the tank or not. For instance, when it is decided to fill the tank during the incoming CTI, e.g. from 9:15 to 9:30 and it still has available storage capacity, the position of the weir F should be set to 1. The controller then writes a control rule into the editor of the SWMM-TSS model in the virtual reality, using the format pre-defined by the software:

```
RULE FILL TANK
IF SIMULATION TIME > 9:15
AND SIMULATION TIME ≤ 9:30
AND TANK VOLUME < 1200
THEN WEIR F SETTING = 1
```

6.2.4.2 HBR

The methodology for HBR is based on MPC too but is far more simple. During the incoming CTI, the retention tank is filled if D1 depth rises above 0.54 m. When the retention tank is full, exceeding stormwater is spilled via CSO. This HBR is representative of the existing strategy applied to the Périnot catchment.

6.2.5 MV curve characterization

According to Bertrand-Krajewski *et al.* (1998), an MV curve can be approximated in a simplified way by a power function:

$$Y = X^{\beta} \qquad \text{(Eq. 6)}$$

where Y is the normalized cumulative pollutant load, X is the normalized cumulative volume and β (beta) is the fitted parameter. Each storm event has its own MV curve and corresponding

fitted β. The curve is meaningful to compare the pollutant load versus flow rate for different storm events.

Figure 52 displays the upstream MV curves and the histograph of the fitted β values for the 31 storm events. The MV curves are derived from both the flow and the TSS concentration arriving at junction nodes U1 and U2. These MV curves are calculated for the period between the start and the end of the storm events.

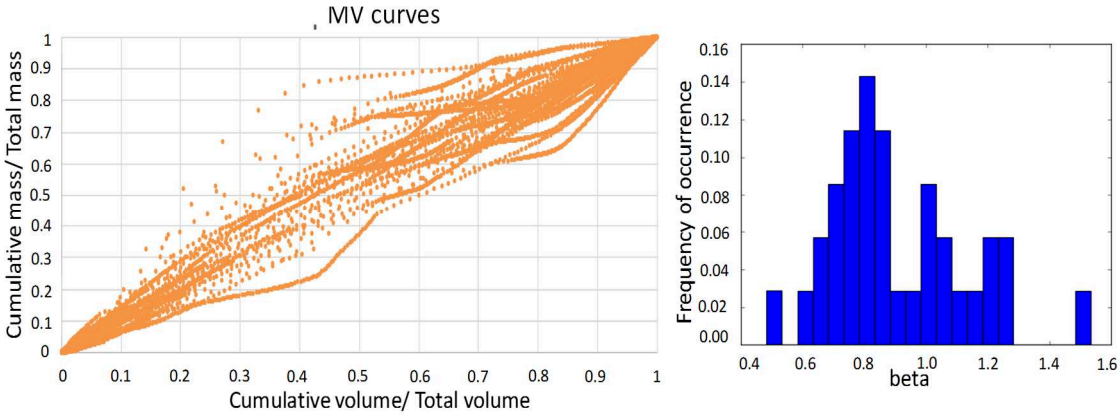

Figure 52. The 31 MV curves and the fitted β distribution obtained from all the storm events in the Périnot catchment.

6.2.6 Sensitivity analysis

There are several parameters which may affect the performance of a control strategy. This study explores: (i) the impact of the length of the CTI and (ii) the size of the retention tank on the performance of the QBR for a set of storm events. Different CTI lengths, i.e. 10 minutes, 30 minutes and 60 minutes, are applied to compare with the initially set length of 15 minutes. Similarly, different volumes of the retention tank, ranging from 600 m^3 to 2500 m^3 depending on the storm events, are also tested to assess the performances compared to the initial case with a volume of 1200 m^3.

6.2.7 Performance indicators

CSO total loads and volumes during the storm events are estimated to evaluate the performance of QBR compared with HBR. In addition, because the 31 storm events have widely varying magnitude of their loads, the results can be presented in terms of percentage difference between QBR and HBR to enable characterization or direct comparison of the benefits between different storm events. Equation (7) shows how the percentage difference of the overflow load for a storm event is calculated:

$$\text{Difference in CSO load} = \frac{Total\ CSO\ Load_{QBR} - Total\ CSO\ Load_{HBR}}{Total\ CSO\ Load_{HBR}} \times 100\ \ (\%) \qquad \text{(Eq. 7)}$$

Given the total CSO load obtained by applying HBR as a reference, a negative percentage difference in CSO load is equivalent to a decrease of the total CSO load discharged to the environment when applying QBR. In other words, this indicates the benefit of QBR over HBR in terms of CSO load. The second performance indicator includes the total loads and volumes transferred to the WWTP.

For sensitivity analysis of the CTI length, it is more meaningful to investigate the impact using only the total amount of the variables, rather than the percentage difference because it is not necessary to compare QBR and HBR. Given the HBR methodology, the impact of the CTI length on its performance is *indeed* trivial.

6.3 Results and discussions

6.3.1 Classification of storm events

Based on the results obtained by implementing the QBR and HBR control strategies on 31 storm events, it is possible to sort these events into three groups with a different range of β values:

- Group 1: $\beta > 1.10$
- Group 2: $0.85 \leq \beta \leq 1.10$
- Group 3: $\beta < 0.85$

Table 18 displays the overall results for each group. The application of QBR results in valuable load reduction for storm events in group 1 and group 2. This leads to an increase of the load transferred to the WWTP. These two groups represent nearly half of the storm events over the studied period. On the other hand, for group 3, the differences between the results of QBR and HBR are mostly insignificant.

Table 18. Summary of overall results obtained in three groups.

		Group 1	Group 2	Group 3
Number of storm events		7	8	16
CSO	Total load, HBR (kg)	3140	5604	11317
	Total load, QBR (kg)	2920	5192	11305
	Total volume, HBR (m^3)	19736	26230	66847
	Total volume, QBR (m^3)	19827	25167	67056
	Total load difference by QBR (%)	-7.00	-7.35	-0.11
	Total volume difference by QBR (%)	0.46	-4.05	0.31
WWTP	Total load, HBR (kg)	8443	10187	25497
	Total load, QBR (kg)	8564	10647	25511
	Total volume, HBR (m^3)	47566	46898	121006
	Total volume, QBR (m^3)	46706	47777	120668
	Total load difference by QBR (%)	1.43	4.52	0.05
	Total volume difference by QBR (%)	-1.81	1.87	-0.28

Group 1, group 2, and group 3 include storm events with MV curves largely below, around, and above the bisector line respectively (as seen on the right graphs of Figure 53, Figure 54, and Figure 55). The bisector line is the line (coloured black in the graphs) with the same ratio of relative load accumulation and relative volume accumulation *(corresponding to a constant concentration during the event).*

Furthermore, QBR helps to reduce markedly the total CSO loads for the majority of the storm events in group 1 (as seen on the left graphs of Figure 53), for almost half of events in group 2 (Figure 54), and for a minority of events in group 3 (Figure 55). Looking at all the storm events with load reduction higher than 5 % for the three groups, the percentages and amounts of load differences do not show a linearly proportional relationship. This may reflect that CSO load reduction due to QBR is independent from the magnitude of the storm event and their MV curves.

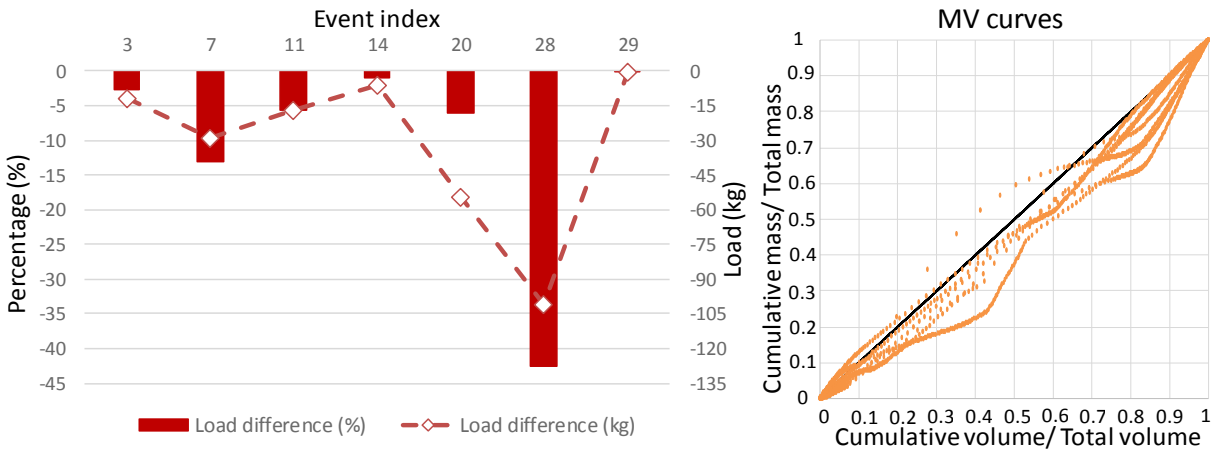

Figure 53. Total CSO load differences (QBR versus HBR) for all 7 storm events in group 1 (left) and their simulated MV curves (right).

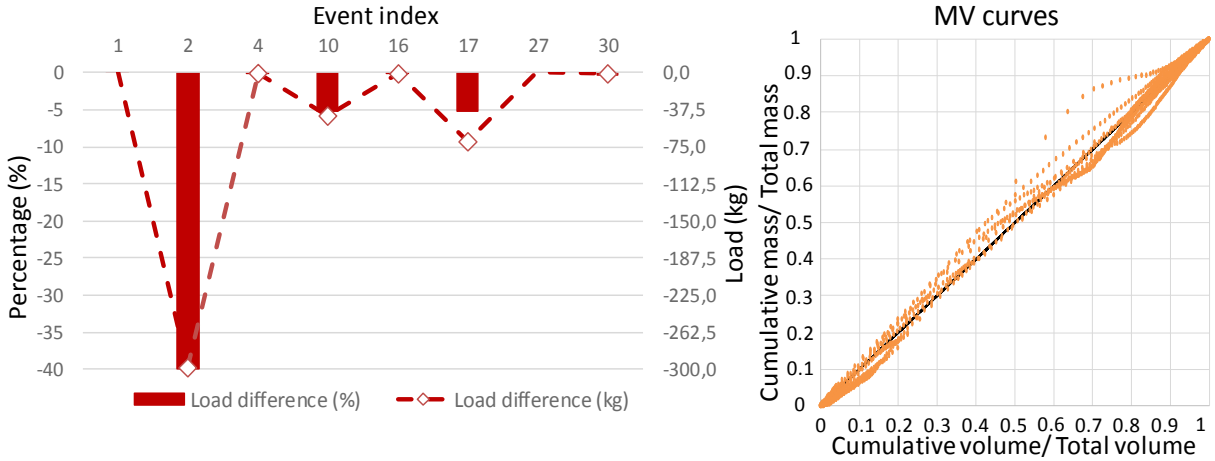

Figure 54. Total CSO load differences (QBR versus HBR) for all 8 storm events in group 2 (left) and their simulated MV curves (right).

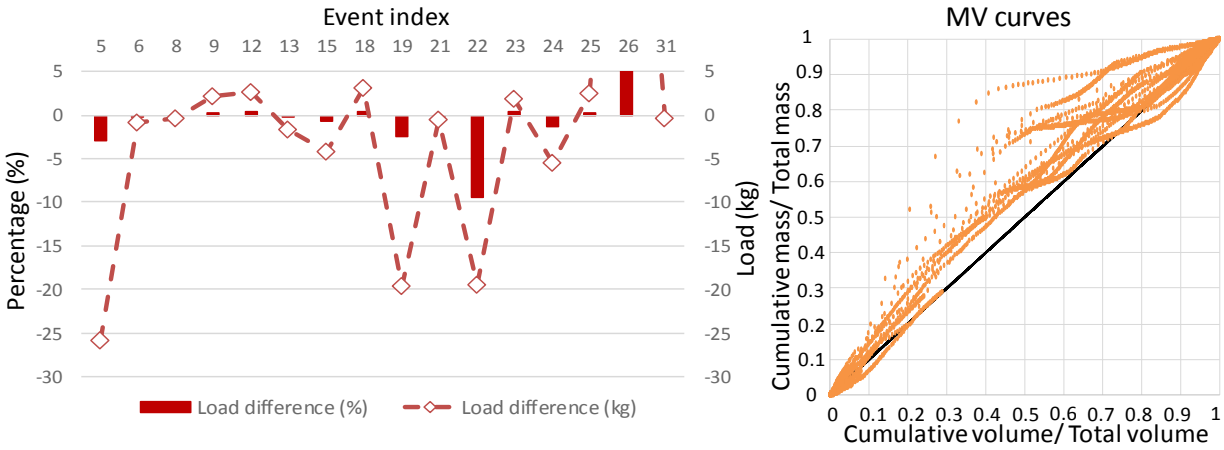

Figure 55. Total CSO load differences (QBR versus HBR) for all 16 storm events in group 3 (left) and their simulated MV curves (right).

The above classification of storm events is seen as comparable to the characterisation of storm event MV curves defined by Lacour (2009) for a few urban catchments in Paris. According to the same author, there are three groups of MV curves with similar ranges of β values (group 1: $\beta > 1.16$, group 2: $0.86 \leq \beta \leq 1.16$, group 3: $\beta < 0.86$) and similar MV curves positions related to the bisector line. Lacour (2009) further proposes that QBR is beneficial for the events from group 1, unlike the events from other groups. The results obtained from the study on Périnot catchment however show that QBR can also be beneficial for events from groups 2 and 3.

6.3.2 Performances of both strategies

In order to analyse the main differences in terms of performance of QBR versus HBR in each group, a couple of typical storm events are selected. This section first looks into storm event #7 in group 1. It has an approximately 1-month return period of rainfall, with a total depth of 15.6 mm and a rainfall duration of 14.5 hours. Figure 56 shows that QBR allows CSO discharges at the beginning of the event and fills the tank during the latter part of the event. This is in agreement with the evolution of the event's upstream MV curve (see the left graph of Figure 59). The grey boxes in Figure 59 highlight the periods when the weir F is opened by QBR to fill the retention tank. These periods obviously contain the highest MV curve gradients, i.e. the most polluted *fraction of* stormwater.

On the other hand, HBR stores all the exceeding stormwater from the start of the event to avoid CSO. Consequently, when the retention tank reaches full capacity, exceeding stormwater with substantially higher TSS loads has to be spilled out. Additionally, the downstream flow to WWTP is well maintained below the limit of 0.3 m^3/s for both strategies. It takes longer time for exceeding stormwater to fill the tank through weir F than to spill through valve C. Thus in both cases, there is always more stormwater in the network during tank filling, which leads to higher flow to the WWTP. In total, the CSO load spilled by QBR during the storm event is 13 % lower than by HBR although the CSO volume is 35.5 % higher.

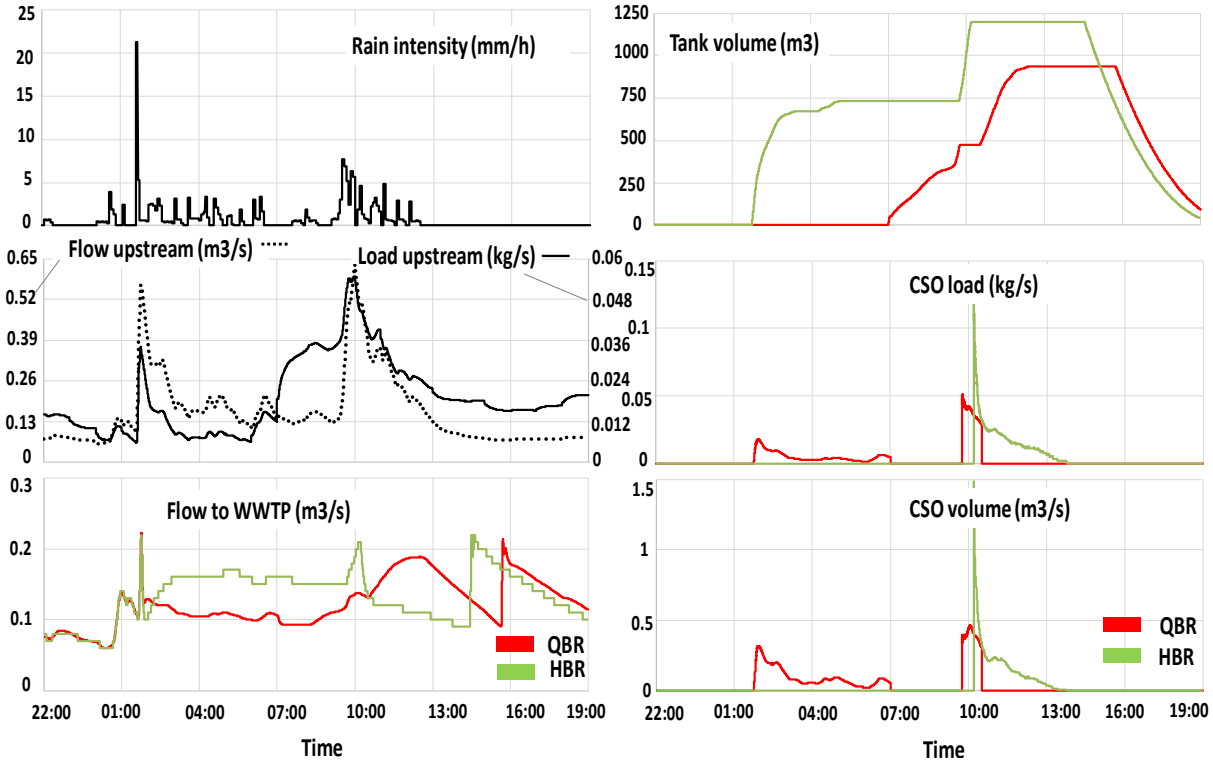

Figure 56. Differences in the results between the two control strategies for storm event #7 (group 1).

Next example is storm event #2 (group 2). Its return period is close to 2 months, with a total rainfall depth of 15 mm and a rainfall duration of 7.25 hours. Figure 57 shows that at the beginning of the event, both HBR and QBR lead to open the weir F to store exceeding stormwater in the retention tank at the same time. HBR then continues to fill the retention tank until it reaches its full capacity at nearly 7:00 AM. In contrast, QBR fills the retention tank over

three separate periods, as indicated by the grey boxes in the middle graph of Figure 59. The first two filling periods (of 1.5 hours and 30 minutes long respectively) correspond to CTIs whose section slopes are ranked either first or second. The final filling period extends much longer (more than 6 hours) because QBR predicts that the network will soon return to dry weather conditions and the retention tank still has storage capacity. It should be noticed that in some situations, although the weir is opened, very limited amount of stormwater can enter the retention tank. This is because the water depths in the network and in the retention tank are almost hydraulically balanced. On the whole, the CSO load spilled by QBR during the storm event #2 is 39.9 % lower than by HBR and the CSO volume is 37.6 % lower too.

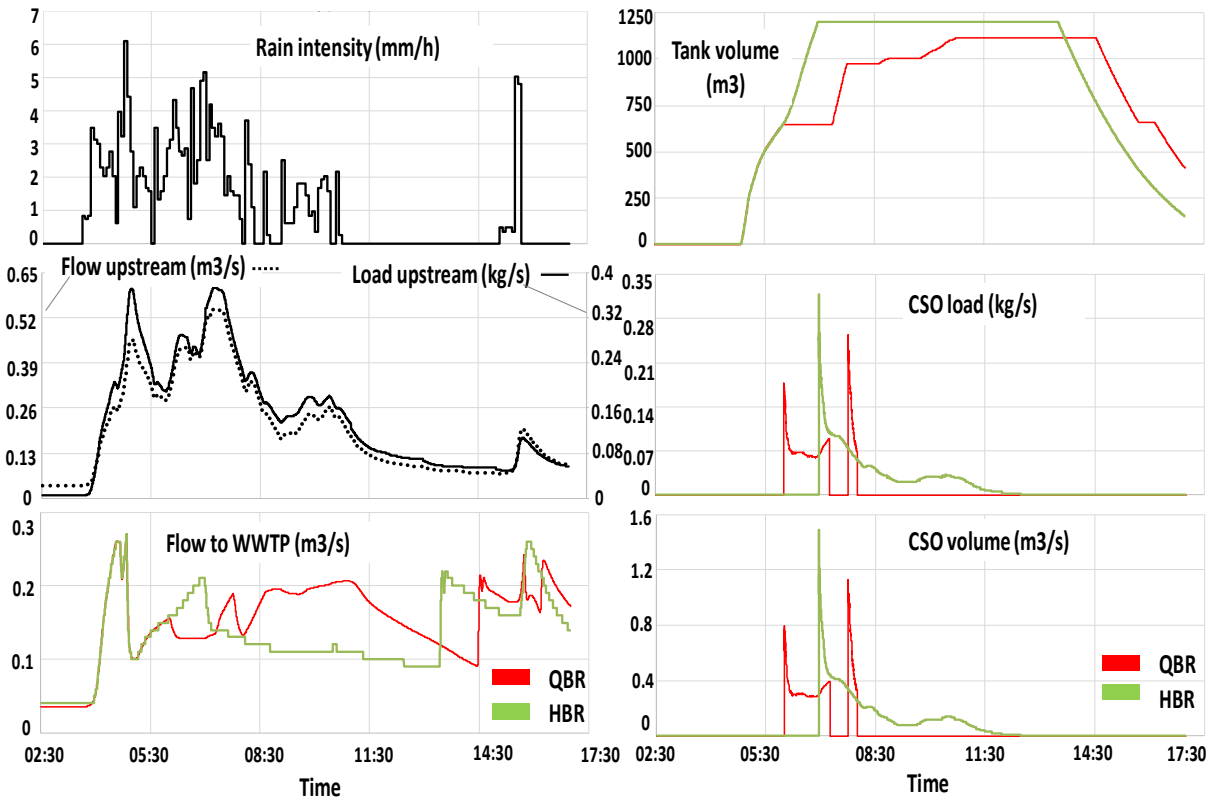

Figure 57. Differences in the results between the two control strategies for storm event #2 (group 2).

For group 3, most of the storm events do not show improved performance by applying QBR. Usually both strategies provide identical or nearly identical actuator settings and performances. This is because the highest MV slope occurs at the beginning of the storm event and along with

large discharge of stormwater. The storm event #31 is an example illustrated in Figure 58. The filling time of QBR (i.e. highest increase in the curve slope, as displayed in the right graph of Figure 59) overlaps the early part of the strong upstream flow period.

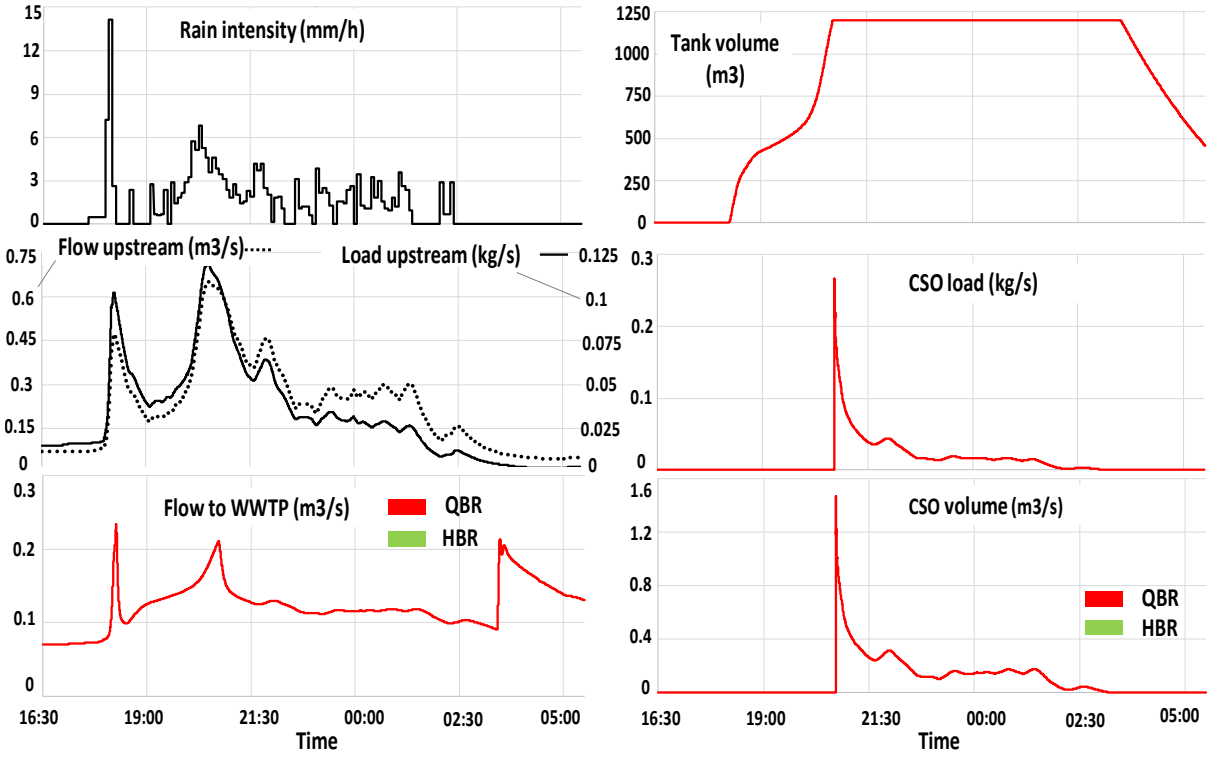

Figure 58. Similarity of the results between the two control strategies for storm event #31 (group 3).

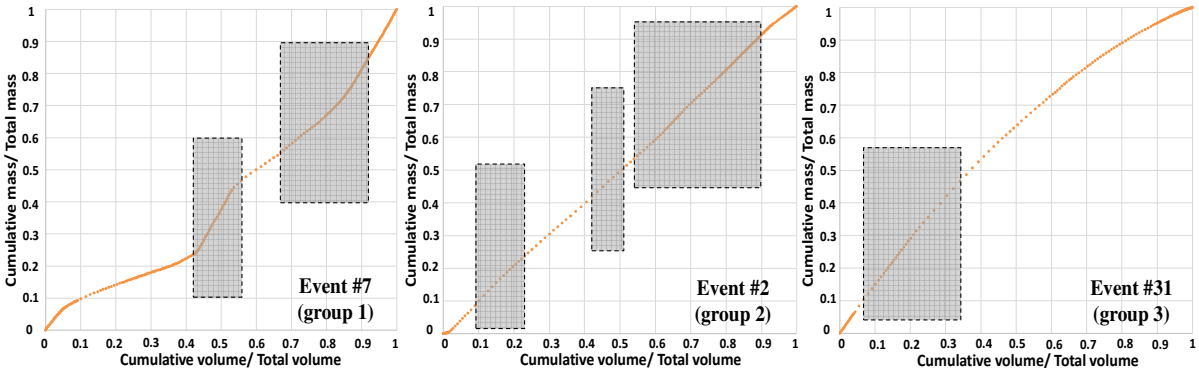

Figure 59. MV curves of the storm events #7 (left), #2 (middle), and #31 (right). Grey box indicates the filling periods of QBR.

Globally, when the MV curve highest gradients occur in the middle or late parts of a storm event (groups 1 and 2), it is highly likely that QBR performs better than HBR. This can be

regarded as an assessment criterion for the possibility of QBR application. There are 11 out of 31 storm events meeting the criterion (five events in group 1, three events in group 2 and three events in group 3). The total CSO load reduction of these storm events alone is around 10 %, with individual reduction values ranging from 3 to 43 %. In fact, the classification of storm events by β range is a relatively simple method to improve the probability of improved performance of QBR compared to HBR. For the dataset used in this study, group 1 tends to give the highest probability to find a storm event meeting the assessment criterion, followed by group 2, and the least by group 3. The results also show that there is no significant linear relationship between CSO load reduction by applying QBR, typical rainfall parameters (e.g. rainfall depth, rainfall duration, and max rainfall intensity over 5 minutes) and the fitted β values (see Appendix A).

6.3.3 Impact of the control time interval

To test the impact of CTI on the performance of QBR, this study picks out randomly two storm events from each group. Figure 60 illustrates that for the tested storm events of group 1 and group 2, decreasing the length of the CTI generally leads to decreasing the amount of total CSO load. Application of QBR with the CTI length of 10 minutes generates the lowest CSO load. *Shorter CTI length means that the optimisation is performed at higher frequency. This can help to improve the performance of QBR.* On the contrary, the CTI length of 60 minutes always shows the worst performance regarding CSO load. The results from group 3 do not show a clear benefit with smaller CTI. This is due to the fact that the retention tank is filled continuously and reaches its full capacity right at the beginning of the storm event, corresponding with the period of strong runoff. The length of the CTI cannot have a significant effect in such cases.

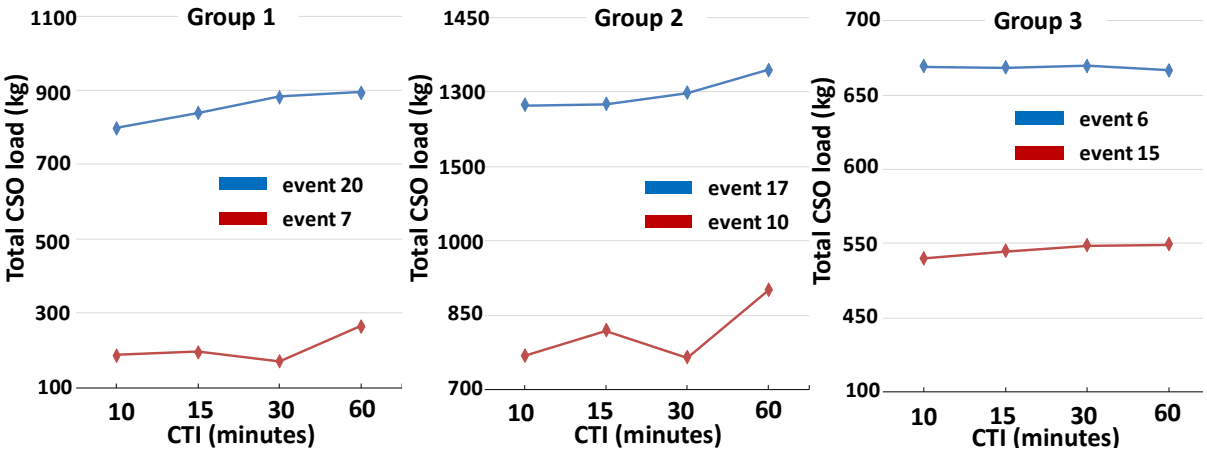

Figure 60. Impact of varying control time intervals (CTI) on the total CSO loads obtained by implementing QBR on tested storm events.

6.3.4 Impact of the retention tank volume

Storm event #20 from group 1 and storm event #2 from group 2 are used to investigate the impact of tank volume on the performance of QBR. Different volumes are tested to draw the complete profile of CSO load differences (between QBR and HBR) with the tank volume, as shown in Figure 61. In both cases, there is a threshold of starting volume, under which QBR cannot bring higher load benefit than HBR (900 m^3 for storm event #2 and 1800 m^3 for storm event #20). Looking back at Figure 57, both strategies fill the tank at the event beginning and at the same time. When the tank volume is merely 900 m^3, it is completely filled during the first filling period of both cases, resulting in the same performance. There is another threshold of ending volume (1950 m^3 for storm event #2 and 2500 m^3 for storm event #20), below which the retention tank can store all the exceeding stormwater, i.e. there is no CSO discharge. This explains why there is no CSO load difference between the two strategies. Besides, the variation in the CSO load difference with different tank volumes is prominent. It is interesting that in both storm events, the performance of QBR rises with increasing volumes, reaches a peak and then drops rapidly. This poses a further question on how to design the volume of a retention tank that works best with a RTC strategy based on water quality information.

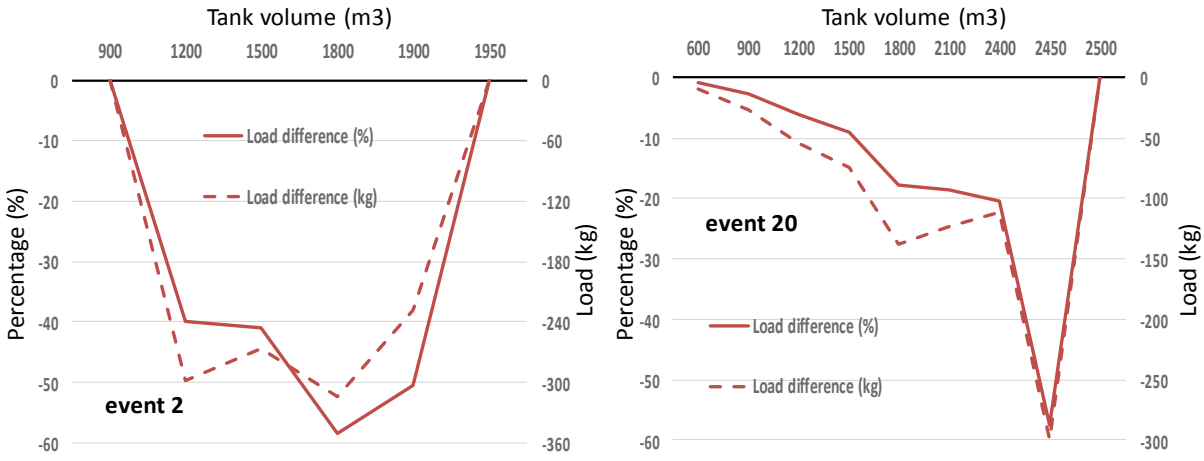

Figure 61. Total CSO load differences (QBR versus HBR) by various tank volumes for the two tested storm events.

6.3.5 Assumption on uncertainties

In addition to the assumption of error free rainfall forecast mentioned above, it is worth noting that the closed-loop control is demonstrated using a physically based model simulator as a virtual reality and without accounting for uncertainties in flow and water quality measurements. These conditions were applied as a first approach to assess the potential benefit of QBR versus HBR. Before implementing QBR in real operation, further works are definitely needed to develop a more complete understanding, including the effects of the mentioned uncertainties. In the next chapter, the author will present a method to quantify the uncertainty in QBR performance due to uncertainty in MV curve prediction.

6.4 Summary

Aiming to reduce CSO loads discharged into the receiving water bodies, a new QBR approach based on MV curves prediction is assessed in the case of the Périnot catchment in Bordeaux, France for a set of 31 storm events over 2 years, and compared with a more traditional HBR approach. It appears that the efficiency of QBR depends on the shape of the predicted MV curve. QBR provides the largest benefit in case of storm events where the steepest gradients of their MV curves appear in the middle or late part of the event duration. This may be considered

as a criterion to evaluate the possible benefit of applying QBR. There are 11 out of 31 storm events meeting this criterion and their total CSO load reduction is approximately 10 %. Reduction values of individual storm events vary between 3 and 43 %.

Accordingly, three types of MV curves may be distinguished as a first approach: groups 1, 2 and 3 with their MV curve respectively below, around, and above the bisector line. According to this typology, group 1 tends to provide the highest probability of storm events meeting the assessment criterion, followed by group 2, and the least by group 3. Furthermore, sensitivity analysis on the impact of CTI illustrates that for storm events in groups 1 and 2, decreasing the length of the CTI generally leads to decreasing the amount of total CSO load or, in other words, improving the efficiency of QBR. Next, the volume of the retention tank is deemed to play an important role in the performance of QBR. Based on the tests applied on the two storm events, the change in the CSO load reduction by QBR (compared to HBR) with different tank volumes is truly significant.

To sum up, the results indicate the true potential of using MV curves for QBR. It could provide an effective alternative to the management of retention tanks to minimise pollutant loads sent to the environment. The simplicity of the approach is clearly an advantage over other RTC solutions which are based on advanced optimisation techniques.

CHAPTER 7: APPLICATION OF THE NEW WATER QUALITY-BASED REAL TIME CONTROL TO THE LOUIS FARGUE CATCHMENT

7.1 Introduction

Results from the proof-of-concept study (chapter 6) show the true potential of applying MV curve prediction for QBR in sewer systems. It brings valuable improvement in terms of CSO load reduction for the Périnot test site. The new QBR strategy is then implemented on the Louis Fargue catchment and, in the same way, compared with a typical HBR strategy. It is interesting to evaluate the robustness of the QBR controller towards a different and much larger system.

Furthermore, this chapter presents the assessment related to the impact of uncertainty of model prediction on the QBR controller performance. This chapter also looks into the sensitivity of storage tank volume on the performance of the two control strategies. By varying the tank volumes, the main goal is: i) to understand the changes in CSO loads obtained by each individual strategy and ii) to compare the CSO load reduction for both strategies. Besides, to serve the extension of QBR to additional retention tanks on the Louis Fargue catchment, sensitivity analyses are also performed to estimate the most useful volumes for QBR of these additional tanks.

7.2 Materials and methods

7.2.1 Control elements

The catchment modelled in this study is the Louis Fargue urban catchment located in Bordeaux, France. As previously mentioned, CSO discharges into the Garonne River come from five CSO points and WWTP bypass. The main interceptor receives and transfers upstream water to the WWTP. Full descriptions and background related to the system are presented in Chapter 4.

One of the enthralling features of the catchment is the great number of retention tanks, which were built within the catchment over decades to protect the downstream urban areas against flooding (see section 4.1). In this research, three tanks, Carmaux, Abria, and Alhambra (blue cylinder symbols in Figure 62), with volumes of 8000 m^3, 6000 m^3 and 1500 m^3 respectively, are selected for implementing the control strategies. The above volumes are lower than the volumes in reality because in order to keep the primary functionality of the above tanks, designed for flooding control, only a fraction of them is used for pollution control. This allows quick recovery of the tank storage capacities, in order to be well prepared when there are new rainfall events coming shortly. Filling and emptying of these tanks are done by adjusting the positions of weirs/gates and pumps respectively. Furthermore, QBR is also applied to the interceptor, in the proximity of Naujac and CDN CSO structures.

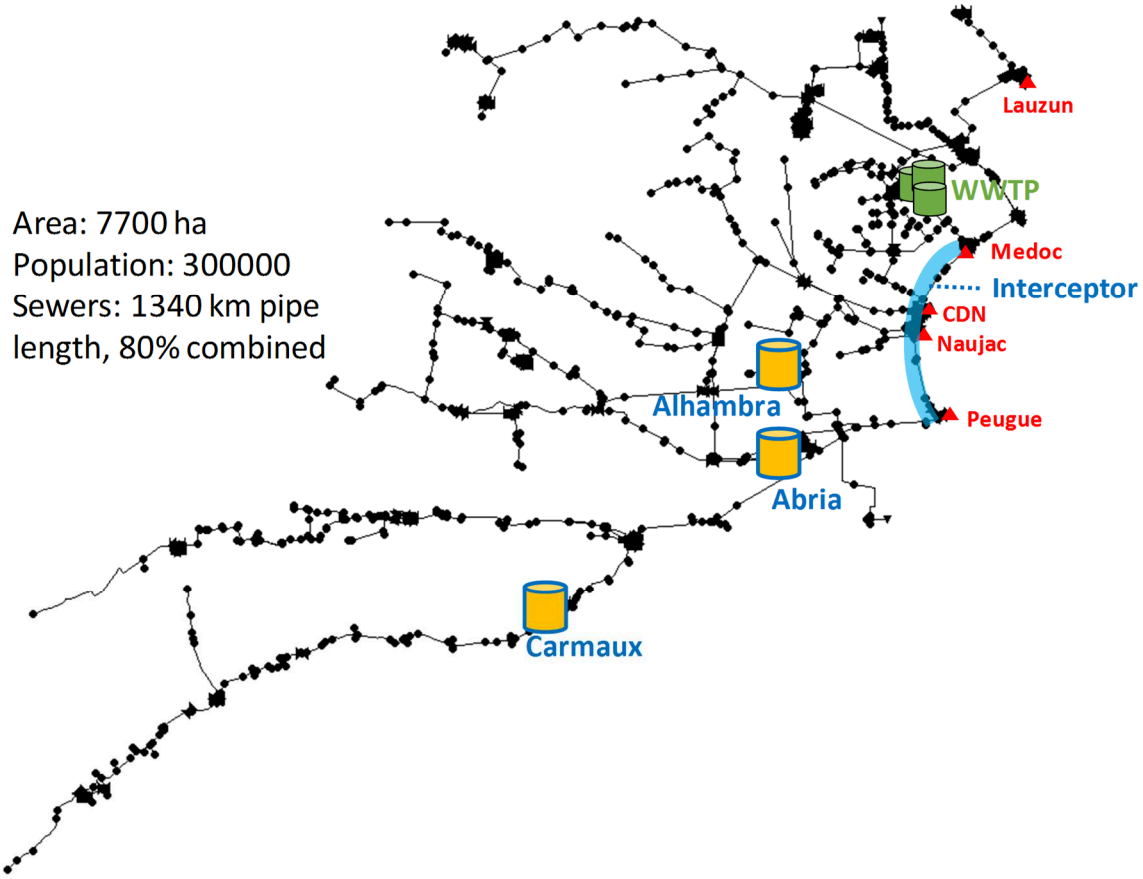

Figure 62. The sewer network with important locations for control.

Configurations of the Carmaux tank are illustrated in Figure 63. Two actuators used for control are weir C1 (to fill the tank) and pump C2 (to empty the tank). Their operational positions are explained in Table 19.

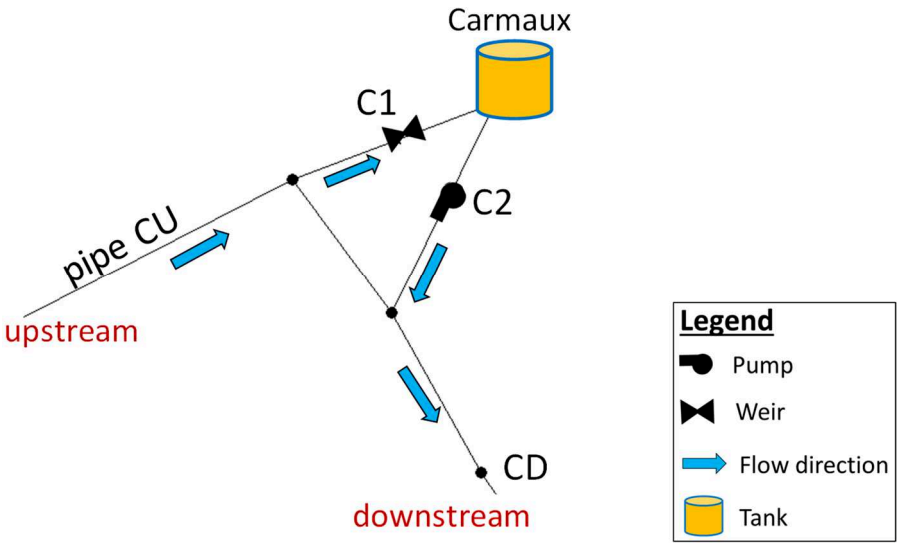

Figure 63. Configurations of the Carmaux site.

Table 19. Operational positions of the actuators to control the Carmaux tank and the way they are controlled by HBR and QBR.

Actuators	Positions	HBR	QBR
Weir C1	0: close (no fill) 1: open (fill the tank)	Open if flow in pipe CU is higher than 0.35 m^3/s.	Settings are based on optimisation (described in section 7.2.3.2)
Pump C2	0: off (no empty) 1: on (empty the tank)	Switched on if node CD depth is lower than 0.22 m.	Same as HBR

Configurations of the Abria tank are illustrated in Figure 64. Three actuators used for control are weir A1 (to fill the tank), pump A2 and pump A3 (to empty the tank). Their operational positions are explained in Table 20.

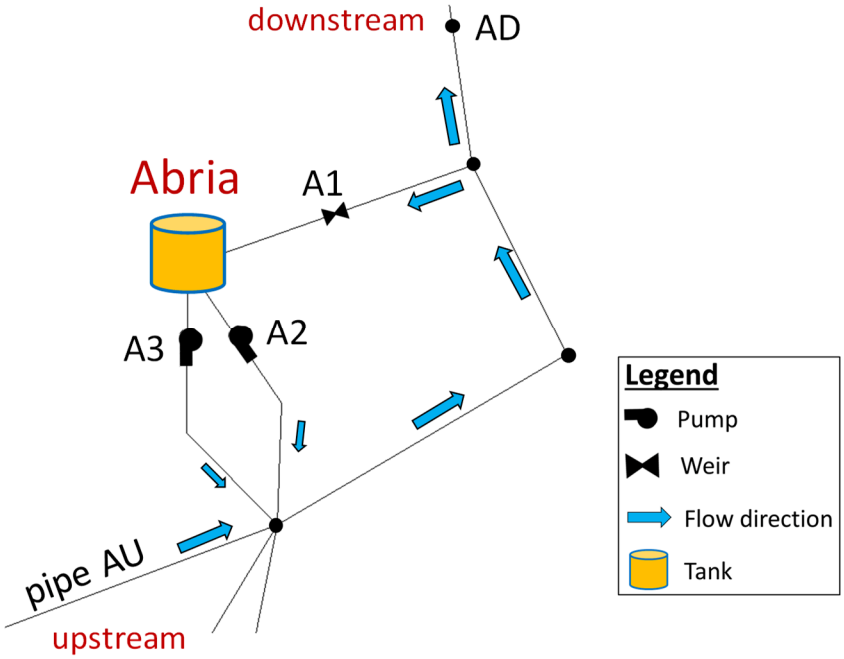

Figure 64. Configurations of the Abria site.

Table 20. Operational positions of the actuators to control the Abria tank and the way they are controlled by HBR and QBR.

Actuators	Positions	HBR	QBR
Weir A1	0: close (no fill) 1: open (fill the tank)	Open if flow in pipe AU is higher than 0.77 m^3/s.	Settings are based on optimisation (described in section 7.2.3.2)
Pump A2	0: off (no empty) 1: on (empty the tank)	Switched on if node AD depth is lower than 0.35 m.	Same as HBR
Pump A3	0: off (no empty) 1: on (empty the tank)	Switched on if node AD depth is lower than 0.35 m.	Same as HBR

Configurations of the Alhambra tank are illustrated in Figure 65. Three actuators used for control are weir H1, weir H2 (to fill the tank), pump H3 and pump H4 (to empty the tank). Their operational positions are explained in Table 21.

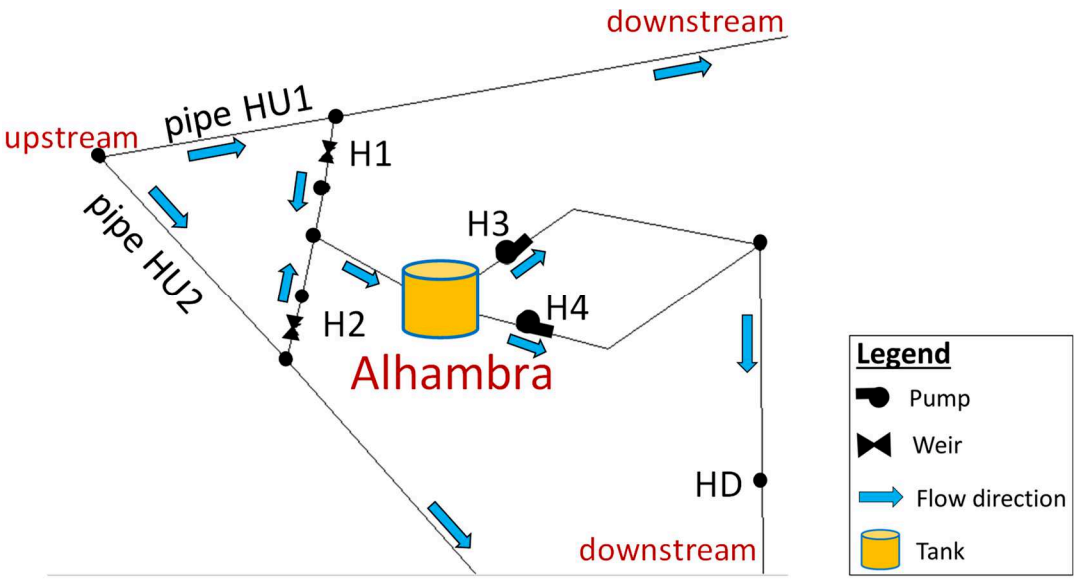

Figure 65. Configurations of the Alhambra site.

Table 21. Operational positions of the actuators to control the Alhambra tank and the way they are controlled by HBR and QBR.

Actuators	Positions	HBR	QBR
Weir H1	0: close (no fill) 1: open (fill the tank)	Open if total flow from pipe HU1 and pipe HU2 is higher than 0.03 m^3/s.	Settings are based on optimisation (described in section 7.2.3.2)
Weir H2	0: close (no fill) 1: open (fill the tank)	Open if total flow from pipe HU1 and pipe HU2 is higher than 0.03 m^3/s.	Settings are based on optimisation (described in section 7.2.3.2)
Pump H3	0: off (no empty) 1: on (empty the tank)	Switched on if node HD depth is lower than 0.47 m.	Same as HBR
Pump H4	0: off (no empty) 1: on (empty the tank)	Switched on if node HD depth is lower than 0.47 m.	Same as HBR

Configurations of the interceptor site are illustrated in Figure 66. Two actuators used for control are weir N (to control CSO at Naujac) and pump C (to transfer water at the CDN outlet to the

interceptor). Their operational positions are explained in Table 22. The other actuators shown in Figure 66 are always switched on in both HBR and QBR.

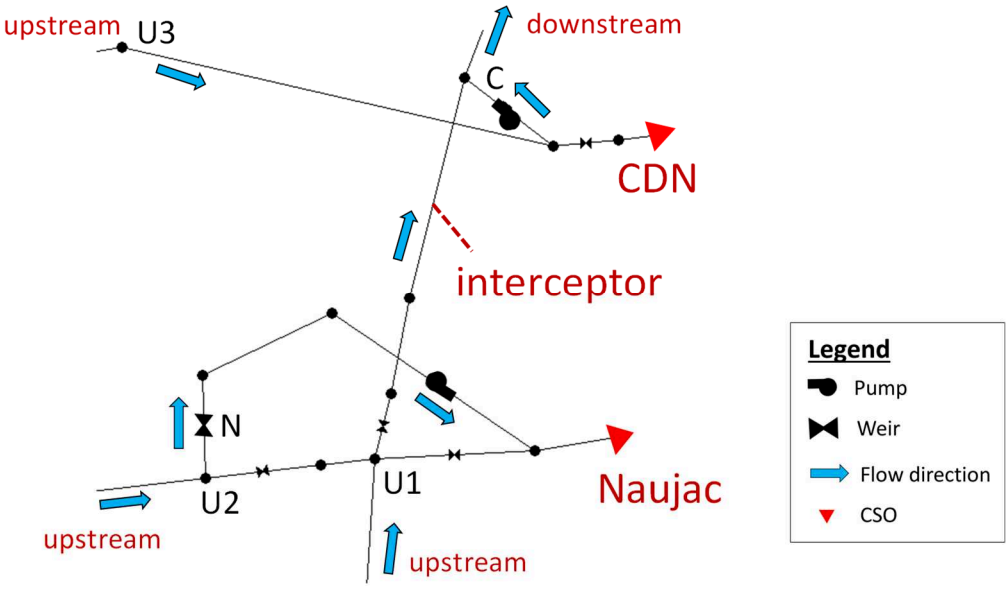

Figure 66. Configurations of the intercetor site.

Table 22. Operational positions of the actuators to control CSOs at the interceptor and the way they are controlled by HBR and QBR.

Actuators	Positions	HBR	QBR
Valve N	0: close (no CSO) 1: open (allow CSO)	Always open to transfer excessive water to the Naujac CSO, which comes from either upstream node U2 or upstream node U1 (reverse flow direction from node U1 to node U2 during wet weather because of big flow in the interceptor).	Settings are based on optimisation (described in section 7.2.3.2)
Pump C	0: off (no transfer) 1: on (transfer water to the interceptor)	Always switched on to transfer water from upstream U3 to the interceptor.	Settings are based on optimisation (described in section 7.2.3.2)

7.2.2 Selection of storm events

With higher numbers of control elements and CSO structures, it is imperative to adapt the controller developed in the proof-of-concept study towards the Louis Fargue catchment. As a first step, this study selects one representative storm event to tune the QBR strategy, i.e. the event on 29 July 2015. The steepest gradients of the chosen event MV curves deem occurring in the middle or late part of the event duration, which is found by the proof-of-concept study (see Chapter 6) as having high probability to achieve valuable CSO load reduction with QBR. Basic rainfall characteristics of this storm event along with its MV curve (exemplified by the MV curve upstream the tank Abria) are presented in Figure 67.

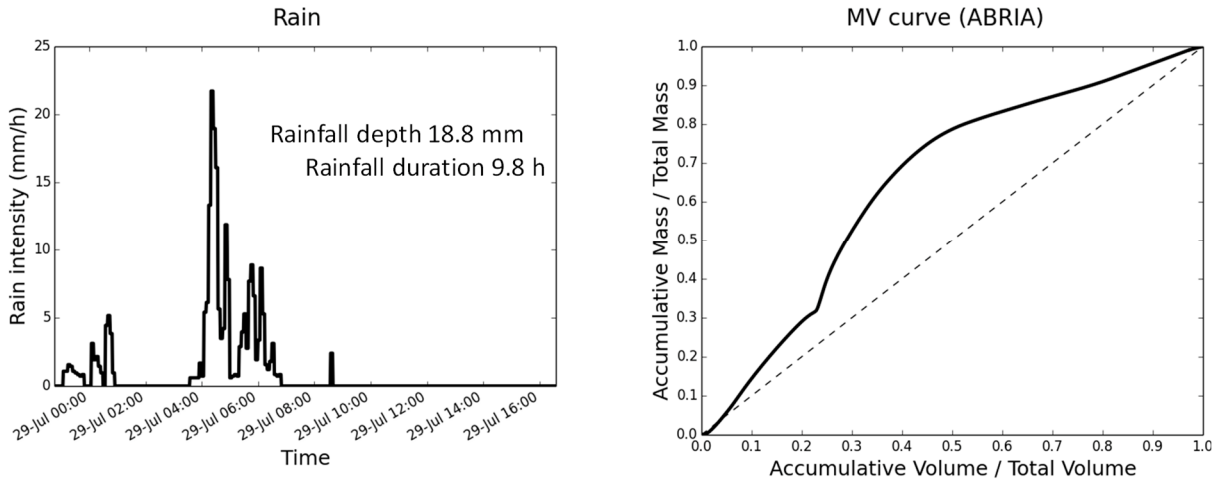

Figure 67. Rainfall characteristics and simulated MV curve of the storm event on 29 July 2015.

The same QBR strategy used in the proof-of-concept study (see section 6.2.4.1) is first applied on the selected storm event. The QBR controller is then tuned by checking the performance of QBR versus HBR at different controlled sites and providing improvement to any identified problem. After tuning the QBR controller with the above storm event, the next step is to implement the strategy on multiple storm events over the long term. The results of this task first help to understand the ability of the QBR controller to cope with situations that are different

from those it is tuned for. The results are equally meaningful to assess the performance of the QBR strategy. The period between October 2015 and December 2016 is chosen to identify appropriate storm events. Extreme storm events (rainfall depth around or more than 30 mm over few days) are not included because the operational priority under these circumstances is flood prevention. Several small storm events having low runoff volumes are also not considered since the controlled retention tanks cannot be filled fully. In the end, there are 19 selected storm events with their rainfall characteristics illustrated in Figure 68.

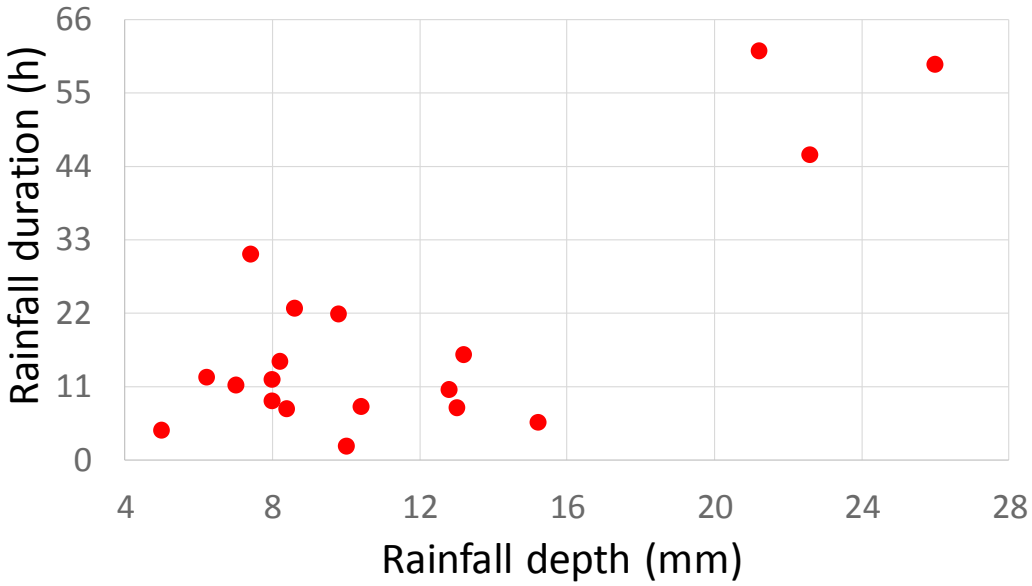

Figure 68. Basic rainfall characteristics of the storm events selected for long term study.

7.2.3 Control methods

For both the HBR and QBR strategies, core principles of control are similar to those in the proof-of-concept study (see section 6.2.4). There is new improvement added to better utilise the whole storage capacity of the retention tanks during storm events, as described below (pages 180-181).

7.2.3.1 HBR

The HBR strategy is based on the current operations of the SN (see section 4.1.2.2). The retention tanks are controlled using hydraulic thresholds. When the flow in an upstream pipe exceeds the threshold of three times dry weather flow, filling of the tanks is done by opening their gates and stopping after full storage capacities are reached. When runoff returns to dry weather conditions and inflow to the WWTP is lower than its hydraulic maximum capacity, pumps are turned on to empty the tanks gradually.

7.2.3.2 QBR

Summary of the control principles for retention tanks

The QBR strategy is based on the receding horizon control principle which utilizes a computer-based platform to simulate processes of reality and to derive control actions through a controller. The control loop of the strategy is illustrated in Figure 69. The algorithm to run the loop is presented in Figure 51b. From the proof-of-concept study on the Périnot catchment, smaller CTI generally leads to better QBR performance, and CTI length longer than 30 minutes can degrade the controller performance considerably (see section 6.3.3). Given the much larger size of the Louis Fargue catchment when compared to the size of the Périnot catchment, the length of the CTI is chosen as 20 minutes. For the SWMM-TSS model, the routing time step and reporting time step are fixed at ten seconds and one minute respectively. These parameter settings can maintain the balance between efficiency of the QBR strategy and the computational cost (e.g. two hours to implement QBR to an 18-hour storm event).

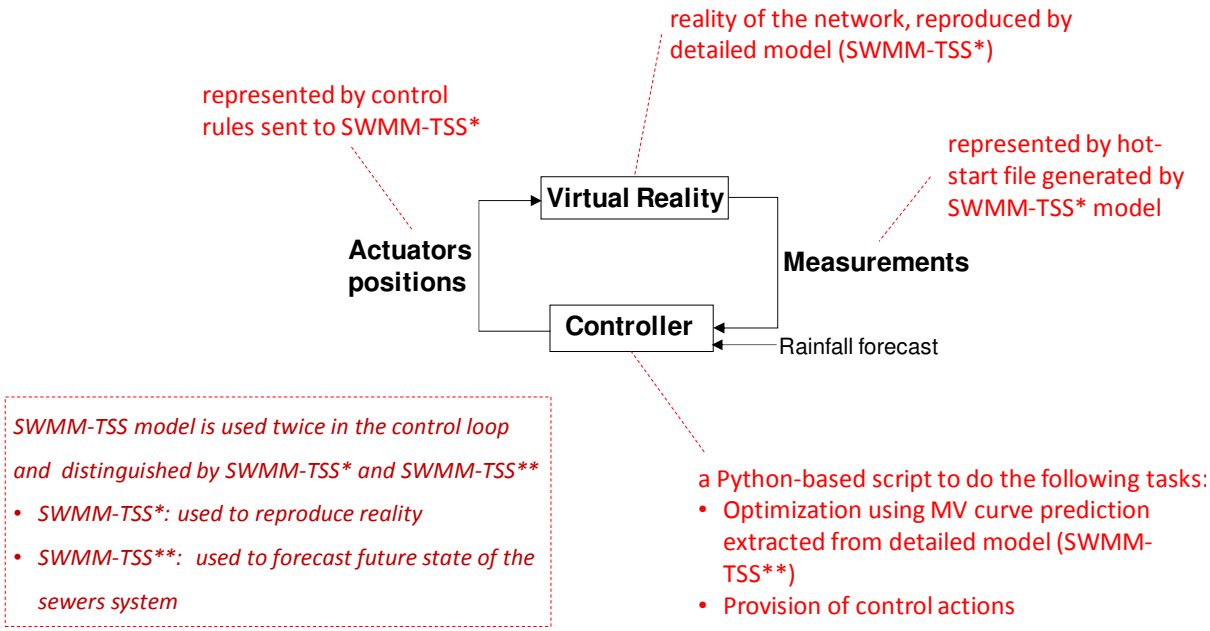

Figure 69. Workflow of the QBR strategy with explanation of each component.

The main differences between the QBR and the HBR strategies are displayed in Figure 70. In particular, Figure 70a shows the predicted flow and TSS flux in a pipe right upstream of a retention tank. With HBR, the tank is completely filled right after the first peak of the flow. QBR only fills the tank during the highest peak of the TSS flux (i.e. the third peak of the flow in this example). Both strategies thus intercept different TSS loads despite utilising the same retention tank volume.

To capture the most appropriate fractions of TSS flux, the QBR controller needs to derive a mass-volume (MV) curve using information from the predicted flow and TSS flux above. This curve represents the evolution of the pollutant load versus the water volume during a storm event, as presented in Figure 70b. From the MV curve, the controller can identify the time window when there is the highest increase of load over volume, corresponding to the sharpest gradient of the MV curve. This time window is then prioritized for filling the tank. Taking a close look at the filling window of QBR versus the one of HBR (red box versus blue box of Figure 70b), it is clear that the slope gradient is higher in the filling window of QBR.

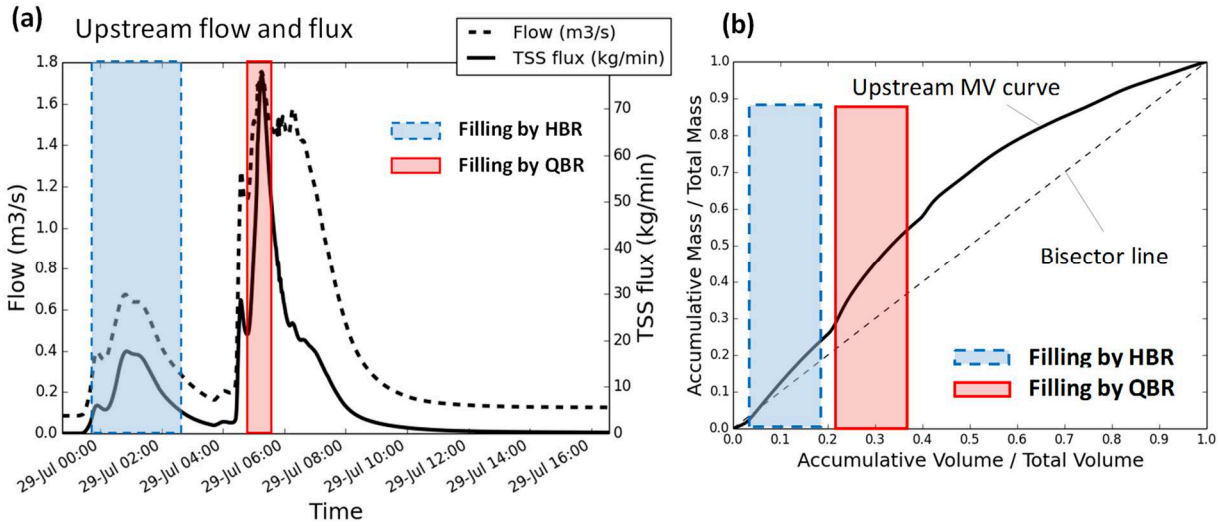

Figure 70. a) Illustration of filling periods by two strategies over flow and TSS flux plots (upstream of the tank); b) Same illustration over the MV curve plot (upstream of the tank).

Improvement added to control of the retention tanks

There are situations when a storm event showing two rainfall periods in which the latter appears a few hours after the previous one (e.g. Figure 71a) and both cause CSO discharges. If the TSS flux from the first period is smaller, the controller gives priority to filling the tank during the second period. However, the controller in the first version was not able to know whether and to what volume the tank could be filled during the first period (see Figure 71b). Improvement has thus been added to the controller developed in the proof-of-concept study to enable it to exploit the available storage capacity of the tank more efficiently. Given much higher TSS flux from the second peak, the controller is also able to estimate the right amount of filling volume during the first peak in order to reserve sufficient storage capacity for the next one (Figure 71c).

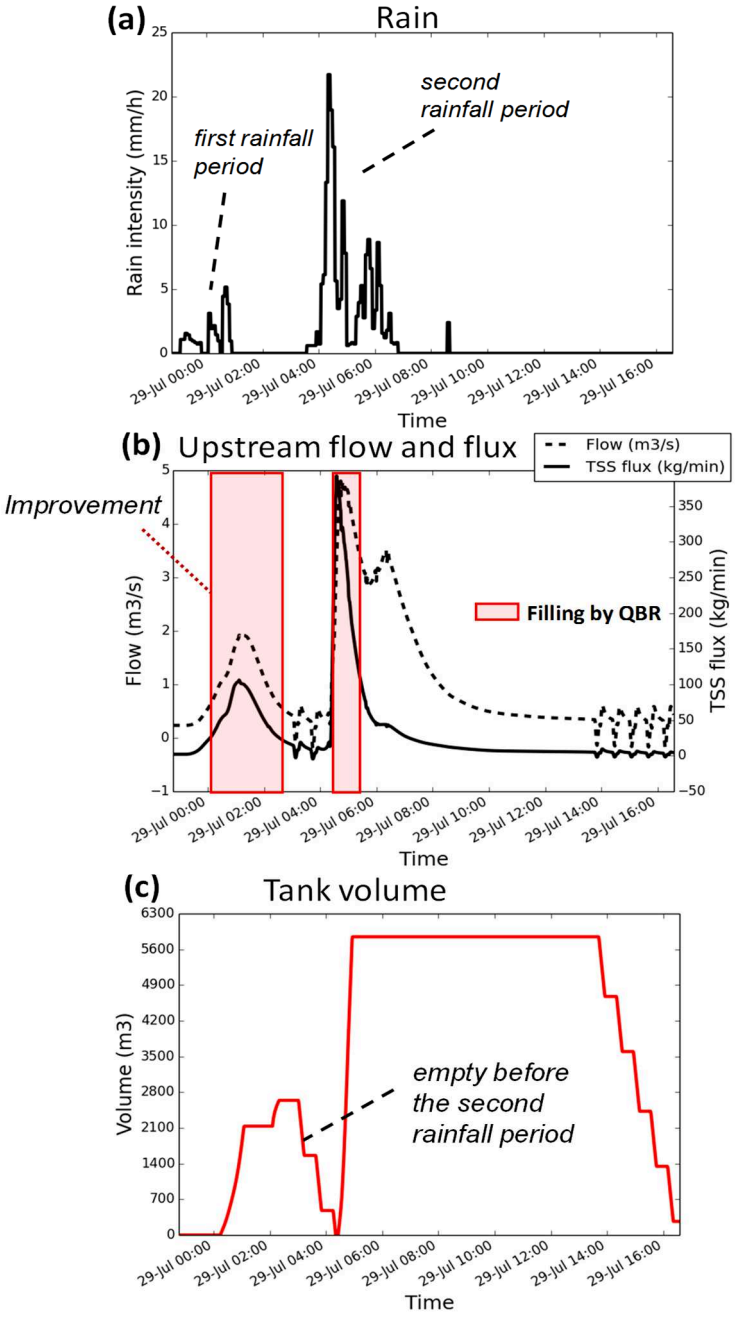

Figure 71. a) Storm event with two rainfall periods; b) Flow and TSS flux dynamics with filling time windows; c) Tank volume during the two rainfall periods.

Control at the interceptor

QBR is also implemented at the interceptor by controlling valve N and pump C (Figure 72a).

Valve N and pump C are always turned on and not controlled with HBR. Valve N allows CSOs

at Naujac during periods of high flows coming from the upstream part of the interceptor. Pump C transfers part of water from CDN's contributory sub-catchments to the WWTP.

The simulated TSS concentration at Naujac is overall higher than at CDN (Figure 72b). Doing optimisation using i) the MV curve, ii) the predicted flow through valve N, and iii) the predicted flows through pump C, the QBR controller can make CSO discharges lower at Naujac and higher at CDN during periods of peak TSS flux, while maintaining the same flow rate directed downstream of the interceptor. Besides, there is a large pipe connected to CDN, acting as an inline storage (4000 m^3 volume) that slows down overflows at CDN. Application of QBR thus can exploit more this advantage.

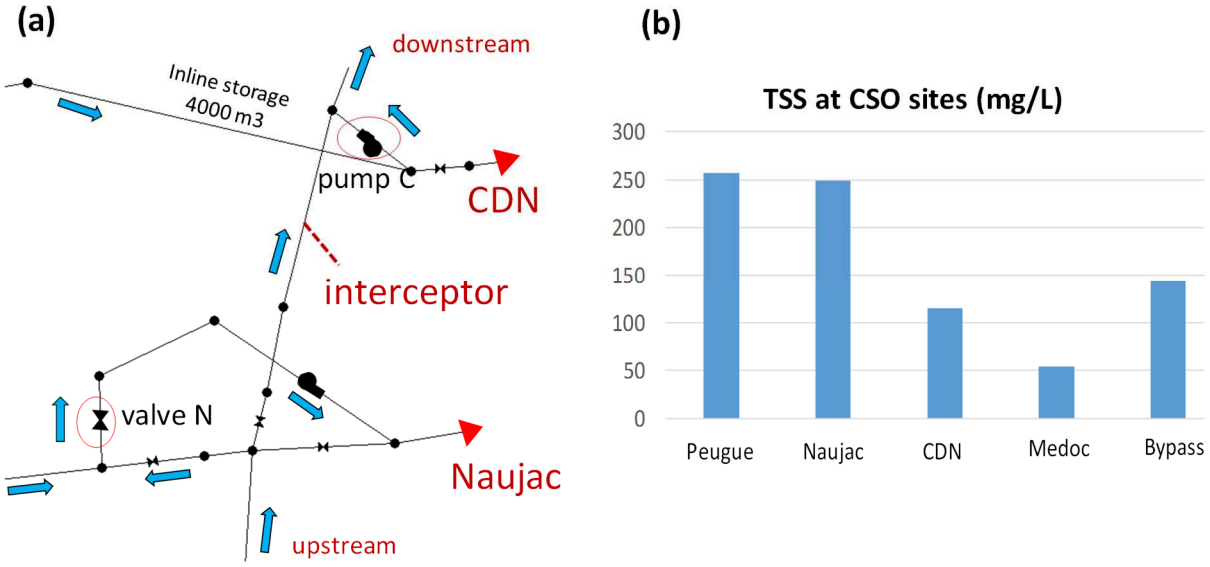

Figure 72. a) Actuators controlled by QBR: pump C and valve N; b) Mean simulated TSS values in 2016 at CSO structures along the interceptor.

7.2.4 Assessment of uncertainty

As mentioned in section 6.3.5, this thesis aims assessing the impact of MV curve prediction uncertainty on the performance of the QBR strategy. To derive an event MV curve, flow and TSS upstream of the retention tank are used. In the control loop, these variables are predicted by the controller that uses the SWMM-TSS model to estimate future states of the system. A

major source of uncertainty in MV curve prediction therefore originates from the flow and TSS prediction uncertainty of the model.

Section 4.3.2 provides the correlation charts of measured and simulated flow and TSS values at Peugue and Naujac over a 15-month period (see Figure 42 and Figure 43). These correlations can be used to derive random samples of flow and TSS time series from the error free time series. 20 % of the correlation data is further removed to eliminate more extreme values, trimming the parts of the probability distribution that are far away from the mean value. The procedure to generate a random sample of flow (and similarly TSS) time series as follows:

(i) First, cumulative distribution function (cdf) of model prediction uncertainty can be derived via the percentage difference (i.e. error) between measured and simulated data from the charts (blue points of the charts in Figure 42 (and Figure 43 for TSS).

(ii) At each time step of flow time series, uniform random number generation in the range [0,1] is utilised to obtain a prediction uncertainty value, through performing linear interpolation on the cdf. Then the error free value of flow at the corresponding time step is used to compute a new value of flow.

$$Q_{new} = Q_{error\ free}(1 + \varepsilon) \quad \text{(Eq. 8)}$$

where Q_{new}: new flow, $Q_{error\ free}$: error free flow, and ε: the error value.

(iii) Repeat step (ii) until a complete time series with errors is generated.

With the four controlled sites by the QBR strategy, 100 random samples of flow and TSS time series each are generated for each site. As computations are long (2 days), only 100 samples are generated in order to carry out a first assessment.

Given the locations of the four controlled sites, the cdf data at Peugue are applied to generate MV curve prediction uncertainty upstream of Carmaux, Abria (both are located within the sub-catchments of Peugue), and the interceptor (closer to Naujac, but main flow in the interceptor

is contributed by runoff from sub-catchments of Peugue) while the remaining site, Alhambra, uses the cdf data at Naujac (receiving the majority of runoff from upstream of Alhambra). The storm event used for the evaluation of uncertainty is the event on 29 July 2015 (see section 7.2.2 above).

7.2.5 Sensitivity analysis

7.2.5.1 Influence of storage tank volume on the controller performance

This thesis aims to investigates the influence of storage tank volume on the performance of the HBR and QBR strategies. Pre-evaluation with a couple of simulations is first carried out to identify feasible ranges of tank volumes for sensitivity test and reduce the number of simulation runs. Outside the range, the CSO load reduction benefit of QBR over HBR is inconsiderable when tank volumes are too small. On the other hand, too big tank volumes result in interception of all excessive stormwater by both strategies, i.e. the same CSO load reductions.

The volume ranges for the Abria, Carmaux, and Alhambra tanks are 2500-15000 m^3, 2000-14000 m^3, and 900-4800 m^3 respectively (as shown in Figure 73). Assuming uniform distributions of the above ranges, Latin Hypercube Sampling is then applied to generate random volumes of the three tanks. A total of 100 combinations of the three tanks volumes are generated resulting in 100 different scenarios/configurations of the Louis Fargue SN (i.e. 100 runs of QBR and HBR each on the Louis Fargue catchment). The simulation results are utilized to assess the total CSO loads obtained by each strategy. The storm event used for the sensitivity analysis is the event on 29 July 2015.

It should be highlighted that for this sensitivity study, the QBR controller does not include control at the interceptor. This ensures that any CSO load difference between the two control strategies is only due to tank control.

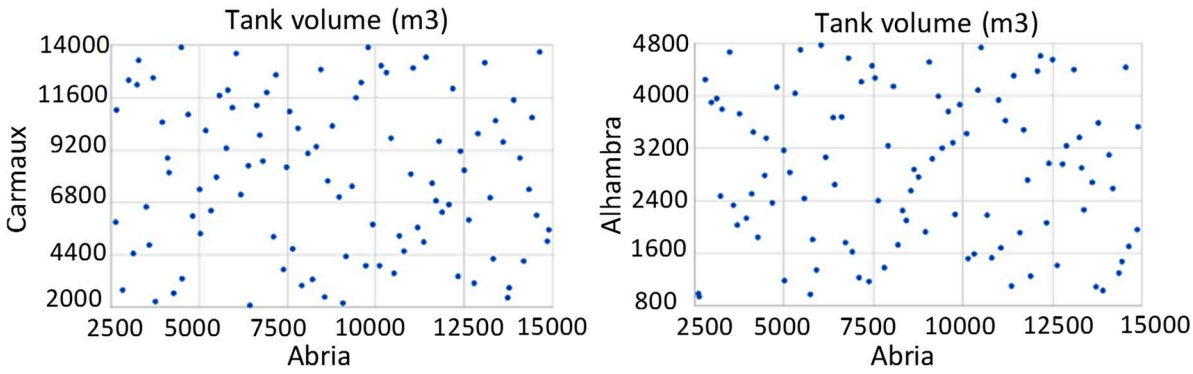

Figure 73. Random generation of volumes of the three tanks.

Ideally the sensitivity analysis should be done using all available storm events and as many generated tank volumes as possible. However, this leads to the increasing cost of computational resources and time. It is also not efficient to choose the storm events for which QBR brings no CSO load reduction benefit over HBR. For the purpose of assessing the impact of tank volumes, one storm event is used.

7.2.5.2 Identification of the tank volumes used for QBR of additional retention tanks

To better exploit the storage capacities of the Louis Fargue catchment, several more retention tanks are planned to be added for the QBR strategy, which is part of the future work of the LIFE EFFIDRAIN project. Sensitivity study is thus performed for the other three retention tanks upstream: Périnot, Bourran, and Chêne Vert (see Figure 19). The results help the selection of the most useful tank volumes used for QBR.

To reduce running time, simulation runs with varying tank volumes are performed separately for each tank model that contains only contributory upstream sub-catchments of the tank, plus few downstream ones (to keep real node depth conditions for tank emptying) (see Figure 74). The model of each new tank is therefore much smaller (in size) than the entire Louis Fargue model. Figure 74 shows the SWMM-TSS models used for the sensitivity study of Périnot, Bourran and Chêne Vert tanks, including their catchment areas. These models are extracted

from the Louis Fargue model. The routing and the reporting time steps of the SWMM-TSS models are set at five seconds and one minute respectively.

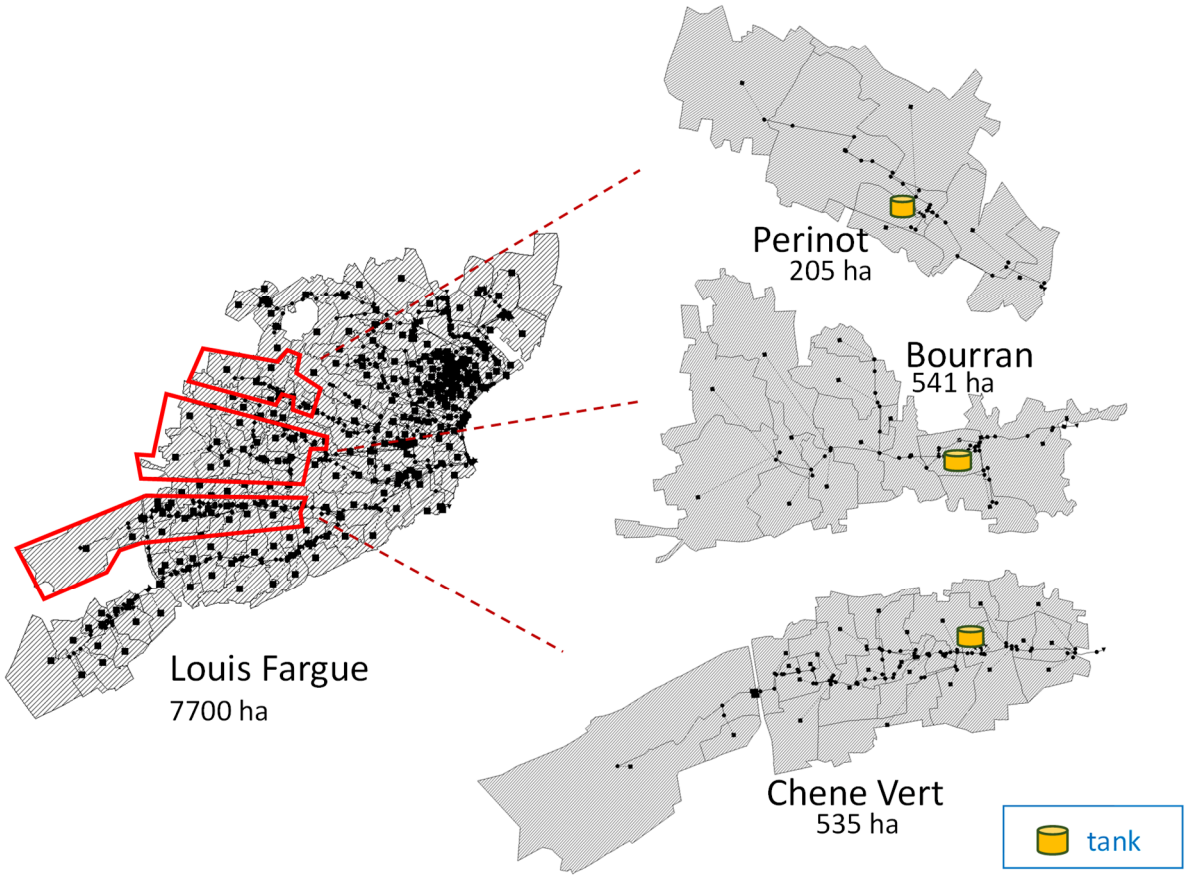

Figure 74. SWMM-TSS models of the Louis Fargue catchment and the three corresponding catchments of Périnot, Bourran and Chêne Vert.

The load interception differences (between QBR and HBR) are used to evaluate the performance of QBR over HBR with varying tank volumes. This is unlike the sensitivity study described in section 7.2.5.1, which is based on assessing the CSO load reduction benefit (on Louis Fargue catchment scale) of QBR over HBR. The ranges of tank volumes and the storm events used for the study are displayed in Table 23. As explained in section 7.2.5.1, the selected events are those having higher CSO load reduction benefit of QBR over HBR. The events are preferably short to minimise the computational time. For each tank, 200 values within its

volume range are randomly generated by Monte Carlo technique, assuming uniform distributions.

Table 23. Ranges of volumes and storm events used for the sensitivity study of Périnot, Bourran and Chêne Vert.

Catchment models	Ranges of tank volumes	Storm events
Périnot	1000 – 5000 m^3	23 April 2016; 26 May 2016
Bourran	3000 – 11000 m^3	09 March 2016; 26 May 2016
Chêne Vert	2000 – 8000 m^3	09 March 2016

7.2.6 Control objectives and performance indicators

In terms of control objectives, the QBR strategy proposes control actions that takes into account the objective function of improving CSO load reduction. The HBR strategy proposes control actions that are solely meant to lower the amount of CSO volumes. Besides, both strategies share the primary control objectives of avoiding flood and maintaining the nominally maximum flow rate sent to the WWTP during storm events.

The performance indicators used to evaluate the QBR and HBR strategies in this chapter are identical to those described in the proof-of-concept study (see section 6.2.7). The indicators include: total CSO load, total CSO volume, total load transferred to the WWTP, total volume transferred to the WWTP. The differences (in amount and percentage) between the QBR and HBR strategies of these indicators are important to compare the strategies. The topmost CSO point (i.e. Lauzun) receives flows from a separate part of the network, which is under static control and does not have any connection with the interceptor or other CSO points. Lauzun is

thus not included in the calculation of the performance indicators to allow proper assessment of the efficiency of the demonstrated strategy.

7.3 Controller performance

7.3.1 Demonstration on the storm event used for tuning

As introduced in section 7.2.2, the QBR controller is first tuned with the storm event on 29 July 2015. The results after tuning show that the QBR controller can give high priority to fill the highest peak of TSS fluxes which happens during the second rainfall period of the storm event. Furthermore, it provides control actions to fill the earlier peaks depending on available storage capacities. In the case of Carmaux tank (see Figure 75), it is decided by the QBR controller to intercept partially the first peak of TSS flux, until reaching 3000 m^3 of water volume in the tank. The remaining higher storage capacity is reserved for the next peak. The HBR strategy intercepts significantly more water volume from the first peak, i.e. 4800 m^3, leaving lower capacity for the next peak. As a result, for Carmaux tank, interception of TSS loads by the QBR strategy is 25.7 % greater than by the HBR strategy. For Abria and Alhambra tanks, the corresponding rates are 37.1 % and 11.4 % respectively. Given higher upstream flow and lower tank volume of Abria compared to Carmaux, Figure 76 shows that the QBR controller can estimate the proper amount to fill during the first peak of TSS flux, allowing fully emptying of the tank before the higher peak of TSS.

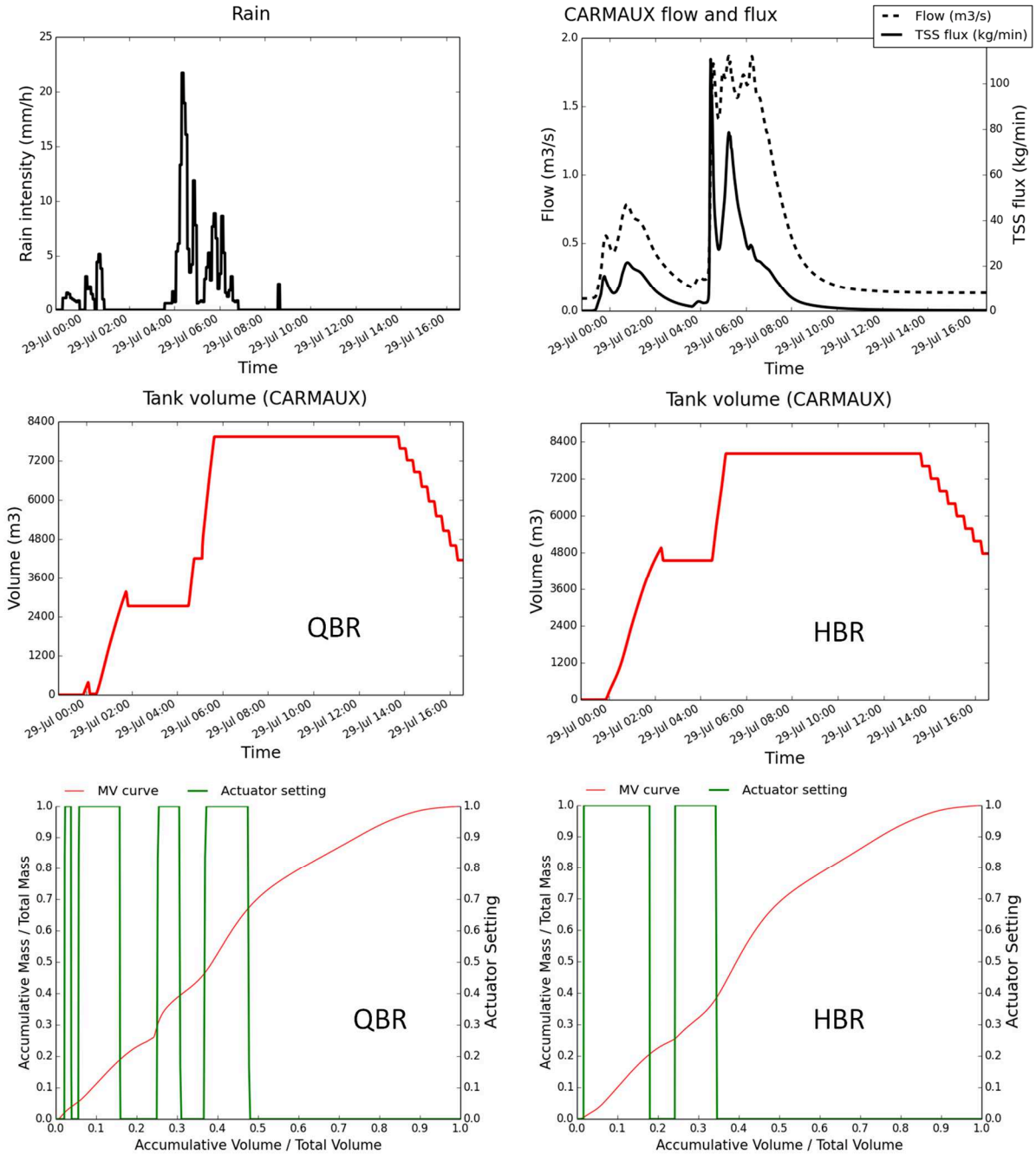

Figure 75. Differences in the results between the two control strategies for the storm event on 29 July 2015 (for Carmaux tank). Actuator setting represents the actuator position (0: close, 1: open to fill the tank).

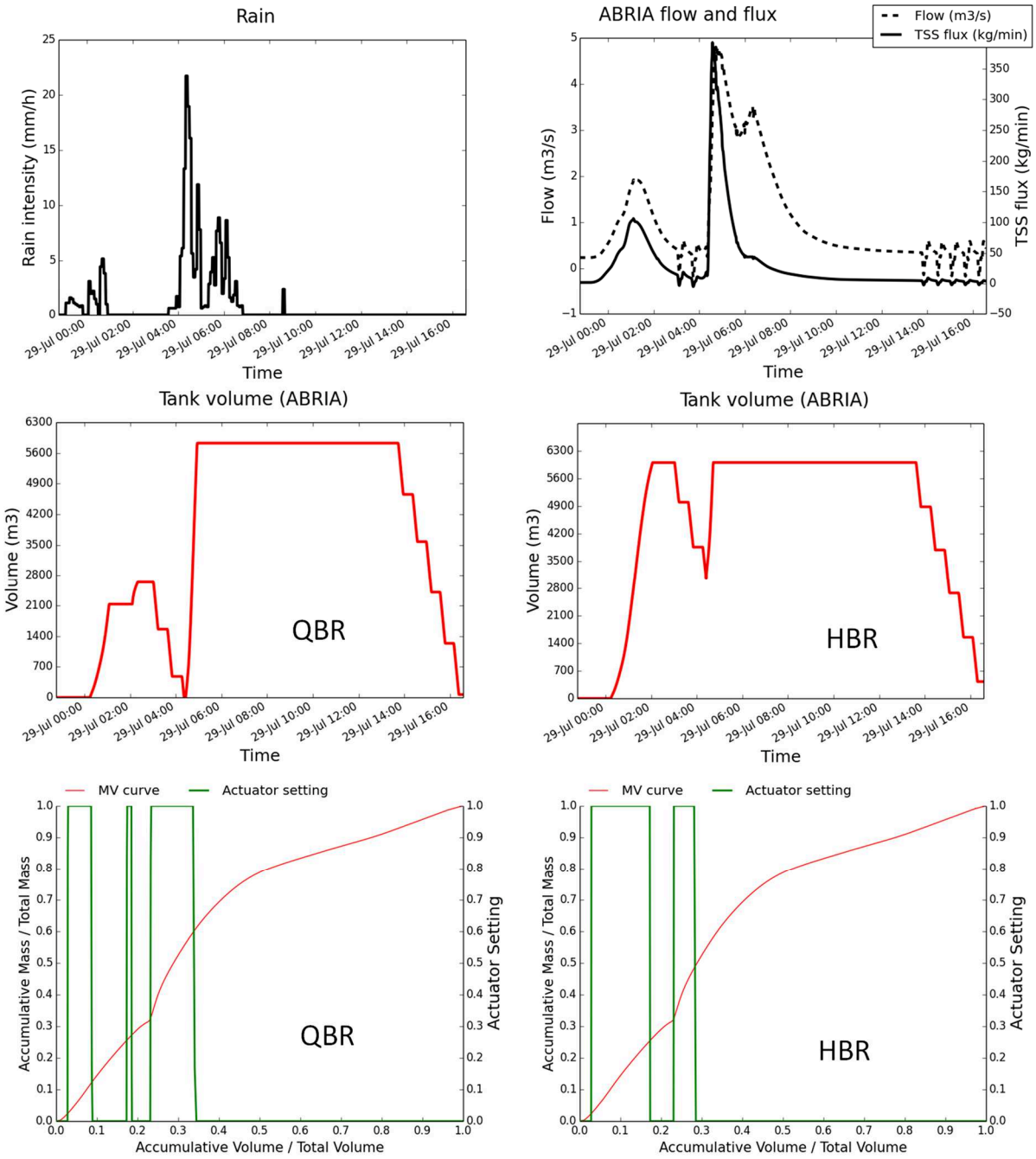

Figure 76. Differences in the results between the two control strategies for the storm event on 29 July 2015 (for Abria tank).

The comparison given in Table 24 represents that for the tested event, QBR produces a 7.5 % CSO load reduction compared to HBR. Compared to HBR, QBR also reduces the CSO volumes slightly (i.e. reduction rate of 1.7 %), which is due to the diversion of CSO flows from Naujac to CDN and the WWTP downstream. Figure 77 shows that the total CSO load and volume at Peugue and Naujac are lower with QBR, because the two tanks Carmaux and Abria are located

wholly within the contributory sub-catchments of Peugue. The reduction at Naujac is due to the control of both the three tanks and the interceptor. More volumes and TSS loads are transferred to the downstream interceptor. Due to the control of the interceptor, QBR generates nearly two times more CSO volumes and TSS loads at CDN, and slightly more to the WWTP bypass. On top of that, more deposit loads in the tanks are found with QBR. The risk of resuspension and higher cost of cleaning the tanks should be taken into account.

Table 24. Performances of QBR and HBR control strategies in terms of CSO volumes and loads (event 29 July 2015).

	QBR		HBR		Difference	
Event	CSO load	CSO volume	CSO load	CSO volume	CSO load	CSO volume
	ton	10^3 m^3	ton	10^3 m^3	%	%
29 July 2015	38.9	124.2	42.1	126.4	-7.5	-1.7

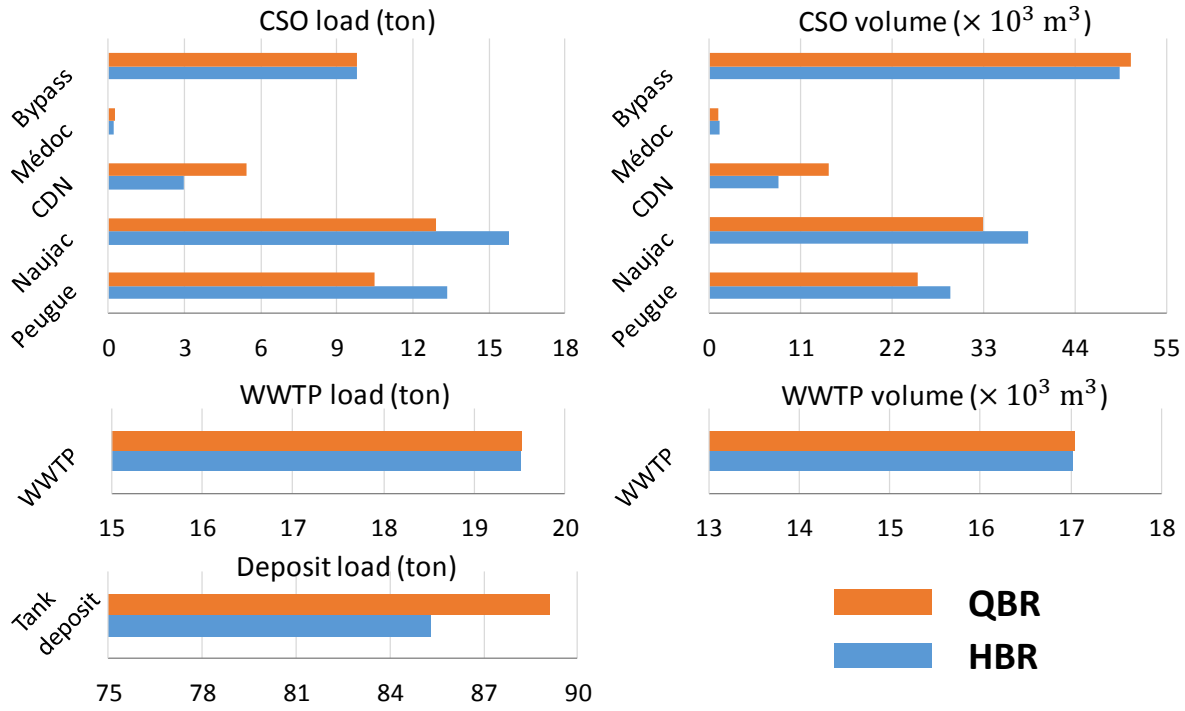

Figure 77. Total TSS loads and water volumes at different outlets along with total deposit loads of the controlled tanks (event 29 July 2015).

7.3.2 Performance of all selected storm events

The results obtained after implementing the two control strategies on 19 selected storm events show that QBR can bring a valuable benefit over HBR, with 17 out of 19 events having load reduction percentage per event varying between 6 and 28.8 % (Figure 78). Total CSO load reduction rate, by QBR over HBR, for all the 19 selected events is approximately 11.5 %. The corresponding total CSO volume reduction rate is 4.8 %.

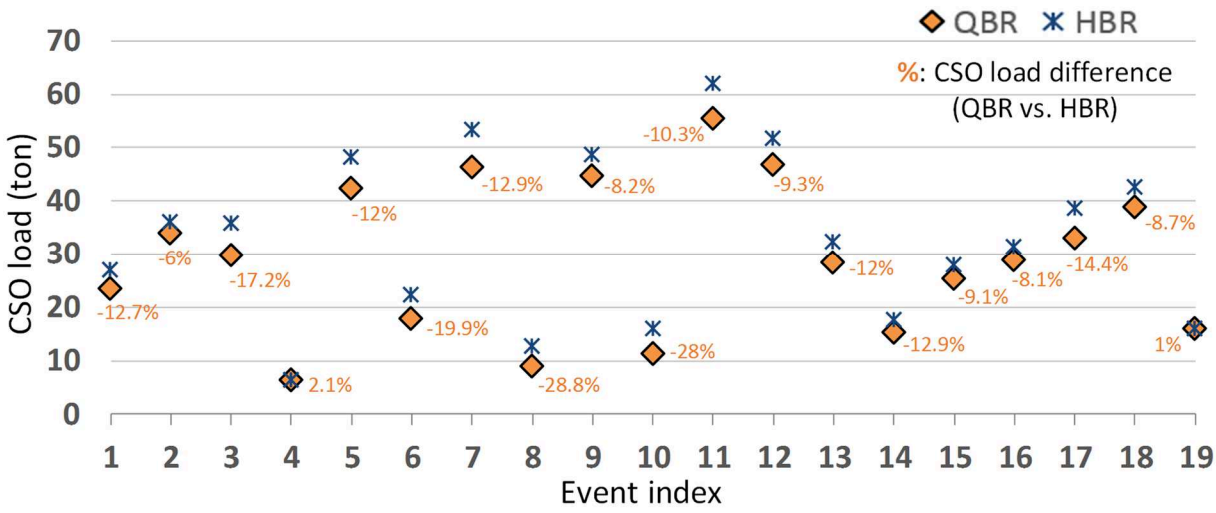

Figure 78. Total CSO loads obtained by both strategies for the 19 selected storm events, together with the CSO load difference between QBR and HBR shown in percentage.

In general, the performance of the QBR strategy is consistent over various storm events. Figure 79 and Figure 80 illustrate an example of the performance on the storm event on 23 April 2016 (event index #2, rainfall depth of 15.2 mm, rainfall duration of 5.6 hours). For tank control, the QBR strategy is capable of identifying the right period (highest TSS load) to maximise the filling of the tank, which leads to a higher mass interception rate of 33.5 % compared to the HBR strategy. For interceptor control, according to Figure 80, the QBR lowers 5.9 tons of TSS loads spilled via Naujac CSO (-28.2 %) and increases 2.4 tons of TSS loads spilled via CDN CSO (70.2 %).

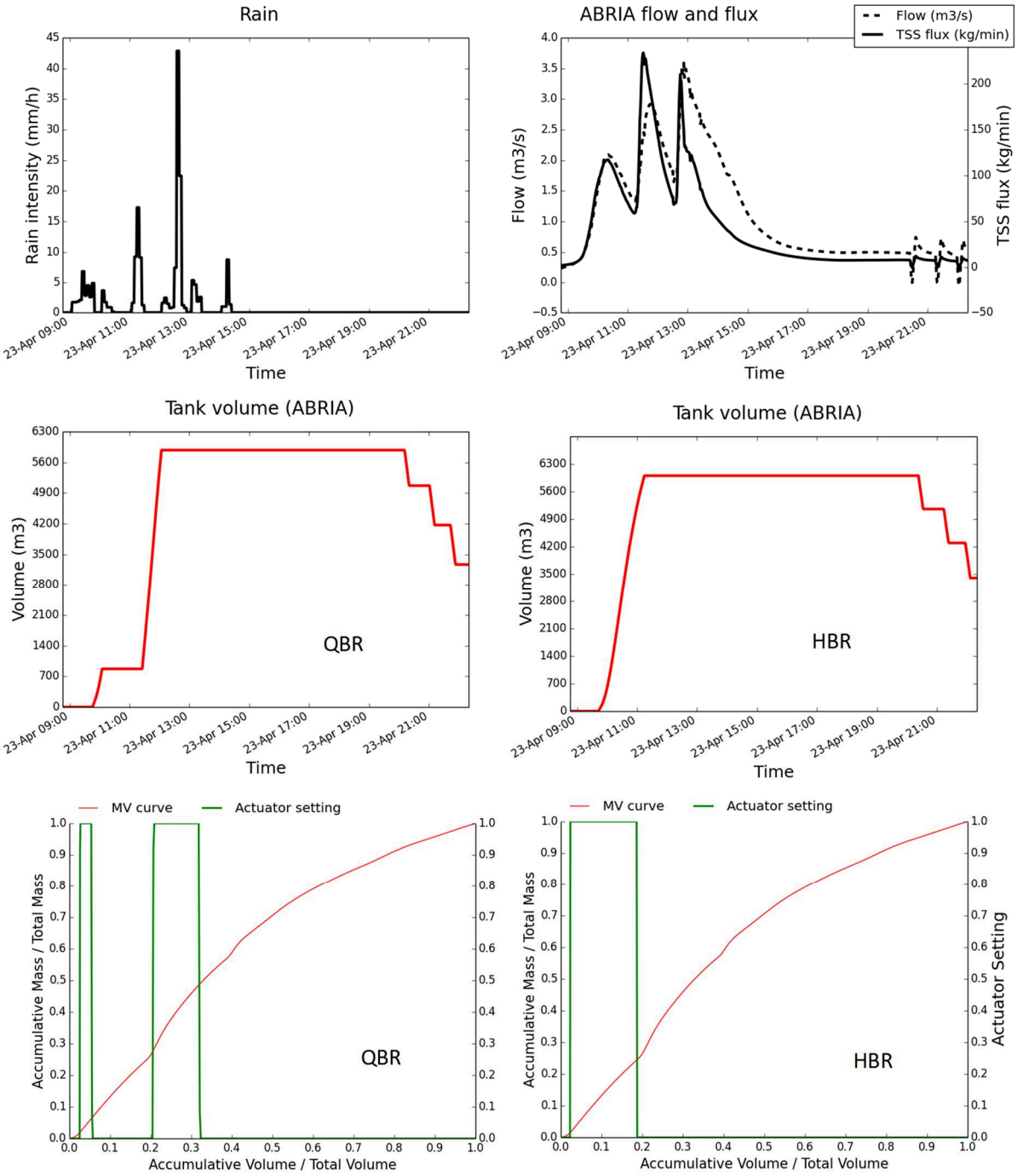

Figure 79. Results of filling Abria tank that demonstrate the QBR controller performance on one of the selected storm events (event on 23 April 2016; event index #12).

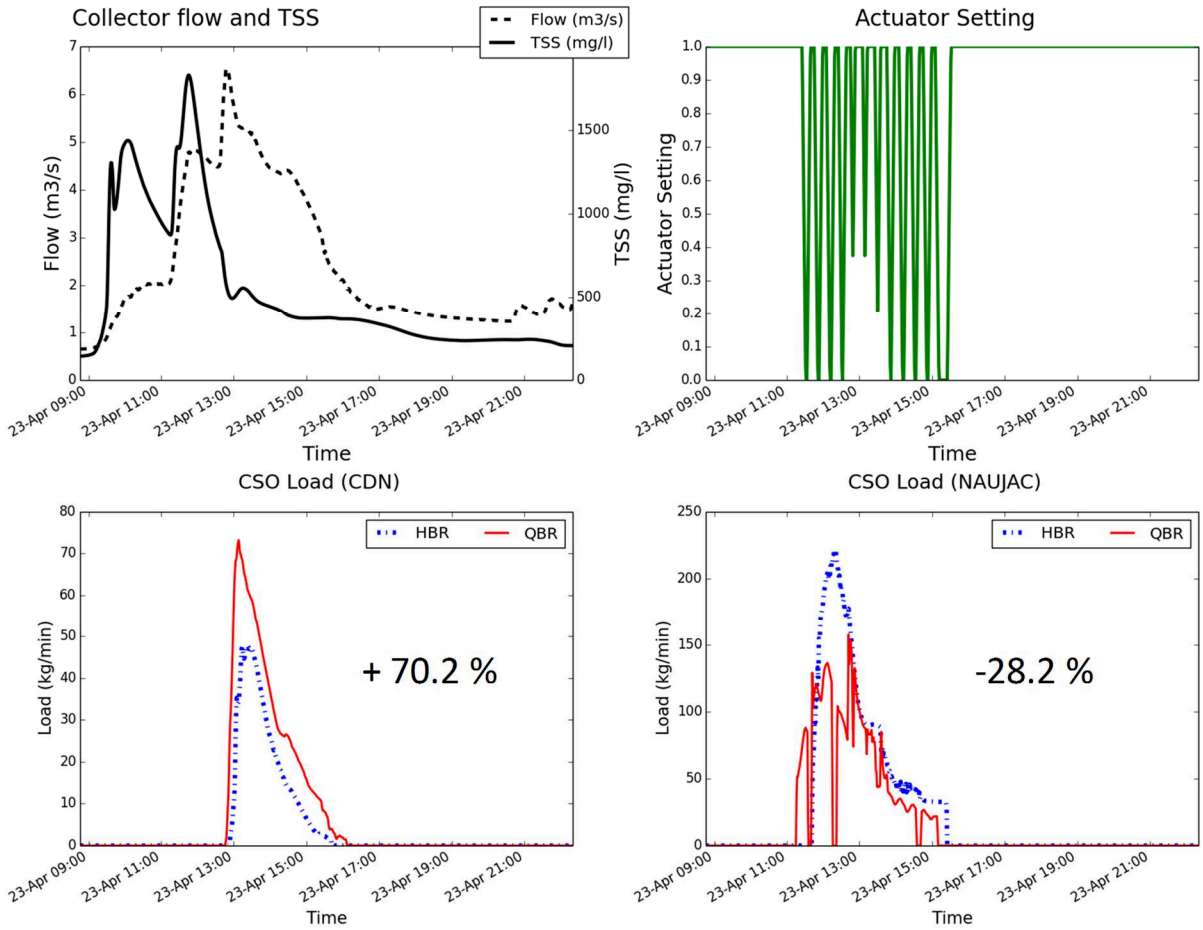

Figure 80. Results of control at the interceptor that demonstrate the QBR controller performance on one of the selected storm events (event on 23 April 2016; event index #12).

7.3.3 Characterisation of the QBR performance by the beta values of event MV curves

Furthermore, the results obtained from the selected storm events are used to sort the performance of QBR according to the MV curve characteristics, i.e. beta values. For each tank, all upstream MV curves of the storm events in which the QBR strategy stores more mass in the tank than the HBR strategy are plotted together with their beta values (see Figure 81, Figure 82, and Figure 83). It is observed from the proof-of-concept study on the Périnot catchment that there are three groups of MV curves (below, around, and above the bisector line) with respectively decreasing possibility of finding storm events benefitting from the QBR strategy. However, this typology deems specific to each catchment and not applicable anymore in the

case of the three controlled tanks of the Louis Fargue catchment. For Carmaux and Abria, the ranges of beta values of the MV curves with QBR benefit nearly overlap with the ranges of beta values of all the 19 storm events, showing that it is not feasible to classify the performance of the QBR according to beta values (see Figure 81 and Figure 82). Besides, it is different from the case of Périnot because a majority of the MV curves with QBR benefit are located above the bisector line. For Alhambra, the number of events with QBR benefit is too few to any draw conclusion (see Figure 83). At present, it seems not feasible to derive any meaningful correlation between the performance of the QBR strategy and the event MV curve characteristics represented by the beta value. In this case, beta is clearly not sufficient to describe accurately the MV curves.

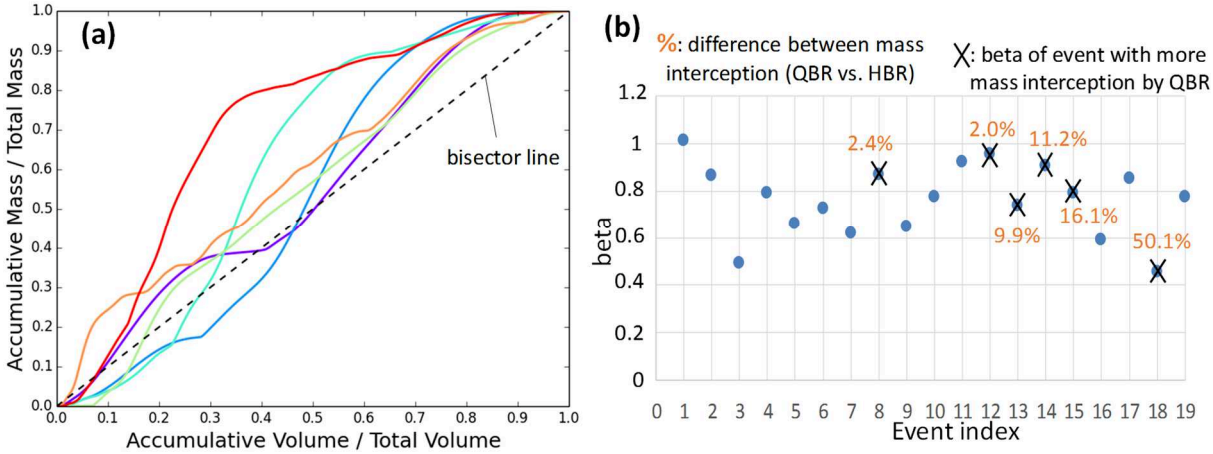

Figure 81. (a) MV curves (upstream of the Carmaux tank) of events for which QBR can intercept more mass in the tank than HBR (at least more than 100 kg). (b): beta values of all 19 MV curves (upstream of the Carmaux tank). Dots with cross mark represent beta values of events displayed in chart (a).

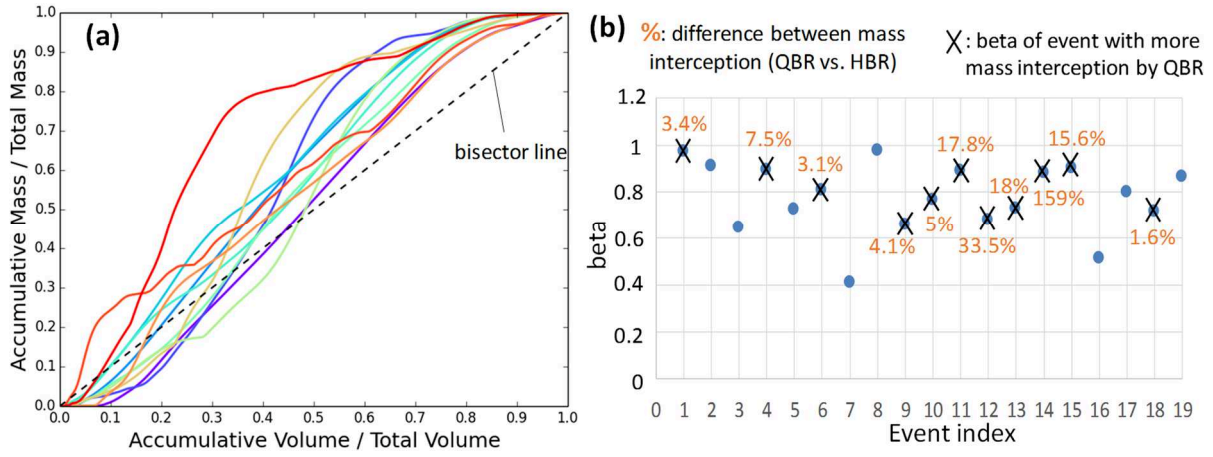

Figure 82. (a) MV curves (upstream of the Abria tank) of events that QBR can intercept more mass in the tank than HBR (at least more than 100 kg). (b): beta values of all 19 MV curves (upstream of the Abria tank). Dots with cross mark represent beta values of events displayed in chart (a).

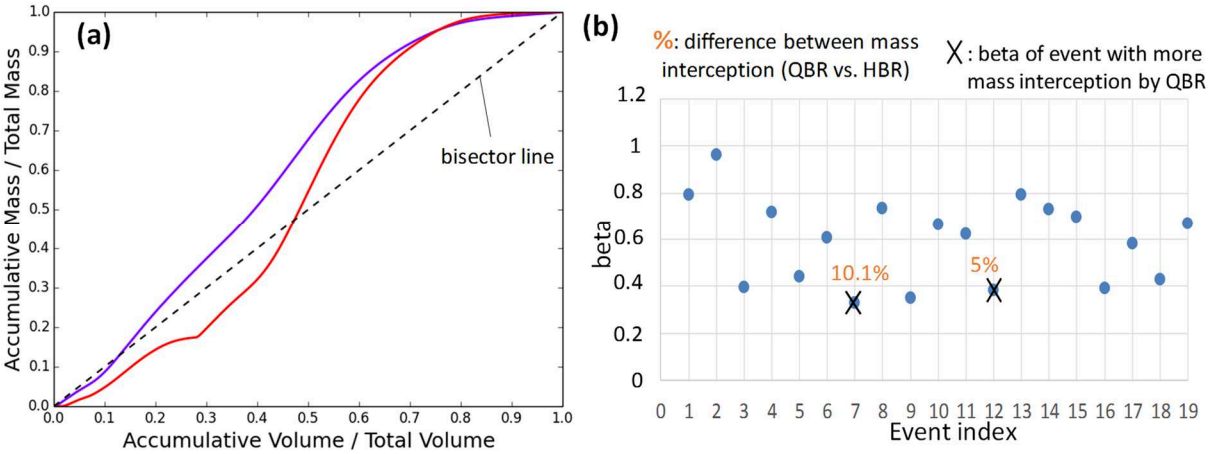

Figure 83. (a) MV curves (upstream of the Alhambra tank) of events that QBR can intercept more mass in the tank than HBR (at least more than 100 kg). (b): beta values of all 19 MV curves (upstream of the Alhambra tank). Dots with cross mark represent beta values of events displayed in chart (a).

7.4 Impact of model prediction uncertainty on the controller performance

Following the procedure of quantifying the uncertainty of the performance of the QBR strategy (section 7.2.4), the left charts of Figure 84 and Figure 85 present histograms of flow and TSS prediction errors of the SWMM-TSS model. The right charts provide the corresponding cdf plots. For each variable (flow and TSS) at each site (Peugue and Naujac), there are approximately 105500 values that are used to derive the charts of the two above figures.

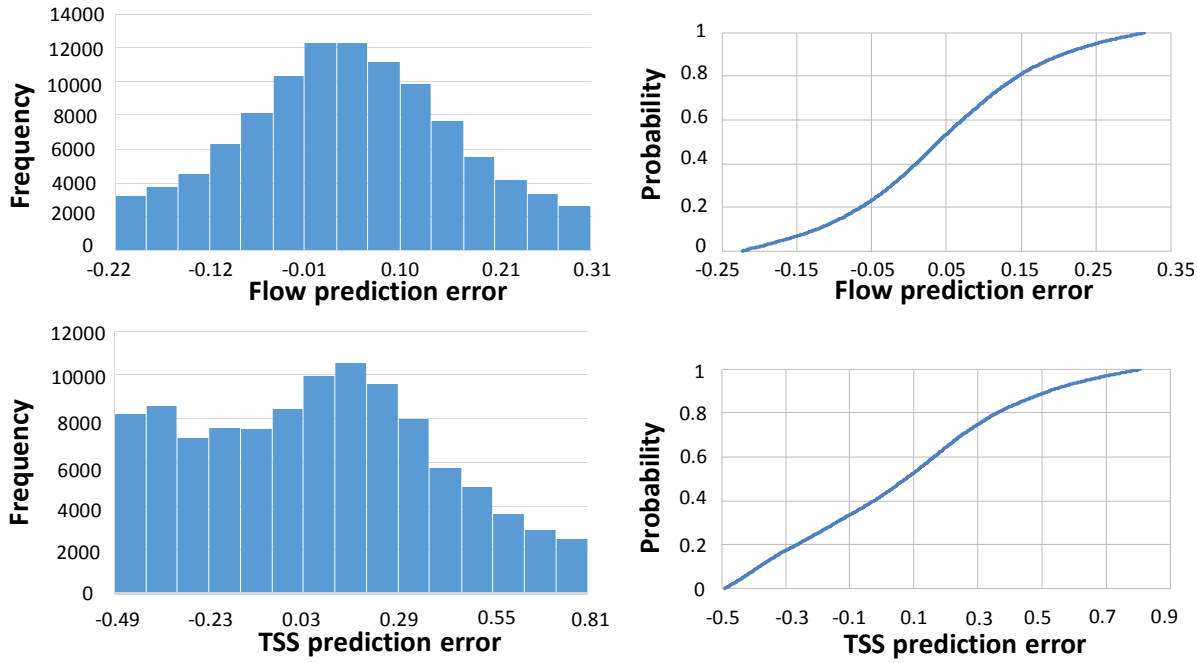

Figure 84. Left charts: histograms of flow and TSS prediction errors (for Peugue). Right charts: flow and TSS cdf charts (for Peugue).

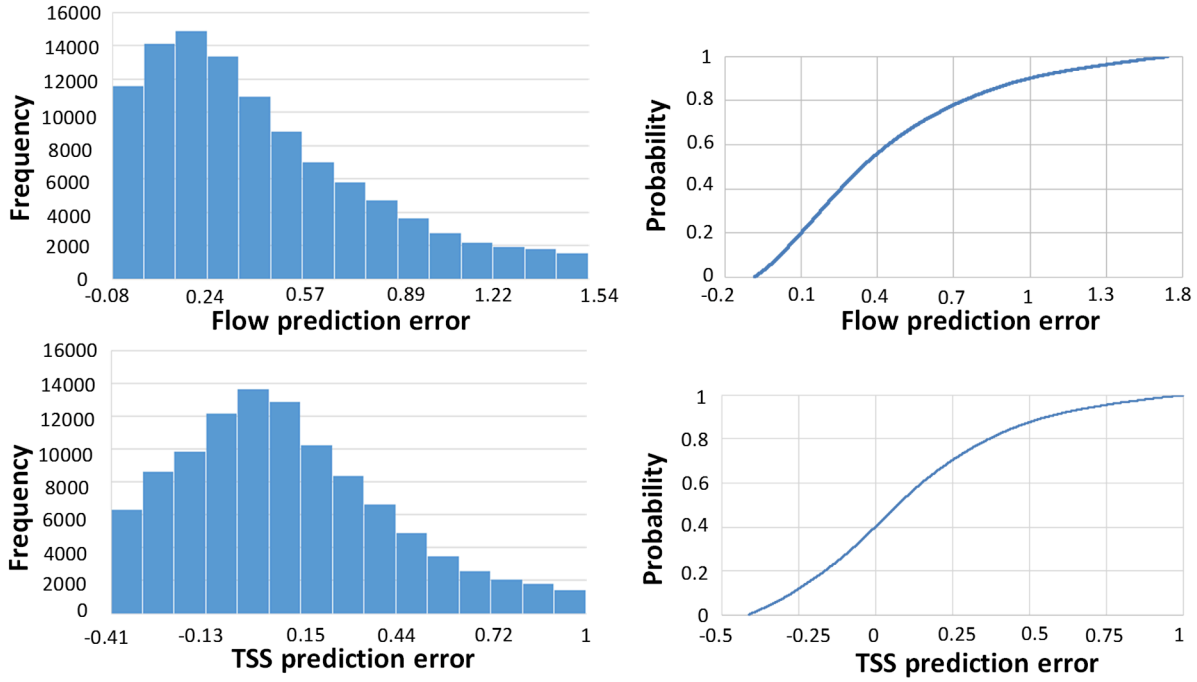

Figure 85. Left charts: histograms of flow and TSS prediction errors (for Naujac). Right charts: flow and TSS cdf charts (for Naujac).

Using the cdf data, random samples of flow and TSS time series are generated for each controlled site. Figure 86 represents an example of the range (from 2.5 percentile to 97.5 percentile) of upstream flow time series samples of Carmaux tank, including the plot of error

free upstream flow time series. Likewise, for the same tank, a corresponding chart for TSS is provided in Figure 87.

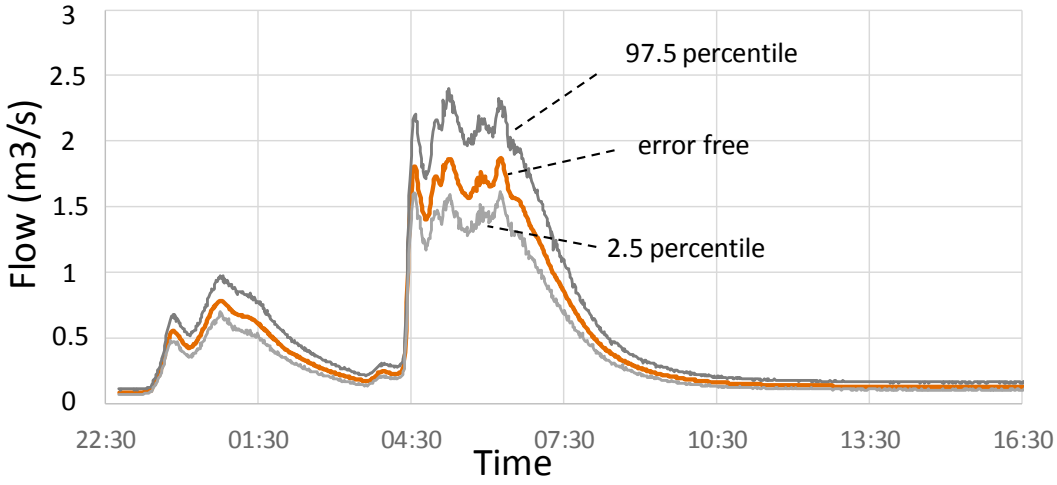

Figure 86. Range of randomly generated flow time series samples, between 2.5 percentile and 97.5 percentile (example for upstream flow of Carmaux tank).

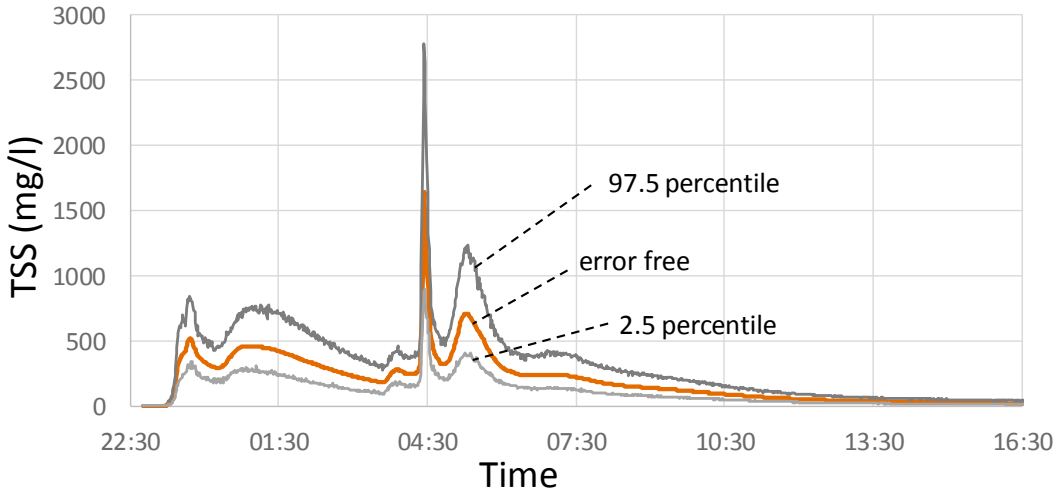

Figure 87. Range of randomly generated TSS time series samples, between 2.5 percentile and 97.5 percentile (example for upstream TSS of Carmaux tank).

As shown in Figure 88, the results obtained after implementing the QBR strategy using MV curve prediction derived by the generated samples of flow and TSS time series at the four controlled locations are presented in terms of the CSO load difference between QBR and HBR. The box plots represent , given the 100 samples of the event MV curves generated for each control site, the range of CSO load differences varies between 5.6 and 8.2 % (or between 2.4

and 3.4 tons). With the median value of 6.4 % (or 2.7 tons), the uncertainty in the CSO load difference can be considered as 7.5 ± 1.1% (or 3.1 ± 0.4 tons). The MV curve prediction is not very sensitive to random uncertainty in flow and TSS prediction uncertainty and as a consequence, the resulting uncertainty range of the QBR performance deems not extensive. In addition, optimisation by QBR is based on estimating the MV curve slope gradients and the stored volumes during each CTI (see section 6.24.1 and section 7.2.3.2), which are derived from predicted flows and TSS upstream the tanks. Consequently, when there is no error in the prediction of these variables, the performance of QBR over HBR should be amongst the top of the 100 simulated samples. This explains why the CSO load difference obtained by the error free prediction is seen as close to the minimum values (i.e. highest CSO load difference) of the box plots.

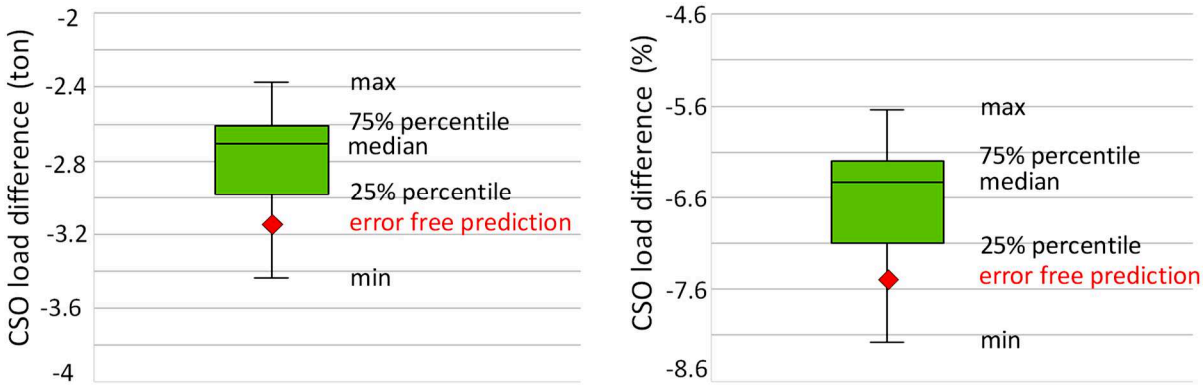

Figure 88. Effect of MV curve prediction uncertainty on the performance of QBR over HBR. Left plot: CSO load difference by ton; right plot: CSO load difference by percentage.

7.5 Impact of the retention tank volume

Figure 89a and Figure 89b show that in both strategies, the larger the tank volumes, the less TSS loads are spilled via CSOs. The slope of the linear regression line indicates the degree of sensitivity of each tank towards the total CSO loads. The Abria tank plays the most important role whereas the Alhambra tank seems insensitive to CSO loads. For Alhambra, the reason

could be due to its much smaller volume when compared to the other ones and the fact that its upstream sub-catchments are minor contributors to CSO loads.

Interestingly, Figure 90 shows that increasing tank volume does not always lead to increasing performance of QBR over HBR. For Abria tank, the benefit of QBR over HBR first grows with larger tank volumes, till reaching a peak (between 6000 m^3 and 8000 m^3) and gradually declining later on. For Carmaux tank, the peak is less clear but also appears in the middle of volume range (between 7000 m^3 and 9000 m^3). To conclude, the choice between the QBR and HBR control strategies should be made in the light of the tank volumes at each site. Sensitivity analysis appears to be important in tank design for QBR strategies.

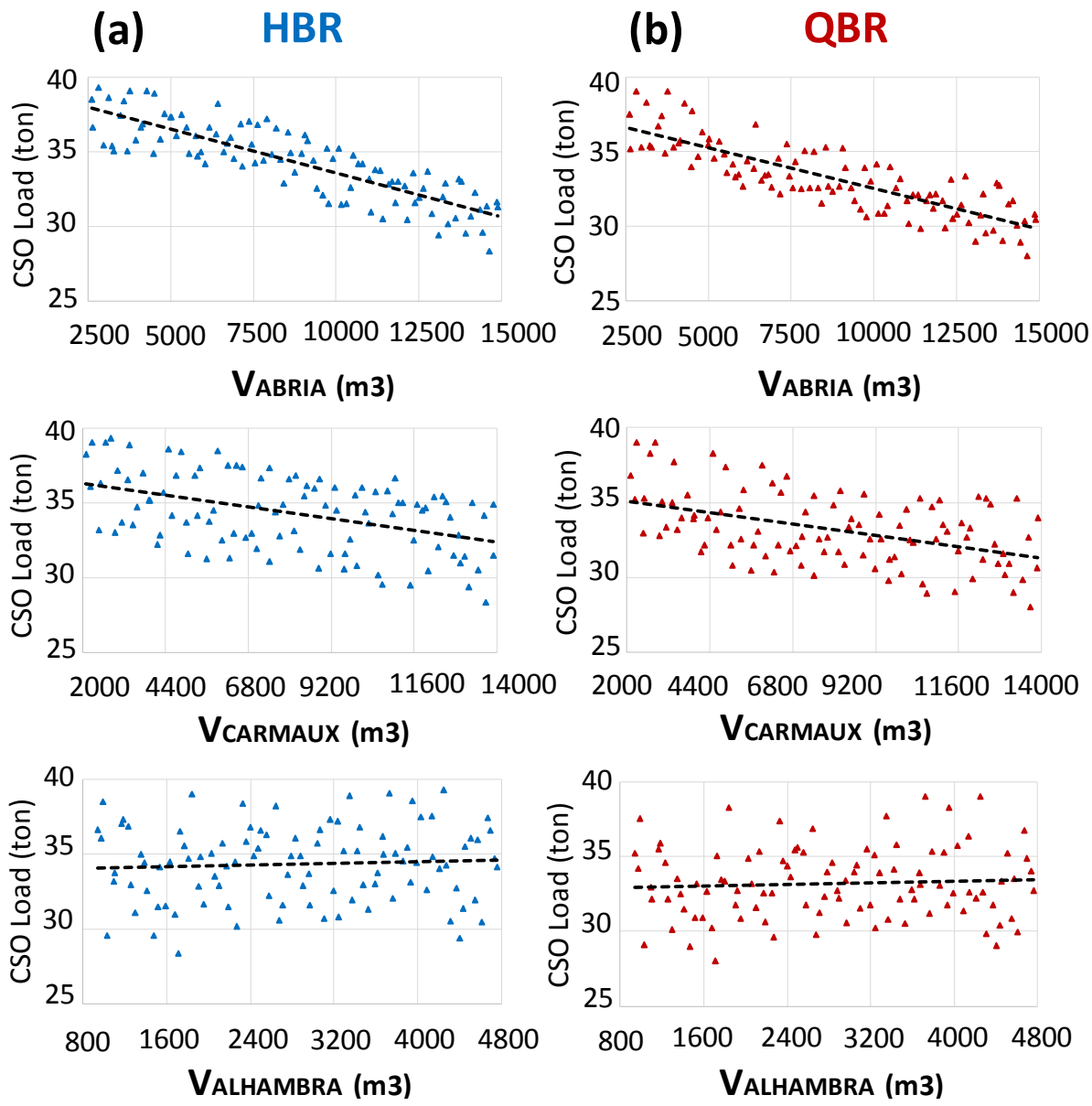

Figure 89. (a) Impact of tank volume (Abria, Carmaux, and Alhambra tanks, event 29 July 2015) on the CSO loads in HBR; (b) in QBR (black dashed line stands for the linear regression line of data).

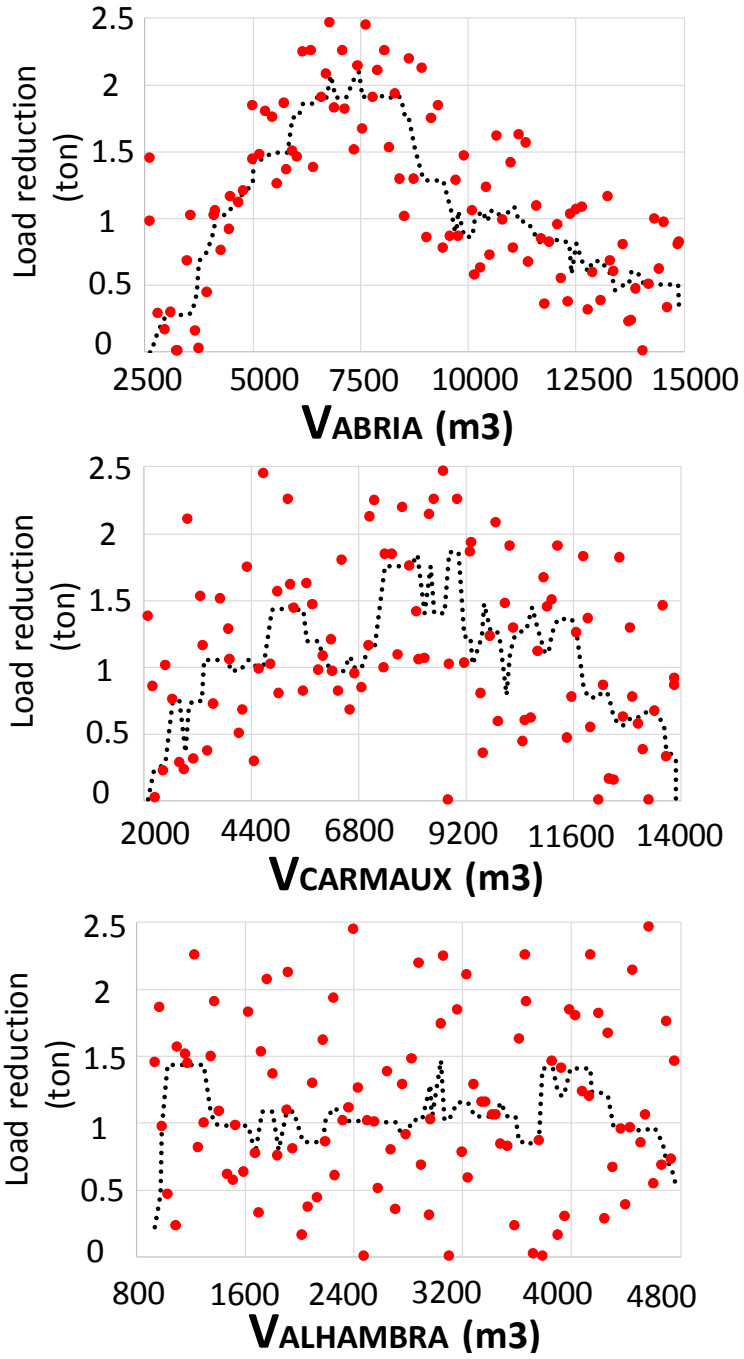

Figure 90. Impact of tank volume (Abria, Carmaux, and Alhambra tanks, event 29 July 2015) on the differences in CSO loads between QBR and HBR (black dotted line represents the moving median line with window width of ten values).

7.6 Volume selection of the additional tanks to be used for QBR

Figure 91 shows the profile of TSS load interception difference (QBR versus HBR) with varying volumes of the Périnot tank for the event on 23 April 2016. The peak values are reached when the tank volumes range between 2300 m^3 and 3300 m^3. There exist cases in which the

TSS load interception difference decreases slightly with a small increase in tank volume, as those circled by black-dotted lines. To understand this issue, the author determines one example range of volume with small change, then picks the minimum and maximum volumes (see Figure 91, 1085 m^3 and 1225 m^3 respectively) to test. The HBR and QBR strategies are re-implemented on the Périnot model, using the same volumes but with one-second routing time step and 30-second reporting time step for the SWMM-TSS model. These settings are smaller than the original ones of five-second routing time step and one-minute reporting time step.

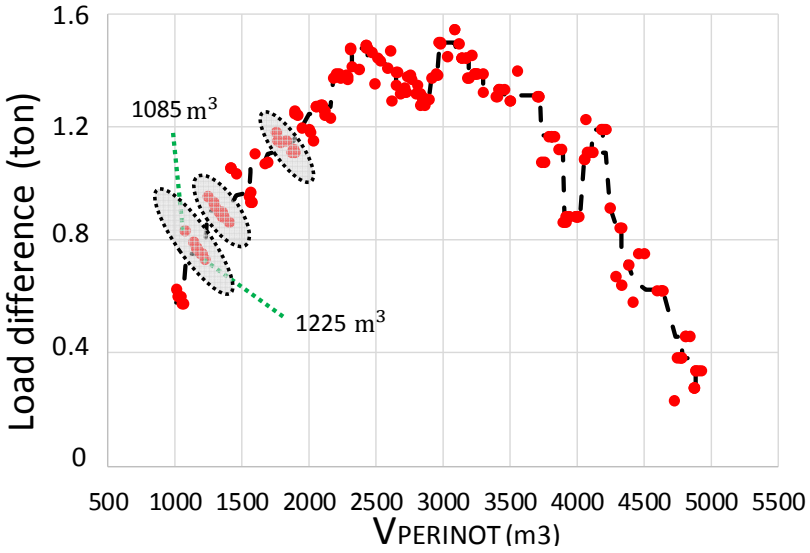

Figure 91. Impact of tank volume (Périnot tank, event 23 April 2016) on the difference in TSS load interception between QBR and HBR (black dotted line represents the moving median line with window width of ten values).

Table 25 provides the comparison between the new results using smaller time steps and the original results. With the original configuration, the QBR performance does not increase when the tank volume increases from 1085 m^3 to 1225 m^3. In contrast, with the new configuration, the intercepted load by QBR increases with increasing tank volume. Similarly, the difference in terms of intercepted load between QBR and HBR also increases.

Table 25. Comparison between two time-step configurations for QBR and HBR on the Périnot catchment (event 23 April 2016).

Tank volume (m^3)	1-minute reporting time step, 5-second routing time step			30-second reporting time step, 1-second routing time step		
	TSS load intercepted by the tank (kg)			TSS load intercepted by the tank (kg)		
	QBR	HBR	Difference (QBR versus HBR)	QBR	HBR	Difference (QBR versus HBR)
1085	1631	794	837	1520	807	713
1225	1631	898	733	1766	899	867

Figure 92 illustrates the weir positions obtained from the original and the new runs when the tank volume is 1225 m^3. This weir is the actuator used to fill the Périnot tank (position 1: fill, position 0: close). In the original run, the weir is opened 30 seconds later than in the new run, which explains the lower TSS load intercepted by the tank. In this case, smaller time-step configuration of the SWMM-TSS model can improve the performance of the QBR strategy.

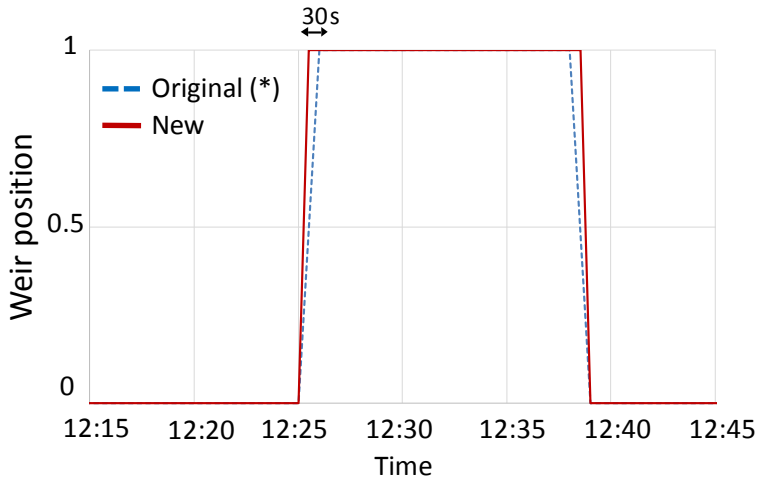

(*) Original run: 1-min reporting, 1-s routing time steps
New run: 30-s reporting, 5-s routing time steps

Figure 92. Comparison between two time-step configurations for QBR on the Périnot catchment (event 23 April 2016).

Figure 93 shows the profile of TSS load interception with varying volumes of the Périnot tank for the event on 26 May 2016. The peak values are reached when the tank volumes range between 3200 m^3 and 3600 m^3. By considering the peak values observed from the event on 23 April 2016, the selected volume of the Périnot tank for QBR could be approximately 3300 m^3.

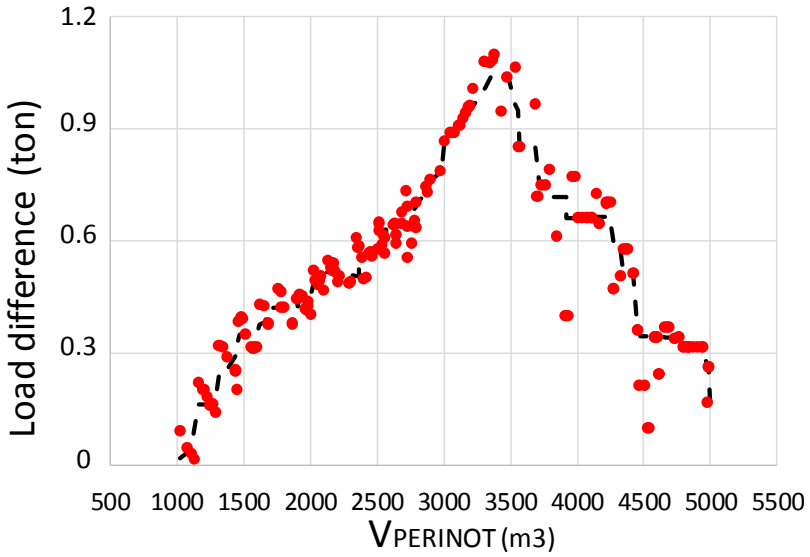

Figure 93. Impact of tank volume (Périnot tank, event 26 May 2016) on the difference in TSS load interception between QBR and HBR (black dotted line represents the moving median line with window width of ten values).

Figure 94 presents the profile of TSS load interception difference with varying volumes of the Bourran tank for the event on 09 March 2016. The peak values are reached when the tank volumes range between 9500 m^3 and 10500 m^3.

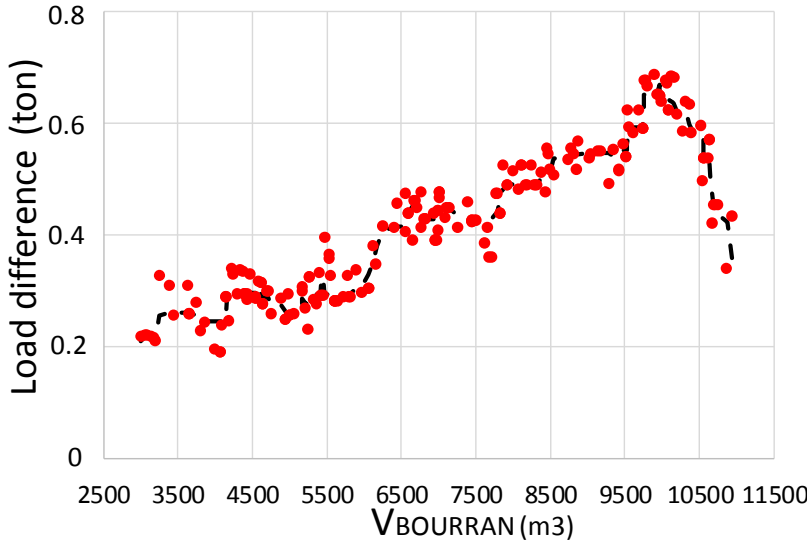

Figure 94. Impact of tank volume (Bourran tank, event 09 March 2016) on the difference in TSS load interception between QBR and HBR (black dotted line represents the moving median line with window width of ten values).

Figure 95 shows the profile of TSS load interception difference with varying volumes of the Bourran tank for the event on 26 May 2016. The peak values are reached when the tank volumes range between 7500 m^3 and 8500 m^3. Given the peak values observed from previous event, the selected volume of the Bourran tank for QBR could be around 8000 m^3.

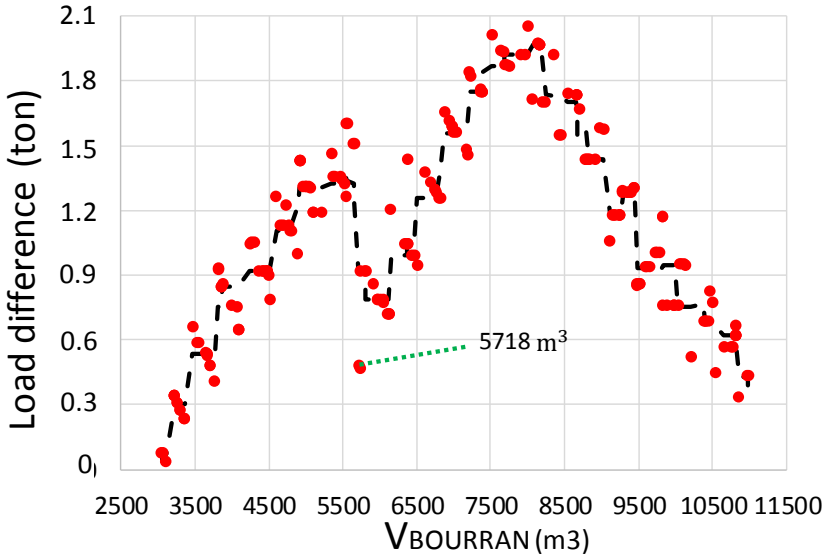

Figure 95. Impact of tank volume (Bourran tank, event 26 May 2016) on the difference in TSS load interception between QBR and HBR (black dotted line represents the moving median line with window width of ten values).

It is also observed from Figure 95 that there is a sharp drop in the load interception difference within the volume range between 5500 m^3 and 6000 m^3. The author picks the lowest value (corresponding to the volume of 5718 m^3) of the load interception differences from that range to investigate the issue. The QBR strategy is re-implemented on the Bourran catchment, using the same volumes and the same time-step configuration of the SWMM-TSS model, but with the CTI of 15 minutes. The original CTI of the sensitivity run is 20 minutes.

Comparison between the results obtained by the original run and the new run of QBR is summarised in Table 26. It is obvious that the QBR controller of the new run (CTI = 15 minutes) outperforms the original one. Load interception difference between QBR and HBR is approximately 1.8 tons, higher than highest load difference obtained within the volume range between 5500 m^3 and 6000 m^3 (see Figure 95).

Table 26. Difference in intercepted TSS load by Bourran tank between two CTI configurations of QBR (event 26 May 2016).

	HBR	CTI = 20 minutes		CTI = 15 minutes	
		QBR	Difference (QBR versus HBR)	QBR	Difference (QBR versus HBR)
TSS load entering the tank (kg)	5440	5920	480	7233	1793

Figure 96a shows that over the storm event duration, there are three peaks of TSS load upstream the tank. With the original run of 20-minute CTI, the QBR controller chooses to intercept the TSS load into the tank for all these peaks, as shown in Figure 96b (TSS load interception) and Figure 96e (weir position to fill the tank). However, in the new run of 15-minute CTI, the controller intercepts the TSS load from the first and the third peaks only. The filling period for the first peak is shorter in the original run, leading to higher remaining tank capacity after filling first peak (see Figure 96c) and as a result, the controller gives decision to fill the second peak.

In brief, the result from the test shows that the drop in the QBR performance could be resolved by shortening the CTI length. This confirms the results shown in section 6.3.3, i.e. a shorter CTI gives a better performance. The difference in performance by changing the CTI duration may be significant.

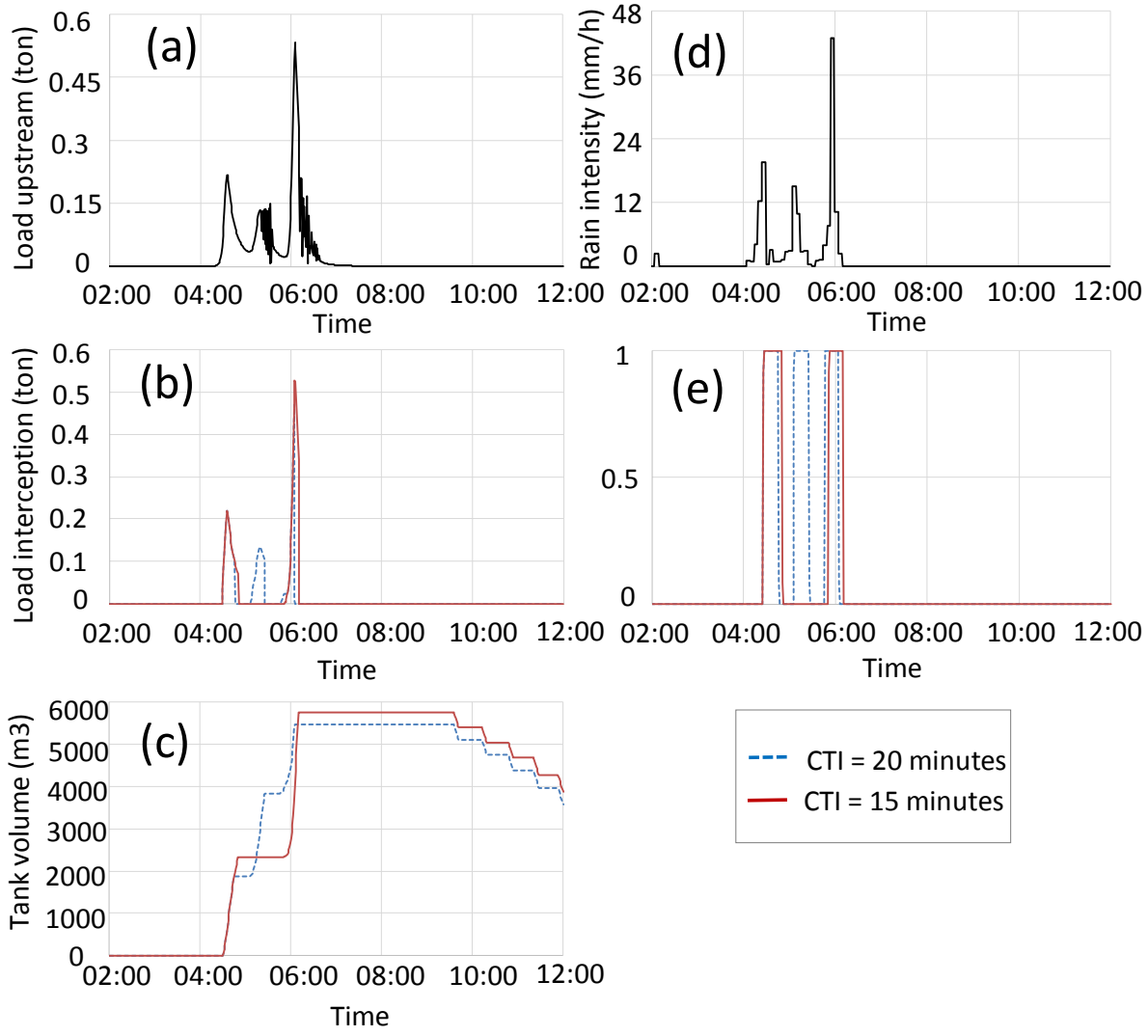

Figure 96. Differences in the results between two CTI configurations of QBR for the event on 26 May 2016 (Bourran tank).

Figure 97 shows the profile of TSS load interception difference with varying volumes of the Chêne Vert tank for the event on 09 March 2016. Using this event, the selected volume of the Chêne Vert tank for QBR could be around 6000 m^3.

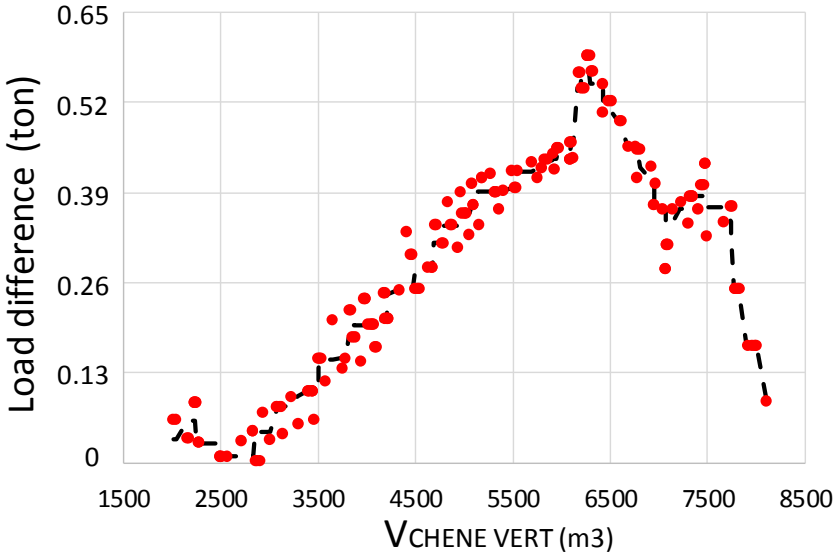

Figure 97. Impact of tank volume (Chêne Vert tank, event 09 March 2016) on the difference in TSS load interception between QBR and HBR (black dotted line represents the moving median line with window width of ten values).

7.7 Summary

Given the proven potential when applied to the small Périnot catchment, the QBR strategy is then implemented at wider scale on the Louis Fargue catchment and compared with a typical HBR strategy that represents current operation of the SN. There are now three tanks taken into account: Carmaux, Abria, and Alhambra with volumes of 8000 m^3, 6000 m^3 and 1500 m^3 respectively selected for control. QBR is also applied at the interceptor to transfer overflows from an upstream CSO point to a downstream one, knowing that the TSS concentration of the first is generally higher than the latter.

Firstly, one representative storm event is selected to tune and test the performance of QBR over HBR. The results show that the QBR strategy is capable of identifying the right period (highest TSS flux) to maximise the filling of the tank, and equally capable of estimating the right amount of filled volumes during other periods to make full of use the tank capacity. For the selected representative event, QBR produces a 7.5 % CSO load reduction when compared to HBR. Secondly, the QBR strategy is implemented on 19 storm events over 15 months. It can be

observed that the performance of the QBR strategy is consistent over various storm events. QBR can bring a valuable benefit over HBR, with 17 out of 19 events having load reduction percentage per event varying between 6 and 28.8 %. Nevertheless, contrarily to the case of the Périnot catchment, for the Louis Fargue catchment, it is not possible to obtain any meaningful correlation between the performance of the QBR strategy and the event MV curve characteristics. This may be due to complex interactions between sub-catchments and storage tanks at the wider scale of the Louis Fargue catchment.

In addition, this chapter evaluates the impact of uncertainty in MV curve prediction (coming from the detailed model prediction uncertainty) on the performance of the QBR strategy, using the same representative storm event. 100 samples of the event MV curves are randomly generated for each of the four controlled sites. The resulting range of CSO load reduction varies between 5.6 and 8.2 % and the median value is 6.4 %. For the representative event, the uncertainty in the CSO reduction of the QBR strategy over the HBR strategy is thus 7.5 ± 1.1% (or 3.1 ± 0.4 tons).

Besides, this chapter looks into the influence of the storage tanks volumes (Abria, Carmaux, and Alhambra) on the performance of the two control strategies. It can be seen from the sensitivity study that a larger storage capacity of the tank can generally reduce CSO load for both strategies. However, the choice between the type of control strategies, QBR or HBR, should take into account the current tank dimensions and locations at the site. This chapter also presents the sensitivity study done separately for each of the three additional retention tanks upstream (Périnot, Bourran, and Chêne Vert), which aims to select the most useful tank volumes used for the extension of QBR to more tanks of the Louis Fargue catchment. Accordingly, the selected volumes for the Périnot, Bourran, and Chêne Vert tanks are 3300, 8000 and 6000 m^3 respectively. Lastly, it has been shown that the QBR performance may also be very sensitive i) to routing and reporting time steps of the model runs and ii) to the duration of the CTI.

CHAPTER 8: GENERAL CONCLUSIONS AND PERSPECTIVES

The concept of real time control appeared more than four thousand years after the first evidences of ancient sewer systems. Since the first installed prototype in the late 1960s, there have been considerable developments of the real time control (RTC) methods for sewer systems. Although literature on water quality-based RTC (QBR) is more limited than hydraulics-based RTC (HBR), the motivation for QBR application has continued to grow over past decades. The increasing interest in QBR mainly comes from the development of sensing technologies and the inclusion of reducing pollutant loads from urban discharges in environmental regulations to protect receiving waters. Past studies justified the possibility of using economic and easy-to-use sensors such as turbidity meter and UV-Vis spectrophotometer for online monitoring of common sewer process variables such as total suspended solids (TSS), chemical oxygen demand or total Kjeldahl nitrogen.

Accordingly, this thesis develops of a new QBR strategy to reduce the amount of CSO loads spilled to receiving waters during storm events. It is meant to be a simple, robust, and nothing-to-lose strategy for combined sewers having retention tanks and controllable actuators. The performance of the QBR strategy is evaluated by comparison with a typical HBR strategy, which represents existing sewers operation in many cities across the world, including the study area of the thesis project: the Louis Fargue catchment in Bordeaux, France. This 7700 ha catchment is part of a larger urban area prone to flooding due to several factors: climate, topography and tidal bore. The catchment is thus equipped with multiple retention tanks, providing abundant storage capacities.

To perform RTC, a SWMM-TSS detailed model to represent reality and forecast future processes is built for the catchment sewer network, using continuously monitoring flow, quality, and rainfall data at four main sub-catchment outlets connected to Peugue, Naujac, Caudéran-Naujac and Lauzun CSO structures. TSS is the quality state variable of the control strategies.

In addition, this thesis utilises available measured data to propose two statistical approaches (i.e. multiple linear regression and random forest regression) for evaluation of the total CSO loads produced by storm events. They were intended for future application in a simplified QBR strategy that should be fast and have reasonable efficiency. These approaches incorporate the techniques of explanatory variable selection and splitting dataset for model calibration and verification.

As a first step, a proof-of-concept study is performed to test the new QBR concept based on MV curve prediction. Basically, the QBR strategy aims identifying the most appropriate period (highest TSS flux) to maximise the filling of the tank while the HBR strategy aims filling the tanks every time the flow rate is higher than its pre-defined threshold. The 205 ha catchment of Périnot is used for implementing the control strategies. This catchment is a small part of the Louis Fargue catchment and includes a CSO structure and a retention tank of 1200 m^3 storage capacity. Over the 31 tested storm events, there are 11 events having valuable CSO load reduction, with reduction values of individual storm events ranging between 3 and 43 %, and reduction value of around 10 % in total. As part of the proof-of-concept study, a sensitivity analysis of the impact of the duration of control time interval (CTI) illustrates that for storm events with QBR benefit, decreasing the length of the CTI generally leads to decreasing the amount of total CSO load or, in other words, improving the efficiency of QBR. Besides, the volume of the retention tank is deemed to play an important role in the performance of QBR.

Based on the tests applied on the two storm events, the change in the CSO load reduction by QBR (compared to HBR) with different tank volumes is considerable.

Next, the QBR strategy is then implemented on the entire Louis Fargue catchment and, in the same way, compared with the HBR strategy. There are three retention tanks which are simulated in the control model: Carmaux, Abria, and Alhambra with volumes of 8000 m^3, 6000 m^3 and 1500 m^3 respectively. Compared to the previous proof-of-concept study, improvement is added to allow the controller to better utilise the entire capacity of the tank capacity. QBR is also applied to the main interceptor of the sewer network to transfer overflows from an upstream CSO point to a downstream one, knowing that the TSS concentration of the first is generally higher than the latter. Using a representative storm event for tuning, the QBR strategy produces a 7.5 % CSO load reduction when compared to HBR. The QBR strategy is also implemented on 19 storm events over a 15-month period. It can be observed that the performance of the QBR strategy is consistent over various storm events. QBR can bring a valuable benefit over HBR, with 17 out of 19 events having load reduction percentage per event varying between 6 and 28.8 %. However, it is not possible to obtain any meaningful correlation between the performance of the QBR strategy and the event MV curve characteristics.

In addition, the study on the Louis Fargue catchment further evaluates the impact of MV curve prediction uncertainty (coming from the detailed model prediction uncertainty) on the performance of the QBR strategy, using the same representative storm event. 100 samples of the event MV curves are randomly generated for each of the four controlled site. For the representative event, the uncertainty of the CSO reduction of the QBR strategy over the HBR strategy is 7.5 ± 1.1% (or 3.1 ± 0.4 tons). Similar to the proof-of-concept study, the influence of the storage tank volume on the performance of the two control strategies QBR and HBR is also investigated. It can be seen from the sensitivity study that a larger storage capacity of the tank can generally improve the amount of CSO load reduction for both strategies. However, the

choice between the type of control strategies, QBR or HBR, should take into account the current tank dimensions and locations within the catchment.

To sum up, the QBR strategy has been tested at different catchment scales and under a large number of storm events. The obtained results of the performance of the strategy are truly promising. The QBR controller is simply based on a fast optimisation method using the gradients of the event Mass-Volume (MV) curve to generate control actions. Compared to other RTC strategies that apply the same model predictive control principles, the new QBR strategy possibly requires less human efforts and time in modelling tool development. It involves the use of only one detailed model for both simulating the processes of reality and forecast future process of the system, along with a simple optimisation approach. There is no need for developing any simplified model or advanced techniques involving numerous model runs to derive an optimal solution.

As the next step, the author thinks that there are several topics arisen from this thesis and interesting for future studies:

- At present, for the Louis Fargue catchment, the QBR strategy was tested only with three tanks. Given 16 existing retention tanks on the catchment, it will be interesting to include several more tanks in control and evaluate how much larger the QBR benefit of CSO load reduction can be.
- Is there any correlation between rainfall characteristics and the performance of the QBR strategy? Is there any correlation between the event MV curve characteristics and the performance of the QBR strategy? Knowing the correlation (if any) is meaningful to decide for which storm events the QBR strategy can be applied with the greatest benefit.
- Is it possible to develop an even more simple and efficient QBR strategy which uses only statistical models (e.g. multiple regression model, random forest model)? For instance, using

rainfall forecast, the total CSO load of each sub-catchment can be quickly computed and recursively updated, facilitating the decisions of allocating excessive stormwater and prioritizing available storage capacities between different sub-catchments according to the magnitude of their CSO loads.

- The controller predicts the event MV curve using error free rainfall data. How will the performance of the QBR strategy be affected if real forecast rainfall data are used (e.g. radar data)?
- The closed-loop control is currently demonstrated using a physically based model simulator as a virtual reality and without accounting for uncertainties in flow and water quality measurements. What happens to the QBR controller performance if these uncertainties are accounted? And how can they be included in the simulation of the model representing reality?

References

Aalderink, R.H. & Lijklema, L. (1985). Water quality effects in surface waters receiving stormwater discharges. *Water in Urban Areas. TNO Committee on Hydrological Research, Proceedings and Information*, 33, 143–159.

Andréa, G., Ahyerre, M., Pleau, M., Pérarnaud, J.-J., Komorowski, F., & Schoorens, J. (2013). Gestion Dynamique des RUTP du bassin versant Louis Fargue à Bordeaux: mise en oeuvre et premiers résultats opérationnels (Louis Fargue catchment area in Bordeaux - Real time control of CSO's: implementation and first operational results). *Proceedings of the 8th International NOVATECH Conference*, Lyon, France, 23-27 June, 10 p.

Angelakis, A. N., Koutsoyiannis, D., & Tchobanoglous, G. (2005). Urban wastewater and stormwater technologies in ancient Greece. *Water Research*, 39, 210–220.

Angelakis, A. N., & Rose, J. B. (2014). *Evolutions of Sanitation and Wastewater Technologies through the Centuries*. London (UK): IWA Publishing, 528 p. ISBN 9781780404844.

Archer, K. J., & Kimes, R. V. (2008). Empirical characterization of random forest variable importance measures. *Computational Statistics & Data Analysis*, 52, 2249–2260.

Ardern, E., & Lockett W.T. (1914) Experiment on the oxidation of sewage without the aids of filters. *J. Soc. Chem. Ind.*, 33, 523–539.

Ashley, R. M., Bertrand-Krajewski, J.-L., Hvitved-Jacobsen, T., & Verbanck, M. (2004). *Solids in sewers.* London (UK): IWA Publishing, 360 p. ISBN 9781900222914.

Ashley, R., Bertrand-Krajewski, J.-L., & Hvitved-Jacobsen, T. (2005). Sewer solids–20 years of investigation. *Water Science and Technology*, 52(3), 73–84.

Bachis, G., Maruéjouls, T., Tik, S., Amerlinck, Y., Melcer, H., Nopens, I., Lessard, P., & Vanrolleghem, P. A. (2015). Modelling and characterization of primary settlers in view of whole plant and resource recovery modelling. *Water Science and Technology*, 72(12), 2251–2261.

Barraud, S., Gibert, J., Winiarski, T., & Bertrand-Krajewski, J.-L. (2002). Implementation of a monitoring system to measure impact of stormwater runoff infiltration. *Water Science and Technology*, 45(3), 203–210.

Barraud, S., Dechesne, M., Bardin, J.-P., & Varnier, J.-C. (2005). Statistical analysis of pollution in stormwater infiltration basins. *Water Science and Technology*, 51(2), 1–9.

Beck, M.B. (1976). Dynamic modeling and control applications in water-quality maintenance. *Water Research*, 10(7), 575–595.

Beeneken, T., Erbe, V., Messmer, A., Reder, C., Rohlfing, R., Scheer, M., Schütze, M., Schumacher, B., Weilandt, M., & Weyand, M. (2013). Real time control (RTC) of urban drainage systems – A discussion of the additional efforts compared to conventionally operated systems. *Urban Water Journal*, 10(5), 293–299

Benedetti, L., Langeveld, J., Comeau, A., Corominas, L., Daigger, G., Martin, C., Mikkelsen, P. S., Vezzaro, L., Weijers, S., & Vanrolleghem, P. A. (2013). Modelling and monitoring of integrated urban wastewater systems: review on status and perspectives. *Water Science and Technology*, 68(6), 1203–1215.

Bertrand-Krajewski, J.-L (1993). Modélisation du transport solide en réseau d'assainissement unitaire: le modèle HYPOCRAS (Modelling of solid transport in a combined sewer network: the HYPOCRAS model). *La Houille Blanche*, 4, 243-255.

Bertrand-Krajewski, J.-L., Briat, P., & Scrivener, O. (1993). Sewer sediment production and transport modelling: A literature review. *Journal of Hydraulic Research*, 31(4), 435–460.

Bertrand-Krajewski, J. L., Chebbo, G., & Saget, A. (1998). Distribution of pollutant mass vs volume in stormwater discharges and the first flush phenomenon. *Water Research*, 32(8), 2341–2356.

Bertrand-Krajewski, J.-L., Laplace, D., Joannis, C., & Chebbo, G. (2000). *Mesures en hydrologie urbaine et assainissement (Measures in urban hydrology and sanitation)*. Paris (France): Technique et Documentation, 794 p. ISBN 2743003804.

Bertrand-Krajewski, J.-L. (2003). Sewer sediment management: some historical aspects of egg-shaped sewers and flushing tanks. *Water Science and Technology*, 47(4), 109–122.

Bertrand-Krajewski, J.-L. (2004). TSS concentration in sewers estimated from turbidity measurements by means of linear regression accounting for uncertainties in both variables. *Water Science and Technology*, 50(11), 81–88.

Bertrand-Krajewski, J.-L., Barraud, S., Lipeme Kouyi, G., Torres, A., & Lepot, M. (2007). Event and annual TSS and COD loads in combined sewer overflows estimated by continuous in situ turbidity measurements. In *Proceedings of the 11th International Conference on Diffuse Pollution* 8p., Belo Horizonte, Brazil.

Bonneton, P., Van de Loock, J., Parisot, J.-P., Bonneton, N., Sottolichio, A., Detandt, G., Castelle, B., Marieu, V., & Pochon, N. (2011). On the occurrence of tidal bores – The Garonne River case. *Journal of Coastal Research*, 64, 1462–1466.

Bordóns C (2000) *Control predictivo: metodología, tecnología y nuevas perspectivas (Predictive control: methodology, technology and new perspectives)*. Departamento de Ingeniería de Sistemas y Automática, Universidad de Sevilla, Aguadulce, Almería.

Borsányi, P., Benedetti, L., Dirckx, G., De Keyser, W., Muschalla, D., Solvi, A. M., Vandenberghe, V., Weyand, M. & Vanrolleghem, P. A (2008). Modelling real-time control options on virtual sewer systems. *J. Environ. Eng. Sci.*, 7(4), 395–410.

Breiman, L. (2001). Random Forests. *Machine Learning*, 45(1), 5–32.

Briat, P. (1995). Lyonnaise des eaux internal Research and Development programs, France.

Brombach, H., Weiss, G. and Fuchs, S. (2005) A new database on urban runoff pollution: Comparison of separate and combined sewer systems. *Water Science and Technology*, 51(2), 119–128.

Butler, D., James Digman, C., Makropoulos, C., & Davies, J. (2018). *Urban drainage*. Boca Raton (USA): CRC Press, 592 p. ISBN 9781498750592.

Campisano A., Schilling, W., & Modica, C. (2000). Regulators' setup with application to the Roma-Cecchignola combined sewer system. *Urban Water*, 2(3) 235-242.

Campisano, A., Cabot Ple, J., Muschalla, D., Pleau, M., & Vanrolleghem, P. A., (2013). Potential and limitations of modern equipment for real time control of urban wastewater systems. *Urban Water Journal*, 10(5), 300–311.

Capodaglio, A. G. (1994). Transfer Function Modelling of Urban Drainage Systems, and Potential Uses in Real-Time Control Applications. *Water Science and Technology*, 29(1–2), 409–417.

Caradot, N., Sonnenberg, H., Rouault, P., Gruber, G., Hofer, T., Torres, A., Pesci, M., & Bertrand-Krajewski, J.-L. (2015). Influence of local calibration on the quality of online wet weather discharge monitoring: feedback from five international case studies. *Water Science and Technology*, 71(1), 45–51.

Cetaqua (2015). Kick-Off LIFE EFFIDRAIN [PowerPoint presentation].

Chebbo, G., Bachoc, A., Laplace, D., & Leguennec, B. (1995). The transfer of solids in combined sewer networks. *Water Science and Technology*, 31(7), 95–105.

Council Directive (1991). Directive of 21 May 1991 concerning urban waste water treatment (91/271/EEC). Off. J Eur. OJ L 135, 30.5.1991, p. 40.

Council Directive (2000). Directive of 23 October 2000 establishing a framework for Community action in the field of water policy (2000/60/EC). Off. J Eur. OJ L 327, 22.12.2000, p. 1–73.

De Feo, G., Antoniou, G., Fardin, H. F., El-Gohary, F., Zheng, X. Y., Reklaityte, I., Butler, D., Yannopoulos, S., & Angelakis, A. N. (2014). The historical development of sewers worldwide. *Sustainability*, 6(6), 3936–3974.

Delgado, S., Alvarez, M., Rodriguez-Gomez, L. E., & Aguiar, E. (1999). H2S generation in a reclaimed urban wastewater pipe. case study: Tenerife (Spain). *Water Research*, 33(2), 539–547.

Delleur, J. W. (2001). New Results and Research Needs on Sediment Movement in Urban Drainage. *Journal of Water Resources Planning and Management*, 127(3), 186–193.

Dembélé, A., Bertrand-Krajewski, J.-L., & Barillon, B. (2010). Calibration of stormwater quality regression models: a random process? *Water Science and Technology*, 62(4), 875–882.

Dembélé, A., Bertrand-Krajewski, J.-L., Becouze, C, & Barillon, B. (2011). A new empirical model for stormwater TSS event mean concentrations (EMCs). *Water Science and Technology* 64(9), 1926–1934.

Durchschlag, A. (1991). Zusammenhang zwischen Mischwasserspeicherung und Kläranlagenablauf (Connection between mixed water storage and wastewater treatment plant effluent). *Zeitschrift Für Stadtentwässerung Und Gewässerschutz* 4.

Erbe, V., & Schütze, M., (2005). An integrated modelling concept for immission-based management of sewer system, wastewater treatment plant and river. *Water Science and Technology*, 52(5), 95–103.

Etcheber, H., Taillez, A., Abril, G., Garnier, J., Servais, P., Moatar, F., & Commarieu, M.V (2007). Particulate organic carbon in the estuarine turbidity maxima of the Gironde, Loire and Seine estuaries: origin and lability, *Hydrobiologia*, 588(1), 245–259.

Etcheber, H., Schmidt, S., Sottolichio, A., Maneux, E., Chabaux, G., Escalier, J.-M., Wennekes, H., Derriennic, H., Schmeltz, M., Quéméner, L., Repecaud, M., Woerther, P., & Castaing, P.

(2011). Monitoring water quality in estuarine environments: lessons from MAGEST monitoring program in the Gironde fluvial–estuarine system. *Hydrol. Earth Syst. Sci.*, 15(3), 831–840.

Feng, J. (2018). *Calibration and Hydraulics-based Control of Water Quality Model in View of Urban Drainage Real Time Control in Bordeaux Metropolitan*. Master thesis, University of Nice Sophia Antipolis (Euroaquae program), France.

Fletcher, T. D., & Deletic, A. (2007). Statistical evaluation and optimisation of stormwater quality monitoring programmes. *Water Science and Technology*, 56(12), 1–9.

Flood, K. (2017). CSO – Oh no! [Blog post]. Retrieved from https://www.dlhowell.com/blog/cso-oh-no/.

Foladori, P. (2015). Urban Stormwater Quality Monitoring. In "*Urban Water Reuse Handbook*" (Eslamian, S.). Boca Raton (USA): CRC Press, pp. 593–605. ISBN 9781482229141.

Fradet, O., Pleau, M., & Marcoux, C. (2011). Reducing CSOs and giving the river back to the public: innovative combined sewer overflow control and riverbanks restoration of the St Charles River in Quebec City. *Water Science and Technology*, 63(2), 331–338.

[France outline map] [Online image] (n.d.). Retrieved from https://www.worldatlas.com/webimage/countrys/europe/outline/frout.htm.

Fricke, K. I., Hoppe, H., Hellmig, M., & Muschalla, D. (2016). 10 years spectrometry based P-RTC in Wuppertal – experiences and enhancements. *Proceedings of the 9th International NOVATECH Conference*, Lyon, France, 4p.

Fronteau, C., Bauwens, W., & Vanrolleghem, P. A. (1997). Integrated modelling: Comparison of state variables, processes and parameters in sewer and wastewater treatment plant models. *Water Science and Technology*, 36(5), 373–380.

Gamerith, V. (2011). *High resolution online data in sewer water quality modelling*. PhD thesis, Technische Universität Graz, Austria.

García, L., Barreiro-Gomez, J., Escobar, E., Téllez, D., Quijano, N., & Ocampo-Martinez, C. (2015). Modeling and real-time control of urban drainage systems: a review. *Advances in Water Resources*, 85, 120–132.

Genuer, R., Poggi, J.-M., & Tuleau-Malot, C. (2010). Variable selection using random forests. *Pattern Recognition Letters*, 31, 2225–2236.

Graham, J. W. (1972). *The Palaces of Crete*. Princeton (USA): Princeton University Press, 269 p. ISBN 9780691035246.

Gray, H.F. (1940). Sewerage in ancient and mediaeval times. *Sewage Works Journal*, 12(5), 939–946.

Granger, D., Lafficher, C., & Maruéjouls, T. (2016). *QualiDO – Evaluation de la qualité des rejets du bassin versant Louis Fargue. Rapport annuel (*QualiDO – Assessment of the quality of discharges from the Louis Fargue catchment. Annual report). Le LyRE, Suez, France.

Grömping, U. (2009). Variable importance assessment in regression: linear regression versus random forest. *The American Statistician*, 63, 308-319.

Gruber, G., Winkler, S., & Pressl, A. (2004). Quantification of pollution loads from CSOs into surface water bodies by means of online techniques. *Water Science and Technology*, 50(11), 73–80.

Gruber, G., Bertrand-Krajewski, J.-L., Beneditis, J. D., Hochedlinger, M., & Lettl, W. (2006). Practical aspects, experiences and strategies by using UV/VIS sensors for long-term sewer monitoring. *Water Practice and Technology*, 1(1), 1–8.

Habib, E., Krajewski, W. F., Nespor, V., & Kruger, A. (2001). Sampling errors of tipping-bucket rain gauge measurements. *J. Hydrolog. Eng*., 6(2), 159–166.

Henze, M., van Loosdrecht, M., Ekama, G. A., & Brdjanovic, D. (2008). *Biological Wastewater Treatment: Principles, Modelling and Design*. London (UK): IWA Publishing, 528 p. ISBN 9781843391883.

Hoppe, H., Messmann, S., Giga, A., & Gruening, H. (2009). Options and limits of quantitative and qualitative online-monitoring of industrial discharges into municipal sewage systems. *Water Science and Technology*, 60(4), 859–867.

Hoppe, H., Messmann, S., Giga, A., & Gruening, H., (2011). A real-time control strategy for separation of highly polluted storm water based on UV–Vis online measurements–from theory to operation. *Water Science and Technology*, 63(10), 2287–2293.

House, M. A., Ellis, J. B., Herricks, E. E., Hvitved-Jacobsen, T., Seager, J., Lijklema, L., Aalderink, H., & Clifforde, I. T. (1993). Urban Drainage – Impacts on Receiving Water Quality. *Water Science and Technology*, 27(12), 117–158.

Hvitved-Jacobsen, T. (1982). The impact of combined sewer overflows on the dissolved oxygen concentration of a river. *Water Research*, 16(7), 1099–1105.

Hvitved-Jacobsen, T., Vollertsen, J., & Nielsen, A. H. (2010). *Urban and highway stormwater pollution: concepts and engineering*. Boca Raton (USA): CRC Press, 367 p. ISBN 9781439826850.

Jaumouillié, P., Larrarte, F., & Milisic, V. (2002). Numerical and experimental investigations of the pollutant distribution in sewers. *Water Science and Technology*, 45(7), 83–93.

Jenkins, D., & Wanner, J. (2014). *Activated Sludge–100 Years and Counting*. London (UK): IWA Publishing, 464 p. ISBN 9781780404936.

Joannis, C., Ruban, G., Gromaire, M. C., Bertrand-Krajewski, J.-L., & Chebbo, G. (2008). Reproducibility and uncertainty of wastewater turbidity measurements. *Water Science and Technology*, 57(10), 1667–1673.

Johansen, N. B. (1985). *Discharge to receiving waters from sewer systems during rain*. Copenhagen (Denmark): Technical University of Denmark, 287 p.

Joseph-Duran, B., Ocampo-Martinez, C., & Cembrano, G. (2014). Hybrid modeling and receding horizon control of sewer networks. *Water Resources Research*, 50(11), 8497–8514.

Jørgensen, M., Schilling, W., & Harremoës, P. (1995). General assessment of potential CSO reduction by means of real time control. *Water Science and Technology*, 32(1), 249–257.

Komorowski, K. (2016). L'évolution de la gestion des eaux pluviales à Bordeaux sur les 30 dernières années (The evolution of stormwater management in Bordeaux over the last 30 years). Session de formation aux techniques de l'assainissement, Suez, France.

Lacour, C. (2009). *Apport de la mesure en continu pour la gestion de la qualité des effluents de temps de pluie en réseau d'assainissement (Contribution of continuous turbidity measurements to the management of effluent quality in sewer systems during wet weather)*. PhD thesis, Université Paris-Est, France.

Lacour, C., Joannis, C., Gromaire, M.-C., & Chebbo, G. (2009). Potential of turbidity monitoring for real time control of pollutant discharge in sewers during rainfall events. *Water Science and Technology*, 59(8), 1471–1478.

Lacour, C., & Schütze, M. (2011). Real-time control of sewer systems using turbidity measurements. *Water Science and Technology*, 63(11), 2628–2632.

Langergraber, G., Fleischmann, N., & Hofstädter, F. (2003). A multivariate calibration procedure for UV/VIS spectrometric quantification of organic matter and nitrate in wastewater. *Water Science and Technology*, 47(2), 63–71.

Langeveld, J. G. (2004). *Interactions within wastewater systems*. PhD thesis, Delft University of Technology, Netherlands.

Langeveld, J. G., Veldkamp, R. G., & Clemens, F. (2005). Suspended solids transport: an analysis based on turbidity measurements and event based fully calibrated hydrodynamic models. *Water Science and Technology*, 52(3), 93–101.

Larrarte, F. (2015). Velocity and suspended solids distributions in an oval-shaped channel with a side bank. *Urban Water Journal*, 12(2), 165–173.

Launay, M. A., Dittmer, U., & Steinmetz, H. (2016). Organic micropollutants discharged by combined sewer overflows – Characterisation of pollutant sources and stormwater-related processes. *Water Research*, 104, 82–92.

Lens, P., Zeeman, G., & Lettinga, G. (2001). *Decentralised Sanitation and Reuse: Concepts, Systems and Implementation*. London (UK): IWA Publishing, 650 p. ISBN 9781900222471.

Leonhardt, G., Sun, S., Rauch, W., & Bertrand-Krajewski, J.-L. (2014). Comparison of two model based approaches for areal rainfall estimation in urban hydrology. *Journal of Hydrology*, 511(4), 880-890.

Lerat-Hardy, A., Coynel, A., Dutruch, L., Pereto, C., Bossy, C., Gil-Diaz, T., Capdeville, M.-J., Blanc, J., & Schäfer, J. (2019). Rare Earth Element fluxes over 15 years into a major European Estuary (Garonne-Gironde, SW France): Hospital effluents as a source of increasing gadolinium anomalies. *Science of the Total Environment*, 656, 409–420.

Lepot, M., Torres, A., Hofer, T., Caradot, N., Grubber, G., Aubin, J.-B., & Bertrand-Krajewski, J.-L. (2016). Calibration of UV/Vis spectrophotometers: A review and comparison of different methods to estimate TSS and total and dissolved COD concentrations in sewers, WWTPs and rivers. *Water Research*, 101, 519–534.

Lofrano, G., & Brown, J. (2010). Wastewater Management through the Ages: A History of Mankind. *Science of the Total Environment*, 408, 5254-5264.

Lund, N. S. V., A. K. V. Falk, A. K. V., Borup, M., Madsen, H., & Mikkelsen, P. S. (2018). Model predictive control of urban drainage systems: A review and perspective towards smart real-time water management. *Critical Reviews in Environmental Science and Technology*, 48(3), 279–339.

Ly, D. K., Maruéjouls, T., Martinez, M., Guasch, R., Ruiloba, L. C., Muñoz, E., Rouge, P., Sun, C., & Cembrano, G. (2017). D5 - Quality monitoring strategy for the pilots. LIFE EFFIDRAIN Project (ref number: LIFE14 ENV/ES/000860).

Ly, D. K., Maruéjouls, T., Joseph-Duran, B., & Muñoz, E. (2018). D10 - Atlantic pilot: pilot set-up and demonstrator configuration. LIFE EFFIDRAIN Project (ref number: LIFE14 ENV/ES/000860).

Malissard, A. (1994). *Les Romains et l'Eau (The Romans and Water)*. Paris (France): Les Belles Lettres, 342 p. ISBN 9782251338149.

Mannina, G., & Viviani, G. (2010). Receiving water quality assessment: comparison between simplified and detailed integrated urban modelling approaches. *Water Science and Technology*, 62(10), 2301–2312.

Maruéjouls, T., Vanrolleghem, P. A., Pelletier, G., & Lessard, P. (2010). Characterisation of retention tank water quality: particle settling velocity distribution and retention time. *Water Quality Research Journal of Canada*, 48(4), 321–332.

Maruéjouls, T., Vanrolleghem, P. A., Pelletier, G., & Lessard., P. (2012). A phenomenological retention tank model using settling velocity distributions. *Water Research*, 46(20), 6857–6867.

Maruéjouls, T., & Montserrat, A. (2016). D3 - Atlantic Pilot Configuration Definition and Preparation. LIFE EFFIDRAIN Project (ref number: LIFE14 ENV/ES/000860).

Maruéjouls, T., Granger, D., Aouichat, F., Lafficher, C., Chadoutaud, E., Pouly, N., & Binet, G. (2017). Suivi de la qualité des eaux unitaires à l'échelle du bassin versant urbain par la mesure en continu (Online monitoring of combined wastewater quality at urban catchment scale). *Techniques Sciences Méthodes*, 10, 35–44.

Maruéjouls, T., & Binet, G. (2018). Impact of two pollutant fluxes calculation methods along with uncertainties on estimation of combined sewer overflow contribution to environmental pollution at the whole urban catchment scale. *Urban Water Journal*, 15(8), 741–749.

Mays, L. W., Sklivaniotis, M. and Angelakis, A. N. (2012). Water for human consumption through the history. In "*Evolution of Water Supply Throughout Millennia*" (Angelakis, A. N., L. W. Mays, L. W., Koutsoyiannis, D., & Mamassis, N.). London (UK): IWA Publishing, pp. 19–42. ISBN 9781843395409.

McCarthy, D. T., Zhang, K., Westerlund, C., Viklander, M, Bertrand-Krajewski, J.-L., Fletcher, T. D., & Deletic, A. (2018). Assessment of sampling strategies for estimation of site mean concentrations of stormwater pollutants. *Water Research*, 129, 297–304.

McQuarrie, A. D. R., & Tsai, C.-L. (1998). *Regression and Time Series Model Selection*. Singapore (Singapore): World Scientific, 480 p. ISBN 9789814497046.

Meirlaen, J. (2002). *Immission based real-time control of the integrated urban wastewater system*. PhD thesis, Ghent University, Belgium.

Métadier, M. (2011). Traitement et analyse de séries chronologiques continues de turbidité pour la formulation et le test de rejets urbains en temps de pluie (treatment and analysis of continuous time series of turbidity for the formulation and test of urban discharges during wet weather). PhD thesis, Institut National des Sciences Appliquées Lyon (INSA Lyon), Lyon, France.

Métadier, M., & Bertrand-Krajewski, J.-L. (2011). Assessing dry weather flow contribution in TSS and COD storm events loads in combined sewer systems. *Water Science and Technology*, 63(12), 2983-2991.

Métadier, M., Binet, G., Barillon, B., Polard, T., Lalanne, P., Litrico, X., & de Bouteiller, C. (2013). Monitoring of a stormwater settling tank: how to optimize depollution efficiency. *Proceedings of the 8th International NOVATECH Conference*, Lyon, France, 10p.

Michelbach, S. & Wöhrle, C. (1994). Settleable Solids from Combined Sewers: Settling, Stormwater Treatment, and Sedimentation Rates in Rivers. *Water Science and Technology*, 29(1–2), 95–102.

Mollerup, A. L., Mikkelsen, P. S., Thornberg, D., & Sin, G. (2017). Controlling sewer systems – a critical review based on systems in three EU cities. *Urban Water Journal*, 14(4), 435–442.

Montgomery, D. C., & Peck, E. A. (1992). *Introduction to linear regression analysis*. New York (USA): Wiley, 544 p. ISBN 9780471533870.

Montserrat, A., Maruéjouls, T., Litrico, X., & Binet, G. (2017). A quality model for combined sewer overflow and sediment description. *Proceedings of the 14th ICUD – International Conference on Urban Drainage*, Prague, Czech Republic, 10-15 September, 373-376.

Moreira, G., Cools, J., Jurkiewicz, K., Kuipers, Y., Petrovicz, D., & Zamparutti, T. (2016). Assessment of Impact of Storm Water Overflows from Combined Waste Water Collecting Systems on Water Bodies (Including the Marine Environment) in the 28 EU Member States – Final Report for Task 1.2. CIRCABC. Belgium: Milieu Ltd.

Muschalla, D., Vallet, B., Anctil, F., Lessard, P., Pelletier, G., & Vanrolleghem, P. A. (2014). Ecohydraulic-driven real-time control of stormwater basins. *Journal of Hydrology*, 511, 82–91

Muste, M., Lee, K., & Bertrand-Krajewski, J.-L. (2012). Standardized uncertainty analysis for hydrometry: a review of relevant approaches and implementation examples. *Hydrological Sciences Journal*, 57(4), 643–667.

Niazi, M., Nietch, C., Maghrebi, M., Jackson, N., Bennett, B. R., Tryby, M., & Massoudieh, A. (2017). Storm water management model: performance review and gap analysis. *J. Sustainable Water Built Environ*, 3(2), 04017002.

Nielsen, P. H., Raunkjær, K., Norsker, N. H., Jensen, N. A., & Hvitved-Jacobsen, T. (1992). Transformation of Wastewater in Sewer Systems – A Review. *Water Science and Technology*, 25(6), 17–31.

Ocampo-Martinez, C. (2010). *Model predictive control of wastewater systems*. Advances in

industrial control. Springer, London (UK): Springer-Verlag London, 217 p. ISBN 9781447157182.

Oliphant, T. E. (2007). Python for scientific computing. *Computing in Science and Engineering*, 9, 10-20.

Painter, H. A. (1958). Some characteristics of a domestic sewage. *Journal of Biochemical and Microbiological Technology and Engineering*, 1(2), 143–162.

Pedregosa, F., Varoquaux, G., Gramfort, A., Michel, V., Thirion, B., Grisel, O., Blondel, M., Prettenhofer, P., Weiss, R., Dubourg, V., Vanderplas, J., Passos, A., Cournapeau, D., Brucher, M., Perrot, M., & Duchesnay, E. 2011 Scikitlearn: Machine learning in Python. *Journal of Machine Learning Research*, 12, 2825–2830.

Pelletier, G., & Bonin, R., 2005. Global optimal real-time control of the Quebec urban drainage system. *Environmental Modelling & Software*, 20, 401–413.

Petruck, A., Cassar, A., & Dettmar, J. (1998). Advanced real time control of a combined sewer system. *Water Science and Technology*, 37(1), 319–326.

Pleau, M., Pelletier, G., Colas, H., Lavallée, P., & Bonin, R. (2001). Global predictive real-time control of Quebec Urban Community's Westerly Sewer Network. *Water Science and Technology*, 43(7), 123–130.

Pleau, M., Colas, H., Lavallée, P., Pelletier, G., & Bonin, R. (2005). Global optimal real-time control of the Quebec urban drainage system. *Environmental Modelling & Software*, 20, 401–413.

Prasad, A. M., Iverson, L. R., & Liaw, A. (2006). Newer classification and regression tree techniques: bagging and random forests for ecological prediction. *Ecosystems*, 9, 181-99.

Prosser, R. (2005). *France (Countries of the World)*. London (UK): Evan Brothers, 61 p. ISBN 9780237528058.

Qin, S.J., & Badgwell, T.A. (2003). A survey of industrial model predictive control technology.

Control Engineering Practice, 11(7), 733–764.

Randrianarimanana, J. J., Lebouc, L., Szturyz, S., & Larrarte, F. (2015). Experimental study of the velocity and suspended solids distribution in wastewater system. In *E-proceedings of the 36th IAHR World Congress* (p. 8). The Hague (Netherlands).

Rauch, W., & Harremoës, P. (1997). Acute pollution of recipients in urban areas. *Water Science and Technology*, 36(8–9), 179–184.

Rauch, W., Aalderink, H., Krebs, P., Schilling, W., & Vanrolleghem, P. (1998). Requirements for integrated wastewater models - driven by receiving water objectives. *Water Science and Technology*, 38(11), 97–104.

Rauch, W., & Harremoës, P. (1999). Genetic algorithms in real time control applied to minimize transient pollution from urban wastewater systems. *Water Research*, 33(5), 1265–1277.

Rauch, W., Bertrand-Krajewski, J.-L., Krebs, P., Mark, O., Schilling, W., Schütze, M., & Vanrolleghem, P. A. (2002). Deterministic modelling of integrated urban drainage systems. *Water Science and Technology*, 45(3), 81–94.

Raudkivi, A. J. (1998). *Loose boundary hydraulics*. Boca Raton (USA): CRC Press, 512 p. ISBN 9789054104483.

Rieger, L., Langergraber, G., Thomann, M., Fleischmann, N., & Siegrist, H. (2004). Spectral in-situ analysis of NO2, NO3, COD, DOC and TSS in the effluent of a WWTP. *Water Science and Technology*, 50(11), 143–52.

Rossman, L. (2015). Storm water management model user's manual version 5.1. US EPA Office of Research and Development, Washington, DC, EPA/600/R-14/413 (NTIS EPA/600/R-14/413b).

Rouge, P., Meseguer, J., Joseph-Duran, B., Maruéjouls, T., Martinez, M., Guasch, R., & Cembrano, G. (2016). D1 - Definition of the Integrated Control Approach Considered in the Demonstrations. LIFE EFFIDRAIN Project (ref number: LIFE14 ENV/ES/000860).

Rudemo, M. (1982). Empirical choice of histograms and Kernel density estimators. *Scandinavian Journal of Statistics*, 9, 65–78.

Saari, H.K., Schmidt, S., Castaing, P., Blanc, G., Sautour, B., Masson, O., Cochran, J.K. (2010). The particulate 7Be/210Pbxs and 234Th/210Pbxs activity ratios as tracers for tidal-to-seasonal particle dynamics in the Gironde estuary (France): implications for the budget of particle-associated contaminants. *Science of the Total Environment*, 408(20), 4784–4794.

Sandoval, S., Torres, A., Pawlowsky-Reusing, E., Riechel, M., & Caradot, N. (2013). The evaluation of rainfall influence on combined sewer overflows characteristics: the Berlin case study. *Water Science and Technology*, 68(12), 2683-2690.

Sandoval, S., & Bertrand-Krajewski, J.-L. (2016). Influence of sampling intake position on suspended solid measurements in sewers: two probability/time-series-based approaches. *Environmental Monitoring and Assessment*, 188, 347.

Sandoval S., & Bertrand-Krajewski, J.-L. (2018). Revisiting conceptual stormwater quality models by alternative linear and non-linear formulations: an event-based approach. *Proceedings of the 11th UDM – International Conference on Urban Drainage Modelling*, Palermo, Italy, 23-26 Sept., 687-690.

Schäfer, J., Blanc, G., Audry, S., Cossa, D., Bossy, C. (2006). Mercury in the Lot–Garonne River system (France): sources, fluxes and anthropogenic component. *Applied Geochemistry*, 21(3), 515–527.

Schilling, W. (1989). *Real-Time Control of Urban Drainage Systems. The State-of-the-Art scientific and Technical Reports No. 2*. IAWQ, London, UK.

Schilling, W., Andersson, B., Nyberg, U., Aspegren, H., Rauch, W., & Harremoës, P. (1996). Real Time Control of wastewater systems. *Journal of Hydraulic Research*, 34(6), 785– 797.

Schilling, W., Bauwens, W., Borchardt, D., Krebs, P., Rauch, W., & Vanrolleghem, P. (1997). On the relation between urban wastewater management needs and receiving water objectives. *Environmental and Coastal Hydraulics: Protecting the Aquatic Habitat, Proceedings of Theme B* 1 & 2, 27, 510–515.

Schmidt, S., Bernard, C., Escalier, J.-M., Etcheber, H., & Lamouroux, M. (2017). Assessing and managing the risks of hypoxia in transitional waters: A case study in the tidal Garonne River (South-West France). *Environmental Science and Pollution Research*, 24(4), 3251–3259.

Schütze, M., Butler, D., & Beck, M. B. (2002). *Modelling, Simulation and Control of Urban Wastewater Systems*. London (UK): Springer London, 362 p. ISBN 9781447101574.

Schütze, M., Campisano, A., Colas, H., Schilling, W., & Vanrolleghem, P. A. (2004). Real time control of urban wastewater systems – where do we stand today? *Journal of Hydrology*, 299(3-4), 335–348.

Schütze, M., Erbe, V., Haas, U., Scheer, M., & Weyand, M. (2008). Sewer system real-time control supported by the M180 guideline document. *Urban Water Journal*, 5(1), 67–76.

Seggelke, K., Löwe, R., Beeneken, T., & Fuchs, L. (2013). Implementation of an integrated real-time control system of sewer system and waste water treatment plant in the city of Wilhelmshaven. *Urban Water Journal*, 10(5), 330–341.

Sickert, E. (1999). Kanalisationen im Wandel der Zeit (Sewerage through the ages). In "*Geschichte der Abwasserentsorgung (History of sanitation)*" (Abwassertechnische Vereinigung). Hennef (Germany): ATV, pp 17–36. ISBN 9783933707086.

Spanakis, S. (1981). He Hydreusi tou Herakliou 829-1939 (The Water Supply to Iraklion 829-1939). Iraklion (Greece): Technical Chamber of Greece, 155 p.

Stanbridge, H. H. (1976). *History of sewage treatment in Britain*. Kent (UK): Institute of Water Pollution Control.

Strecker, E., Urbonas, B., Quigley, M., Howell, J., & Hesse, T. (2002). *Urban Storm Water BMP Performance Monitoring, A Guidance Manual for Meeting the National Storm Water BMP Database Requirements*. Washington, DC.

Sun, S., & Bertrand-Krajewski, J.-L. (2012). On calibration data selection: The case of stormwater quality regression models. *Environmental Modelling & Software*, 35, 61-73.

Sun, S., & Bertrand-Krajewski, J.-L. (2013). Input variable selection and calibration data selection for storm water quality regression models. *Water Science and Technology*, 68(1), 50-58.

Sun, S., Barraud, S., Castebrunet, H., & Aubin, J.-B (2015). Long-term stormwater quantity and quality analysis using continuous measurements in a French urban catchment. *Water Research*, 85, 432–442.

s::scan Messtechnik GmbH. (2011). *Manual Spectrometer Probe V2*, November 2011 Release.

Tanaka, N., & Hvitved-Jacobsen, T. (1998). Transformations of wastewater organic matter in sewers under changing aerobic/anaerobic conditions. *Water Science and Technology*, 37(1), 105–113.

Vallet, B., Muschalla, D., Lessard, P., & Vanrolleghem, P. A. (2014). A new dynamic water quality model for stormwater basins as a tool for urban runoff management: Concept and validation. *Urban Water Journal*, 11(3), 211–220.

van Daal, P., Gruber, G., Langeveld, J., Muschalla, D., & Clemens, F. (2017). Performance evaluation of real time control in urban wastewater systems in practice: review and perspective. *Environmental Modelling & Software*, 95, 90-101.

van den Broeke, J., Langergraber, G., & Weingartner, A. (2006). On-line and in-situ UV/vis spectroscopy for multi-paramter measurements: a brief review. *Spectroscopy Europe*, 18(4), 15–18.

Vanrolleghem, P. A., Schilling, W., Rauch, W., Krebs, P., & Aalderink, H. (1999). Setting up measuring campaigns for integrated wastewater modelling. *Water Science and Technology*, 39(4), 257–268.

Vanrolleghem, P. A., Benedetti, L., & Meirlaen, J. (2005). Modelling and real-time control of the integrated urban wastewater system. *Environmental Modelling & Software*, 20(4), 427–442.

Vaze, J., & Chiew, F. H. S. (2003). Comparative evaluation of urban storm water quality models. *Water Resources Research*, 39(10), 1280.

Versini, P.-A., Joannis, C., & Chebbo, G. (2015). *Guide technique sur le mesurage de la turbidité dans les réseaux d'assainissement (Technical guide on turbidity measurement in wastewater systems)*. Paris (France): Onema, 82 p. ISBN 9791091047432.

Vezzaro, L., Christensen, M. L., Thirsing, C., Grum, M., & Mikkelsen, P. S. (2014). Water quality-based real time control of integrated urban drainage systems: a preliminary study from Copenhagen, Denmark. *Procedia Engineering*, 70, 1707–1716.

Vollertsen, J., & Hvitved-Jacobsen, T. (2002). Biodegradability of wastewater – a method for COD-fractionation. *Water Science and Technology*, 45(3), 25–34.

Vuorinen, H. S., Juuti, P. S., & Katko, T.S. (2007). History of water and Health from ancient civilizations to modern times. *Water Science and Technology*, 7(1): 49–57.

Wager, S., Hastie, T., & Efron, B. (2014). Confidence Intervals for Random Forests: The Jackknife and the Infinitesimal Jackknife. *Machine Learning Research*, 15(1), 1625-51.

Webster, C. (1962). The sewers of Mohenjo-Daro. *Journal Water Pollution Control Federation*, 34(2), 116-123.

Weerts, A.H., & Serafy, Y.H. (2006). Particle filtering and Ensemble Kalman Filtering for state updating with hydrological conceptual rainfall-runoff models. *Water Resources Research*, 42(9), W09403.

Weyand, M. (2002). Real-time control in combined sewer systems in Germany–Some case studies. *Urban Water*, 4, 347–354.

Willems, P. (2001). Stochastic description of the rainfall input errors in lumped hydrological models. *Stochastic Environmental Research and Risk Assessment*, 15, 132–152.

Winkler, S., Zessner, M., Saracevic, E., & Fleischmann, N. (2008). Intelligent monitoring networks – Transformation of data into information for water management. *Water Science and Technology*, 58(2), 317–322.

Wiuff, R. (1985). Transport of suspended material in open and submerged streams. *Journal of the Hydraulics Division*, 111(5), 774–792.

Appendices

Appendix A: CORRELATION BETWEEN CSO LOAD REDUCTION AND TYPICAL RAINFALL PARAMETERS

It is interesting to examine the linear correlation between various variables such as: CSO load difference between QBR and HBR, rainfall parameters, and beta values. Equation (1) describes the Pearson Product-Moment Correlation (PPMC) coefficient used in this study to measure the correlation of two variables, e.g. *X* and *Y*.

$$PPMC = \frac{\sum_{i=1}^{n}(X_i-\overline{X})(Y_i-\overline{Y})}{\sqrt{\sum_{i=1}^{n}(X_i-\overline{X})^2}\sqrt{\sum_{i=1}^{n}(Y_i-\overline{Y})^2}} \quad \text{(Eq. 1)}$$

where $\boldsymbol{X_i}$ and $\boldsymbol{Y_i}$ are individual values of *X* and *Y* (i.e. obtained from each storm event), $\overline{\boldsymbol{X}}$ and $\overline{\boldsymbol{Y}}$ are the corresponding means of the individual values. The PPMC coefficient varies from -1 to 1, in which 1 represents a perfectly positive linear relationship and -1 represents a perfectly negative one.

The main goal of the correlation test is to examine whether there exist linear correlations between: (i) CSO load reduction versus rainfall parameters, (ii) CSO load reduction versus β values, and (iii) β versus rainfall parameters. Initially the computation of PPMC coefficients are done for all 31 storm events but the results show no linear correlation (see Table 1).

Table 1. PPMC matrix for different variables for all the 31 storm events.

	β	CSO load reduction (kg)	CSO load reduction (%)	Rainfall depth (mm)	Rainfall duration (h)	Max rainfall intensity, 5 minutes (mm/h)
β	1					
CSO load reduction (kg)	0.18	1				
CSO load reduction (%)	0.28	0.84	1			
Rainfall depth (mm)	-0.34	-0.05	-0.12	1		
Rainfall duration (h)	-0.12	0.01	0.00	0.52	1	
Max rainfall intensity, 5 minutes (mm/h)	-0.38	-0.17	-0.17	0.33	0.03	1

Similar PPMC coefficients are then calculated only for the 11 storm events having valuable CSO load reduction, with reduction values of individual storm events ranging between 3 and 43 %. Table 2 reports the computation of PPMC coefficients for various pairs of variables from these 11 storm events. CSO load reduction is represented by two variables, including both the quantity and percentage difference. However, it is clear from the results that very low correlation values are found. Furthermore, graphical representation of storm events in terms of rainfall depth and rainfall duration (Figure 1) gives no hint to distinguish the three groups through basic rainfall characteristics. Lastly, the correlations between β and other variables indicate that for this dataset, the fitted β of all storm events cannot be estimated by statistical methods such as linear regression with input variables from the tested rainfall characteristics.

Table 2. PPMC matrix for different variables from the 11 storm events meeting the assessment criterion.

	β	CSO load reduction (kg)	CSO load reduction (%)	Rainfall depth (mm)	Rainfall duration (h)	Max rainfall intensity, 5 minutes (mm/h)
β	1					
CSO load reduction (kg)	-0.06	1				
CSO load reduction (%)	0.13	0.79	1			
Rainfall depth (mm)	-0.06	0.25	-0.02	1		
Rainfall duration (h)	-0.05	0.16	0.13	0.32	1	
Max rainfall intensity, 5 minutes (mm/h)	-0.04	-0.25	-0.35	0.35	-0.61	1

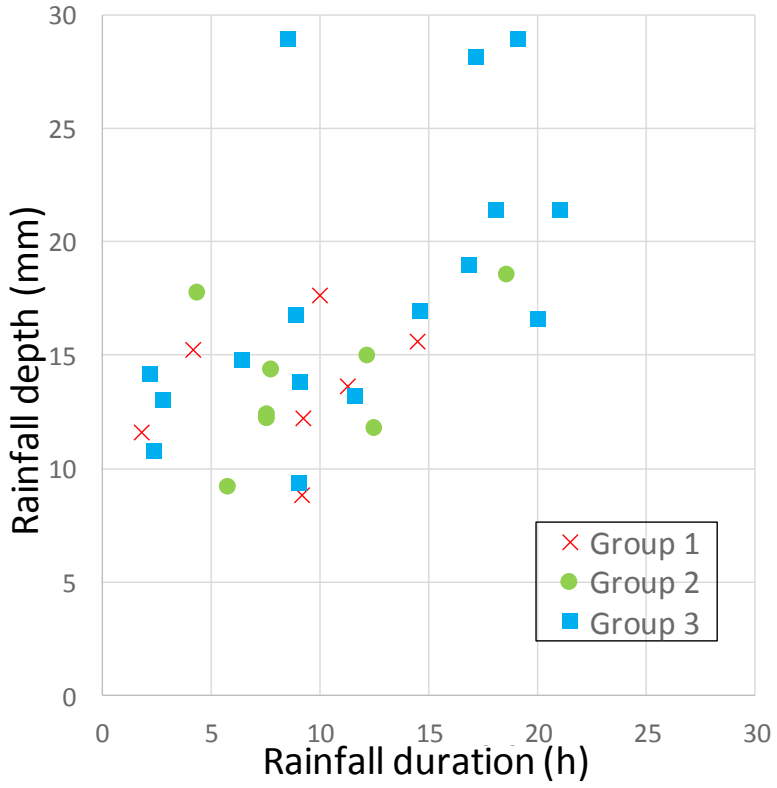

Figure 1. Rainfall depths and rainfall durations of the 31 storm events.

Appendix B: STORM EVENTS USED FOR TESTING THE CONTROL STRATEGIES

Table 1. Storm events used for the proof-of-concept study on Périnot catchment.

(Rainfall data were extracted from Périnot rain gauge).

Event	Start	End	Rainfall depth (mm)	Rainfall duration (hour)
1	18/04/2015 14:00	19/04/2015 00:00	12.40	7.58
2	10/06/2015 02:30	10/06/2015 18:30	15.00	12.17
3	13/06/2015 00:30	13/06/2015 11:00	11.60	1.83
4	28/07/2015 22:00	29/07/2015 13:00	14.40	7.75
5	07/08/2015 23:30	08/08/2015 21:30	14.40	16.83
6	12/08/2015 23:30	13/08/2015 11:00	16.00	6.42
7	13/08/2015 22:00	14/08/2015 19:00	15.60	14.50
8	22/08/2015 19:00	23/08/2015 13:00	17.00	14.58
9	11/09/2015 23:00	12/09/2015 14:30	13.20	11.58
10	02/10/2015 22:00	03/10/2015 16:00	18.60	18.60
11	17/10/2015 22:00	18/10/2015 14:00	8.80	9.17
12	27/10/2015 02:30	28/10/2015 00:00	16.60	20.00
13	20/11/2015 16:30	21/11/2015 13:00	29.00	19.08
14	09/03/2016 03:00	09/03/2016 16:30	13.60	11.33
15	20/03/2016 16:30	21/03/2016 02:00	10.80	2.33
16	09/04/2016 02:30	09/04/2016 15:00	12.20	7.58
17	23/04/2016 08:00	23/04/2016 18:00	17.80	4.33
18	09/05/2016 05:00	10/05/2016 04:00	21.40	18.08
19	21/05/2016 17:30	22/05/2016 19:30	27.62	17.17
20	26/05/2016 01:00	26/05/2016 12:00	15.20	4.17
21	28/05/2016 09:00	28/05/2016 17:00	14.20	2.17
22	28/05/2016 23:30	29/05/2016 07:00	13.00	2.75

23	17/06/2016 04:00	18/06/2016 04:00	21.40	21.00
24	04/08/2016 08:30	04/08/2016 20:30	9.40	9.00
25	13/09/2016 15:00	14/09/2016 04:30	29.00	8.50
26	30/09/2016 18:00	01/10/2016 08:30	13.80	9.08
27	05/11/2016 01:00	05/11/2016 13:00	9.20	5.75
28	08/11/2016 21:30	09/11/2016 17:30	11.40	9.25
29	03/02/2017 20:30	04/02/2017 12:30	17.60	10.00
30	28/02/2017 02:30	28/02/2017 17:30	11.80	12.50
31	03/03/2017 16:30	04/03/2017 05:30	16.80	8.92

Table 2. Storm events used for the case study of Louis Fargue catchment

(Rainfall data were extracted from Abria rain gauge).

Event	Start	End	Rainfall depth (mm)	Rainfall duration (hour)
1	17/10/2015 23:15	18/10/2015 22:00	8.00	8.92
2	27/10/2015 03:15	28/10/2015 09:00	8.20	14.83
3	30/01/2016 13:45	02/02/2016 21:15	22.60	45.75
4	22/02/2016 21:45	24/02/2016 18:00	7.40	30.83
5	01/03/2016 22:45	02/03/2016 23:15	13.20	15.83
6	18/03/2016 05:15	19/03/2016 04:00	5.00	4.50
7	20/03/2016 17:45	23/03/2016 14:00	10.00	2.17
8	26/03/2016 21:45	30/03/2016 03:00	6.20	12.42
9	31/03/2016 06:15	03/04/2016 00:00	12.80	10.50
10	04/04/2016 13:45	06/04/2016 22:00	7.00	11.17
11	09/04/2016 03:15	11/04/2016 23:15	13.00	7.83
12	23/04/2016 08:45	24/04/2016 03:00	15.20	5.58
13	09/05/2016 02:15	11/05/2016 00:00	8.60	22.67
14	06/06/2016 13:15	08/06/2016 01:00	8.00	12.08
15	15/06/2016 21:15	20/06/2016 19:00	21.20	61.42
16	04/08/2016 10:45	05/08/2016 04:00	8.40	7.67
17	04/11/2016 23:45	05/11/2016 22:00	10.40	8.00
18	08/11/2016 16:15	14/11/2016 02:00	26.00	59.33
19	22/11/2016 13:15	24/11/2016 22:00	9.80	21.92

Appendix C: SCIENTIFIC ACTIVITIES DURING THE THESIS

Attended conferences, workshops and scientific courses

The 9th International NOVATECH Conference, Lyon, France, 28 June-01 July 2016.

Simulation workshop: Real-time control and integrated modelling (organised by Otto-von-Guericke University of Magdeburg/Germany and ifak e. V. Magdeburg), Lyon, France, 01 July 2016.

The 23rd European Junior Scientists Workshop on Monitoring Urban Drainage Systems (organised by Sewer Systems & Processes Working Group of the IWA – IAHR Joint Committee on Urban Drainage), Chichilianne, France, 15-20 May 2017.

PhD course (2.5 ECTS): Modelling of Integrated Urban Drainage-Wastewater Systems (organised by Technical University of Denmark, Université Laval, and Czech Technical University), Prague, Czech Republic, 06-09 September 2017.

The 14th ICUD – International Conference on Urban Drainage, Prague, Czech Republic, 10-15 September 2017.

The 11th UDM – International Conference on Urban Drainage Modelling, Palermo, Italy, 23-26 September 2018.

Professional course: the 4th Advanced course on Innovative Wastewater Treatment and Mathematical Modelling (organised by International Water Association Task Group on Membrane Modelling and Control), Palermo, Italy, 27-30 September 2018.

Published and submitted journal papers

Ly, D. K., Maruéjouls, T., Binet, G., Litrico, X., & Bertrand-Krajewski, J.-L. (2018). Evaluation of two statistical approaches for estimating pollutant loads at adjacent combined sewer overflow structures. *Water Science and Technology*, 78(3), 699–707.

Ly, D. K., Maruéjouls, T., Binet, & Bertrand-Krajewski, J.-L. (2019). Application of Stormwater Mass-Volume Curve Prediction for Water Quality-based Real Time Control in Sewer Systems (*Urban Water Journal*, doi: 10.1080/1573062X.2019.1611885).

Published international and national conferences

Ly, D. K., Maruéjouls, T., & Bertrand-Krajewski, J.-L. (2017). Evaluation of two statistical approaches for estimating pollutant loads at adjacent combined sewer overflow structures. *Proceedings of the 14th ICUD – International Conference on Urban Drainage*, Prague, Czech Republic, 10-15 September, 1477-1485.

Ly, D.K., Maruéjouls, T., Binet, G., & Bertrand-Krajewski, J.-L. (2018). Potential of using mass-volume curve prediction for water quality-based real time control. *Proceedings of the 11th UDM – International Conference on Urban Drainage Modelling*, Palermo, Italy, 23-26 September, 700-704.

Joseph-Duran, B., Maruéjouls, T., Ly, D. K., Meseguer, J., & Cembrano, G. (2018). Comparison of Volume-based and Pollution-based Model-Predictive Controllers for Combined Sewer Network Regulation. *Proceedings of the 11th UDM – International Conference on Urban Drainage Modelling*, Palermo, Italy, 23-26 September, 5 p. (Contributor).

Maruéjouls, T., Feng, J., & Ly, D. K. (2019). Critère de flux de polluants pour évaluer la conformité des réseaux d'assainissement : Est-ce pertinent ? Comment le mettre en œuvre ? *Conférence ASTEE-SHF Fonctionnement des systèmes d'assainissement : l'arrêté du 21 juillet 2015, esprit et pratiques*, Colombes, France, 05-06 February, 5 p (Contributor).

Ly, D.K., Bertrand-Krajewski, J.-L., Binet, G., & Maruéjouls, T. (2019). A water quality-based control strategy to reduce CSO pollutant loads. (accepted for oral presentation at *the 10th International NOVATECH Conference*, Lyon, France, 01-05 July, 4 p.).

Ly, D.K., Bertrand-Krajewski, J.-L., Binet, G., & Maruéjouls, T. (2019). Influence of storage tank volume on combined sewer overflow load savings for volume based and quality based real time control strategies. (accepted for oral presentation at *the 9th SPN – International Conference on Sewer Processes & Networks*, Aalborg, Denmark, 27-30 August, 2 p.).

Joseph-Duran, B., Muñoz, E., Meseguer, J., Maruéjouls T., Ly, D. K., & Cembrano, G. (2019). Integrated Sewer Network and WWTP Real-Time Control. (accepted for oral presentation at *the 9th SPN – International Conference on Sewer Processes & Networks*, Aalborg, Denmark, 27-30 August, 2 p.) (Contributor).

Other international publications

Ly, D. K., Maruéjouls, T., & Bertrand-Krajewski, J.-L. (2017). A regression model to estimate pollutant load at adjacent combined sewer overflow structures. *Proceedings of the 23rd European Junior Scientists Workshop*, Chichilianne, France, 15-20 May, 4 p.

Ly, D. K., Maruéjouls, T., Martinez, M., Guasch, R., Ruiloba, L. C., Muñoz, E., Rouge, P., Sun, C., & Cembrano, G. (2017). D5 - Quality monitoring strategy for the pilots. LIFE EFFIDRAIN Project (ref number: LIFE14 ENV/ES/000860), 134 p.

Sun, C., Cembrano, G., Ly, D. K., Maruéjouls, T., Martinez, M., Guasch, R., Ruiloba, L. C., Muñoz, E., Rouge, Joseph-Duran, B., & Meseguer, J. (2017). D6 - Mathematical modelling of the RTC strategies (MPC and Rule-based): conceptual definition and mathematical modelling. LIFE EFFIDRAIN Project (ref number: LIFE14 ENV/ES/000860), 54 p (Contributor).

Joseph-Duran, B., Muñoz, E., Urrea, M., Ly, D. K., Meseguer, J., Cembrano, G., Maruéjouls, T., Guasch, R., & Martinez, M. (2017). D8 - Description of the demonstrator used in the pilots: MPC- and rule-based. LIFE EFFIDRAIN Project (ref number: LIFE14 ENV/ES/000860), 53 p (Contributor).

Ly, D. K., Maruéjouls, T., Joseph-Duran, B., & Muñoz, E. (2018). D10 - Atlantic pilot: pilot set-up and demonstrator configuration. LIFE EFFIDRAIN Project (ref number: LIFE14 ENV/ES/000860), 76 p.

Ly, D. K., Maruéjouls, T., Joseph-Duran, B., Meseguer, J., & Muñoz, E. (2018). D14 - Atlantic pilot: pilot demonstrations and environment impact assessment. LIFE EFFIDRAIN Project (ref number: LIFE14 ENV/ES/000860), in progress.

Appendix D: CURRICULUM VITAE

PERSONAL INFORMATION

Duy Khiem Ly

dkly1310@gmail.com

Skype dkly10

WORK EXPERIENCE

April 2016 - Present

PhD candidate

Suez Water France – Le LyRE, Bordeaux, France

- Working in the LIFE EFFIDRAIN European project to demonstrate integrated real time control strategies of urban wastewater systems for environmental protection. My tasks included:
  - Monitoring of hydraulics and wastewater quality sensors (turbidity meters and spectrometers) and data treatment.
  - Review of major wastewater quality processes in the sewer and the treatment plant.
  - Development of hydraulics and water quality models.
  - Definition and implementation of control strategies for combined sewer systems.
  - Result analysis and performance assessment.

October 2013 – March 2016

Research engineer

Nanyang Technological University, Energy Research Institute @ NTU, Singapore

- Main projects – duties:
  - Modelling and Impact Assessment of Maximum Desalination Capacity along Singapore's Northern Shores – development of brine and total suspended solids models to evaluate the impact of existing and projected Desalination Plants outfall discharges to the receiving waters.
  - Feasibility Study for Marine Renewable Energy Test Sites in Singapore – project management, scope definitions, contract negotiations, permitting application for environmental impact assessment, geotechnical investigation, measurements of water depth and flow velocity, development of detailed models.

March 2013 – August 2013

Intern engineer

DHI Water & Environment (S) Pte. Ltd., Singapore

- Project – duties: Evaluation of the potential effects of Sumatra squall-generated waves on coastal structures and offshore activities in Singapore. – characterisation of the squalls and building of a wave model to assess the effects.

May 2011 – August 2011

Research assistant

National University of Singapore, Dept. of Civil Engineering, Singapore

- Project – duties: Evaluation of the effect of sewer leaks on surface water quality in urban catchment area. – application of COMSOL (CFD) software to build a model including main hydraulics, water quality processes and to investigate of the impact.

EDUCATION AND TRAINING

April 2016 - Present

PhD – Thesis title: "Water quality-based real time control of combined sewer systems "

DEEP Laboratory, National Institute of Applied Sciences of Lyon (INSA Lyon), France

Attended the following courses:

- Simulation workshop on Real-time Control and Integrated Modelling (France, 2016).
- European Junior Scientist Workshop on monitoring urban drainage systems (France, 2017).
- Advanced course on Modelling of Integrated Urban Drainage-Wastewater Systems (Czech Republic, 2017).
- Advanced Course on Innovative Wastewater Treatment and Mathematical

Modelling (Italy, 2018).

September 2011 – August 2013

Master of Science in Hydroinformatics and Water Management

Erasmus Mundus Euro-Aquae Master Course

- **Semester 4 at DHI Water & Environment (S) Pte. Ltd., Singapore**
  Intern project: Squall-generated wave model for Singapore.
- **Semester 3 at Brandenburg University of Technology, Germany**
  Subjects: Numerical simulation: free surface and groundwater modelling, Information and process modelling in hydro-engineering projects, Geometric modelling and presentation methods, Monitoring, data acquisition and documentation, Hydro-Europe working as virtual company.
- **Semester 2 at Newcastle University, United Kingdom**
  Subjects: Hydroinformatics & Integrated river basin management, Numerical methods & Computational hydraulics, Introduction to modelling of floods, Hydroinformatics Systems Development, Climate change: vulnerability, impacts and adaptation.
- **Semester 1 at Nice-Sophia Antipolis University, France**
  Subjects: Hydrology & Hydraulics, Mathematics & Physics, Computer skills, database & GIS – ICT, Introduction to aquatic environment management, Web-based collaborative engineering.

August 2007 – May 2011

Bachelor of Civil Engineering (Honours)

National University of Singapore, Singapore

- **Main subjects:** Geotechnical engineering, Transportation engineering, Financial accounting, Construction project management, Critical thinking and writing, Hydraulics, Water science & Technology, Water & wastewater engineering 1, Solid and hazardous waste management, Introduction to GIS & remote sensing, Water resources engineering.
- **Exchange program:** 1 semester at University of Waterloo, Canada (2010).
- **IARU Global Summer program:** 3-week course on landscape sustainability by University of Copenhagen, Denmark (2009).

PERSONAL SKILLS

Mother tongue(s): Vietnamese

Other language(s)

	UNDERSTANDING		SPEAKING		WRITING
	Listening	Reading	Spoken interaction	Spoken production	
English	C2	C2	C2	C2	C2
French	B1	B1	B1	B1	B1

Levels: A1/A2: Basic user - B1/B2: Independent user - C1/C2 Proficient user (European Framework of Reference for Languages)

Communication skills

- team work: I have worked in various teams with diverse professional backgrounds and expertise.
- intercultural skills and mobility: I have lived and worked in many countries, experiencing and adapting to different cultures and lifestyles.

Organisational / managerial skills

- I was involved in management tasks of a technical project and played key role in coordinating and promoting regional collaborations between Southeast Asian partners, through organizing technical workshops and MoU signing events.

Technical skills and competences

- Hydraulic and quality modelling of sewer systems.
- Development of model predictive controllers.
- Installation, maintenance of wastewater quality sensors, and data treatment.
- Statistical modelling and uncertainty quantification: multiple linear regression, random forest.
- Knowledge of fundamental and innovative processes of wastewater treatment.
- Softwares and programming languages:
  - proficient with EPA SWMM, Python, and Microsoft Office applications.
  - used to work with HEC-RAS, Matlab, EPANET, MIKE 2D, MIKE 3D, COMSOL.
  - was basically trained to use GPS-X, DHI West, SIMBA, GIS.

Driving licence

A, B

ADDITIONAL INFORMATION

Journal Articles

- Application of Stormwater Mass-Volume Curve Prediction for Water Quality-based Real Time Control in Sewer Systems. *(Urban Water Journal, doi: 10.1080/1573062X.2019.1611885).*
- Evaluation of two statistical approaches for estimating pollutant loads at adjacent combined sewer overflow structures. *Water Science &Technology*, 78 (3), 699–707.
- Modelling sewage leakage to surrounding groundwater and stormwater drains. *Water Science &Technology*, 66 (12), 2659–2665.

Selected conference and workshop proceedings

- Influence of storage tank volume on combined sewer overflow load savings for volume based and quality based real time control strategies. *The 9th International Conference on Sewer Processes & Networks*, Aalborg, Denmark, 2019.
- A water quality-based control strategy to reduce CSO pollutant loads. *The 10th International NOVATECH Conference*, Lyon, France, 2019.
- Potential of Using Mass-Volume Curve Prediction for Water Quality-based Real Time Control. *The 11th International Conference on Urban Drainage Modelling,* Palermo, Italy, 2018.
- Comparison of Volume-based and Pollution-based Model-Predictive Controllers for Combined Sewer Network Regulation. *The 11th International Conference on Urban Drainage Modelling*, Palermo, Italy, 2018.
- Evaluation of two statistical approaches for estimating pollutant loads at adjacent combined sewer overflow structures. *The 14th ICUD - International Conference on Urban Drainage*, Prague, Czech Republic, 2017.
- A regression model to estimate pollutant load at adjacent combined sewer overflow structures. *The 23rd European Junior Scientists Workshop*, Chichilianne, France, 2017.
- Impacts of Sewer Leaks on Surrounding Groundwater and Surface Water Quality in Singapore. *American Geophysical Union, Fall Meeting, California, USA, 2011.*

Book chapter

- Characteristics of Sumatra Squalls and Modelling of the Squall-Generated Waves. *Advances in Hydroinformatics* (2017), Springer Water.

Appendix E: SOMMAIRE GENERAL DES RESULTATS MAJEURS DE LA THESE

Cette thèse vise à développer une nouvelle stratégie de gestion en temps réel (GTR) basée sur la qualité de l'eau (QBR pour *Quality Based Real time control*). Cette stratégie a été testée sur le réseau d'assainissement unitaire (RAU) Louis Fargue de Bordeaux afin de réduire la charge de polluants aux déversoirs d'orage (DO). La réduction des charges aux DO est calculée puis comparée avec une approche de GTR plus classique de RAU, qui est basée sur l'hydraulique (HBR pour *Hydraulics Based Real time control*). Compte tenu de l'objectif ci-dessus, les principales étapes du travail mené sont les suivantes :

i. Revue des principaux processus influençant la qualité dans les RAUs et les stations de traitement des eaux usées (STEU), associés aux effets environnementaux néfastes causés par les rejets urbains dans les eaux réceptrices.
ii. Revue des concepts sous-jacents, des classifications, des motivations et de la mise en œuvre des méthodes de GTR des RAUs.
iii. Examen des stratégies de mesurage des polluants en vue de GTR basées sur la qualité de l'eau (QBR).
iv. Définition d'un nouveau concept de QBR, comprenant la configuration de la simulation, de l'algorithme et d'un contrôleur basé sur Python qui fournit les actions de contrôle appropriées pendant les évènements pluvieux.
v. Étude de validation de principe sur un petit site d'essai portant sur un nombre suffisamment important d'évènements (c'est à dire 31 événements).
vi. Application à l'échelle d'une ville, sur le RAU Louis Fargue, avec évaluation de la performance lors d'évènements représentatifs et à long terme.

vii. Étude de sensibilité sur l'influence du volume du réservoir de rétention sur la performance de GTR basé sur la qualité et étude de l'impact de l'incertitude de prédiction du modèle sur les performances du régulateur.

Les trois premières étapes sont basées sur des études bibliographiques. Elles sont étroitement liées et fournissent des connaissances pertinentes à l'élaboration de la nouvelle stratégie QBR. L'étape iv implique le développement conceptuel de la nouvelle stratégie QBR. Pour réaliser cette étape, l'auteur a tenté de proposer plusieurs concepts avant d'atteindre le choix le plus pertinent. Par exemple, dans un premier temps les travaux ont été orientés vers l'utilisation de modèles de régression, qui sont rapides et simples pour prédire les processus de qualité de l'eau. Bien que ce concept statistique n'ait pas été approfondi, les résultats de l'élaboration des modèles de régression sont stimulants et méritent d'être présentés dans cette thèse. Les trois dernières étapes sont consacrées à l'élaboration et à la démonstration de la nouvelle stratégie QBR.

Selon l'objectif et les étapes décrites ci-dessus, la structure de cette thèse de doctorat est formée de huit chapitres. Le Tableau 1 présente les grandes lignes de la thèse, y compris le contenu principal de chaque chapitre:

Tableau 1. Structure de la thèse

Chapitre 1	▪ Connaissances de base pour mieux comprendre le domaine des réseaux d'assainissement urbain. ▪ Le projet, les objectifs et la structure de la thèse.
Chapitre 2	▪ Examen des principaux processus de qualité dans les RAUs et les STEUs, associés aux effets nuisibles sur l'environnement causés par les rejets urbains dans les plans d'eau récepteurs. ▪ Examen des concepts sous-jacents, des classifications, des motivations et de la mise en œuvre des méthodes GTR pour les RAUs.
Chapitre 3	▪ Examen des stratégies de mesurage des polluants pour le QBR.
Chapitre 4	▪ Description de la zone d'étude de cas, base de données et modèle hydrodynamique détaillé sélectionné.
Chapitre 5	▪ Élaboration de deux approches statistiques pour estimer les charges totales de évènements aux DO: régression linéaire multiple contre forêt aléatoire en régression.
Chapitre 6	▪ Démonstration de l'étude de validation de principe pour la nouvelle stratégie QBR.
Chapitre 7	▪ Explication de la stratégie de référence et application de la nouvelle stratégie à grande échelle sur le bassin de collecte Louis Fargue. ▪ Évaluation de la nouvelle stratégie basée sur la qualité par rapport à la stratégie de référence basée sur l'hydraulique (HBR vs. QBR). ▪ Analyse de sensibilité sur l'influence du volume du réservoir de rétention et évaluation de l'impact de l'incertitude de prédiction par le contrôleur.
Chapitre 8	▪ Conclusions et perspectives de la thèse.

Le Chapitre 1 donne d'abord un aperçu des fonctions et des composants de RAU et de STEU, ainsi que de leur raccordement. Les eaux usées provenant des points de consommation sont

collectées et transportées via le RAU à la STEU pour y être traitées avant d'être rejetées dans les eaux réceptrices. Dans les RAUs, les eaux pluviales sont transportées avec les eaux usées dans les mêmes canalisations. Malgré la différence de fonctions, RAU et STEU sont directement liés et fournissent tous deux des rejets (par l'intermédiaire des DO et des effluents de STEU) dans les eaux réceptrices.

L'histoire évolutive de ces deux systèmes est résumée, à partir des premiers vestiges d'anciens drains de rues trouvés au Pakistan (dès 2500 AEC). Les étapes clés de l'histoire sont présentées dans ce chapitre, par exemple le plus grand RAU ancien : Cloaca Maxima ou la découverte du procédé des boues activées. La deuxième partie du Chapitre 1 clarifie les aspects liés à la thèse. La thèse s'inscrit dans le cadre du projet LIFE EFFIDRAIN, qui comprend deux sites : le pilote Atlantique et le pilote Méditerranéen. Le site Atlantique faisant référence au bassin versant de Louis Fargue à Bordeaux est la zone d'étude de la thèse. L'objectif principal de la thèse est le développement d'une nouvelle stratégie (appelée QBR pour *Quality Based Real time control*) pour le RAU de Louis Fargue afin de réduire les charges de polluants des DO pendant les évènements pluvieux.

Les connaissances clés sur les principaux processus liés à la qualité de l'eau et au transport des polluants dans les RAUs ainsi que les effets dominants de ces processus sur les eaux réceptrices sont présentés au Chapitre 2. L'accumulation et le lessivage des surfaces, le transport dans les conduites, la conversion biochimique des polluants et les procédés dans les réservoirs de stockage sont des considérations clés pour les RAUs. En outre, les effets dominants de ces processus sur les eaux réceptrices, c'est-à-dire les effets aigus, différés et cumulatifs, sont examinés en mettant l'accent sur les effets aigus par temps de pluie, comme l'appauvrissement

en oxygène, qui sont une préoccupation majeure dans l'évaluation des effets des DO sur les milieux récepteurs (dont c'est le cas dans ce travail).

Le Chapitre 2 met aussi en lumière des concepts importants liés à la GTR, tels que sa définition, la boucle de régulation et ses éléments. Les classifications des méthodes GTR selon différents critères sont également décrites. Il existe de nombreux critères pour distinguer le type de contrôle, comme le degré d'automatisation, le degré de contrôle, l'extension physique, le moment de l'entrée, l'objectif de contrôle et la méthode de développement de la stratégie de contrôle. En ce qui concerne l'objectif de contrôle, la GTR peut être classé en deux catégories : HBR (visant à réduire le volume d'eau polluée entrant dans les eaux réceptrices) et QBR (visant à réduire les charges polluantes entrant dans les eaux réceptrices). Aussi, ce chapitre explique plus en détail la méthode de contrôle prédictif, qui peut être caractérisée par l'horizon de contrôle et les principes d'optimisation. Enfin, l'évolution de GTR dans le temps est évoquée avec l'introduction de multiples études issues de la littérature. Depuis le premier prototype installé aux États-Unis à la fin des années 1960, les méthodes GTR ont connu un développement considérable. Bien que la documentation sur le QBR soit plus limitée que celle sur le HBR, la motivation pour l'application du QBR n'a cessé de croître au cours des dernières décennies. L'intérêt croissant pour le QBR provient principalement du développement des technologies de détection et de l'inclusion de la réduction des charges polluantes provenant des rejets urbains dans la réglementation environnementale.

Le Chapitre 3 fournit des connaissances sur les facteurs importants à considérer dans les stratégies de surveillance : les variables d'état, les méthodes de suivi des polluants et les méthodologies d'installation des capteurs de qualité des eaux. Les MES (Matières En Suspension), la DCO (la Demande Chimique en Oxygène) ou l'NTK (l'Azote Total Kjeldahl)

peuvent être considérées comme des variables d'état pour le QBR des réseaux d'assainissement. Des études antérieures ont justifié la possibilité d'utiliser des capteurs économiques et faciles à utiliser tels que des spectrophotomètres UV-Vis et des turbidimètres pour le suivi en ligne de ces variables d'état. Les valeurs de concentrations en polluants peuvent être obtenues grâce à un étalonnage local, qui correspond à la corrélation entre les données de turbidité de ces capteurs et les données analysées en laboratoire des campagnes d'échantillonnage.

Des capteurs de qualité de l'eau peuvent être installés au niveau des DO pour quantifier la dynamique des processus et des charges polluantes par temps de pluie. L'information sur la qualité de l'eau à d'autres endroits, comme les entrées et les sorties des STEUs et des bassins de rétention, et les dérivations secondaires avant les jonctions où l'eau s'écoule dans la dérivation principale est utile pour modéliser et mettre en œuvre des décisions de contrôle.

Ensuite, deux méthodes de déploiement des capteurs sont présentées et comparées : l'installation directe et l'installation hors-ligne. L'installation directe est utilisée dans cette étude parce qu'elle permet d'éviter les complications liées à la demande d'espace, de ressources et de permis supplémentaires auprès des autorités et qu'elle ne pose pas le problème du décalage dans le temps des mesures dues au pompage. De plus, une revue de la littérature sur l'impact du positionnement des différents capteurs de qualité sur les concentrations de polluants dans l'eau est effectuée et l'un des points saillants est le risque de gradients verticaux élevés dans le profil de concentration de MES en raison des couches épaisses de sédiments.

Le chapitre 4 se compose de trois sections principales. La première partie présente d'abord le contexte du bassin versant de Louis Fargue à Bordeaux, qui est sujet aux inondations en raison de plusieurs facteurs : climat, topographie et marée. En conséquence, une stratégie de protection contre les inondations a été mise en œuvre par la municipalité depuis 1982. Un grand nombre

de bassins de rétention, de tunnels et de stations de pompage ont été construits ainsi que le centre de télé-contrôle RAMSES (Régulation de l'Assainissement par Mesures et Supervision des Equipements et Stations) pour gérer les RAUs et éviter les inondations. Ensuite, la première section fournit également une description détaillée du bassin Louis Fargue. Le bassin de 7700 ha dispose d'un vaste réseau de bassins de rétention d'une capacité de stockage pouvant atteindre environ 1000000 m^3. Actuellement, la plupart de ces réservoirs sont exploités par contrôle local dynamique ou statique pour protéger le bassin versant des inondations. En outre, depuis 2013, un système de Gestion Dynamique (GD) global basé sur le volume, a été mis en place en aval du bassin versant de Louis Fargue afin de réduire encore les inondations et les volumes des DO. Les eaux réceptrices de RAU peuvent être exposées au risque d'épuisement de l'oxygène.

Pour cette recherche, les données de qualité (ici turbidimètres), les données hydrauliques (capteurs de débit, de vitesse et de niveau) et les données pluviométriques (pluviomètres) sont recueillies d'octobre 2015 à mai 2017. Des capteurs hydrauliques et de qualité en ligne sont installés au niveau des points de captage secondaires, juste en amont des structures des DO suivants : Peugue, Naujac, Caudéran-Naujac et Lauzun. Des campagnes d'échantillonnage sont également menées pour dériver les corrélations entre la turbidité et MES, qui est sélectionnée comme variable d'état pour le contrôle dans cette étude. Pour effectuer la GTR, une tâche essentielle consiste à élaborer un modèle détaillé qui peut simuler la qualité de l'eau principale et les processus hydrauliques à l'intérieur de RAU. Le modèle utilisé pour le bassin versant de Louis Fargue est le modèle SWMM-TSS, basé sur la version 5.1.11 de SWMM de la US Environmental Protection Agency, associé à une bibliothèque améliorée des modèles de la qualité de l'eau définie par l'utilisateur qui permet une meilleure reproduction des systèmes de traitement des eaux usées par transport solide. De plus, la procédure de configuration du modèle détaillé de la qualité pour la zone d'étude est élaborée, ainsi que les résultats représentatifs lors de la comparaison entre les données observées et les données modélisées. En général, la

performance du modèle est considérée comme satisfaisante (hydraulique) et acceptable (pour les pollutographes de MES) pour permettre la comparaison des performances du QBR avec le HBR.

Dans le chapitre 5, les résultats de la modélisation des charges de MES au niveau de trois DO dans le bassin versant de Louis Fargue, Bordeaux (France) montrent que l'ensemble des Variables Explicative (VEs) dépend à la fois de l'approche de modélisation, Régression Linéaire Multiple (RLM) ou Forêts Aléatoires (FA) et varie selon la structure de DO. Pour l'ensemble de données disponibles, la FA nécessite moins de VE que la RLM. La technique des agrégats pour sélectionner les événements représentatifs appropriés pour l'étalonnage du modèle améliore clairement la prévisibilité du modèle pour les deux approches. Le RLM présente de plus faibles écarts d'erreur en raison de la sélection des données d'étalonnage et de meilleures performances des résultats de vérification. Toutefois, les incertitudes des valeurs simulées en calibration et vérification des modèles FA sont jugées inférieures à celles des modèles RLM.

Compte tenu des résultats actuels, le présent document constitue un moyen utile d'évaluer les charges des DO au moyen de modèles de régression. En plus de l'utilisation typique de RLM, FA peut être une alternative intéressante à considérer. Il est possible d'améliorer encore les modèles à des fins opérationnelles en appliquant une analyse de sensibilité à l'impact de l'incertitude type des mesures des précipitations et en élargissant l'ensemble de données par la collecte et l'analyse de données supplémentaires pour inclure davantage d'événements de déversement. Aux fins de la présente étude, les modèles de régression élaborés et plus performants sont destinés à une application ultérieure dans le cadre d'une stratégie simplifiée de QBR. La prévision des précipitations permet de calculer rapidement et de mettre à jour de façon récursive la charge totale de chaque sous-bassin hydrographique, ce qui facilite les

décisions d'attribution des eaux pluviales excessives et de hiérarchisation des capacités de stockage disponibles entre les différents sous-bassins en fonction de l'importance de leurs charges en polluants aux DO.

Dans le but de réduire les charges déversées dans les eaux réceptrices, une nouvelle approche QBR basée sur la prédiction des courbes masse-volume (MV) est développée au Chapitre 6. La performance du QBR est appliquée au bassin versant du Périnot à Bordeaux, en France, pour une série de 31 évènements pluvieux sur 2 ans, et comparée à une approche HBR plus traditionnelle. Il semble que l'efficacité du QBR dépend de la forme de la courbe MV prédite. Le QBR offre le plus d'intérêt dans le cas de pluie où les pentes les plus raides sur les courbes MV apparaissent au milieu ou à la fin de la durée de l'événement. Cela peut être considéré comme un critère pour évaluer l'intérêt potentiel de l'application du QBR. Onze des 31 évènements répondent à ce critère et leur réduction totale de la charge déversée est d'environ 10 %. Les valeurs de réduction des évènements individuels varient entre 3 et 43 %.

En conséquence, on peut distinguer trois types de courbes MV : les groupes 1, 2 et 3 avec leur courbe MV respectivement en dessous (Figure 1), autour (Figure 2) et au-dessus de la ligne bissectrice (Figure 3). Selon cette typologie, le groupe 1 a tendance à fournir la probabilité la plus élevée d'évènements répondant au critère d'évaluation, suivi du groupe 2, et le moins élevé du groupe 3. De plus, l'analyse de sensibilité sur l'impact de l'intervalle de temps de contrôle (ITC) montre que pour les évènements appartenant aux groupes 1 et 2, la diminution de la durée de l'ITC entraîne généralement une diminution de la charge totale aux DO ou, en d'autres termes, une amélioration de l'efficacité du QBR. Ensuite, le volume du réservoir de rétention est considéré comme jouant un rôle important dans la performance du QBR. D'après les essais

effectués lors des deux évènements, le changement dans la réduction de la charge aux DO par le QBR (par rapport au HBR) avec des volumes de réservoir différents est vraiment significatif.

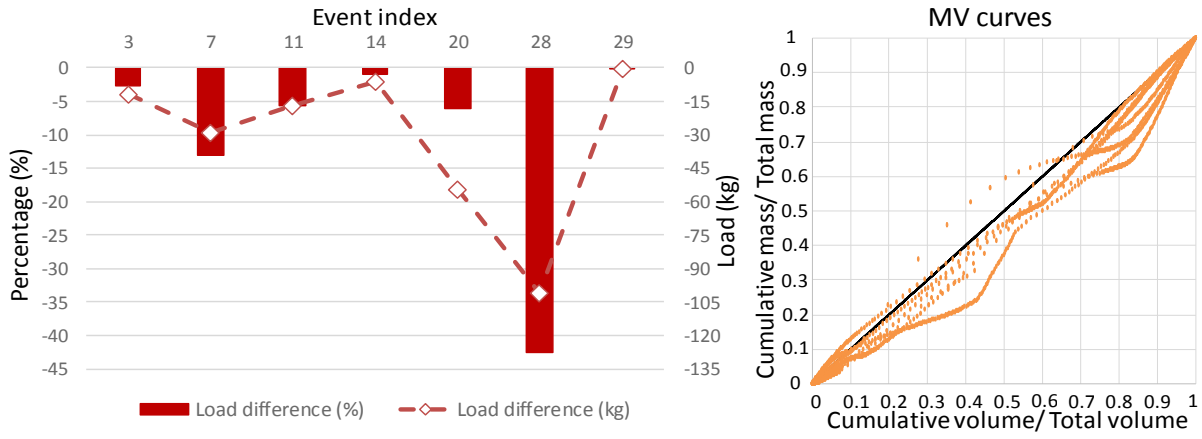

Figure 1. Différences de charge totales aux DO (QBR versus HBR) pour l'ensemble des 7 évènements du groupe 1 (à gauche) et leurs courbes MV simulées (à droite).

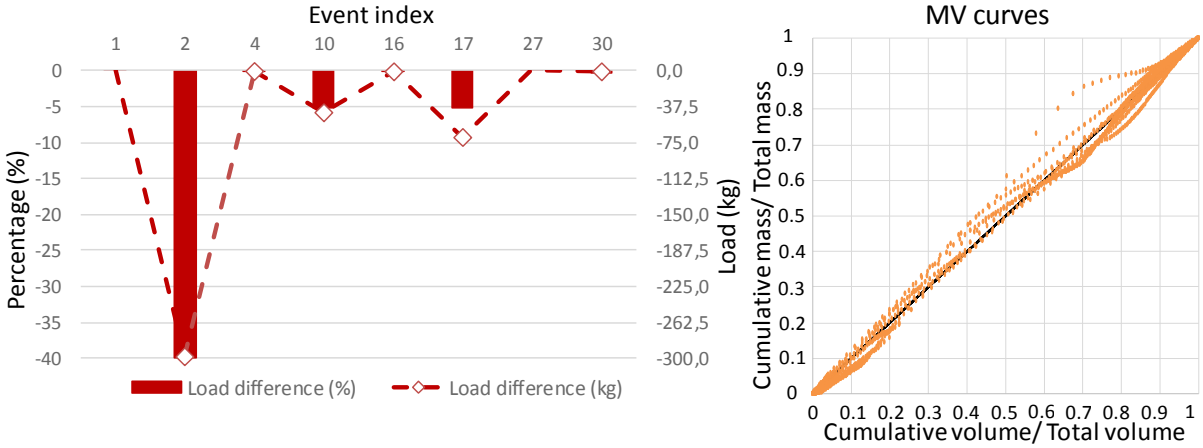

Figure 2. Différences de charge totales des CSO (QBR versus HBR) pour l'ensemble des 8 évènements du groupe 2 (à gauche) et leurs courbes MV simulées (à droite).

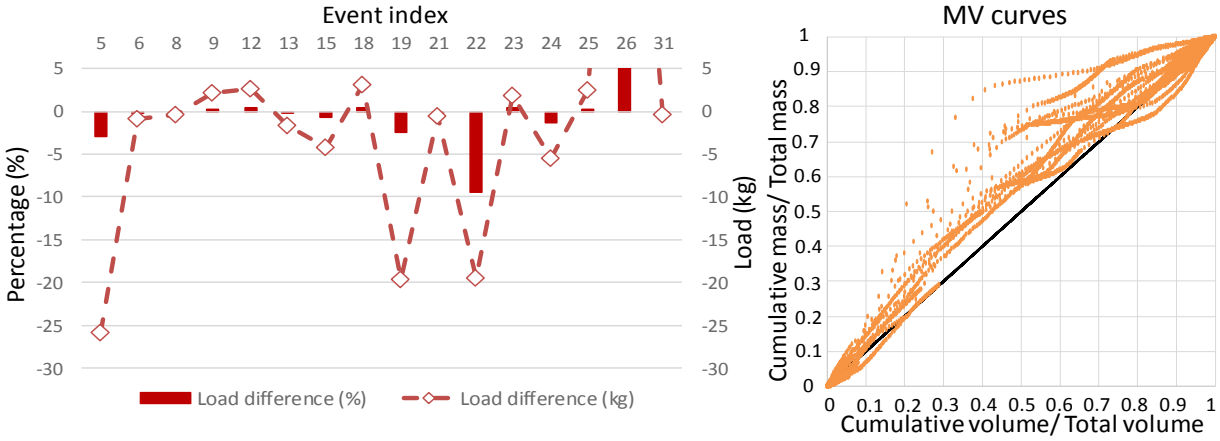

Figure 3. Différences de charge totales des CSO (QBR versus HBR) pour l'ensemble des 16 évènements du groupe 3 (à gauche) et leurs courbes MV simulées (à droite).

En résumé, les résultats indiquent le potentiel réel de l'utilisation des courbes MV pour le QBR. Elle pourrait constituer une alternative efficace à la gestion des bassins de rétention pour minimiser les charges polluantes rejetées dans l'environnement. La simplicité de l'approche est clairement un avantage par rapport aux autres solutions GTR qui sont basées sur des techniques d'optimisation avancées.

Compte tenu des résultats positifs lorsqu'elle est appliquée au petit bassin versant du Périnot, la stratégie QBR est ensuite mise en œuvre sur le bassin versant de Louis Fargue et comparée à une stratégie HBR typique qui représente le fonctionnement actuel de RAU. Ce travail est effectué au chapitre 7. Trois réservoirs sont pris en compte : Carmaux, Abria et Alhambra avec des volumes de 8000 m^3, 6000 m^3 et 1500 m^3 respectivement sélectionnés pour le contrôle. Le QBR est également appliqué sur du stockage en ligne au niveau de l'intercepteur des quais pour transférer les débordements d'un DO amont (Naujac) vers un DO aval (Caudéran-Naujac), sachant que la concentration de MES du premier est généralement plus élevée que celle du second.

Au préalable, un événement pluvieux représentatif est sélectionné pour régler et tester la performance du QBR par rapport au HBR. Les résultats montrent que la stratégie QBR est capable d'identifier la meilleure période (flux de MES le plus élevé) pour maximiser le remplissage du réservoir, et également d'anticiper les volumes à venir pour utiliser au mieux la capacité du réservoir (voir Figure 4). Pour l'événement représentatif choisi, QBR produit une réduction de 7.5 % de la charge au DO par rapport au HBR.

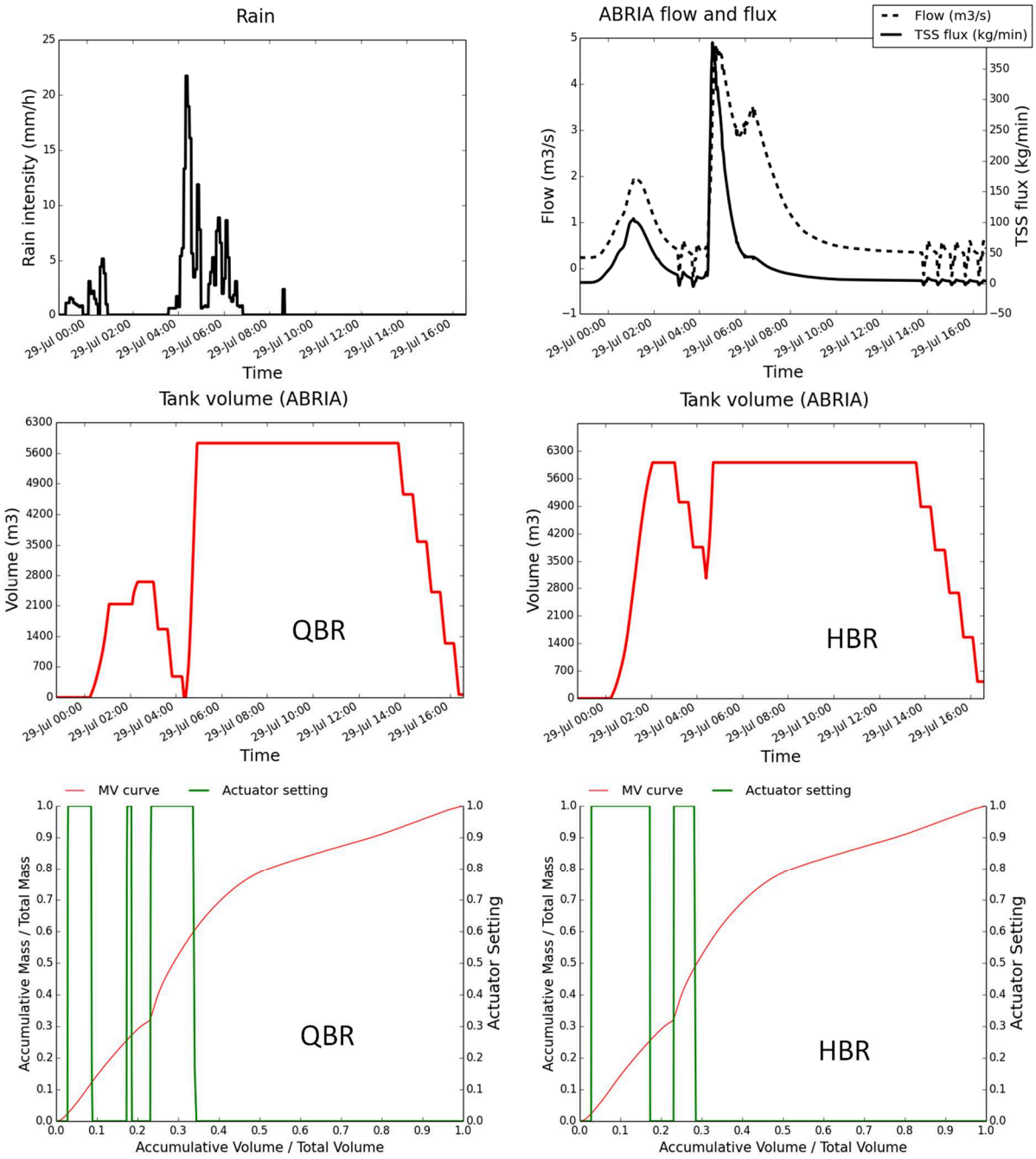

Figure 4. Différences dans les résultats entre les deux stratégies de lutte pour l'évènement du 29 juillet 2015 (pour le réservoir Abria).

Deuxièmement, la stratégie QBR est mise en œuvre pour 19 évènements sur une période de 15 mois (voir Figure 5). On peut observer que la performance de la stratégie de QBR est constante au cours de diverses évènements. QBR peut apporter un avantage précieux par rapport à HBR, avec 17 des 19 événements ayant un pourcentage de réduction de charge par événement variant

entre 6 et 28.8 %. Néanmoins, à la différence du cas du bassin versant de Périnot, pour le bassin versant de Louis Fargue, il n'est pas possible d'obtenir une corrélation significative entre la performance de la stratégie QBR et les caractéristiques de la courbe MV événement.

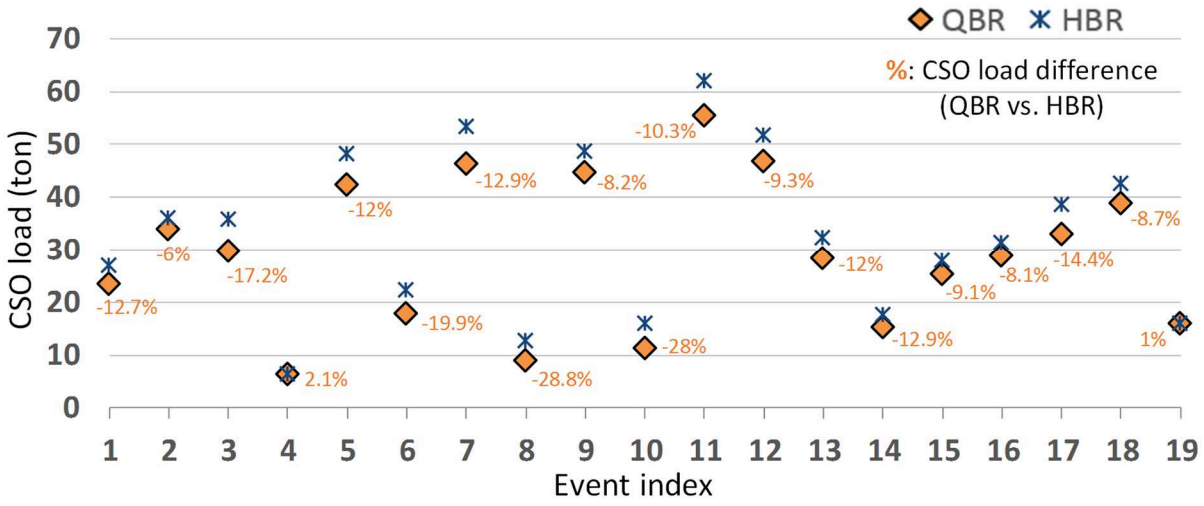

Figure 5. Charges totales des CSO obtenues par les deux stratégies pour les 19 évènements sélectionnées, ainsi que la différence de charge des CSO entre le QBR et le HBR, en pourcentage.

En complément, ce chapitre vise l'évaluation de l'impact de l'incertitude de la prévision de la courbe MV (provenant de l'incertitude de prévision détaillée du modèle) sur la performance de la stratégie QBR, en utilisant le même événement pluvieux représentatif. 100 échantillons des courbes MV des événements sont générés de façon aléatoire pour chacun des quatre sites contrôlés. La plage de réduction de la charge aux DO qui en résulte varie entre 5.6 et 8.2 % et la valeur médiane est de 6.4 %. Pour l'événement représentatif, l'incertitude dans la réduction de la stratégie QBR par rapport à la stratégie HBR est donc de 7.5 ± 1.1 % (ou 3.1 ± 0.4 tonne).

En outre, le Chapitre 7 examine l'influence du volume du réservoir de stockage (Abria, Carmaux et Alhambra) sur la performance des deux stratégies de contrôle. L'étude de sensibilité montre qu'une plus grande capacité de stockage du réservoir peut généralement réduire la charge des CSO pour les deux stratégies. Il est intéressant de noter que la Figure 6 montre que l'augmentation du volume du réservoir n'entraîne pas toujours une augmentation de la

performance du QBR par rapport au HBR. Pour le réservoir Abria, l'avantage du QBR sur le HBR augmente d'abord avec l'augmentation du volume du réservoir, jusqu'à atteindre un pic (entre 6000 m^3 et 8000 m^3) et diminue progressivement par la suite. Pour le bassin de Carmaux, le pic est moins clair mais apparaît également au milieu de la plage de volume (entre 7000 m^3 et 9000 m^3). Le réservoir de l'Alhambra semble insensible aux charges déversées. En général, le choix entre le type de stratégie de contrôle, QBR ou HBR, devrait tenir compte des dimensions et de l'emplacement actuel des réservoirs sur le site.

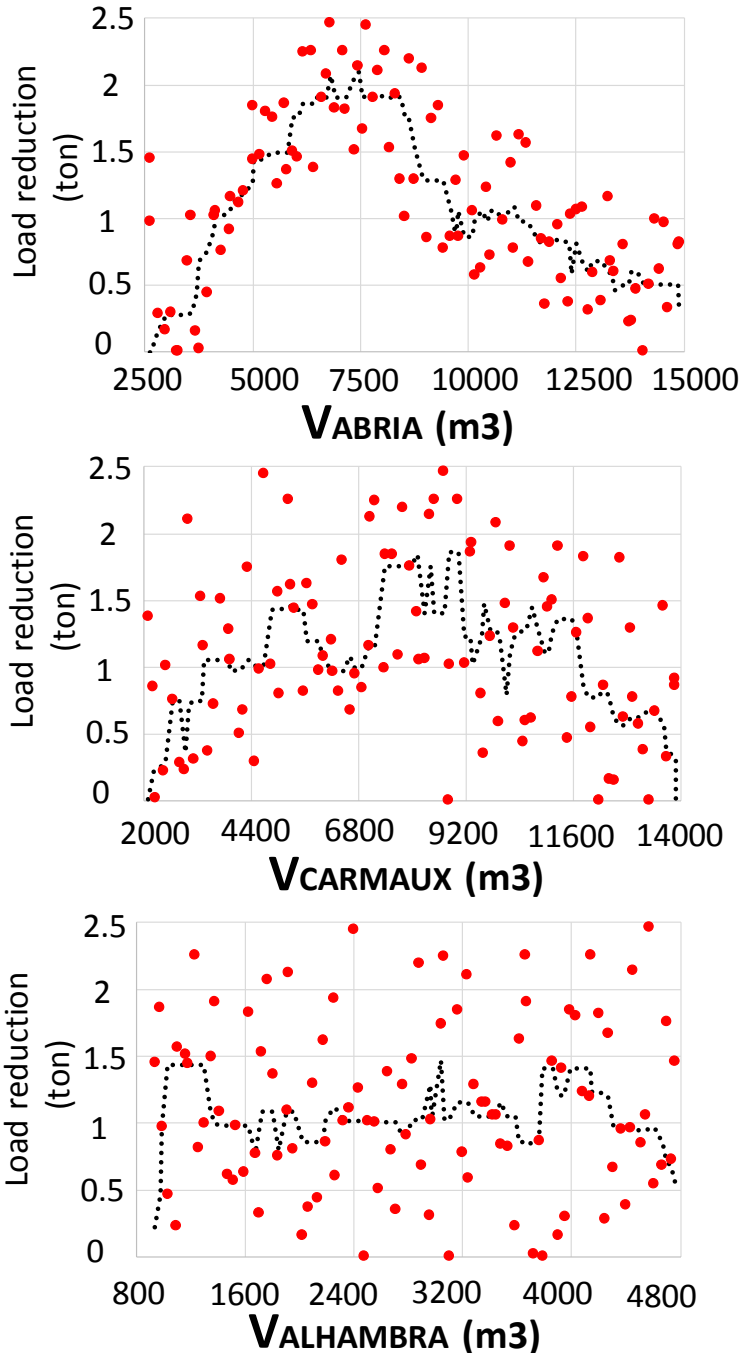

Figure 6. Impact du volume des réservoirs (Abria, Carmaux et Alhambra, événement du 29 juillet 2015) sur les différences de charges des CSO entre QBR et HBR (la ligne pointillée noire représente la ligne médiane mobile avec une largeur de fenêtre de 10 valeurs).

Enfin, le Chapitre 7 présente également l'étude de sensibilité réalisée séparément pour trois bassins de rétention supplémentaires en amont du réseau (Périnot, Bourran et Chêne Vert). Cette étude vise à sélectionner les volumes de bassin les plus utiles pour l'extension du QBR à

plusieurs bassins sur le périmètre de Louis Fargue. Ainsi, les volumes retenus pour les bassins Périnot, Bourran et Chêne Vert sont respectivement de 3300, 8000 et 6000 m^3.

FOLIO ADMINISTRATIF

THESE DE L'UNIVERSITE DE LYON OPEREE AU SEIN DE L'INSA LYON

NOM : LY DATE de SOUTENANCE : 28/05/2019

Prénoms : DUY KHIEM

TITRE : WATER QUALITY-BASED REAL TIME CONTROL OF COMBINED SEWER SYSTEMS

NATURE : Doctorat Numéro d'ordre : 2019LYSEI032

Ecole doctorale : MEGA DE LYON (MECANIQUE, ENERGETIQUE, GENIE CIVIL, ACOUSTIQUE) - ED162

Spécialité : Génie Civil

RESUME :

Real time control (RTC) is considered as a cost-efficient solution for combined sewer overflow (CSO) reduction as it optimises the available capacity of sewer networks. RTC helps to prevent the need for construction of additional retention volumes, increases the network adaptability to changes in water management policies, and above all alleviates the environmental impact of CSOs. Following increasing interest in water quality-based RTC (QBR), this thesis demonstrates a simple and nothing-to-lose QBR strategy to reduce the amount of CSO loads during storm events. The performance of the QBR strategy, based on Mass-Volume (MV) curves prediction, is evaluated by comparison to a typical hydraulics-based RTC (HBR) strategy. A proof-of-concept study is first performed on a small catchment of 205 ha to test the new QBR concept using 31 storm events during a two-year period. Compared to HBR, QBR delivers CSO load reduction for more than one third of the events, with reduction values from 3 to 43 %. The QBR strategy is then implemented on the Louis Fargue catchment (7700 ha) in Bordeaux, France and similarly compared with the HBR strategy. By implementing QBR on 19 storm events over 15 months, its performance is consistent, bringing valuable benefits over HBR, with 17 out of 19 events having load reduction varying between 6 and 28.8 %. The thesis further evaluates the impact of MV curve prediction uncertainty (due to model prediction uncertainty) on the performance of the QBR strategy, using a representative storm event. The resulting range of uncertainty is limited. Besides, results of the sensitivity study show that the choice of the QBR or HBR strategy, should take into account the current tank volumes and their locations within the catchment.

MOTS-CLÉS : combined sewer overflow, mass-volume curve, pollutant load, real time control, sensitivity analysis, storage tank

Laboratoire (s) de recherche : Laboratoire DEEP (Déchets Eaux Environnement Pollutions)

Directeur de thèse : Jean-Luc BERTRAND-KRAJEWSKI

Président de jury : Sylvie BARRAUD

Composition du jury :

MUSCHALLA, Dirk	TU GRAZ	Rapporteur
CAMPISANO, Alberto	UNIVERSITY OF CATANIA	Rapporteur
BARRAUD, Sylvie	INSA LYON	Examinatrice
CHEBBO, Ghassan	ENPC	Examinateur
MARUÉJOULS, Thibaud	SUEZ EAU France	Co-encadrant de thèse
BERTRAND-KRAJEWSKI, Jean-Luc	INSA LYON	Directeur de thèse